THE MEASUREMENT AND INTERPRETATION OF HEAT FLOW IN THE MEDITERRANEAN AND BLACK SEAS

by

ALBERT J. ERICKSON

S.B., Brown University
(1964)

SUBMITTED IN PARTIAL FULFILLMENT OF THE
REQUIREMENTS FOR THE DEGREE OF
DOCTOR OF PHILOSOPHY

at the

MASSACHUSETTS INSTITUTE OF TECHNOLOGY

and the

WOODS HOLE OCEANOGRAPHIC INSTITUTION

June, 1970

Signature redacted

Signature of Author.....
Joint Program in Oceanography, Massachusetts Institute of Technology - Woods Hole Oceanographic Institution, and Department of Earth and Planetary Sciences, and Department of Meteorology, Massachusetts Institute of Technology, June 1970

Signature redacted

Certified by .....
Thesis Supervisor

Signature redacted

Accepted by .....
Chairman, Joint Oceanography Committee in the Earth Sciences, Massachusetts Institute of Technology - Woods Hole Oceanographic Institution

The Measurement and Interpretation of Heat Flow in the Mediterranean and Black Seas

by

Albert Joseph Erickson

Submitted to the Joint Oceanographic Committee in the Earth Sciences, Massachusetts Institute of Technology and Woods Hole Oceanographic Institution, on June, 1970, in partial fulfillment of the requirements for the degree of Doctor of Philosophy.

ABSTRACT

The average of 33 heat flow measurements located throughout the eastern Mediterranean Sea is 0.74±0.30 HFU. No correlation exists between the observed heat flow and other types of geophysical data. The variability of the heat flow data is slightly higher in areas of rough sea floor relief.

The average of 24 heat flow values in the western Mediterranean is 2.33±1.01 HFU, over 50% greater than the world average of 1.4 HFU and nearly three times the average measured flux through the eastern Mediterranean. The mean of 12 measurements located in the Mediterranean west of Sardinia and Corsica is 1.83±0.55 HFU. Heat flow values ranging from 1.35 to 3.15 HFU are distributed throughout the western Mediterranean basin without any apparent pattern.

The average of 12 heat flow values in the Tyrrhenian Sea is 2.83±1.07 HFU. An area of uniformly high heat flow (3.38±0.16 HFU) exists in the southeastern half of the Tyrrhenian basin. Measurements on and north of the Tyrrhenian abyssal plain are more variable and high values (up to 4.14 HFU) are found throughout the entire basin.

The average of 19 heat flow measurements in the Black Sea is 0.84±0.32 HFU. The average flux through the eastern and western halves of the Black Sea is nearly equal. Measurements at which the highest values were

obtained tend to be located on the margins of the Black Sea, rather than in the central basin. This pattern is probably caused by thermal refraction of heat away from the thickly sedimented basin and a lower sedimentation rate on the margins. Sedimentation in the Black Sea has reduced the equilibrium heat flow by a factor of two or more. The equilibrium heat flow through the floor of the Black Sea, corrected for the effects of both sedimentation and refraction, is estimated as 2.7 HFU.

Environmental corrections to the heat flow values measured in the Mediterranean are smaller. The average equilibrium heat flow through the eastern and western Mediterranean Seas is estimated to be 0.9 and 2.9 HFU, respectively.

The abnormally high and low heat flux through the floors of the western and eastern Mediterranean, respectively, may be interpreted in terms of plate tectonics. The western Mediterranean and, in particular, the Tyrrhenian Sea, has many of the geophysical properties of a marginal sea behind an island arc system, including abnormally high heat flow. Conversely, the eastern Mediterranean, located seaward of the Cretan island arc, may be underlain by lithospheric material sinking beneath the Aegean Sea and depressing the isotherms in the upper mantle, thus producing the observed regionally low heat flux.

Thesis Supervisor ..... M. Gene Simmons
Professor, Department of Earth and Planetary Sciences, Massachusetts Institute of Technology

TABLE OF CONTENTS

Page

Page

*The appendices have been omitted from copies of this report scheduled for normal distribution. They are available upon request from the author.

LIST OF FIGURES

LIST OF TABLES

THE MEASUREMENT AND INTERPRETATION OF HEAT FLOW IN THE MEDITERRANEAN AND BLACK SEAS

by

Albert Joseph Erickson

INTRODUCTION

1.1 REGIONAL SETTING

Tectonic processes ranging from continental drift to volcanic activity depend upon thermal energy for their existence. Knowledge of the thermal state of the upper mantle beneath the Mediterranean-Alpine area can provide important constraints on possible models of its origin and history. The marine heat flow measurements reported in this thesis are a first step to provide reliable data relevant to the thermal state of the upper mantle in this extremely interesting area.

The Mediterranean and Black Seas, along with the Adriatic and Caspian Seas, are located in the western third of the zone of Cenozoic tectonic activity which extends from the Strait of Gibraltar east to the island arcs of the East Indies (Holmes, 1965). The Eurasian continental block north of the Alpine zone has been generally stable since the Late Paleozoic Hercynian orogeny. The stable African, Arabian, and Indian crustal blocks form the southern boundary of the zone (Klemme, 1958).

The generally east-west alignment of the zone of Alpine folding and geologic evidence for north-south compression (Brinkmann,1960) have resulted in a widely-held belief that the zone marks the area affected by the collision of remanents of the proto-continent Gondwanaland with the Eurasian continental mass. Recent advances in

geophysical techniques, particularly the use of paleomagnetic data (Raven, 1960) and the recognition that processes within the upper mantle can determine the configuration and mobility of the earth's crust (Shimazu, 1967; Menard and Chase, 1965; Bott, 1965) have strengthened the basic hypothesis that the Alpine zone is an area of north-south compression. The small ocean basins within the Alpine zone are, in themselves, of unusual scientific interest because they have many geophysical characteristics of both oceanic and continental areas (Menard, 1967; Ritsema 1969a). Geologic evidence, reviewed by De Booy (1969) and Pannekoek (1969), suggests that areas in the western Mediterranean now covered by 2 or 3 km of water and underlain by thin crust and upper mantle structure characteristic of oceanic areas, formerly were sources of elastic, terrigenous sediment now immobilized in the flysch sequences of the Alps, Appenines, and Atlas mountains. Within the eastern and western Mediterranean Seas, arcuate structures characterized by seismic, volcanic, and tectonic activity are similar geophysically to Pacific island arcs. The Mediterranean arc structures and ocean basins may be a consequence of the attempted assimilation of continental crust within the asthenosphere, as discussed by McKenzie (1969).

1.2 GEOGRAPHIC SETTING

The western Mediterranean Sea is the entire body of water west of Italy and Sicily. It is cut longitudinally by the islands of Sardinia and Corsica into the Tyrrhenian basin to the east and the western Mediterranean basin to the west (Figure 1). The Balearic abyssal plain, the Alboran basin, the Rhone fan, and various continental and island rises are distinguished within the western Mediterranean basin as separate physiographic provinces in Figure 2. Similarly, the Tyrrhenian basin includes the Tyrrhenian abyssal plain, and the Sardinian, Corsican, and Sicilian island rises, as well as the continental rise west of Italy. In this manuscript, the phrase Tyrrhenian basin refers to the deeper, southern half of the Tyrrhenian Sea.

The shallow water area between Sicily and Africa, referred to as the Sicilian platform, divides the eastern and western Mediterranean Seas. The eastern Mediterranean includes the Ionian Sea west of Greece and the Levant Sea south and east of Crete. The deepest areas in the eastern Mediterranean are located in the southwestern Ionian Sea and along the southwestern coast of Greece (see Figure 3).

The Cretan island arc consists of the islands of Rhodes, Karpathos, Crete, Andikithera, and Kithera. The Mediterranean ridge is a broad, arcuate topographic bulge

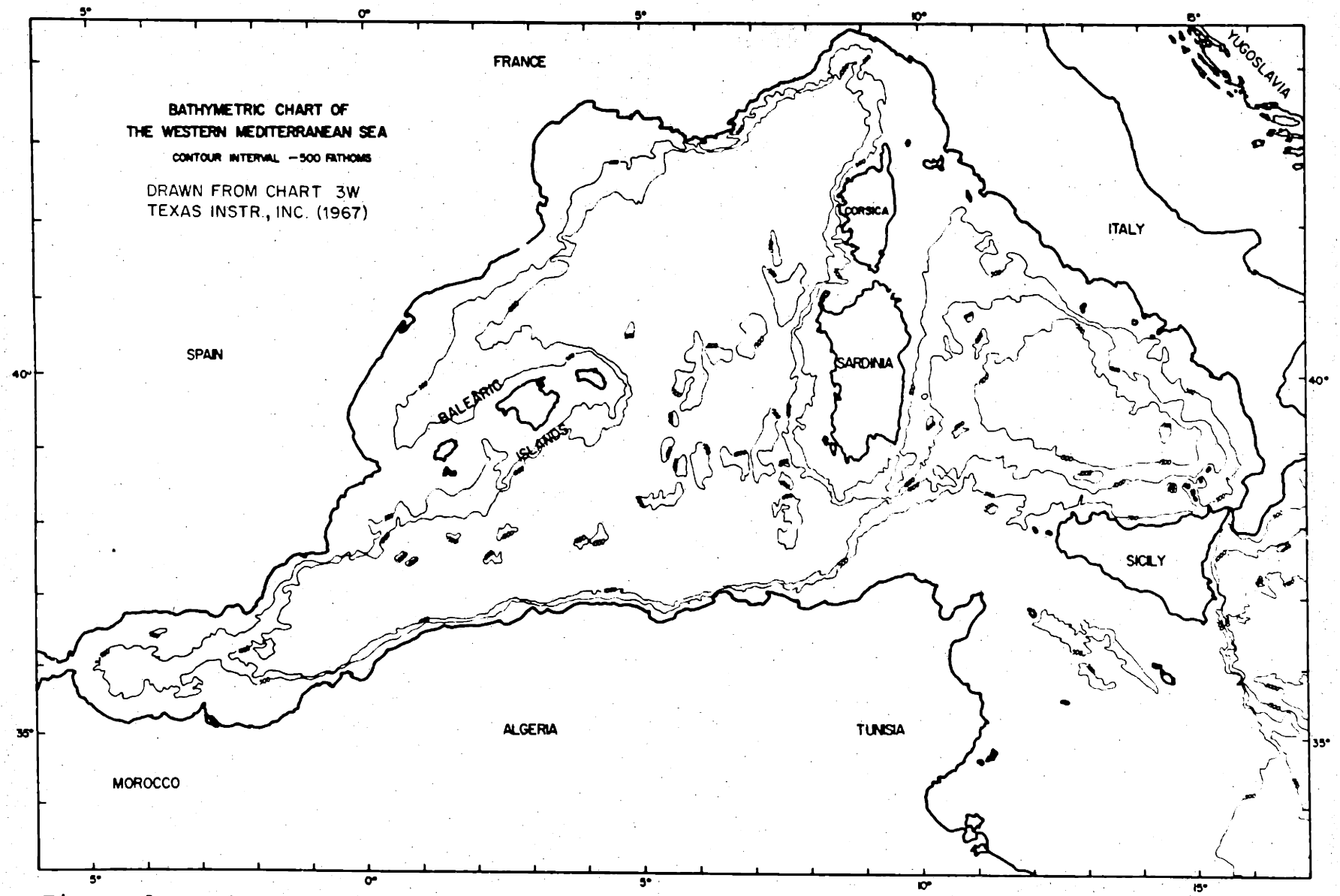

Figure 1. Bathymetric map of the western Mediterranean Sea.

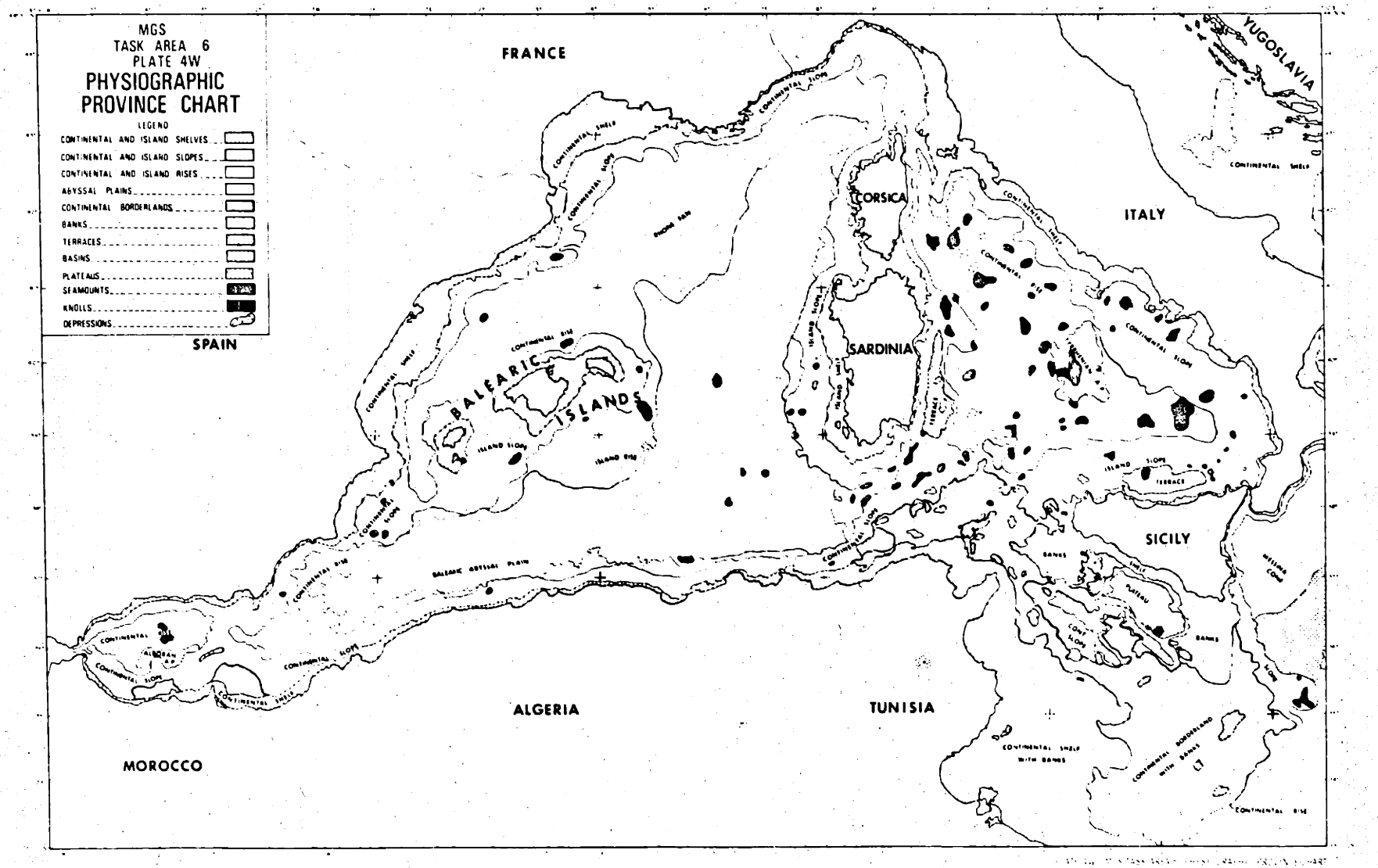

Figure 2. Physiographic provinces in the western Mediterranean Sea.Drawn from Chart 4W,Texas Instr.,Inc.(1967)

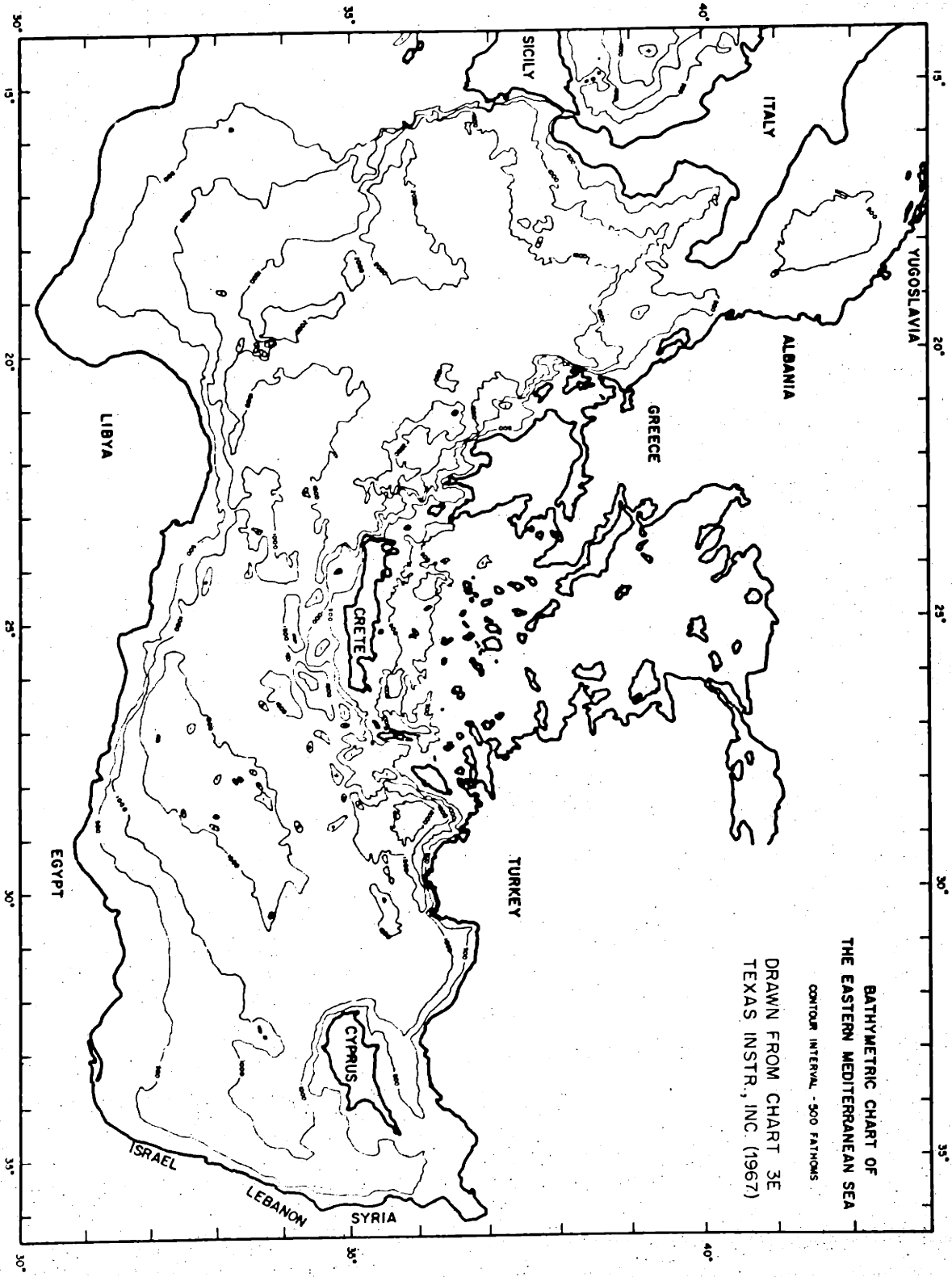

Figure 3. Bathymetric map of the eastern Mediterranean Sea.

separated from the Cretan island arc on the north by the Hellenic trough system, and flanked on the south by topographic lows at the base of the African continental rise. It extends from the heel of Italy eastwards almost to Cyprus (Figure 4). Cyprus forms the southwestern edge of the shallow Cilicia plateau, which extends north and east from Cyprus to Turkey and Lebanon, respectively.

It will be convenient to refer to the eastern, western, and central deep-water portions of the Black Sea as the eastern, western, and central Black Sea basins, although, as shown in Figure 5, the basins are not defined bathymetrically. The margins of the Black Sea are defined as that part of the seafloor shallower than 2000 m, and vary from a width of a few tens of kilometers south of the Crimean peninsula to hundreds of kilometers in the shallow, northwestern corner.

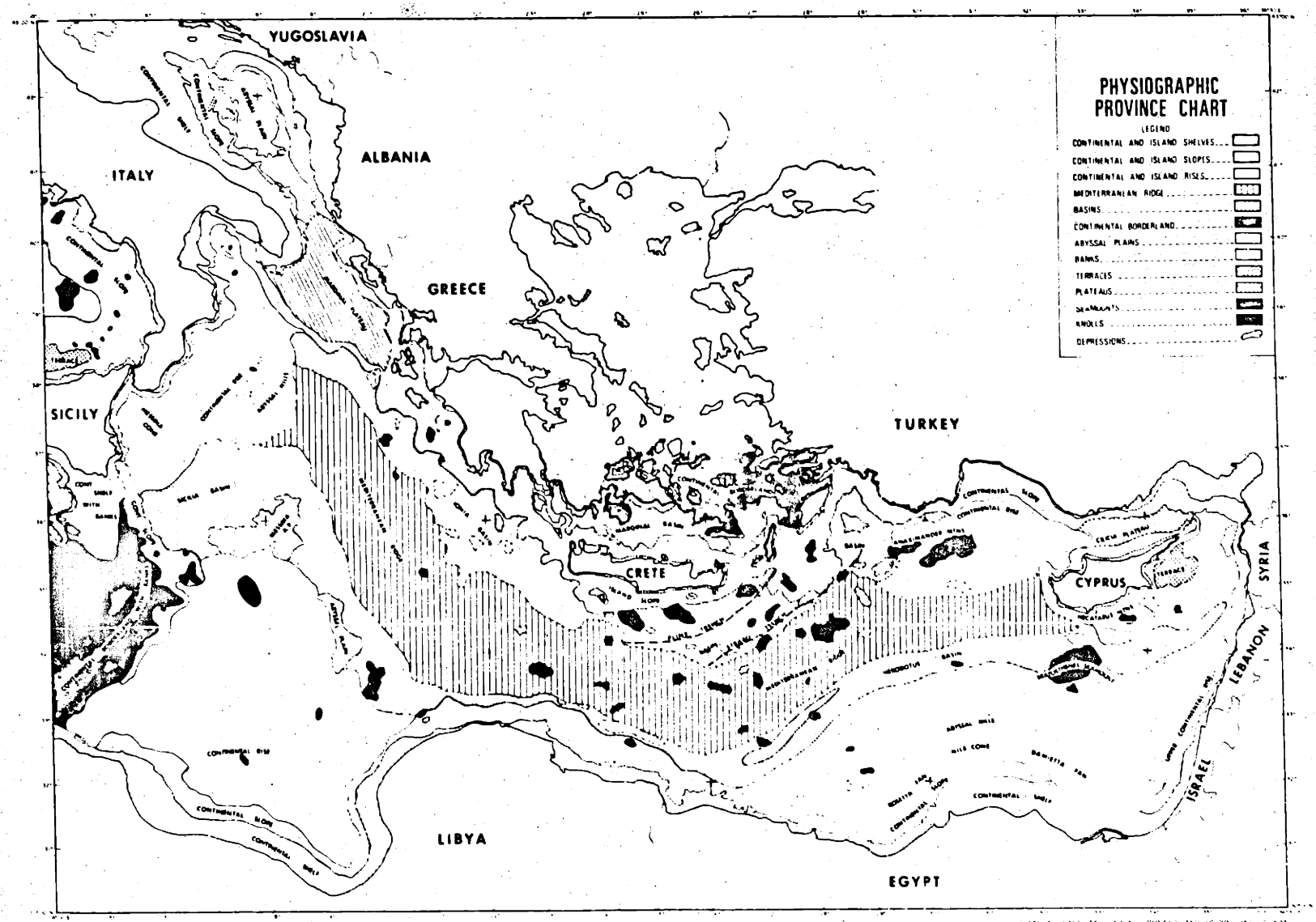

Figure 4. Physiographic provinces in the eastern Mediterranean Sea. Drawn from Chart 4E, Texas Instr.,Inc.(1967).

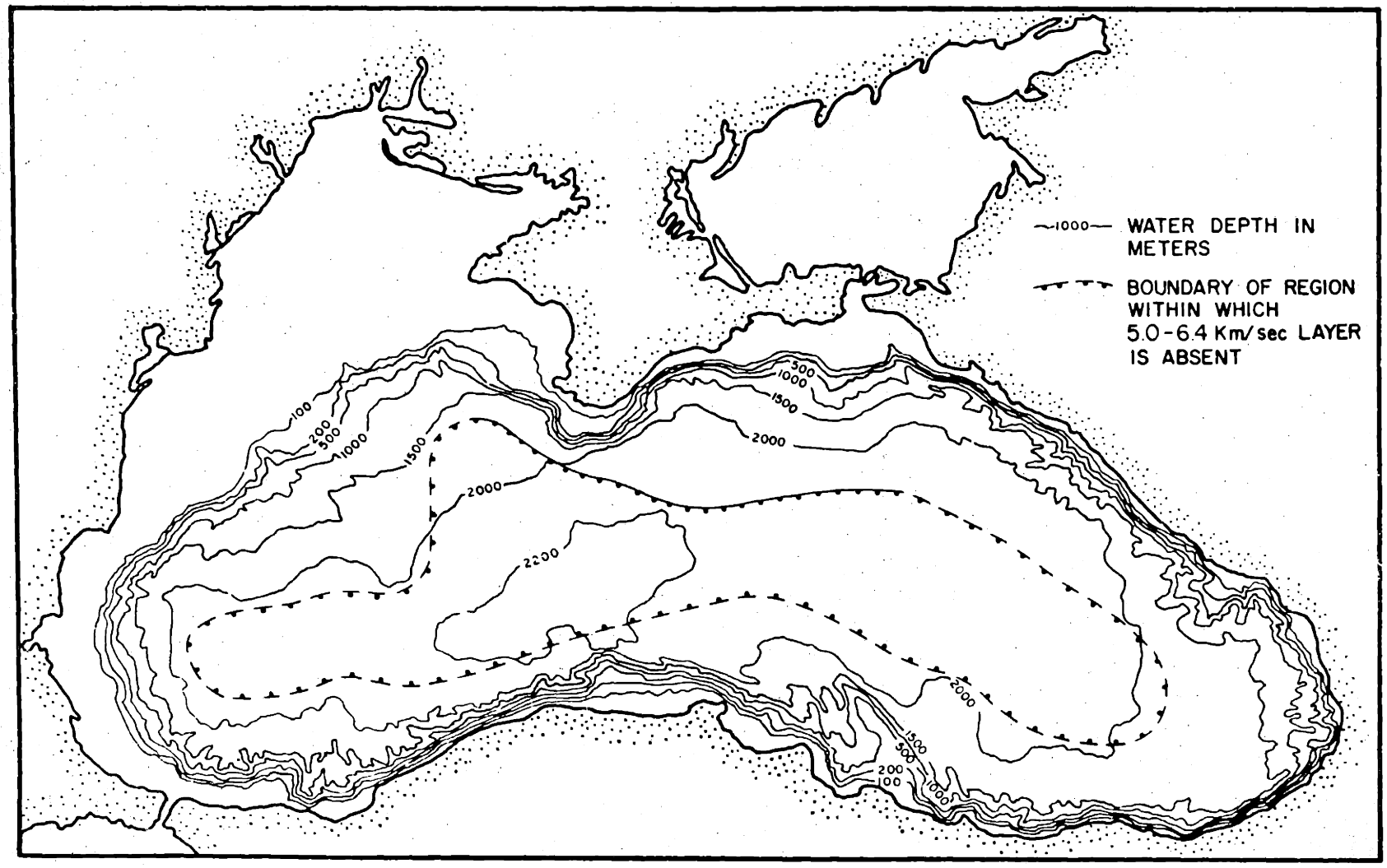

Figure 5. Bathymetric map of the Black Sea.Also shown is region within which the "granitic" layer is absent. From Mindeli et al. (1965)

1.3 REVIEW OF GEOPHYSICAL DATA

A broad understanding of geophysical data from the Mediterranean-Alpine region is necessary in order to provide a framework in which to interpret the new heat flow data presented in this thesis. In the next section data relevant to the general area is presented, followed by sections in which the geophysical characteristics of the western and eastern Mediterranean and Black Seas are reviewed.

1.31 Alpine-Mediterranean Area

1.311 Earthquake Distribution and Mechanisms

The Mediterranean is part of a broad, east-west trending seismic zone that includes the Himalayas. Narrow branches pass southeastward through the Red Sea and westward from Gibraltar to the mid-Atlantic ridge. Although the seismicity of the Mediterranean-Alpine area is higher than that in the more stable areas to the north and south, the average level of activity is only a fraction of that associated with the island arc structures around the Pacific.

Studies of the regional seismicity of Europe and the Mediterranean by Kárník (1967), and more recently by Dorman and Barazangi (unpublished data, 1968), reveal that seismic activity is strongly concentrated on the Balkan peninsula along the eastern coast of the Adriatic Sea,

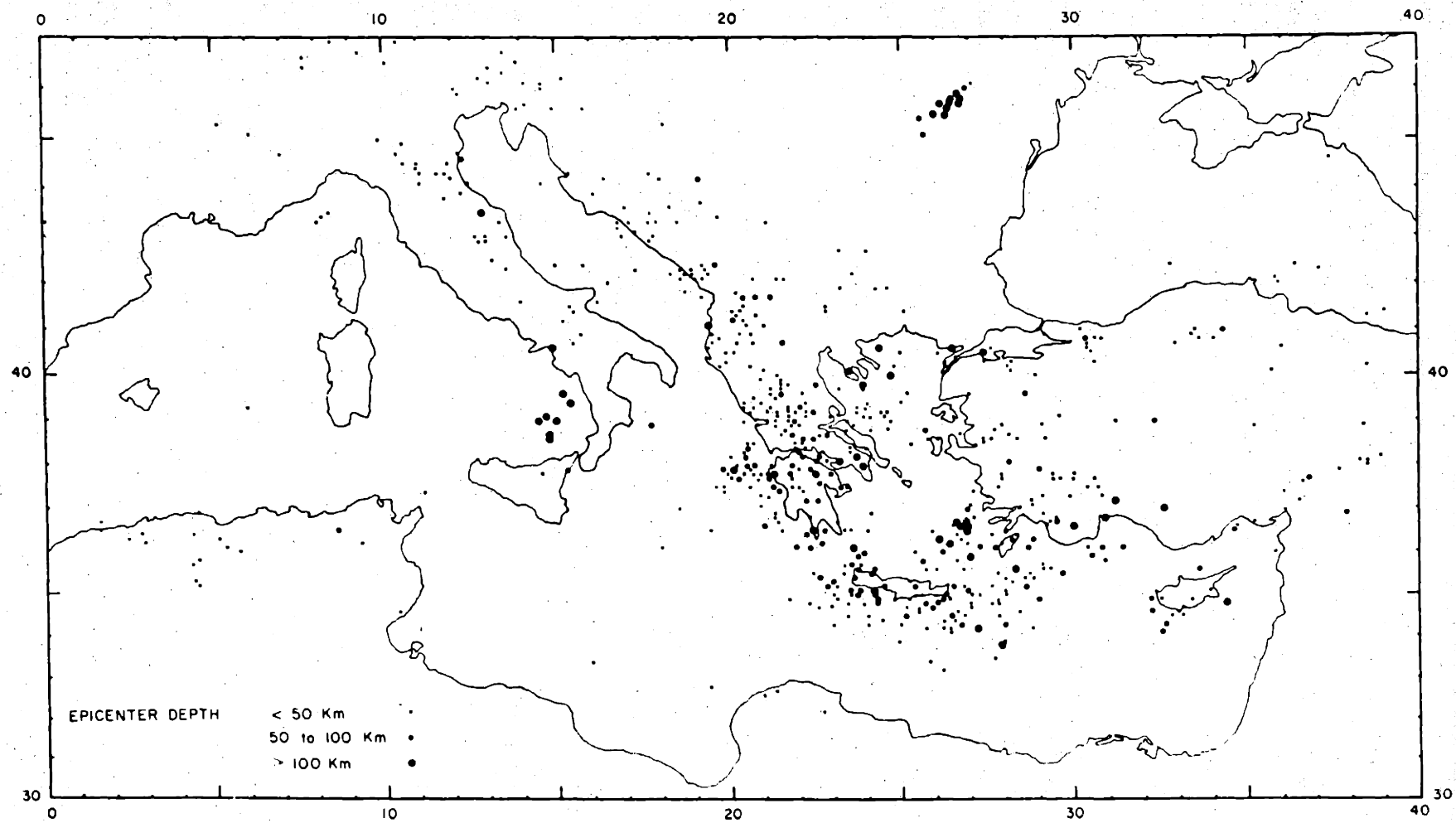

Figure 6. Seismicity of the Mediterranean between 1961 and 1967. Note the localization of intermediate depth earthquakes beneath the Tyrrhenian Sea and in the vicinity of the Cretan arc. From Dorman and Barazangi (personal communication, 1968).

and extends southeast in a broad arc to include southern Greece, the Aegean Sea, western Turkey, and parts of the northern Levant Sea (see Figure 6). Areas of moderate seismicity include the southern Tyrrhenian Sea and the Appenine peninsula, the Caucasus, the Carpathians, and the Mediterranean coast of North Africa. Earthquakes are absent in most of the other regions.

Only two deep focus earthquakes have occurred outside the Pacific seismic belt; one at a depth of 450 km beneath the southern Tyrrhenian Sea and another, 600 km beneath southern Spain. Intermediate depth (50 to 300 km) events occur beneath the Tyrrhenian Sea, the southern Aegean, and the Mediterranean Sea near the Cretan arc. Additional mantle earthquakes are found in the Carpathians and Caucusus mountains, and beneath western Turkey and the Caspian Sea.

Seismic activity is concentrated along the western and southern coasts of Greece, with well defined maxima in the Ionian Sea near the entrance to the Gulf of Corinth and in the area of Crete and Rhodes (Galanopoulos, 1963). Within the southern Aegean Sea, shallow and intermediate depth earthquakes are uniformly distributed north as far as the inner volcanic arc. Delibasis and Galanopoulos (1968) reported that the maximum epicentral depth increases eastwards from about 100 km at 20°E to 200 km at 28°E. No evidence is found for the occurrence of the foci on a plane dipping beneath the Aegean Sea, as might

be expected by analogy with other arcuate island chains. Earthquakes are absent in the Ionian and Levantine basins south of the axis of the Mediterranean ridge. Both shallow and intermediate depth epicenters exist near Cyprus and the Hecataeus mountains.

Ritsema (1969a) reviewed source mechanisms and orientations of the principle stresses for eastern Mediterranean earthquakes. He noted that shallow earthquakes occurring along the Dalmatian coast and in western Greece were of the transcurrent fault type and involved sinistral fault motions along roughly NW-SE striking fault planes. Earthquakes in the vicinity of Greece, the Aegean Sea, and the Cretan arc are characterized by transcurrent faulting on steeply dipping planes due to primarily horizontal tensional stresses. Shirokova (1967) arrived at essentially the same conclusions after studying the mechanisms of shallow focus earthquakes.

Ritsema (1969a) noted that focal mechanisms of earthquakes occurring within the mantle usually show greater uniformity and are of a different type than shallow ones. Only a few solutions for mantle quakes exist for the eastern Mediteranean. These are generally consistent with either thrusting of the mainland of Greece over the Ionian Sea or upward motion of the Ionian Sea relative to the mainland.

Ritsema (1969b) reached similar conclusions regarding the distribution and mechanisms of earthquakes

in and adjacent to the Tyrrhenian Sea. Within the last 50 years, 25 quakes of magnitude 5 or larger have been detected in the southern Tyrrhenian Sea to depths as great as 450 km. Although the intermediate and deep foci are not distributed along a well-defined plane dipping beneath the Calabrian arc, foci near land are mostly between 40 and 100 km deep and increase in depth further seaward to between 210 and 320 km. Ritsema noted that the maximum stress for these earthquakes generally dips about 60° towards the west-northwest, in accord with a tectonic model in which oceanic lithosphere dives in an oblique angle under the continental plate.

Dextral transcurrent movement along east-west fault planes is characteristic of earthquakes which occur eastward from the mid-Atlantic ridge past the Strait of Gibraltar and along the Mediterranean coast of North Africa, as well as along the northern Anatolian fault zone. Western Turkey and the southern Aegean are characterized by northeast-southwest faulting. The change in the direction of movement from east-west to northeast-southwest occurs in the area of maximum seismic activity between Rhodes and Crete.

Earthquakes within the Black Sea are confined to the narrow continental margins and are particularly numerous at depths between 10 and 40 km in a small area southeast of the Crimean peninsula. Zverev and Mironova (1967) observed unusually high attenuation of intermediate

velocity compressional waves in the vicinity of the zone of high seismicity. Levitskaya (1961) noted the tendency for the distribution of epicenters to dip at about 45° beneath Crimea.

Intense local seismicity in the Vrancea region of the Carpathian mountains west of the Black Sea is evident above the moderate seismic activity associated with the remainder of the Carpathian mountain chain. Radu and Purcaru (1964) noted that only 10% of the 450 events which occurred between 1935 and 1962 in the Vrancea region were shallower than 100 km. Shocks occur either at depths greater than 100 km, or shallower than 60 km; the region between is essentially aseismic. First motion studies of earthquakes deeper than 100 km show the maximum compressive stress is horizontal and perpendicular to the general tectonic trend. Ez (1964) analyzed recent tectonic movements in the region and concluded that the earthquakes reflect differential vertical movement along the boundaries of the Carpathian tectonic block which is rising while the adjacent areas are sinking.

A seismic zone associated with the northern Anatolian fault parallels the south coast of the Black Sea. Over 16 m of right lateral horizontal and 4 m of vertical displacement have occurred along this fault over a period of 18 yr (Ketin, 1957). An apparent westward migration of epicenters of 1650 km along the fault zone between 1930 and 1953 was suggested by Kárník (1964).

Other seismic zones exist within and south of the Sea of Marmora, along the eastern coast of the Aegean Sea, and in south-central Turkey (Lahn, 1949). Preliminary fault plane solutions for Anatolian earthquakes by Canitez and Üçer (1967) show that both vertical and horizontal motions occur in response to compressional and tensional forces.

The existence of a belt of earthquakes extending from the eastern end of the Black Sea southeast across the Caucasus into the Caspian Sea and east into south central Asia was noted by Tskhakaya (1961) and Solov'ev (1961). The epicenters of the 400 earthquakes investigated were, almost without exception, located in the upper 10 km of the crust. Of the 5 earthquakes constituting exceptions, 3 had epicenters between 70 and 80 km deep and were situated in the eastern part of the Caucasus; the remaining 2 earthquakes occurred at depths of 100 and 150 km beneath the Caspian Sea. Caucasian earthquake mechanisms generally involve horizontal or subhorizontal compressive stresses oriented perpendicular to the trend of surface features (Shirokova, 1967).

1.312 Upper Mantle Structure

The structure and seismic properties of the upper mantle are known in greater detail beneath the western Mediterranean than beneath the eastern Mediterranean. The

dispersion curve obtained for Love and Rayleigh waves traveling between Algeria and Spain was described by Payo (1965) as "typically oceanic". Payo (1967) repeated this conclusion in a later paper and added the observation that a significantly thicker and lower velocity crust exists beneath the eastern Mediterranean.

The shear velocity structure beneath the western Mediterranean basin was studied by Berry and Knopoff (1967) using phase velocity data obtained with long-period vertical seismometers. An ultra-low shear velocity (4.10 ± 0.05 km/sec) channel exists only 50 km below the central part of the basin and drops to a depth of 100 km around the margins, as shown in Figures 7 and 8. Berry and Knopoff found it necessary to introduce a layer of higher velocity material into their model between the 7.7 km/sec refracting layer found by Fahlquist (1963) at a depth of 12 km, and the top of the low-velocity channel.

Recently Payo (1969), using both phase velocity dispersion and travel time data, successfully modeled the western Mediterranean crustal and upper mantle velocity structure using the same sedimentary layers as were used in Berry and Knopoff's (1967) model, which were, in turn, based on Fahlquist's (1963) seismic refraction data. Payo determined a similar upper mantle structure which included slightly higher shear velocity in the low velocity channel (4.20 rather than 4.10 km/sec) and an 8 km rather than a 4 km thick basaltic layer as proposed by Berry and

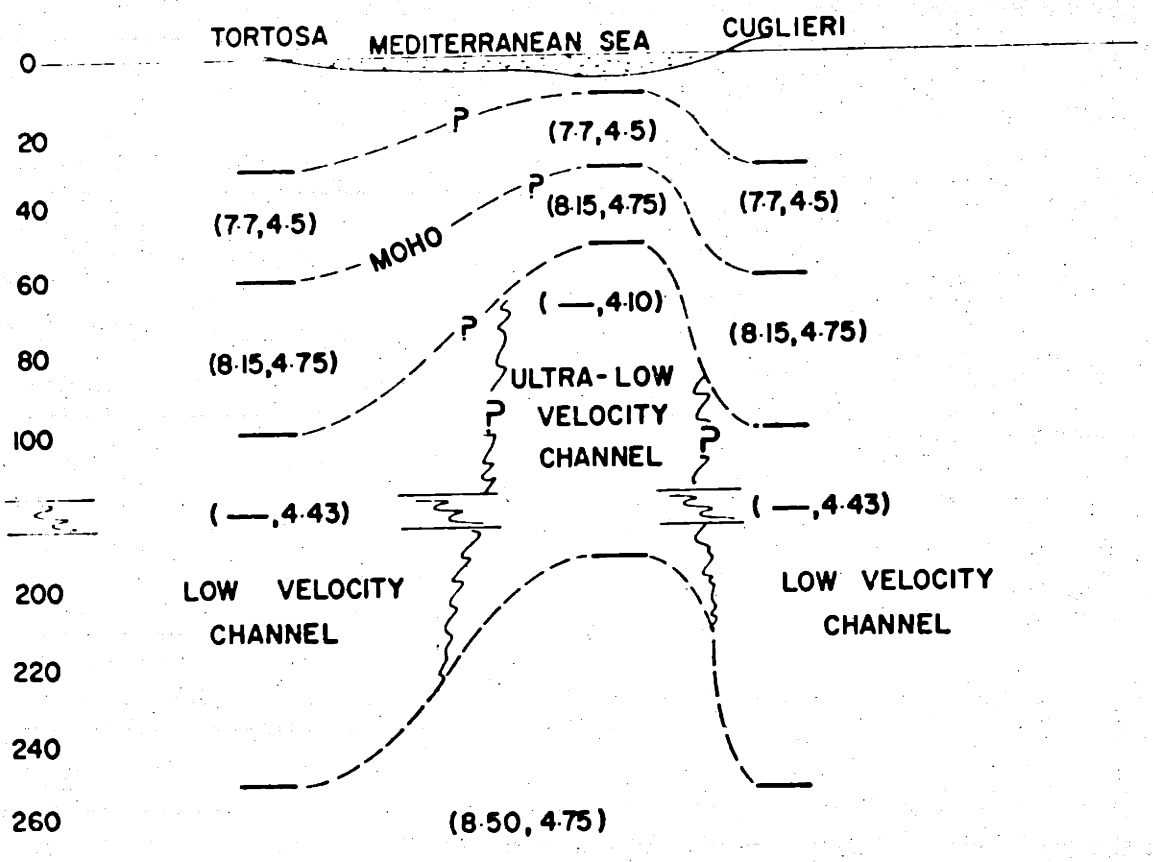

Figure 7. Upper mantle structure beneath the western Mediterranean along an east-west traverse. Numbers in parentheses are the compressional and shear velocities, respectively. Note the depth discontinuity at a depth of 100 km. From Berry and Knopoff (1967).

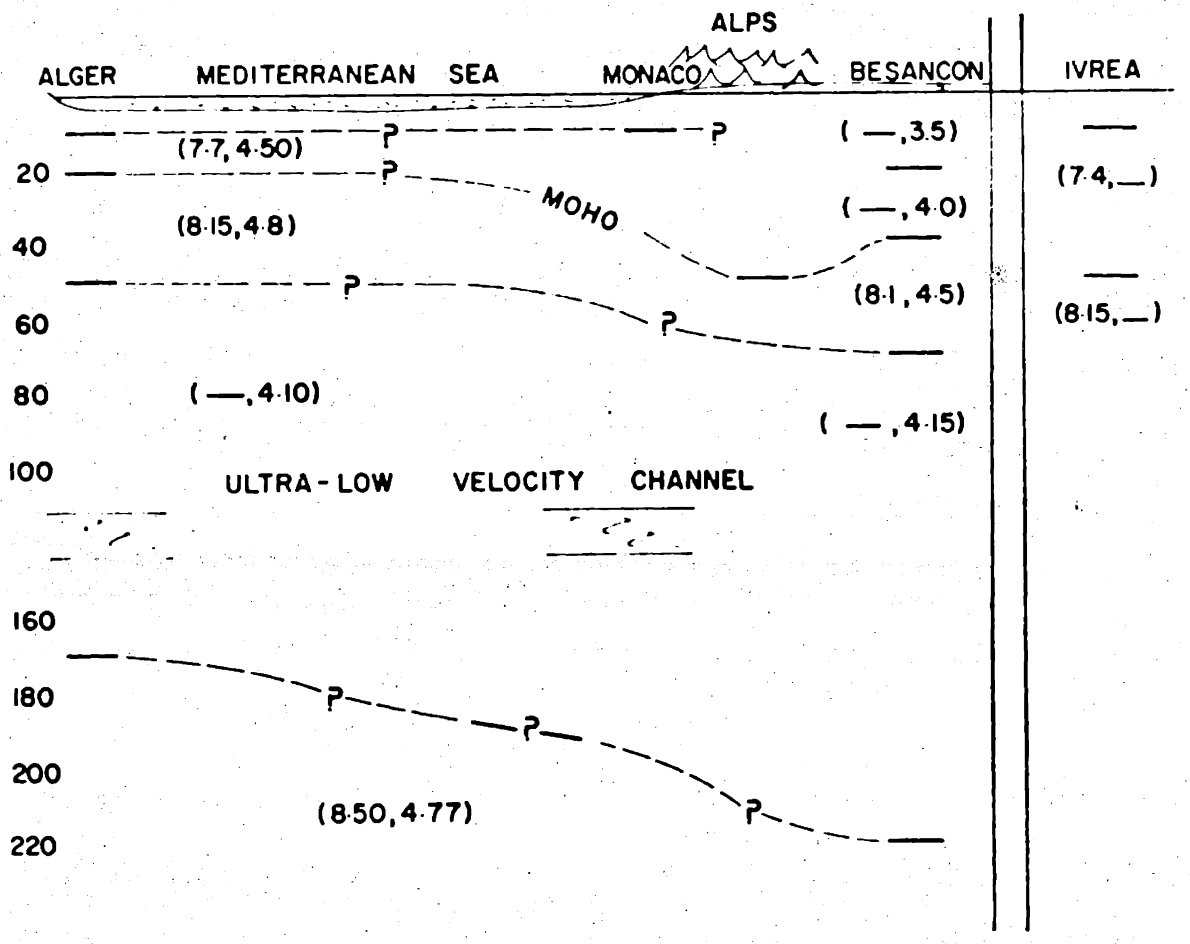

Figure 8. Upper mantle structure beneath the western Mediterranean Sea along a north-south traverse from the Alps to Africa. Numbers in parentheses are the compressional and shear velocities, respectively. Note the depth discontinuity at a depth of 100 km. From Berry and Knopoff (1967).

Knopoff (1967).

Both surface wave dispersion and body wave travel time data have been interpreted as indicating the existence of an important low velocity zone in the upper mantle beneath the eastern Mediterranean Sea at a depth of 100 to 150 km (Payo, 1967, 1969). Papazachos (1969), using phase velocity data from Rayleigh waves propagating between Athens and Helwan, determined a crustal thickness of 19 km with an "extra-thick" sedimentary layer and a low shear velocity (4.3 km/sec) layer between the depths of about 59 and 219 km. The phase velocity of Rayleigh waves traveling south from Athens to Helwan is greater than for waves traveling from Helwan to Athens, and Papazachos (1969) suggested that a sloping Mohorovicic discontinuity (down to the north) is probably responsible.

Molnar and Oliver (1969) studied lateral variations in the attenuation of short-period shear (S_n) waves traveling along different paths through the uppermost mantle above the low velocity zone. On a worldwide scale, they found that S_n waves propagate very efficiently across the stable regions of the earth, the continental shields, and deep-ocean basins, but that propagation is very inefficient for paths which cross the crests of the mid-ocean ridge system or the concave sides of most island arcs. They interpret these observations in terms of plate theory, as indicating that "the part of the strong outer shell, or lithosphere, in the mantle is discontinuous

with gaps in it at the ridges and island arcs."

S_n waves propagate efficiently along paths which cross the Baltic shield and western Europe. High attenuation of shear waves was observed when paths included Cenozoic orogenic areas. Transmission of S_n waves is inefficient for paths across the western Mediterranean Sea; the eastward extent of the low Q zone is not well defined, but may terminate beneath the Ionian Sea. East of Crete S_n waves propagate through the upper mantle beneath the eastern Mediterranean, however, no transmission occurs for paths north of the Cretan arc which include either western Turkey or the Aegean Sea.

1.313 Published Heat Flow Data

The estimation of the average heat flux through the crust of the earth is made difficult by the global distribution of heat flow values. Reliable data is available from slightly more than 25% of the earth's surface; data is lacking from large parts of Africa, South America and Antarctica, and from high latitudes in all of the major oceans. In addition, a disproportionate number of marine heat flow measurements are located in the axial regions of the mid-oceanic ridges. The arithmetic mean of all heat flow data (1.65 HFU)* and the mean of the heat flow values averaged over 5° by 5° regions (1.52 HFU) calculated by Horai and Simmons (1969) are probably higher than the

* 1.0 heat flow unit (HFU) is equal to 10^{-6} cal/cm^{2}sec.

global average. Langseth (1969) estimated the average heat flow by extrapolating existing data into areas where no measurements were available, based on the observed correlation between geologic province and heat flux. He calculated a global mean flux of 1.35 HFU, and suggested that this value should be increased to 1.4 HFU to account for heat lost through volcanic activity at the mid-ocean ridges. The value of 1.4 HFU appears to be the best estimate of the average heat lost through the crust and will be used to represent "normal" or "average" heat flow throughout this manuscript.

Heat flow has already been determined by other investigators in the Mediterranean Sea. The measurement by Bullard and Day (1961) on the Alboran abyssal plain was one of the early measurements made at sea. The results of this and later measurements are listed in Table 1. Heat flow values at stations CH21-18 and CH43-27 have unacceptably large uncertainties and will not be considered further. Three of the remaining reliable measurements are located in the western Mediterranean, the fourth measurement is in the Ionian Sea. The measurements, located in widely separated and dissimilar physiographic regions, range from 0.64 HFU in the Ionian Sea to 2.50 HFU near the base of the Rhone fan.

The average of 11 marine heat flow measurements from the southern Adriatic Sea is 1.32 ± 0.34 HFU (Lavenia, 1967). Values range from 0.87 to 1.24 HFU in the southern

PUBLISHED MEDITERRANEAN HEAT FLOW DATA

STATION NUMBER	POSITION Lat.	Long.	DEPTH (m)	SEAFLOOR DESCRIPTION	GRADIENT (°C/m)	THERM. COND.*	HEAT FLOW (HFU) **	REF.
B+D-8	35°58'N	04°34'W	1251	Alboran Abyssal Plain	0.057	2.13	1.25	1
CH21-18	39°31'N	05°26'E	2830	Balearic Abyssal Plain	--	--	(>0.87)	2
CH21-19	42°14'N	07°09'E	2728	Base of Rhone Fan	--	--	2.50	2
ZEP-32	40°37'N	05°50'E	2720	Base of Rhone Fan	0.056	2.20	1.2	3
CH43-25	35°47'N	17°29'E	4036	Messina Abyssal Plain in Ionian Sea	0.032	(2.00)	0.64	4
CH43-27	38°47'N	15°04'E	2013	Northwestern flank of Stromboli	0.021-0.091	(2.00)	(0.42-1.83)	4

* Thermal conductivity in mcal/cm sec °C, values in parentheses estimated

** Heat flow in parentheses not used in data analysis

References:

1. Bullard and Day (1961)
2. Lister (1963)
3. Nason and Lee (1964)
4. Birch and Halunen (1966)

Table 1

Adriatic basin. Higher values (1.98 to 2.48 HFU) were measured on the walls of the basin; these values may be an indication of slumping, thermal refraction, or of an instability in bottom water temperature. Although the reliable determination of the heat flux through the southern Adriatic is of great geophysical interest, it appears unwise to incorporate Lavenia's data without careful evaluation of the extent to which it is representative of the equilibrium regional heat flow.

Seven heat flow values have been reported from the Black Sea. Sysoyev (1963) measured the thermal gradient in the floor of the Black Sea using 2 reversing mercury thermometers 2 m apart attached to the outside of a coring device. Sysoyev estimated the thermal conductivity of the Black Sea sediments to be 4.0 KU* and calculated an average heat flux of 1.92 HFU. Lubimova (1966) used a more realistic value of 1.9 KU for the thermal conductivity and recomputed the heat flux. Again using Sysoyev's thermal gradient data, she obtained an average flux of 0.87 HFU (Table 2). The average of 383 thermal conductivity measurements made on Black Sea sediments by the author is 2.18 KU; using this value an average heat flux of 1.05 HFU is obtained.

Lebedev et al. (1967) attempted to correct these heat flow measurements for the effects of both rapid sedimenta-

* 1.0 conductivity unit (KU) is equal to 1 mcal/cm sec ^{o}C.

PUBLISHED BLACK SEA HEAT FLOW DATA

STATION	DEPTH (m)	POSITION N.LAT.	POSITION E.LONG.	THERMAL GRADIENT (°C/m x 10^{-2})	THERMAL CONDUCTIVITY (mcal/cm sec °C)	HEAT FLOW (HFU)
4742	2179	43°38'	36°28'	3.0	1.9 (Assumed)	0.57
4745	1714	41°53'	40°28'	4.5	"	0.86
4750	2170	42°48'	37°38'	6.5	"	1.24
4751	2216	43°18'	34°02'	5.5	"	1.04
4752	2197	42°33'	34°02'	4.5	"	0.86
4753	1840	43°28'	31°23'	5.0	"	0.95
4754	1300	41°38'	29°38'	4.5	"	0.86

From LUBIMOVA (1966)

Table 2

tion and refraction of heat due to the contrast in thermal conductivity between the crystalline rocks at the margins and the thick sediments in the Black Sea depression. These two factors, according to Lebedev et al., reduce the deep-seated heat flux by 25%. Correcting for these effects, they estimated the average heat flux through the Black Sea basin as 1.2 to 1.6 HFU.

Non-linear temperature-depth profiles were observed by the author in the upper few meters beneath the Black Sea floor. These 7 measurements may not be representative of the regional heat flow due to the rather short interval over which Sysoyev (1963) measured the gradient and the irability of temperature determinations at only two points to detect a variable thermal gradient. For this reason, they are not included in the following analysis.

No heat flow data is available for Africa north of the equator, from the countries adjacent to the eastern Mediterranean, or from any area in southern Europe (except the hydrothermal areas in Italy) within 200 km of the Mediterranean. Clark (1961) and Clark and Niblett (1956) obtained four values ranging from 1.9 to 2.2 HFU, and a fifth value of 1.4 HFU, in railroad tunnels through the Swiss and Austrian Alps. Initially they attributed the above average heat flow to heat generated in thickened granitic roots beneath the Alps. Recently Clark and Jäger (1969) estimated the rates of erosion above three of the tunnels from apparent ages of

rocks metamorphosed during the Alpine orogeny and from the depth of burial compatible with the observed mineralogy. They concluded that 30 to 50% of the observed heat flow is a consequence of denudation, and that the heat flow through the Alps is generally less than 1.5 HFU.

Extensive geothermal investigations in Austria and Hungary (Boldizsár, 1968, 1967a, 1967b, 1964) and in Czechoslovakia (Čermák, 1967, 1968a, 1968b) have resulted in the delineation of an area of high heat flow over the entire Hungarian basin (see Figure 9). Seven heat flow values in the basin range from 1.50 to 3.31 HFU and average 2.4 HFU. The highest heat flow is observed where the Tertiary sediment cover is thinnest. Refraction of heat due to the thermal conductivity contrast between the Mesozoic and Paleozoic basement and the poorly conducting Tertiary sediments is responsible for the observed local variations in heat flux. Three heat flow values near the inner edge of the Carpathian mountains adjacent to the northeastern edge of the Hungarian Basin range from 2.45 to 2.60 HFU and confirm the regional extent of the high heat flow anomaly associated with the Hungarian basin. The Vienna basin, shown as VB in Figure 9, is located between the eastern Alps and the western Carpathians and separates the Hungarian basin to the south from the Bohemian massif to the north. Heat flow in the Vienna basin increases southward towards the Hungarian basin. Čermák (1968a) measured

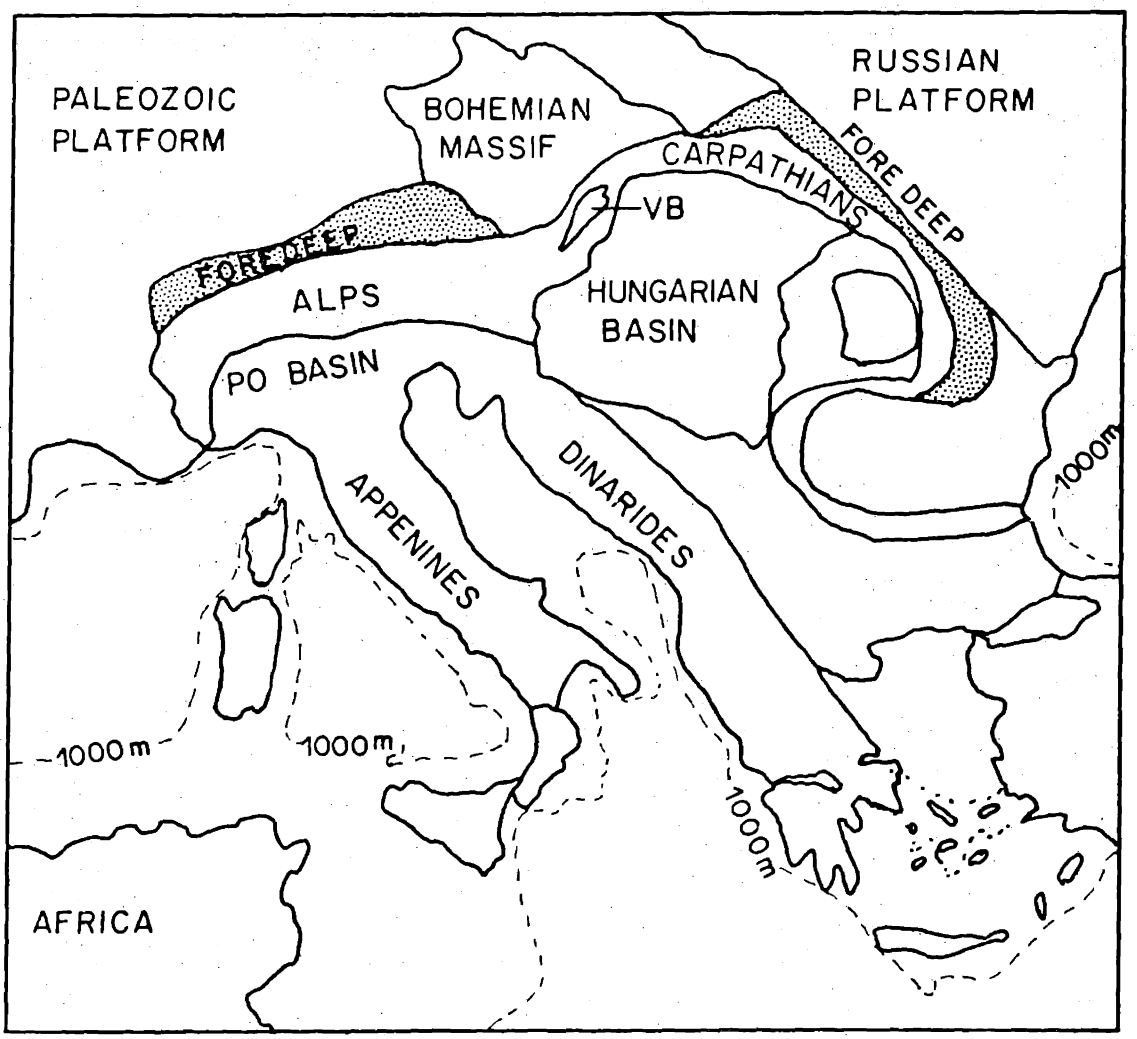

Figure 9. Schematic index map showing the major tectonic features in southeastern Europe. Location of the Vienna basin is designated by the letters 'VB'.

heat flow of 1.32 HFU in the central basin, and values of 1.57 and 2.22 HFU at locations in the southern Vienna basin. Boldiszár (1968) also observed increasing thermal gradients southward across the Vienna basin. He assumed a thermal conductivity of 4 KU for the Tertiary sediments in the basin and estimated an average heat flow of 1.2 HFU. The discrepancy between Čermák's and Boldiszár's results may be due to Boldizsár's assumed value for the thermal conductive being too low.

The Vienna basin is underlain by basement equivalent to the flysch in the Carpathian foredeep. Boldizsár proposed that average or slightly below average heat flow exists in the flysch zone of the Alps and Carpathians and extends eastward from Switzerland to the Ukraine. Four (preliminary) heat flow values in the Czechoslovakian part of the Carpathian foredeep range from 1.3 to 1.5 HFU (Čermák, 1968b). Two additional values further east in the foredeep are reported by Boldizsár (1968) as being in the range 0.75 to 0.84 HFU and 1.1 to 1.3 HFU, respectively.

The average of 40 heat flow values in the Bohemian massif is 1.61±0.26 HFU (Čermák, 1968a). The average heat flow (1.41±0.21 HFU, n = 6) is slightly lower in the Paleozoic blocks which form the basement of the massif than the mean (1.49±0.05 HFU, n = 9) in the late Paleozoic coal basins. The average of 14 heat flow measurements in the area of the massif overlain by thick Cretaceous sedi-

ments is 1.71±0.30 HFU. Čermák remarked that the correlation of heat flow with the geology of individual tectonic units is very good, and that geologically older units are usually characterized by lower heat flow than younger formations.

The region extending east from the Carpathians to the Caspian Sea is geologically, structurally, and thermally complicated. Within the zone of Alpine folding, heat flow is high in the Greater Caucasus and low in the adjacent foredeeps. Heat flow values increase regularly from the axes of Cenozoic foredeeps towards the limbs; the increase is gradual in the direction of the stable Paleozoic platform. However a sudden increase of between 1 and 2 HFU occurs in the zone where the foredeep adjoins the Greater Caucasus (Makarenko, Smirnov, and Sergivenko, 1968).

The Stavropol uplift, located on the Hercynian platform northeast of the Greater Caucasus, is the site of a well-defined heat flow maximum of 2.05 HFU (average of 32 measurements), possibly associated with Tertiary magmatic activity (Makarenko, Polak, and Smirnov, 1968).

Because of the production of oil and gas in the area, the region of the Apsheron peninsula west of the Caspian Sea has been the subject of extensive geothermal investigations. Within this region both positive and negative thermal anomalies are created by the conversion of kinetic energy into thermal energy, changes in temperature

associated with expansion or compression of gas through tectonic or artificial processes, and exothermic or endothermic chemical reactions. Mass transport of heat associated with the removal or replacement of oil by diffusion through porous rock can also create local thermal anomalies. High heat flow anomalies are observed over mud volcanoes both on land and beneath the Caspian Sea.

Lebedev et al. (1967) distinguished geothermal zones coinciding with the main tectonic elements of the Crimean peninsula. Furthest to the north, on the southern margin of the Russian platform, heat flow values range from 0.62 to 0.79 HFU (Lubimova, 1964), similar to values obtained on other Pre-Cambrian shields. The Paleozoic Hercynian platform south of the Russian platform is characterized by highly variable heat flow values ranging from 0.8 to 2.5 HFU, with an average flux of about 1.3 HFU (Lebedev et al., 1967). They attributed the variability to the effects of topography, structures in the sedimentary complex, and regional differences in the history of sedimentation. Heat flow values between 1.1 and 1.2 HFU are found in the Crimean mountains north of the Black Sea coast. Two regions of slightly high heat flow exist in the vicinity of the Kerch peninsula between the Black and Azov Seas, and are considered to result from the movement of fluids in a highly permeable fault zone in the one case, and associated with oil and gas deposits, in the second (Lebedev et al., 1967).

The average of 18 closely-spaced heat flow measurements in southwestern Iran is 0.87 HFU (Coster, 1947). Coster corrected the heat flow measurements for the effect of a post-glacial temperature increase of 5°C and obtained a value of 1.18 HFU for the equilibrium heat flux.

1.314 Volcanic and Fumarole Activity

Heat flow data in the Mediterranean region can be supplemented by the cautious consideration of recent or continuing volcanic and fumarole activity. Areas of hydrothermal activity not directly associated with volcanism are not necessarily evidence of hyperthermal activity (discussed by Mazor, 1968).

Extensive volcanic activity is present on the Ethiopian Danakil peninsula and within the Gregory and Albertine rift valleys of central and east Africa respectively--all rather far removed from the area of investigation. Egypt was the site of Upper Cretaceous and Oligocene volcanism, and minor fumarole activity is still found near Cairo (El-Hinnawi, 1965). The existence of hot springs in Tunisia is noted by Scheffer (1964), but, as mentioned above, the implications are unclear. The proximity of Tunisia to the Italian volcanic provinces suggests that the hot springs may be fumaroles.

Intense volcanic activity is in progress on the

Arabian peninsula. Nineteen active volcanoes and fumaroles exist adjacent to, and within, the Red and Arabian Seas (Neuman van Padang, 1963; and Richard and Neuman van Padang, 1957). Nearer the Mediterranean, intensive Quaternary volcanism has occurred at four major centers in Iran, but only three nearly extinct volcanoes and a few hot springs remain (Gansser, 1966). Poorly documented evidence of volcanic activity exists for the Dead Sea rift valley, and Neuman van Padang (1963) concluded that no activity remains at this time.

Over 200 hot mineral springs are located along the Jordan and Suez rift valleys (Mazor, 1968). The abnormally high surface water temperatures are caused by heating of the water due to deep circulation, rather than by unusually high thermal gradients (Rosenthal and Eckstein, 1968). They stress that reliable temperature-depth data exist only for the southwestern part of the Dead Sea region.

Turkey is characterized by enormous amounts of Tertiary volcanic products (Blumenthal and van der Kaaden, 1964). Volcanic activity practically ceased during the Pleistocene and only three volcanoes are now active. Two active volcanoes and four major areas of fumarole activity in southern Greece and in the southern Aegean Sea are distributed in an arcuate zone parallel to and about 150 km behind the Cretan arc. Their locations are shown in Figure 10. Volcanic products in

Figure 10. Locations of active volcanoes and fumarole fields in the southern Aegean Sea. Note that the volcanoes are arranged in an arc inside and concentric with the Cretan arc.

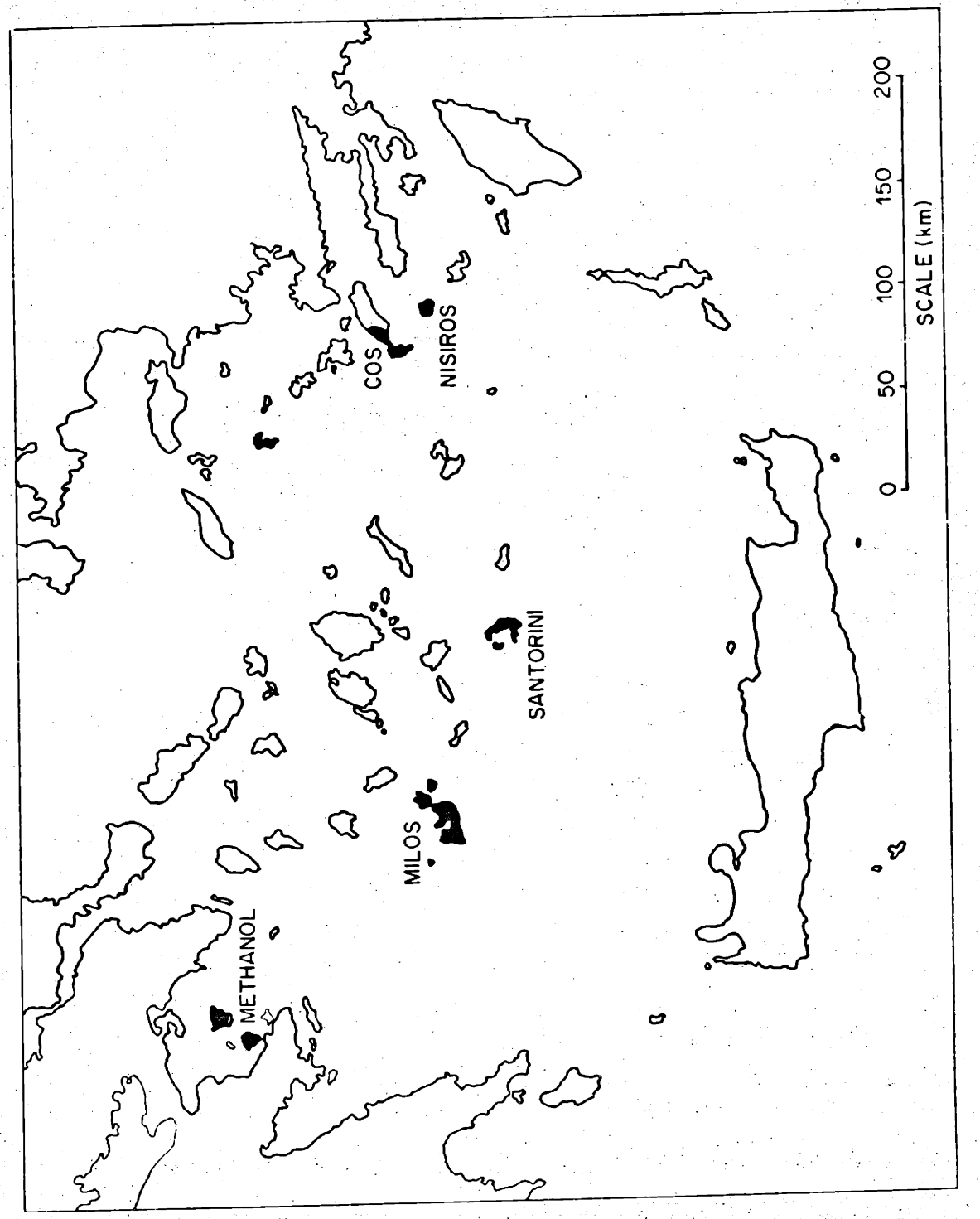
METHANOL
MILOS
SANTORINI
COS
NISIROS
0
50
100
150
200
SCALE (km)

these areas are andesitic or dacitic.

Two areas of unusual hydrothermal activity near the Tyrrhenian coast in central Italy are almost certainly the result of Quaternary volcanic activity. Boldizsár (1963) estimated the heat flow as 6 to 14 HFU at Larderello, and Cataldi (1967) measured thermal gradients as high as 300°C/km in the geothermal area near Monte Amiata (see Figure 11). The reliability of the thermal measurements in both areas is suspect because the gradient was determined at shallow depth in an area where extensive circulation of water through the surface rocks may have decreased the thermal gradient, and thus the heat flow values obtained by Boldiszár and Cataldi are minimum values.

The locations of active volcanoes in and around the Tyrrhenian Sea are shown in Figure 11. Volcanism began in southern Italy during the Paleozoic and increased in intensity until the present time. Extensive volcanic activity began along the Italy Tyrrhenian coast during the Eocene and increased in area to include the islands of Sardinia and Sicily, as well as to form the Aeolian islands north of Sicily and the Pontine islands west of Naples.

The majority of the eruptive centers, including those active during the Quaternary, are extinct; only 6 volcanoes and one major volcanic center are active (Imbo, 1965). Three of the 6 are near Naples; they include Vesuvius and the Phlegraen fields on the Italian mainland,

Figure 11. Locations of Tertiary volcanic products and hydrothermal areas in and around the Tyrhennian Sea. The names and positions of volcanoes which are presently active are shown. Note that present volcanic activity is distributed in an arcuate pattern generally concentric with the Calabrian arc.

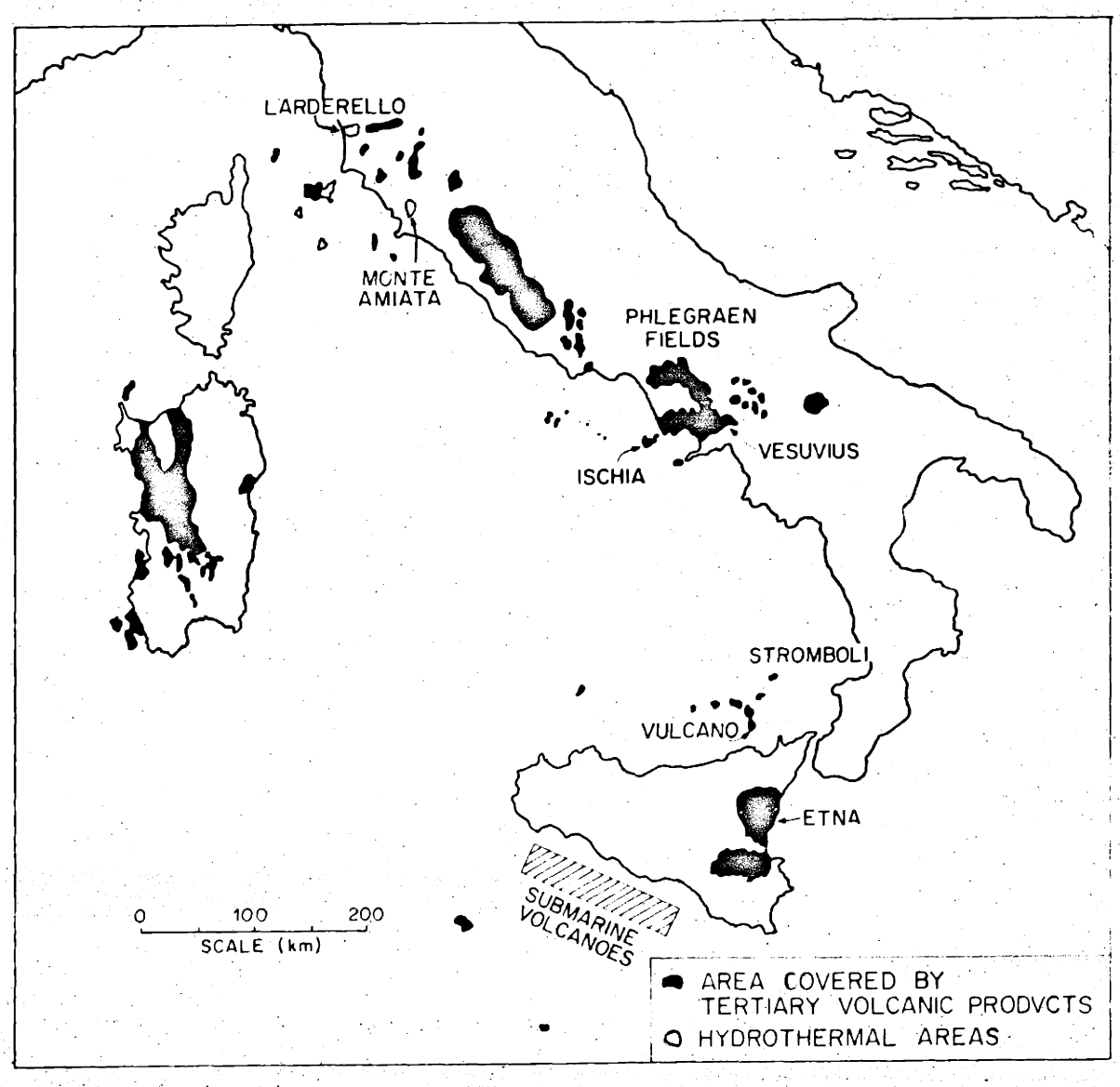
LARDERELLO
MONTE AMIATA
PHLEGRAEN FIELDS
VESUVIUS
ISCHIA
STROMBOLI
VULCANO
ETNA
SUBMARINE VOLCANOES
0 100 200
SCALE (km)
AREA COVERED BY TERTIARY VOLCANIC PRODVCTS
HYDROTHERMAL AREAS

and the island of Ischia in the Tyrrhenian Sea. The active volcanoes Stromboli and Vulcano are located in the Aeolian islands and Etna is in Sicily. Several scattered eruptive centers are distributed in a band up to 20 km wide about 50 km southwest of Sicily. Magnetic and bathymetric data substantiating their existence was presented by Zarudzki (unpublished manuscript, 1968).

Gasparini and Adams (1969) determined K-Ar ages of rocks from several volcanoes in southern Italy. Volcanism commenced almost simultaneously at a number of locations along a line parallel to and seaward of the present Tyrrhenian Sea coast. All of the volcanic activity occurred during the last 7 m.y., with younger volcanoes migrating further and further inland.

In addition to their high potassium content, "Mediterranean" volcanic rocks characteristic of central and southern Italy contain greater concentrations of uranium and thorium than volcanic products from any other area (Imbo, et al., 1968). Locardi (1968) determined the radioactivity of what he believes is the "parent" magma characteristic of central Italy. Uranium and thorium occur in quantities of 25 and 110 ppm, respectively, with 7.1% potassium.

The origin of these highly potassic and radiogenic volcanics is uncertain. Hurley et al. (1966) argued, based on ratios of $^{87}Sr/^{86}Sr$ and Sr-abundance, that the potassium-rich lavas are the result of the assimilation

of ancient continental sialic rocks within the upper mantle.

1.315 Paleomagnetic Data

Measuring the direction of remanent magnetization in rocks and accepting the assumptions that 1.,the earth's average magnetic field has closely approximated that due to a geocentric dipole oriented parallel to the present axis of rotation throughout geologic time, and 2., that rocks can retain the characteristics of the ambient magnetic field for geologically long periods, permits one to reconstruct the latitude and orientation of the continents at various times in the past. Cox and Doell (1960) discussed the reliability of the dipole assumption, and the mechanisms and characteristics of acquired remanent magnetization in rocks. Eurasia west of the Urals, and Africa, with the exception of zones affected by Alpine tectonics, appear to have behaved as structural units at least since the Hercynian orogeny, and possibly since the Early Paleozoic (Briden, 1968; Creer, 1968; and Nairn, 1960). A comparison of the polar wandering curves of Africa and Eurasia suggests that both continents have undergone large displacements relative to one another and to the magnetic poles.

The paleomagnetic data thus far available is unable to supply the details of this movement. Recently Girdler

(1968) and McElhinny et al. (1968) summarized the evidence for movement of Africa relative to the magnetic poles. Northward movement of over 60° during the Paleozoic was followed by little or no movement from the Early Mesozoic to the Middle or Early Cretaceous. Since this time Africa moved northward 20° and rotated counterclockwise until 10 m.y. ago, when a small clockwise rotation may have occurred (Girdler, 1968). McElhinny et al. (1968) suggested that Africa was displaced northward 20° between 70 and 100 m.y. ago, and underwent largely rotational and/or longitudinal movement during the Tertiary. In summary, Africa appears to have moved northward in two major epochs of drift. The first epoch occurred during the Paleozoic and was followed by an interval of 150 to 200 m.y. during most of the Mesozoic in which little or no latitudinal movement occurred. Beginning in the Late Mesozoic, 20° of additional latitudinal and an unknown amount of longitudinal movement took place, probably largely confined to the first half of the Tertiary (Nairn, 1964; Raja et al., 1966; and McElhinny and Wellman, 1969).

Within the Alpine zone between Africa and Europe, paleomagnetic data has been used to delineate large crustal blocks which appear to have had a similar history of tectonic movement. In addition, the nature of the movement has been studied by comparing the direction

of remanent magnetization within the crustal block under consideration with the direction found in adjacent "stable" structural units.

The Iberian peninsula has rotated 30 to 40° counter-clockwise about a vertical axis in the northern Pyrenees since the Permian (Girdler, 1968; Van der Voo, 1967, 1969; Van Dongen, 1967). Analysis of the bathymetry and the shape of linear magnetic anomalies observed in the Bay of Biscay by Matthews and Williams (1968) is consistent with this conclusion. Jones and Funnell (1968) and Jones and Ewing (1969) presented arguments that the Bay of Biscay contains a Cretaceous age seismic reflector, identified from seismic profiling and coring. If this is so, opening of the bay must have been completed prior to the Cretaceous.

This finding conflicts with data presented by Watkins and Richardson (1968), who are of the opinion that at least half of this rotation has occurred since the Eocene. They observed a systematic difference between the declination of the directions of remanent magnetization in Eocene basalts near Lisbon and magnetic declinations in rocks from stable Europe. Van der Voo (1968) criticised their conclusion on the basis of their failure to apply a correction to the observed declinations for tectonic deformation of the basalt flow subsequent to its having acquired its remanent magnetization. After correcting for dip, Van der Voo found no significant

discrepancy between the results from the Iberian peninsula and stable Europe, and repeated his conclusion that the rotation had indeed been completed before the Eocene.

Ashworth and Nairn (1965) and Nairn and Westphal (1967) studied the paleomagnetism of rocks from Corsica and suggested that the most probable interpretation of the data is that Corsica has rotated $53^{\circ} \pm 14^{\circ}$ counter-clockwise since the Permian, although a later paper by Westphal (1967) quoted by Van der Voo and Zijderveld (1969) called for only 20° of rotation. Unpublished results for Sardinia show a 40° counterclockwise rotation (Zijderveld, in preparation, 1969).

Counter-clockwise movement of Alpine crustal blocks has been suggested by Van Hilten (1962), De Boer (1965), and Van Hilten and Zijderveld (1966) for northern Italy, in the Carpathian mountains by Kotasek and Krs (1965), and by Van Dongen et al. (1967), Gregor and Zijderveld (1964), Van der Voo (1968), and Helsley and Nur (unpublished manuscript, 1969) for Alpine regions in Syria, Israel, and Turkey. Helsley and Nur and Van der Voo noted similarities in the Upper Mesozoic virtual pole positions of Lebanon, Syria, Israel and Africa, and suggested that Africa and the Alpine folded zone south of the stable Eurasian continental block may have behaved as a structural unit at least since the Lower Cretaceous.

In addition to rotation of the Alpine crustal units, large-scale, generally westward translations of Europe

south of the Alps relative to the stable European platform have been postulated. Schwarz (1963) and De Boer (1965) using data from the Spanish Pyrenees and northern Italy, proposed that the Alpine region has undergone up to 4800 km of northwestward movement relative to Europe. Van Hilten and Zijderveld (1966) speculate that the southern Alps were connected to northern Africa, and that both behaved as a structural unit until the Tertiary when the Alpine crustal blocks were "smeared off" against Europe just as Africa terminated its northwestward movement relative to Eurasia. Visscher (1967) pointed out that the similar spore-pollen assemblages found in Upper Permian evaporite sequences within Europe and the Alps are not consistent with displacements on the order of thousands of kilometers since that time. A recent re-examination of the paleomagnetic inclinations found in the Alpine zone and within stable Europe removed the necessity to postulate movements of this magnitude (Zijderveld et al., in press, 1970).

Another type of paleomagnetic evidence, based on the analysis of magnetic anomalies associated with reversals of the earth's magnetic field as recorded in actively spreading ocean ridges, was used by Le Pichon (1968) to estimate the amount and rate of relative movement between the African and Eurasian crustal blocks. Le Pichon estimated that the Alpine-Himalayan region is undergoing compression in response to closure between

Africa and Eurasia at a rate increasing eastward from 1.9 cm/yr at Gibraltar to 5.6 cm/yr at the longitude of Tibet. Between 200 and 500 km of crustal shortening appear to have taken place in this region since the Late Miocene.

1.32 Western Mediterranean Sea

1.321 Gravity Data

De Bruyn (1955) published maps showing Bouguer and isostatic gravity anomalies over Europe and the Mediterranean Sea. Coverage in the Mediterranean is based upon pendulum gravity measurements made in submarines; those made by French and Italian observers may be 5 to 15 mgal too high. De Bruyn's Bouguer gravity anomaly map was calculated assuming a Bouguer density of 2.67 gr/cm^3.

The principle features of the Bouguer anomaly field in the western Mediterranean are the positive (up to 225 mgal) values over the deep water areas of the Balearic basin west of the southern tip of Sardinia, in the southern half of the Tyrrhenian Sea, and east of the Sicilian platform in the Ionian Sea. Lower, but still strongly positive anomalies extend westward from the southern Balearic abyssal plain almost to the Alboran basin. Further north, a region of low positive anomalies associated with the Balearic island platform protrudes northeast into the strongly positive anomalies character-

istic of the deep water region.

A region of low, positive anomalies coincident with Sardinia and Corsica separates larger positive anomalies over the Balearic basin and the southern Tyrrhenian Sea. A large negative Bouguer anomaly (-110 mgal) is present south of the Tyrrhenian Sea over central Sicily (Harrison, 1955). A large positive anomaly over the southeastern tip of Sicily connects with positive anomalies in the Ionian Sea.

Isostatic gravity anomalies are generally positive in the western Mediterranean and along the western coast of Italy. The southern Tyrrhenian is characterized by a broad positive isostatic anomaly greater than 50 mgals. Similar anomalies exist in smaller areas in the northern Tyrrhenian Sea and in the central and western Balearic basin.

1.322 Magnetic Data

Vogt and Higgs (1969; 1968a; and 1968b) presented the results of an aeromagnetic survey conducted by the U.S. Naval Oceanographic Office in 1957. North-south track lines, spaced 16 km apart, were flown at an altitude of 305 m over large portions of the eastern and western Mediterranean Seas.

The Balearic basin is characterized by long wavelength (50 to 100 km), low amplitude (100 gamma),

generally amoeboid-shaped magnetic anomalies (Vogt and Higgs, 1968a) (see Figure 12). Within the Alboran basin, north of the Balearic islands, and west of Sardinia and Corsica, considerable variation in the residual magnetic intensity is apparent. Generally east-west trending magnetic anomalies are parallel to the bathymetric features. The proximity of the Alboran basin to volcanoes on the coast of North Africa is compatible with a volcanic origin for the anomalies. North-south residual anomalies occur west of Sardinia and Corsica in a region of generally rough bottom relief.

Large amplitude magnetic anomalies are found within the Tyrrhenian Sea near volcanic seamounts and in areas of rough bottom topography. In the extreme northern end of the Tyrrhenian Sea high amplitude, northward trending anomalies exist parallel to, and near the base of, the Corsican island rise. Additional large magnetic anomalies occur in an area west of Naples, renown for its present and past volcanic activity. The most extensive group of high amplitude anomalies, located in the southeastern end of the Tyrrhenian Sea, is generally directly associated with topographic highs or ridges thought to be of volcanic origin.

1.323 Crustal Structure

The location of seismic refraction profiles obtained

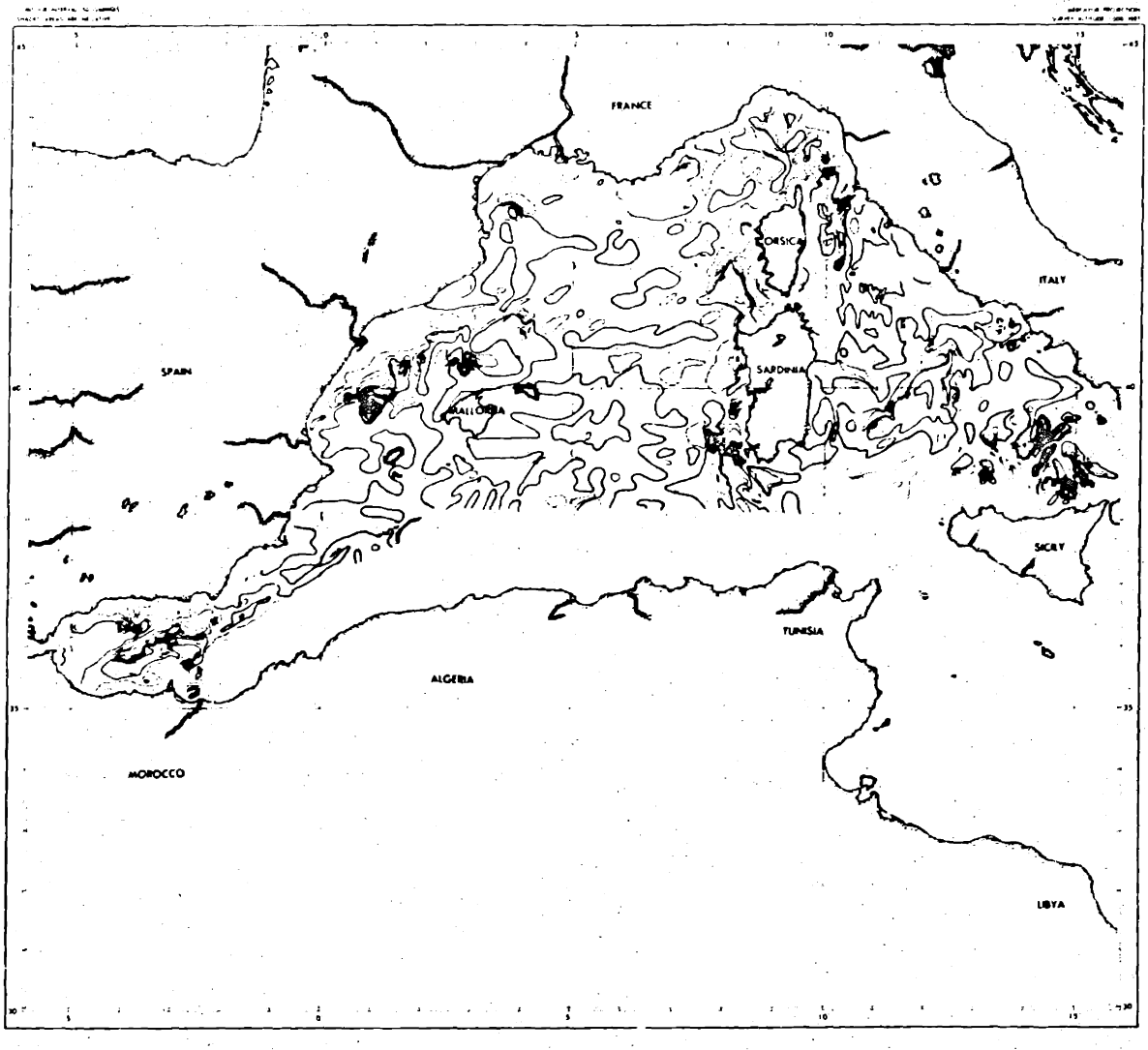

Figure 12. Residual magnetic anomalies over the western Mediterranean Sea. Contour interval 50 gammas. Shaded areas are negative. From Vogt and Higgs (in preparation, 1969).

in the western Mediterranean basin by Moskalenko (1967), Fahlquist (1963), Ewing and Ewing (1959) are shown in Figure 13.

The velocity structure of the crust along line AA' is shown in Figure 14. It can be seen that the Moho occurs at a depth of 11 km beneath the Balearic abyssal plain and sinks to greater depths to the northeast and southwest. Mantle material beneath the Moho is characterized by unusually low compressional velocities; at two of the four locations where mantle arrivals were recorded the velocity is only 7.7 km/sec.

A layer of 6.5 to 7.1 km/sec material about 3 km thick occurs above the mantle at most locations along AA', although at profile 4 5.8 to 6.0 km/sec material rests directly on normal mantle. 5 to 6 km of intermediate velocity (4.0 to 6.0 km/sec) material occurs beneath 1 or 2 km of unconsolidated and semi-consolidated sediment.

Profile 194, consisting of two unreversed profiles, is located in 2.8 km of water on the Balearic abyssal plain west of the southern tip of Sardinia. The length of the profile (22 km) was not sufficient to detect refracting material below the 7 km/sec layer observed at a depth of about 10 km. 2.5 to 3.0 km of 5.2 km/sec material and 4 to 6 km of 2 to 4 km/sec material are present above the 7 km/sec layer.

Profile 198 was situated southwest of the Balearic Islands in 2.8 km of water over the western Balearic

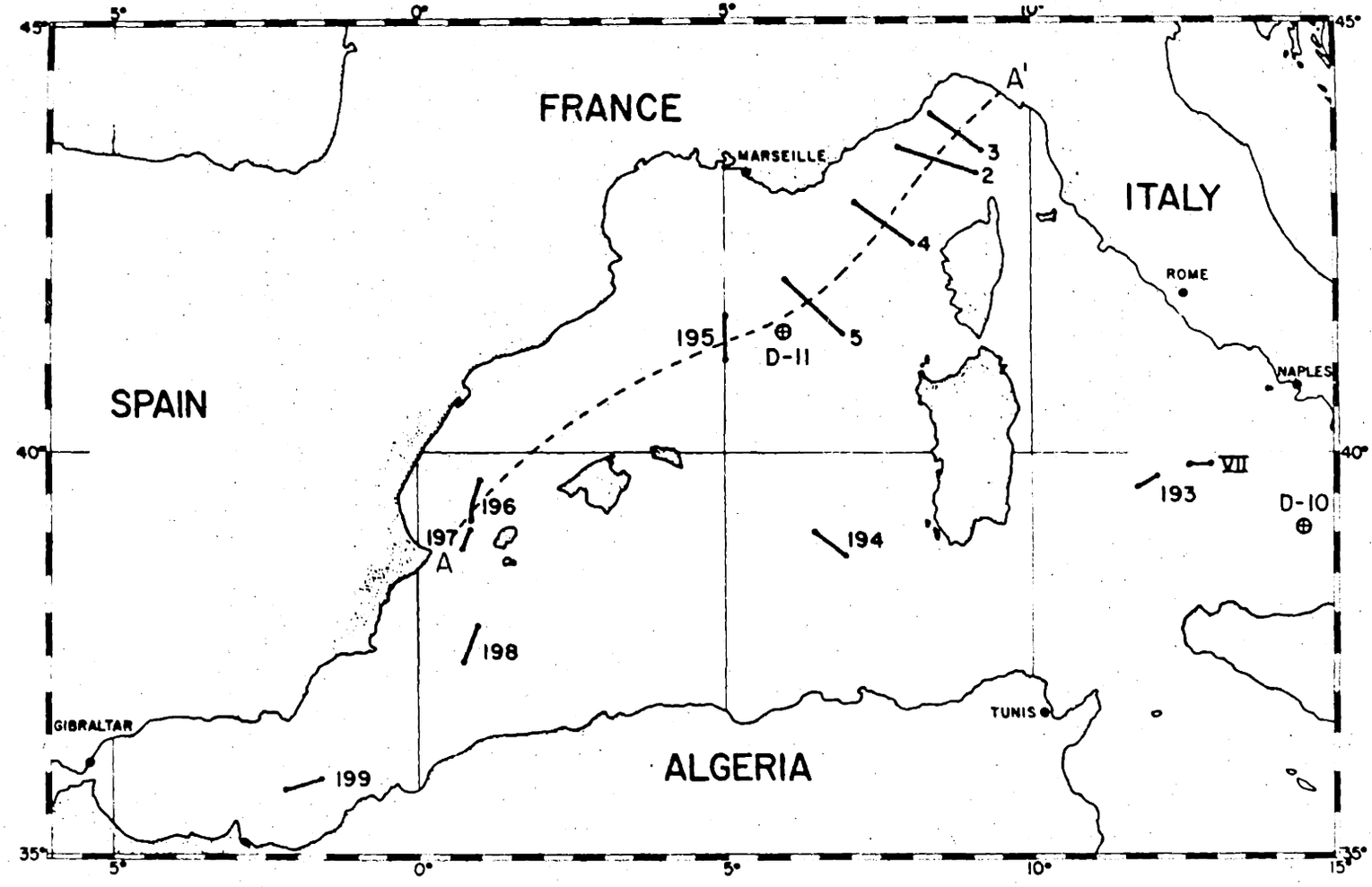

Figure 13. Locations of seismic refraction profiles in the western Mediterranean Sea. Profiles D-10 and D-11 from Ewing and Ewing (1959), profile VII from Moskalenko (1967), others from Fahlquist (1963). After Fahlquist (1963).

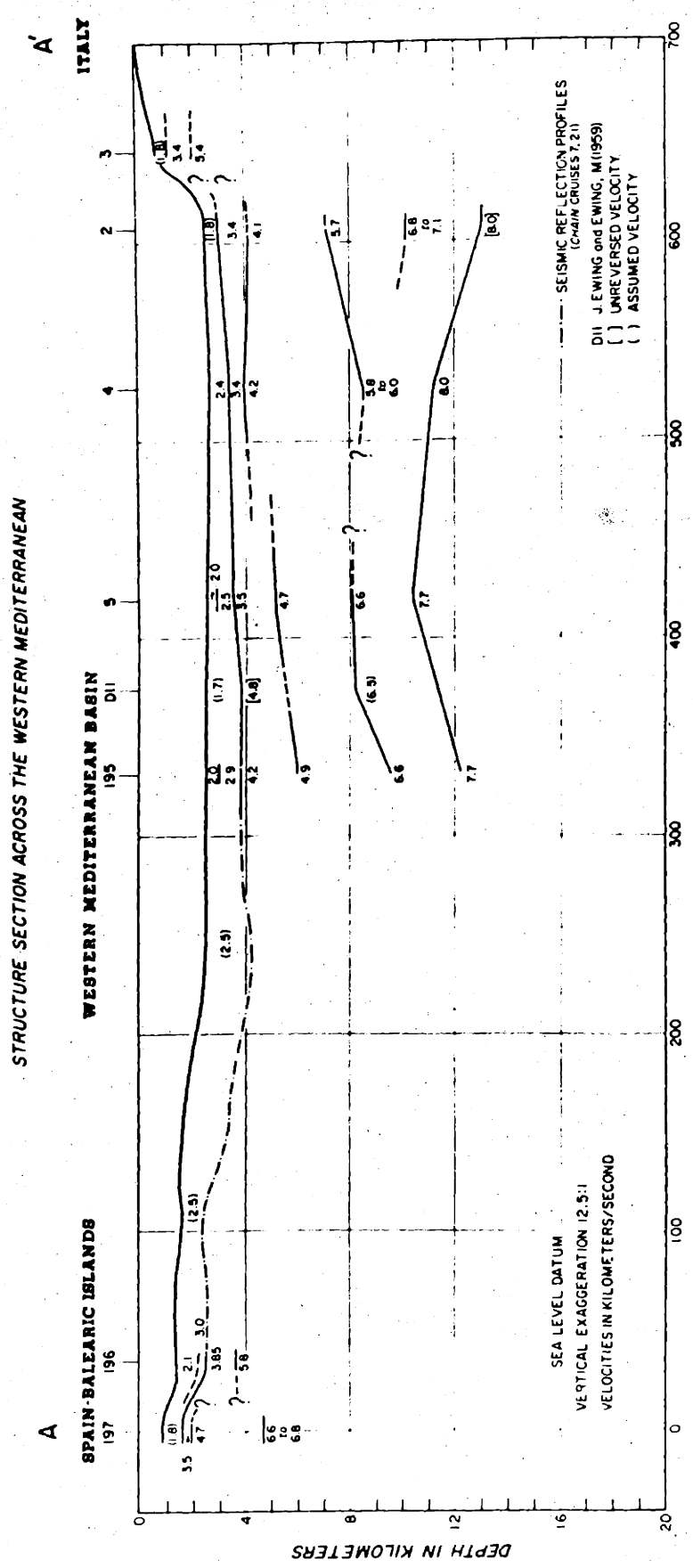

Figure 14. Crustal structure beneath the western Mediterranean basin along line AA' of Figure 13. From Fahlquist (1963).

abyssal plain. Despite a length of over 50 km, no mantle arrivals were observed. Material with a velocity of 6.8 km/sec was detected at a depth of 8 km. This layer is overlain by 5.6 km/sec material and other intermediate and lower velocity layers.

Profile 199 was situated in the extreme southwestern margin of the Balearic basin in about 2 km of water. Material with an apparent velocity of 7.7 km/sec was detected at a depth of 7.75 km (5.75 km beneath the sea floor). 3.3 km of 5.1 km/sec and 1.65 km of 2.9 km/sec material overlay the 7.7 km layer. The extremely shallow depth to the 7.7 km/sec material and the fact that the profile is unreversed should be taken into consideration before associating the 7.7 km/sec refracting layer with the upper mantle (Fahlquist, 1963).

The results of a short, unreversed refraction profile (D-10) across a large volcanic seamount in the southeastern end of the Tyrrhenian basin were reported by Ewing and Ewing (1959). A refracting layer with a compressional wave velocity of 4.9 to 5.7 km/sec was observed 0.9 to 1.2 km below the sea floor. At profile VII Moskalenko (1967) observed from 0.75 to over 2 km of 4.0 and 5.0 km/sec material, possibly underlain by deeply buried layered reflectors. Refracted waves from 3.92 to 4.36 km/sec material a few hundred meters beneath the seafloor were observed in an unreversed refraction profile (196) across the central Tyrrhenian basin

(Fahlquist, 1963). A refracting layer with velocities between 7.28 and 6.69 km/sec was located 2.2 to 3.0 km below the basin. Fahlquist identified this high velocity material with basalt on the basis of known volcanism north of Sicily and the presence of numerous volcanic seamounts in the Tyrrhenian basin.

1.33 Eastern Mediterranean Sea

1.331 Gravity Data

Free-air gravity anomalies as large as -240 mgal extend in a broad arc south of Crete from western Greece to the Rhodes abyssal plain (see Figure 15). This region of negative free-air anomalies coincides with the Mediterranean ridge and widens to include the Pliny and Strabo trenches with even greater free-air anomalies. A second, narrower, arc of low gravity extends southeast from the Rhodes abyssal plain, passes through Cyprus, and bends northeast towards the Gulf of Iskenderon. Large positive free-air (100 mgal), Bouguer (250 mgal) and isostatic (173 mgal) anomalies associated with the ultrabasic Troodos massif on Cyprus (Gass and Masson-Smith, 1963) and smaller positive anomalies over the Anaximander and Hecateus seamount complexes consitute a major, local interruption of this second arc.

Gravity increases abruptly northward across the Cretan arc and isostatic and free-air anomalies over 100 mgal

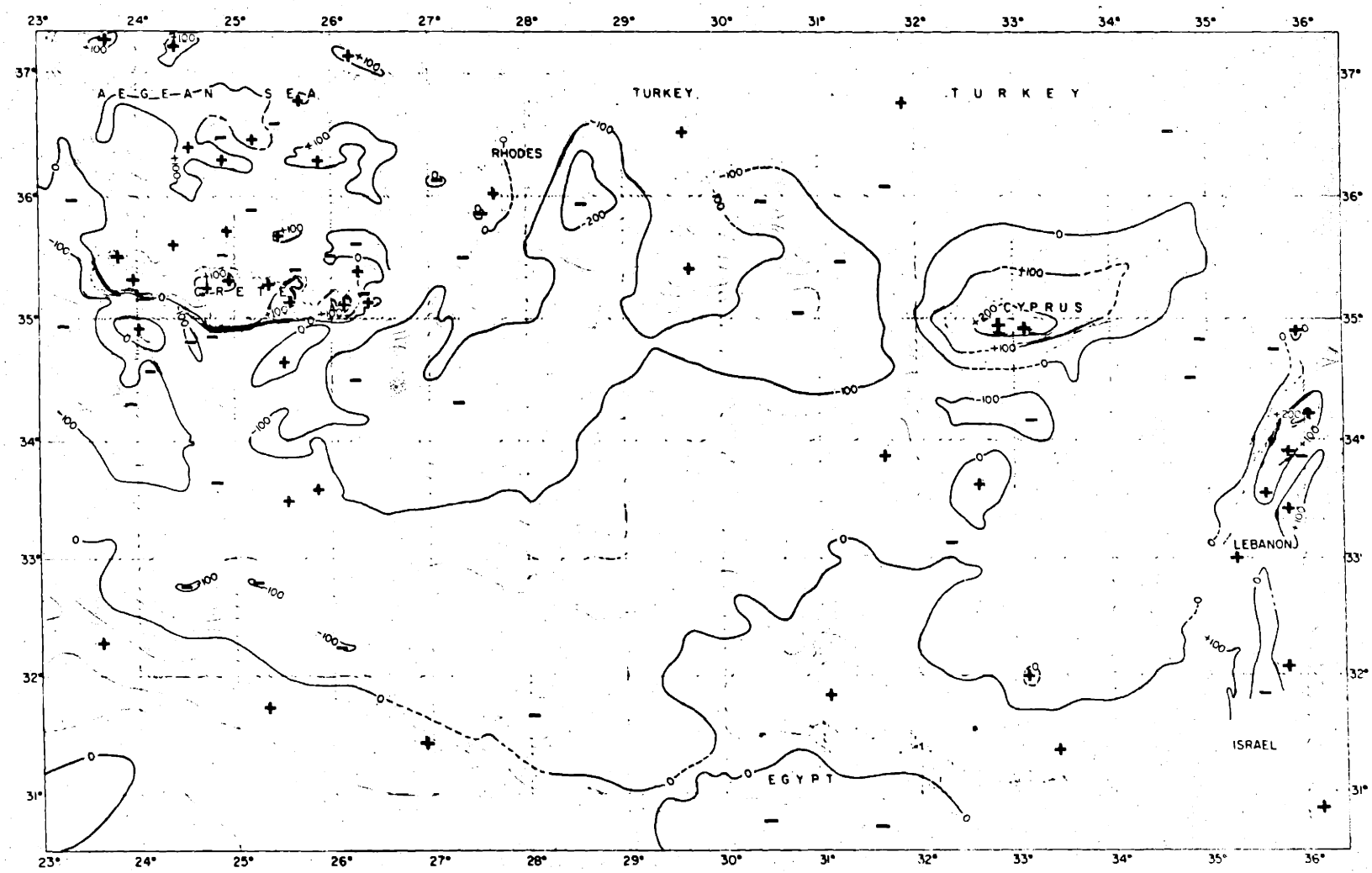

Figure 15. Free-air gravity anomalies over the eastern Mediterranean Sea. Contour internal 20 mgal. From Woodside and Bowin (1970).

are present in the southern Aegean Sea. Bouguer anomalies are positive over the shallow Aegean Sea and negative over deeper water within the Hellenic trough system (Harrison, 1955). A similar relationship was observed in the Crimea-Black Sea region by Woollard (1962).

1.332 Magnetic Data

The residual magnetic field over the eastern Mediterranean and Aegean Seas was described by Vogt and Higgs (1968b). Complex magnetic anomalies of several hundred gammas amplitude exist southeast of Sicily (Figure 16). Short-wavelength anomalies locally exceeding 500 gammas amplitude occur over a topographic high which extends eastward into the Ionian basin. Zarudzki (unpublished manuscript, 1968) interpreted the strong magnetic anomalies above the tectonically deformed and geophysically complex area south of Sicily as evidence of past and continuing volcanic activity.

An area of low amplitude (50 gamma), long wavelength (100 km), magnetic anomalies coincides with the Mediterranean ridge and the area characterized by large, regional, negative free-air gravity anomalies. Weak north-south trends in the residual field may be a consequence of both having obtained the aeromagnetic data along north-south flight lines and failure to correct for temporal variations in the earth's magnetic field. Trenches north and south of Crete, as well as the Cretan arc itself, are magnetically

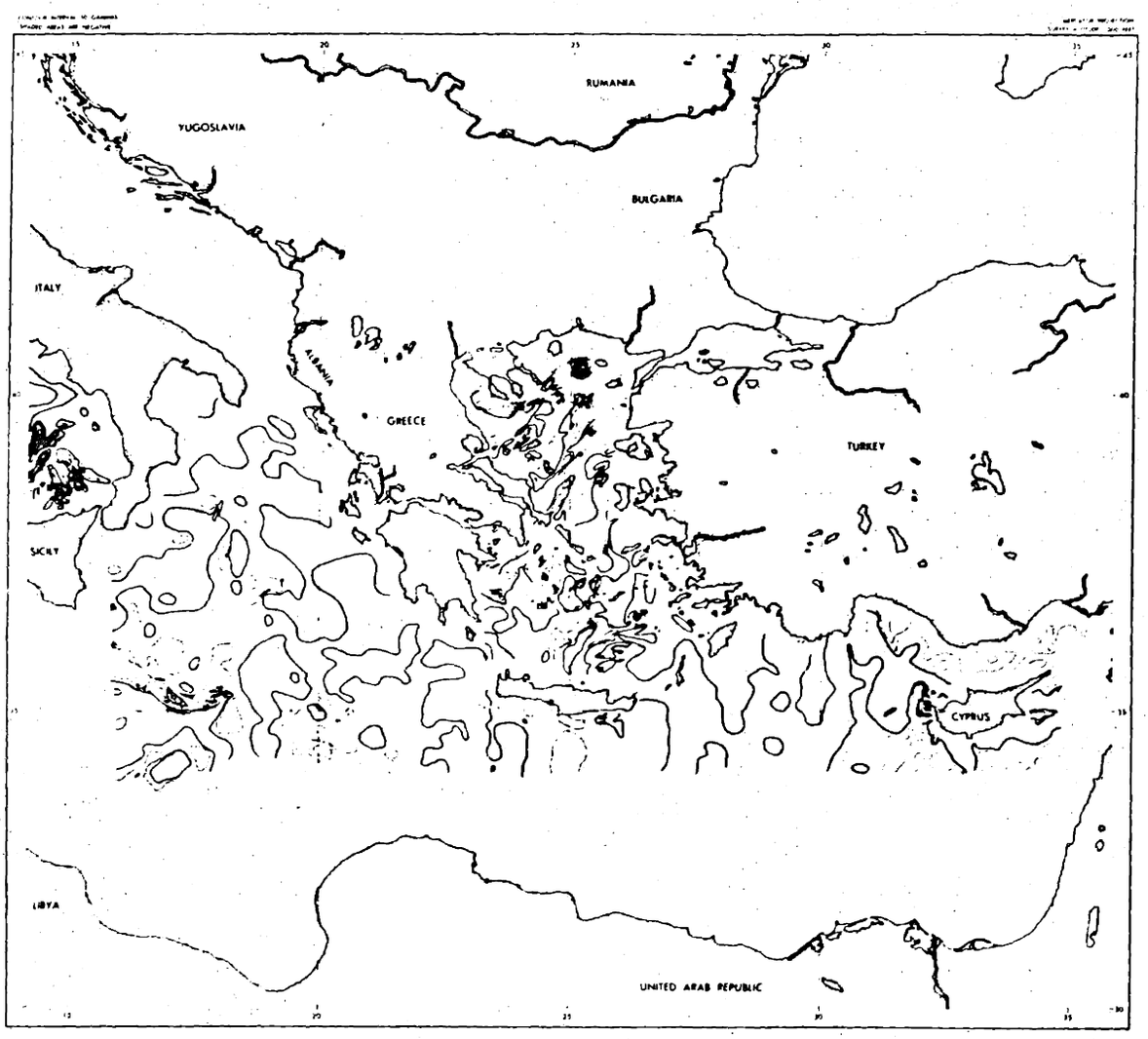

Figure 16. Residual magnetic anomalies over the eastern Mediterranean Sea. Contour interval 50 gammas. Shaded areas are negative. From Vogt and Higgs (1969).

quiet.

Northeast-southwest trending magnetic anomalies in the northern half of the Aegean Sea may be due to the seaward extension of bodies of Mesozoic granite exposed in western Turkey. Large magnetic anomalies present along a northeast trending valley in the northwestern Aegean may indicate a tensional origin for the rift, with subsequent intrusion of igneous material of high magnetic susceptibility (Vogt and Higgs, 1969). Although magnetic anomalies exist in the vicinity of volcanic structures in the southern Aegean Sea, the regional northeast trends continue beneath areas with no apparent volcanic history.

An arcuate band of high amplitude (200 gamma) magnetic anomalies extends from Cyprus northeast towards the Gulf of Anatolia and northwest into the Gulf of Iskenderon, "supporting the tectonic continuity of Cyprus with Alpine thrust belts on the mainland" (Vogt and Higgs, 1969). Zarudzki et al. (unpublished manuscript, 1969) found no evidence from marine magnetic data for the seaward extension of the intense north-south magnetic anomalies observed over Cyprus and described by Gass (1968).

Magnetic disturbances are absent over the Ptolemy and Anaximander seamount complexes. Although the Hecataeus mountains south of Cyprus are magnetically quiet, the Eratosthenes seamount further south is covered by a weak magnetic low.

In summary, the eastern Mediterranean, despite its rugged relief, is magnetically quiet except near Cyprus, where ultrabasic and basic rocks which outcrop on and around the Troodos massif are responsible for north-south oriented anomalies reaching an amplitude of over 2000 gammas. Large magnetic anomalies in the Aegean Sea can be attributed to volcanic activity in the form of seamounts, ridges, or islands.

1.333 Crustal Structure

The thickness and velocity characteristics of the crust and upper mantle beneath the eastern Mediterranean are largely unknown. A refracting layer with compressional wave velocity between 4.2 and 5.0 km/sec is present beneath 0.3 to 0.4 km of unconsolidated sediment in the Ionian Sea and south of Cyprus (Gaskell and Swallow (1953) and Ewing and Ewing (1959). In an unreversed seismic refraction profile on the Mediterranean ridge south of Rhodes, Moskalenko (1966) observed three refracted waves with apparent velocities of 2.8, 3.7, and 4.7 km/sec. The velocity in the sediment was assumed to increase linearly with depth from 1.5 km/sec at the surface to 2.5 km/sec at the top of the 3.7 km/sec layer. Moskalenko estimated that 0.6 km of unconsolidated sediment and 0.5 km of semi-consolidated sediment rest on at least 2 km of 4.7 km/sec material, if the 4.7 km/sec layer is underlain by a 6.0 km/sec layer whose refracted

arrivals are barely first arrivals at the end of the profile.

In a second unreversed seismic refraction profile across the deep-water Levantine basin south of the Mediterranean ridge, Moskalenko observed approximately 0.6 km of unconsolidated sediment resting directly on a 4.7 km/sec layer 1.8 to 2.0 km thick. A 6.1 km/sec layer 1.5 to 1.8 km thick and higher velocity (7.0 to 7.5 km/sec) material are present beneath the 4.7 km/sec material. Five north-south reflection profiles from the African coast to the Hellenic trough provide further data relating to the structure of the upper crust. The travel time to reflecting surfaces was determined at 50 km intervals and thicknesses were computed using velocities determined in the refraction survey whose results have been described. The total thickness of sediment on the African continental slope increases towards the deep-water area. Over the Mediterranean ridge the unconsolidated and semi-consolidated sediments attain thicknesses of 0.5 km and 0.5 to 0.6 km, respectively.

Moskalenko (1966) proposed that the 4.7 km/sec refracting layer is consolidated Mesozoic sediment on the basis of its correlation with the structure beneath the African continental margin as known from seismic reflection profiles and deep drilling in northern Egypt. In this interpretation, the 6.1 km/sec refracting interface corresponds to the base of the sedimentary section

beneath Africa and extends northwards beneath the continental margin, the Herodotus basin, and the Mediterranean ridge to the Hellenic trough. The total thickness of the sedimentary section is approximately constant at 2.0 to 2.5 km across the Levantine basin and thickens to 2.0 to 3.5 km over the Hellenic trough province to the north.

Ryan (1969a) combined seismic profiler data and a sedimentary time base derived from a study of the stratigraphy of eastern Mediterranean cores to provide information on the sedimentary and tectonic history of the eastern Mediterranean. He noted the widespread occurrence of a characteristic seismic reflector and estimated its age as 4.3 ± 0.3 m.y. using the local sedimentation rate and depth to the reflector, as well as the age of pelagic foraminfera found in a core believed to have sampled the reflector.

Ryan noted increasing sediment deformation northward across the Mediterranean ridge. Sedimentary layers conformable to the seafloor are confined to shallower and shallower depths below the seafloor in this direction. Deformation takes the form of short-wavelength fracturing and faulting in the north and gradually changes into broad, low amplitude folding at the southern edge of the Mediterranean ridge. A core taken on the Mediterranean ridge contained turbidite layers bearing reworked Eocene nanoplankton characteristic of the Nile River (Ryan,

1969a), in accord with the previous existence of an abyssal plain on the site of the present uplifted Mediterranean ridge. Recent turbidite sequences occur above the level of the basin adjacent to the southern margin of the ridge, suggesting that deformation of a former abyssal plain has occurred here more recently than further to the north. Hersey (1965) also concluded that the intensely deformed layers in the eastern Mediterranean were once flat-lying abyssal plain sediments similar to sediments now present in the Tyrrhenian and Balearic basins. Northward dipping strata beneath the Rhodes abyssal plain and a similar sequence of layers dipping and thickening northward beneath the Pliny trench south of Crete are in accord with these hypotheses (Ryan, 1969a).

Temporal as well as spatial variations in the depositional process are suggested by the widespread presence of an acoustically transparent layer beneath the stratified, ponded, turbidite-type deposits found in all Mediterranean abyssal plains. The ratio of the observed thicknesses of the transparent and stratified layers indicates that deposition by ponding began after 80% of the total sequence was laid down--that is, within the last million years (Ryan, 1969b).

Hersey (1965) noted that recent sediments have bypassed the flanks of the Nile cone and are found only near the top of, or at the base of the cone. Deeper,

older, reflectors can be traced from shallow water northward beneath 1 km of sediments deposited in the Herodotus abyssal plain. At the eastern end of the Mediterranean the continental platform appears to consist of at least one kilometer of horizontally layered sediment underlain by rough basement.

1.34 Black Sea

1.341 Gravity Data

A generalized Bouguer gravity map published by Malovitskiy and Neprochnov (1966) is shown in Figure 17. A positive Bouguer gravity anomaly exists over the deep portion of the Black Sea, with maximal values over the deep water regions beneath which "granitic" material, characterized by a compressional wave velocity between 5.4 and 6.4 km/sec, is thin or absent (Balavadze and Mindeli, 1965).

Neprochnov et al. (1967) used the results of deep seismic sounding in the Black Sea south of Crimea to explain why the Crimean mountains, in contrast with most other Alpine mountains, are characterized by positive Bouguer gravity anomalies. They concluded that the high positive anomalies are related to a rise of the dense "basaltic" layer and a thinning of the lighter "granitic" layer beneath the mountains.

The absence of a direct correspondance between the

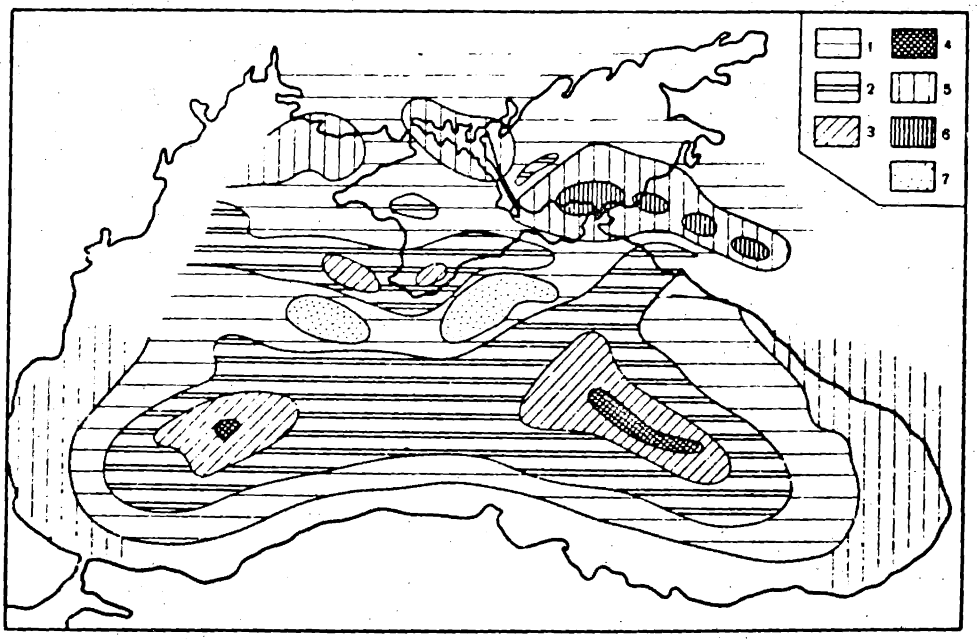

Figure 17. Bouguer gravity anomalies over the Black Sea.

1 - slightly positive anomalies.
2 - regional, moderately positive anomalies.
3 - local, moderately positive anomalies.
4 - extremely high, positive anomalies.
5 - small, negative regional anomalies.
6 - large, negative anomalies.
7 - local, negative anomalies.

From Malovitskiy and Neprochnov (1966)

depth of the Moho and the observed Bouguer anomaly within the central Black Sea basin was noted by Neprochnov (1968). Burakovskiy (1966) analysed gravity data along north-south deep seismic sounding profiles over the northern continental margins of the west, central and eastern Black Sea and observed regional differences in the relation between the gravity field and crustal structure. Within the western Black Sea, and to a smaller extent along the profile south of Crimea, the observed gravity anomaly is up to 200 mgal greater than the value predicted from the observed crustal structure. Burakovskiy (1966) concluded that the upper mantle beneath the western Black Sea is unusually dense and reflects different stages in the development of the eastern and western parts of the Black Sea.

1.342 Magnetic Data

Residual magnetic anomalies in the Black Sea south of 44°N are shown in Figure 18 from Anonymous (1965). Residual anomalies in the eastern half of the Black Sea trend northwest, generally parallel to the structural trends in the adjacent Caucasus mountains. The northwest trend of the anomalies is less well-defined in the western half of the Black Sea where the trend of the anomalies swings more to the northeast parallel to the fold axes of the Pontic mountains along the Turkish coast. Bowin (unpublished manuscript, 1970) computed the depth to

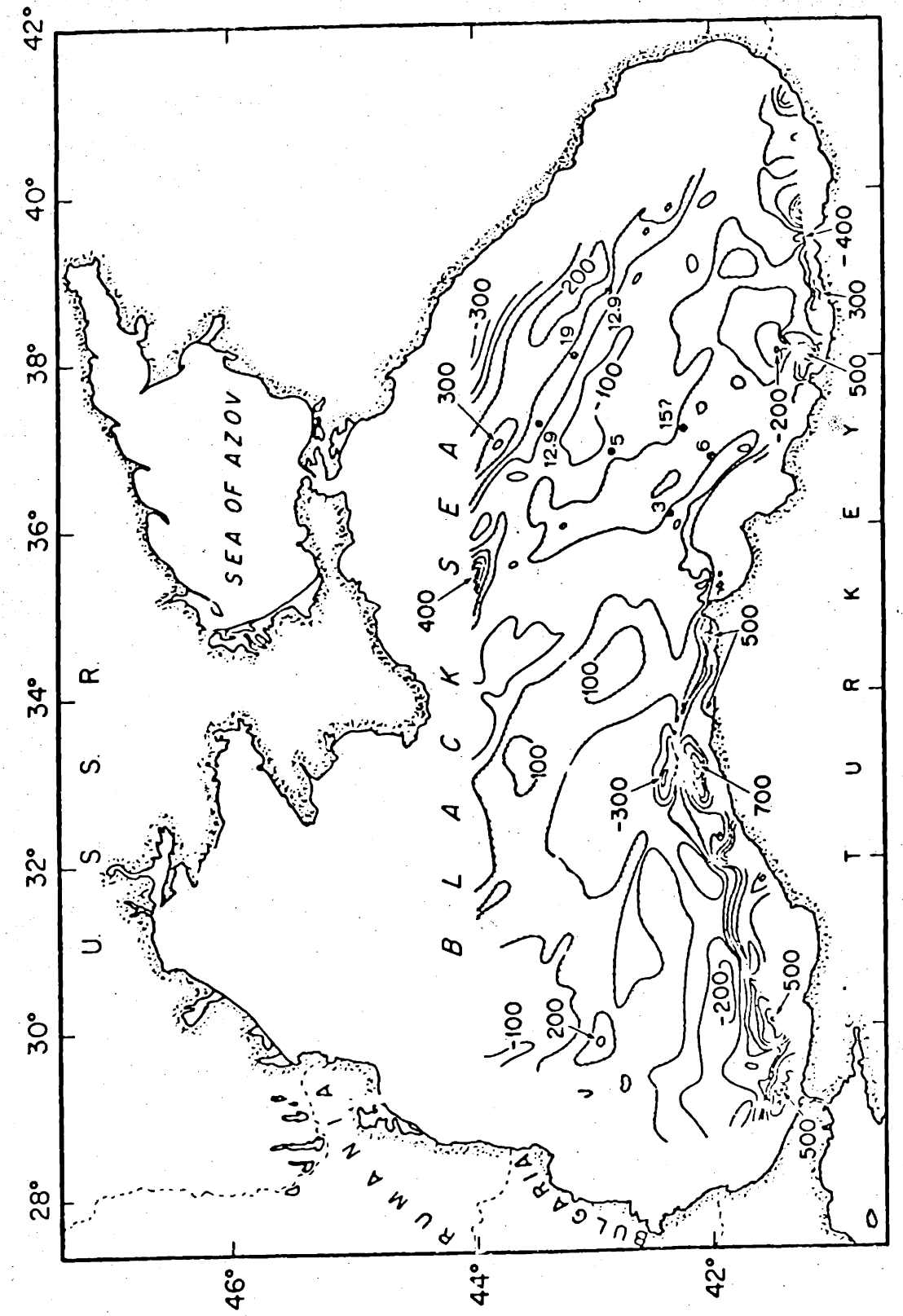

Figure 18. Residual magnetic field over the Black Sea. Contour interval is 100 gammas; shaded areas are positive. From Bowin (unpublished manuscript,1970)

magnetic basement at several locations in the eastern half of the Black Sea. If the magnetic anomalies are caused by tabular bodies of uniform magnetization extending to great depth, the bodies are located from 3 to 19 km beneath the seafloor. Thus the magnetic anomalies may be due to bodies within the sedimentary column as well as to contrasts in the magnetic properties of the basement layer.

1.343 Crustal Structure

Neprochnov et al. (1967) measured apparent velocities between 2.4 and 5.0 km/sec in the sedimentary column beneath the Black Sea. Two distinct arrivals with velocities of 3.0 km/sec and between 4.0 and 4.5 km/sec were observed at some locations. The 4.0 to 4.5 km/sec layer lies at a depth of 6 to 10 km and is from 4 to 8 km thick. Variations in average velocity, the occurrence of discontinuous horizontal or sub-horizontal refracting horizons possessing a wide range of velocities, and regional differences in thickness are also observed.

Balavadze and Mindeli (1965), using gravity and deep-seismic profiling data, determined that the sediment attains a maximum thickness of about 14 km southwest of Crimea. The sediment thins to about 11 km in the center of the sea and to 5 km in the northwestern shallow water area.

Material with velocities between 5.0 and 6.0 km/sec,

usually identified with rocks of granitic composition or with metamorphosed sediments, is either thin or absent beneath the sedimentary layer in the central basin (Mindeli et al., 1966). As shown in Figure 19, the sediment rests directly upon material with a seismic velocity between 6.4 and 7.0 km/sec. The thickness of the 6.4 to 7.0 km/sec material, frequently referred to as the "basaltic" layer, ranges from 6 to 23 km. The base of the "basaltic" layer in the central Black Sea is elevated and the crustal thickness is only 22 km. Near the margins, the surface of the "basaltic" layer sinks to depth of 20 to 23 km, except in the vicinity of Crimea, where the layer appears to rise beneath the Crimean mountains. Around the margins of the Black Sea material with a compressional velocity of 6.2 to 6.4 km/sec appears between the thinning low-velocity layer associated with the sediments and the deepening basaltic layer and attains a thickness of 10 to 15 km near the continent (Neprochnov et al., 1967). Considerable relief at the boundaries between the "basaltic", "granitic", and sedimentary layers are observed away from the abyssal regions. A layer of 5.0 to 6.0 km/sec material, possibly metamorphosed sediment, was observed between the sedimentary and "granitic" layers south of Crimea.

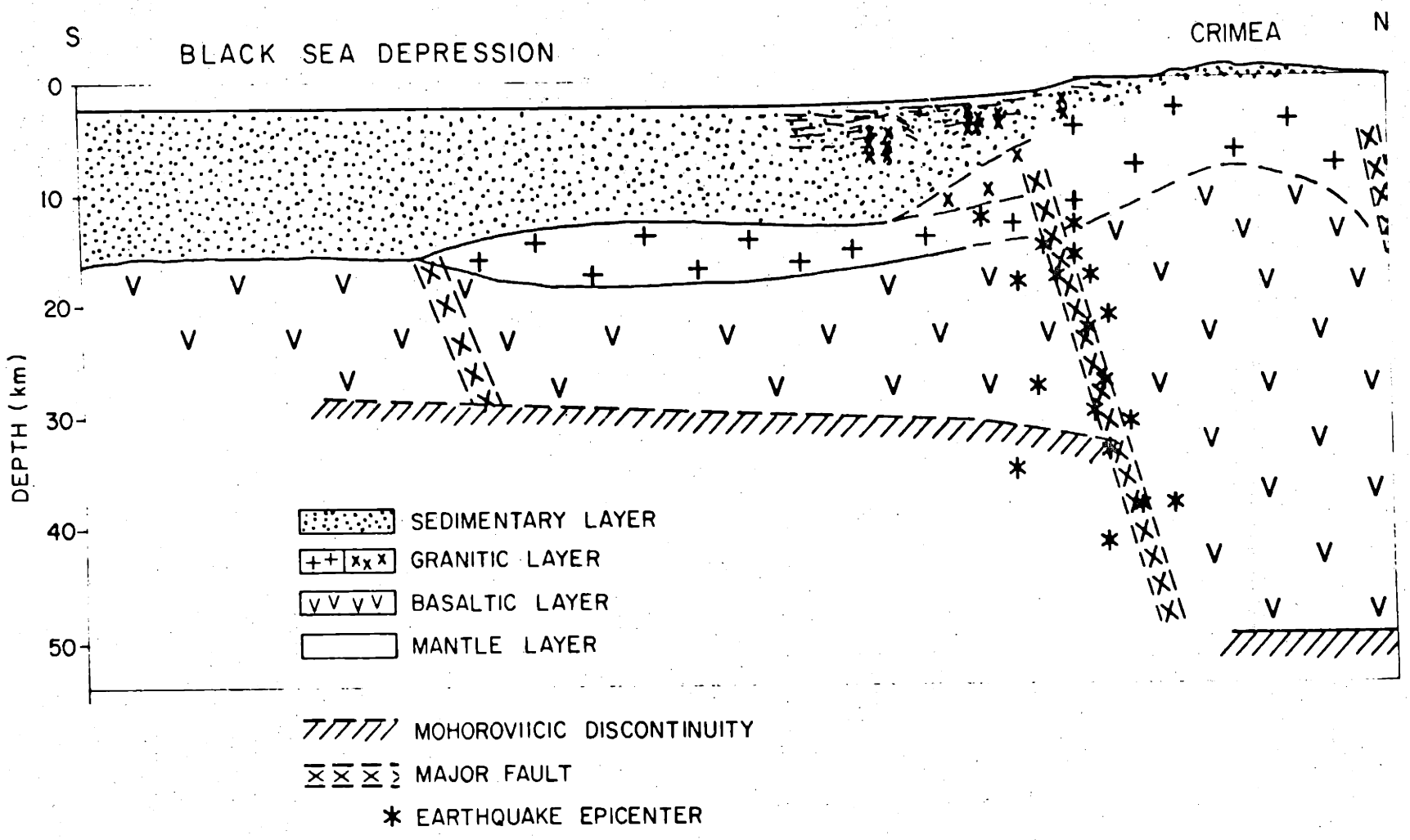

Figure 19. Crustal structure beneath the Black Sea south of Crimea. After Subbotin et al. (1968).

DISCUSSION OF DATA

2.1 EQUIPMENT AND TECHNIQUE

All of the new heat flow data presented in this paper were obtained using equipment similar to the Ewing thermograd described by Langseth (1965). From 4 to 8 outrigger-type thermistor probes were used to measure the temperature in the sediment along a corer 2 to 12 m long (Figure 20). Another thermistor probe located at the top of the core weight provided a semi-continuous temperature record in the water column above the sea floor, as well as a reference to which temperatures measured beneath the sea floor could be compared. Absolute values of water temperature obtained using the thermal gradient recorder were usually within 0.02°C of bottom water temperatures determined using reversing mercury thermometers.

There are at least three different classes of errors which contribute to the uncertainty in a particular heat flow value. These are listed below.

1. Error in measuring the thermal gradient.
2. Error in measuring the thermal conductivity.
3. Error in estimating the heat flow from thermal gradient and conductivity measure-

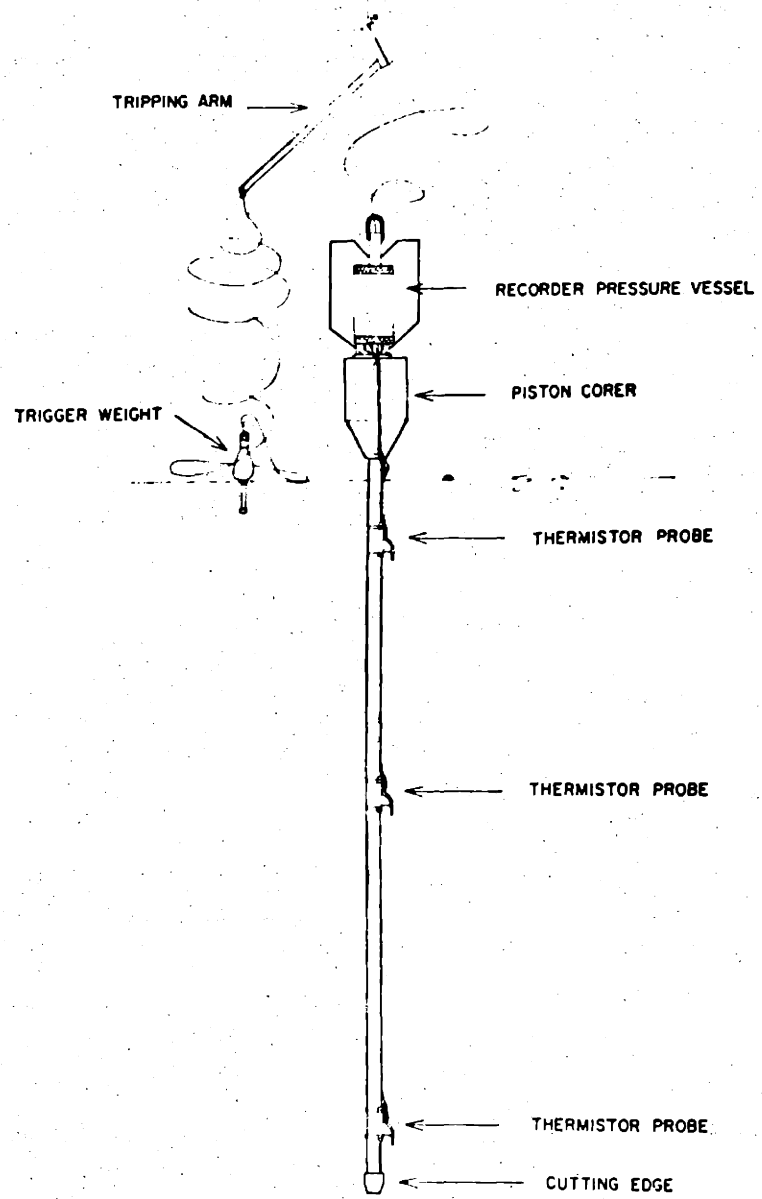

Figure 20. Piston corer with thermal gradient recorder and outrigger-type thermistor probes. After Langseth (1965)

ments at discrete intervals.

In addition, environmental effects determine the extent to which a heat flow measurement is representative of the regional heat flow.

2.11 Thermal Gradient Measurements

The error in the thermal gradient is determined by factors relating to the temperature sensor (stability and calibration of the thermistor and construction of the probe), to the thermal gradient recorder (sensitivity, linearity, alignment of optics, tolerance of precision resistors), and by factors peculiar to each measurement (amount and angle of penetration into the sea floor, the establishment of thermal equilibrium between the temperature sensors and the sediment, measurement of spacing between temperatures sensors). The temperature increase at each probe after penetration can be measured to 0.002^{o}C, however failure of the probes to reach thermal equilibrium with the sediment can render this sensitivity meaningless for some measurements. Distances between probes are known to about 1%. Under normal conditions, when care is taken to reduce errors inherent in the temperature sensor and the thermal gradient recorder, the largest error is due to the failure of the temperature sensors to attain thermal equilibrium with the sediment.

In cases where 3 or more probes penetrated the sediment, or where at least 2 probes and an estimate of penetration allowed the use of the water temperature as a third point, the probable error in the gradient was estimated by computing the maximum and minimum gradients which could be drawn through the temperature increase versus depth plots. Half of the difference between the maximum and minimum possible gradients was considered to be the probable error. Temperature increases which appeared well determined were weighted more heavily than poorly measured increases associated with temperature fluctuations due to movement of the corer in the sea floor, or failure of the probe to approach thermal equilibrium. Where only two points existed on the temperature increase versus depth plot, the possible error assigned was similar to the possible error associated with other measurements made in the general area using the same equipment and techniques. For measurements where a sufficient number of temperature-depth data points were available to define a non-linear gradient, the measurement was considered unreliable and not included in the data analysis unless at least the deepest 3 temperature-depth points defined a straight line. In this case the error associated with the measurement was estimated in the usual manner, neglecting the upper, non-linear, data points. The minimum possible error in the thermal gradient is estimated to be 5%.

Temperature-depth data and profiles for all measurements discussed in this manuscript are presented in Appendices I and II, respectively.

2.12 Thermal Conductivity Measurements

Thermal conductivity was measured on the sediment obtained at the same location as the thermal gradient measurement using the needle-probe technique described by Von Herzen and Maxwell (1959). The total error in a single thermal conductivity measurement includes errors in determining the rate of heat generation per unit length of the needle-probe and measuring the rate of the temperature increase in the sediment due to the heat released by the needle. Additional errors arise from failure of the needle-probe and sediment to fulfill criteria for a continuous linear heat source in an infinite, isotropic medium. Von Herzen and Maxwell (1959) obtained agreement between thermal conductivity values measured using the needle-probe and steady-state techniques to 3 or 4 %.

The effect of decompression and shipboard handling on the thermal properties of the cored sediment is poorly understood. The expansion of interstitial gases and the possible loss of water or rearrangement of mineral grains--sometimes easily observable as areas of excess water or graded, washed, portions of the cores--may result in

non-representative thermal conductivity values. Thermal conductivity values determined using an in situ thermal conductivity probe developed at the Scripps Institute of Oceanography are in good agreement with shipboard needle-probe measurements made on material obtained in gravity cores at the same location (Sclater et al., 1969).

The thermal conductivity values measured aboard ship were corrected for the effects of higher pressure and lower temperature at the sea floor using the corrections suggested by Ratcliffe (1960). Conductivity data measured by M.I.T. personnel, from which the harmonic mean conductivity used in the final heat flow calcuation was computed, is presented in Appendix III.

A sampling error exists due to the measurement of the conductivity at discrete intervals, rather than continuously along the core. The sampling error was defined for all stations as the standard deviation of the conductivity measurements about the harmonic mean divided by the square root of the number of individual measurements. At stations for which the thermal conductivity was estimated from measurements made on nearby cores a probable error of 10% was assigned.

The heat flow value at each station is the product of the average thermal gradient and the harmonic mean thermal conductivity. Strictly speaking, the heat flow value determined by averaging the flux through different intervals below the seafloor, each with a

characteristic gradient and thermal conductivity, should be even more representative than that obtained by averaging over the entire core. This method was not used because conductivity variations within the cores were generally small and because of the difficulty of assigning sections of core to intervals over which the gradient was determined. The probable error in the heat flow measurement was estimated to be the sum of the probable errors in the average thermal gradient and conductivity values.

2.2 ENVIRONMENTAL CORRECTIONS

The main reason for measuring heat flow is toobtain information relating to thermal conditions in the upper mantle. The measured heat flow does not necessarily give an accurate indication of the thermal regime in the mantle. Both transient and steady state disturbances can cause the observed heat flux to differ substantially from the geophysically relevant heat flow which would be observed if such disturbances did not exist. The environmental corrections are applied to the observed heat flux in an attempt to obtain heat flow data which is representative of the thermal state of the upper mantle.

In order for a heat flow measurement to be representative of the regional heat flux out of the upper mantle, the following conditions must exist on or beneath the sea floor:

1) The sea floor must be flat, undisturbed, and composed of material possessing uniform, isotropic thermal conductivity,

2) the sea floor must be maintained at constant temperature and position, and

3) heat transfer through the sediment must be entirely by conduction, rather than by convection or any form of mass transfer.

It is likely that these conditions are nearly satisfied over large areas of the deep ocean basins.

However, in relatively shallow, tectonically active basins such as the Mediterranean and Black Seas, most of the conditions mentioned above cannot be assumed. In the following sections the extent to which different environmental conditions can effect the observed heat flow is discussed and where sufficient data exist, estimated.

2.21 Sedimentation at Constant Rate

In many areas of the deep ocean sedimentation rates are low enough that the heat required to warm the sediment and maintain the equilibrium thermal gradient is small compared to the heat flow. In small ocean basins located within or adjacent to continental areas, sedimentation may occur at such a rapid rate that a significant fraction of the equilibrium heat flow is absorbed in warming the rapidly accumulating sediment, and the thermal gradient at or near the sediment-water interface will then be smaller than that which would exist without sedimentation (Figure 21).

Estimation of the effect of sedimentation on the thermal gradient requires knowledge of the sedimentation rate and type throughout the history of the ocean basin. It is fair to say that were such information available, the geological and geophysical problems could be considered at least half solved; the history of the Mediterranean and Black Seas is intimately connected with

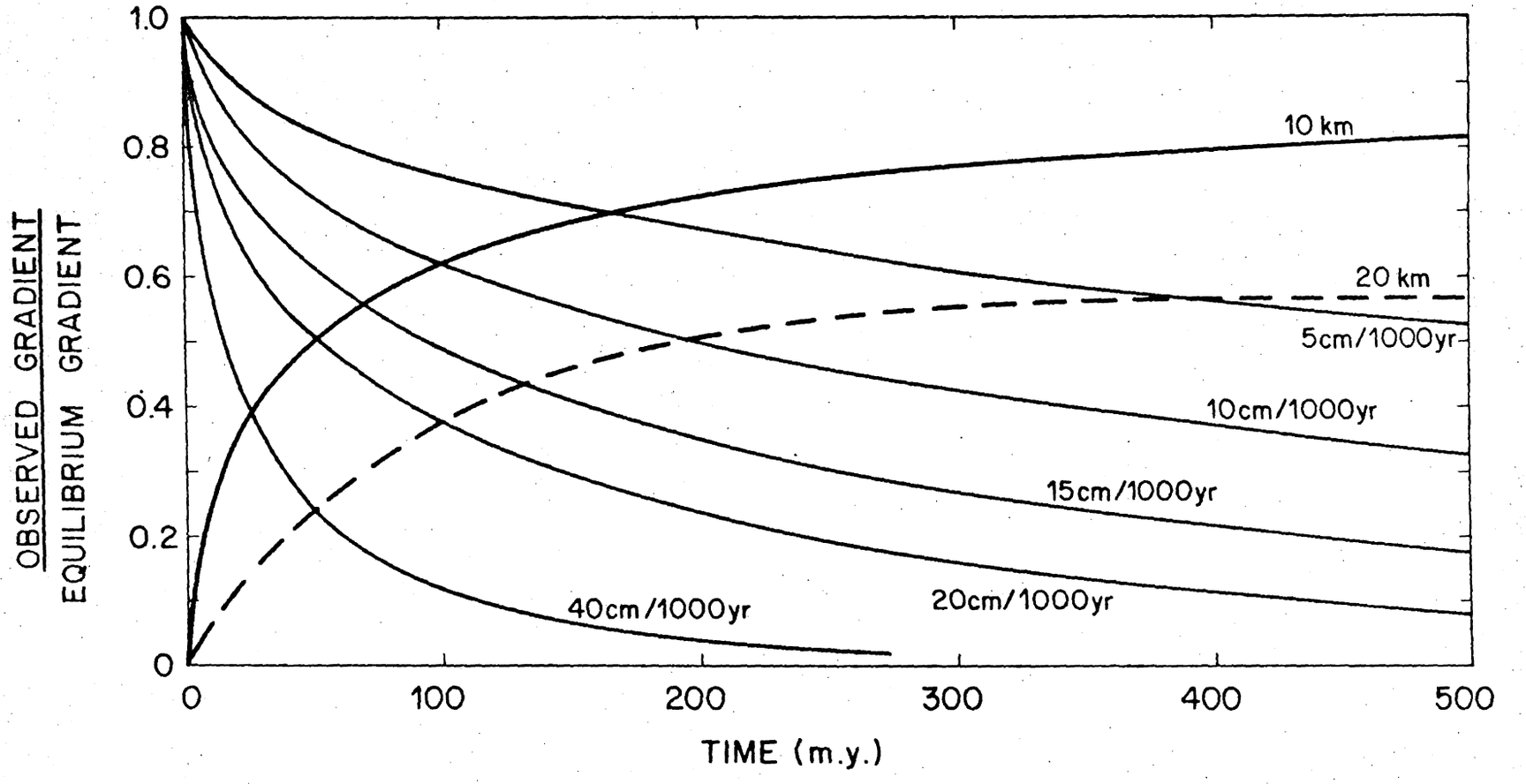

Figure 21. The reduction of the thermal gradient due to sedimentation, as a function of sedimentation rate and duration. A thermal diffusivity of 0.002 cm^2/sec is assumed for the sediment. The heavy solid and dashed curves show the reduction due to the deposition of 10 and 20 km of unconsolidated sediment over different intervals of time.

the age, origin, and geological history of the adjacent areas from which the sediment now present in the basins was derived. Of particular importance is the identification of the 4.0 to 6.0 km/sec refracting layer, present throughout the Mediterranean, as consolidated or metamorphosed sediment or crystalline basement. The sedimentation effect was estimated on the assumption that the sedimentation rate can be approximated by dividing the "expanded" thickness of the sedimentary column, calculated as the total thickness of unconsolidated sediment required to produce the observed sediment thickness, by the estimated duration of sedimentation. It is further assumed that the same sedimentation correction is valid throughout a particular basin. Although some areas, such as the Rhone fan, the Nile cone, or the Mediterranean ridge, are now receiving sediment at unusually high or low rates, their sedimentary histories are assumed to be similar to the long-term histories of the basins in which they are located. With few exceptions, regions receiving sediment at anomalous rates have been doing so for a geologically short time. Heat flow values from these areas may require second order sedimentation corrections; however, the absence of reliable data on which to base these corrections has led to qualitative, rather than quantitative, corrections. These are discussed below in reference to individual measurements.

2.22 Sudden Sedimentation or Erosion

The sudden addition or removal of a layer of sediment can alter the thermal gradient beneath the sea floor. Von Herzen and Uyeda (1963) showed that the sudden deposition of a layer of sediment is unlikely to have an important effect on the average heat flow value computed from heat flow measurements made in different sedimentary environments.

Ryan's (1969b) successful correlation of eastern Mediterranean sediment cores was possible because the characteristic thickness of interruptions in the regional stratigraphic succession (< 1 m) was small compared to the core length (10 m). The disturbance to the thermal gradient caused by the deposition of 1 m of sediment decreases rapidly both with time and depth beneath the seafloor. Von Herzen and Uyeda (1963) calculated that the thermal gradient observed at the seafloor attains 90% of its original value within 10 years and is within a few percent of the equilibrium value after 100 years. Most estimates of the sedimentation rate in the Mediterranean Sea range between 30 cm/1000 yrs and 5 cm/1000 yrs; if sedimentation were to occur entirely by the periodic, sudden deposition of layers of sediment 1 m thick, the probability of coring such a layer within 100 years after it was deposited would be small. Furthermore, the existence of a significant disturbance to

the thermal gradient would be obvious if the gradient were determined by temperature measurements at several points over an interval thicker than the recently deposited layer. Although abnormally low heat flow values may be due to the effects of sudden deposition, it is unlikely that the regional heat flow average computed from widely-spaced measurements would be seriously affected.

The removal of sediment, either through erosion of the sea floor by currents or by slumping of sediments off of slopes, can increase the observed gradient near the sea floor. Carslaw and Jaeger (1959, p. 61) gave the temperature T(x,t) at depth x beneath an infinite half-space of uniform thermal diffusivity k which was originally at temperature T_1+Gx, and whose surface was maintained at zero temperature beginning at t=0.

$$T(x,t) = T_1 \, erf\left(x/\sqrt{\pi k t}\right) \qquad \text{Equation 1}$$

The thermal gradient $G_{obs}(o,t)$ at the seafloor (x=0) is then

$$G_{obs}(o,t) = T_1/\sqrt{\pi k t} + G \qquad \text{Equation 2}$$

The temperature change T_1 can be rewritten to include the sediment thickness Δx removed.

$$T = G\Delta x \qquad \text{Equation 3}$$

Substituting T_1 into Equation 2, the observed gradient

$$G_{obs}(o,t) = \frac{G\Delta x}{\sqrt{\pi k t}} + G = G(1+\alpha) \qquad \text{Equation 4}$$

where $\alpha(\Delta x, t)$ is the fractional disturbance to the gradient. Figure 22 shows α calculated for various layer thicknesses and elapsed times since removal. The disturbance to the thermal gradient at the sea floor due to the removal of 1 m of sediment with a thermal diffusivity of 0.002 cm^2/sec is only 7% after 1 year and less than 1% after 50 years. The sudden removal of greater thicknesses of sediment can seriously change the thermal gradient for much longer periods. Slumps of this magnitude, though possible, are very infrequent and are not an important source of error in the computation of the regional heat flow.

2.23 Water Temperature Variations

Temperature fluctuations in the bottom water pro-

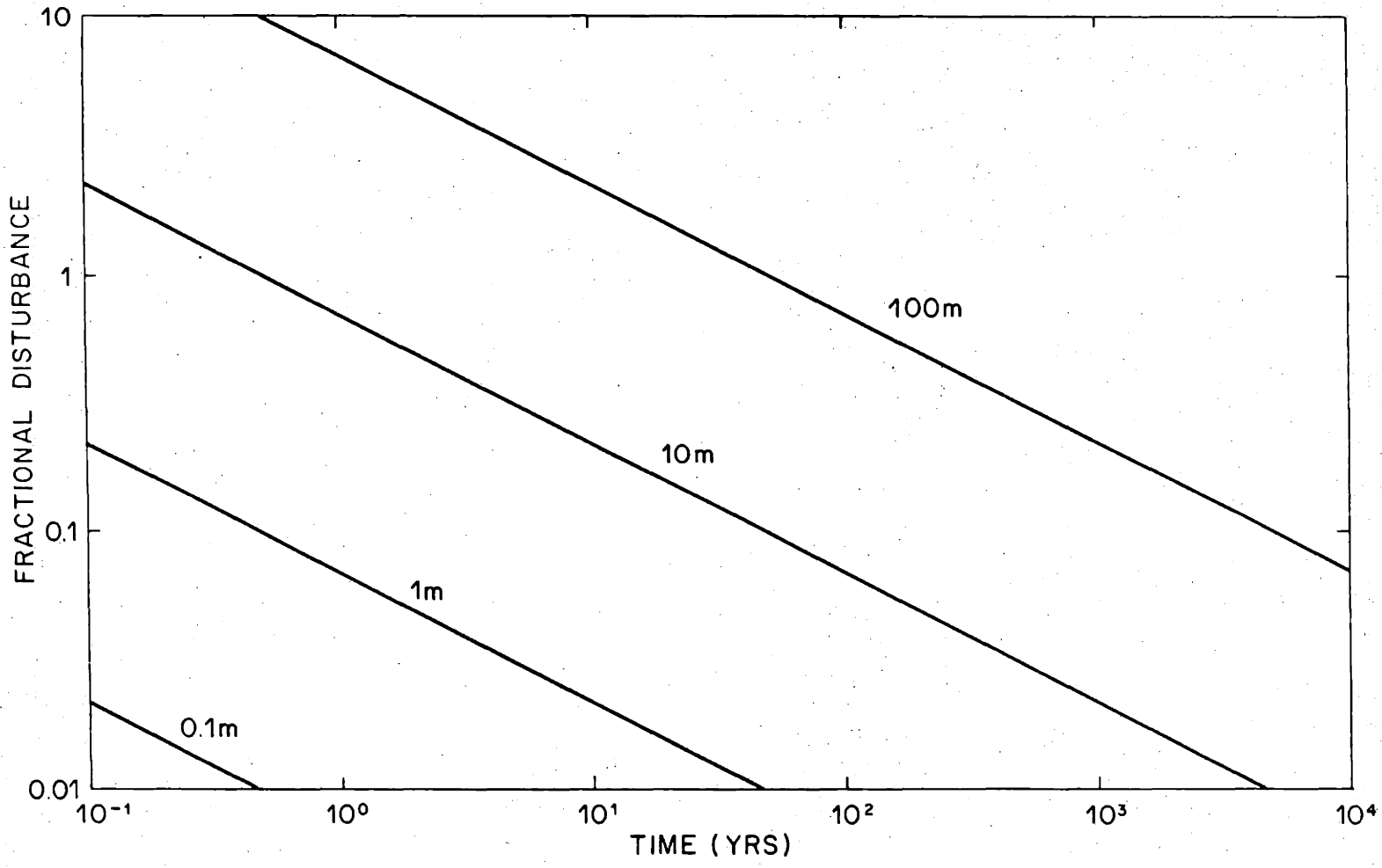

Figure 22. The effect on the geothermal gradient of the sudden removal of various thicknesses of sediment with a thermal diffusivity of 0.002 cm^2/sec. The ratio of the observed thermal gradient to the steady-state thermal gradient is shown for different lengths of time since removal.

pagate into the sea floor and change the geothermal gradient in the sediment. Short-period temperature oscillations are dominated by a semi-diurnal periodicity associated with internal tidal waves (Lee and Cox, 1966). Higher frequency oscillations with periods of several minutes and amplitudes of up to several tenths ^{o}C were observed by Gordon et al. (1966) and Gretener and Simmons (1967) in the Caribbean and Gulf of Mexico, respectively.

Annual temperature variations are absent below 500 m in the northeastern Pacific (Lee and Cox, 1966). The circulation and production of bottom water in the Mediterranean and Black Seas are significantly different from the same processes in the major oceans, and it is not surprising that a seasonal change of about $0.2^{o}C$ was observed in hydrographic data presented by Miller (1963).

The propagation of a thermal disturbance of the form $T_o\cos(wt)$ in the water into sediment having uniform thermal diffusivity k is described by Equation 1 (Carslaw and Jaeger, p. 65, 1959).

$$T(x,t) = T_o\exp(-Kx)\cos(wt-Kx) \qquad \text{Equation 1}$$

The wave number K and the wavelength λ of the temperature wave are given by Equations 2 and 3, respectively.

$$K = \sqrt{\omega/2k} \qquad \text{Equation 2}$$

$$\lambda = 2\pi/K \qquad \text{Equation 3}$$

Assuming a thermal diffusivity of $k = 0.002$ cm^2/sec, the wavelength of the semidiurnal and annual oscillations are about 35 cm and 9 m, respectively. The amplitude of the temperature disturbance decays exponentially with depth and is reduced to $0.0019T_o$ at a depth of one wavelength. Thus, for thermal gradient measurements at depths equal to or greater than λ, the effect of temperature variations is negligible. The thermal gradients discussed in this manuscript were measured over depths of 2 to 12 m beneath the sea floor, and are thus unaffected by semidiurnal variations.

The wavelength of the temperature wave associated with annual water temperature variations is comparable to the interval over which the gradient was measured. If annual temperature variations occur in the bottom water of the Mediterranean and Black Seas, the temperature-depth measurements described in this manuscript should show the effects of these variations.

The amplitude and shape of the thermal perturbation beneath the sediment due to a yearly temperature change of 0.2°C is shown in Figure 23. The existence of a temperature-depth distribution of this shape in the sediment would be easily detectable, regardless of the time of the year,

Figure 23. The family of nonlinear temperature-depth curves beneath the sea floor due to sinusoidal variations of the bottom water temperature with an amplitude 0f 0.2°C and a period of 1 yr. Note the distinctly nonlinear relationship between temperature and depth in the top few meters of sediment, regardless of the phase of the sea floor temperature disturbance.

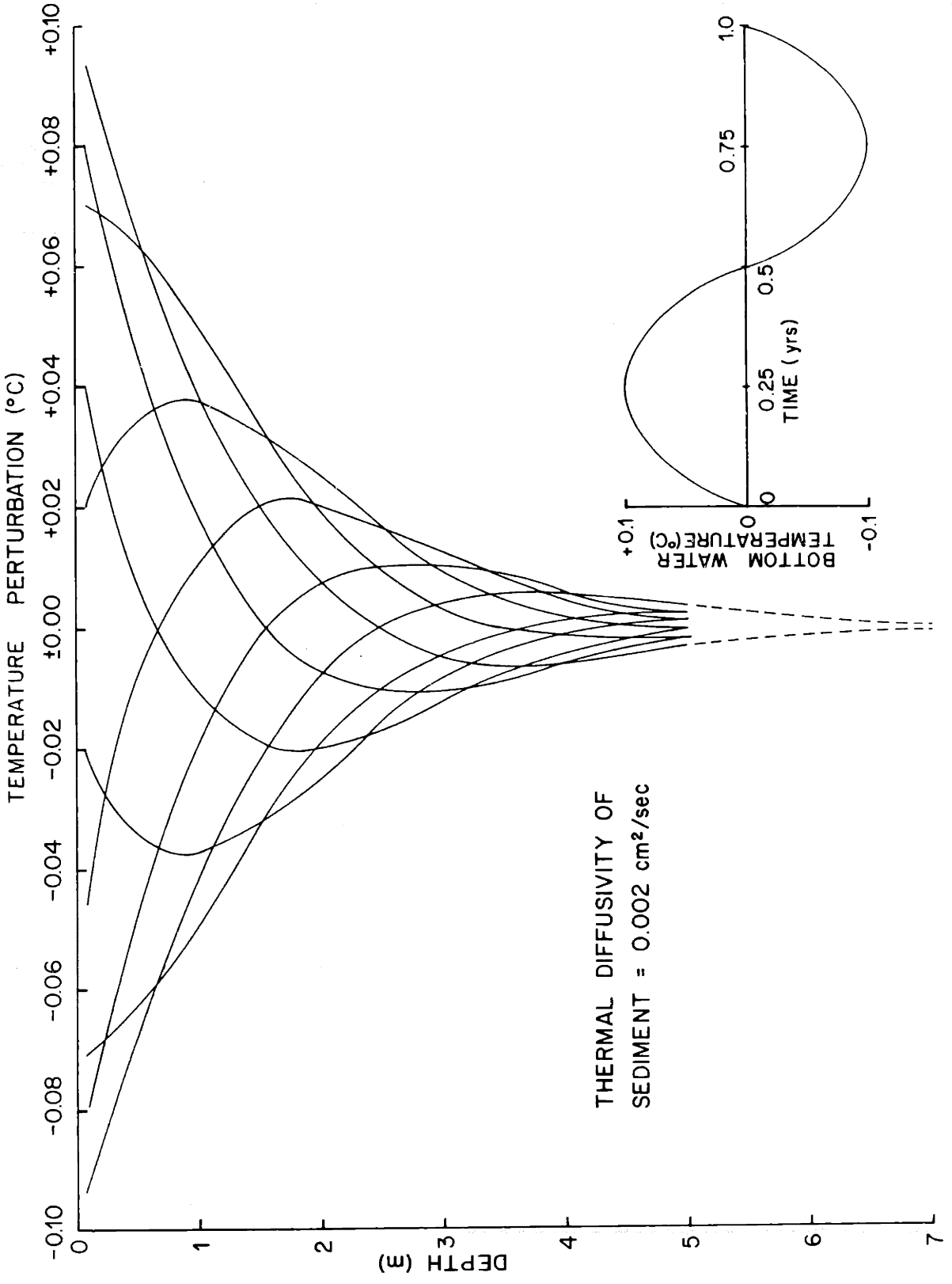
TEMPERATURE PERTURBATION (°C)
-0.10
-0.08
-0.06
-0.04
-0.02
±0.00
+0.02
+0.04
+0.06
+0.08
+0.10
DEPTH (m)
0
1
2
3
4
5
6
7
THERMAL DIFFUSIVITY OF
SEDIMENT = 0.002 cm²/sec
BOTTOM WATER
TEMPERATURE(°C)
+0.1
0
-0.1
0
0.25
0.5
0.75
1.0
TIME (yrs)

Figure 23

with the equipment and measurement techniques used to obtain the heat flow data. Nonlinear gradients are generally absent beneath the Mediterranean Sea, and where present in the Black Sea are of a different form (see Sections 2.322 and 2.523).

Gradual changes in bottom water temperature in response to long-term changes in climate can affect the thermal gradient in the sediment to depths of hundreds or even thousands of meters beneath the seafloor. Although the perturbation to the equilibrium thermal gradient may be large, the curvature of the gradient is usually too small to be detectable by temperature measurements over an interval of a few tens of meters or less. The Black and Mediterranean Seas have responded thermally to the series of glacial and interglacial periods which have characterized the Late Pleistocene. The way in which they have responded is poorly understood.

The method of Birch (1948) can be used to estimate the relative importance of past climatic variations on the geothermal gradient. Birch approximated the thermal history of the earth by breaking up the whole interval of time into smaller intervals, over each of which the surface temperature was considered to be constant. The temperatures disturbance $T(x,t)$ at the depth x in a semi-infinite slab of uniform diffusivity k, due to a temperature disturbance of amplitude $\Delta T(t)$ and duration Δt, ending t years ago is

$$T(x,t) = \Delta T(t) \cdot W(t, \Delta t, k, x) \qquad \text{Equation 1}$$

where

$$W(t, \Delta t, k, x) = Erf\left[\frac{x}{\sqrt{4k(t-\Delta t)}}\right] - Erf\left[\frac{x}{\sqrt{4kt}}\right] \qquad \text{Equation 2}$$

W(t, Δt, k, x) can be viewed as a weighting function which is a measure of the contribution of a past thermal event at the surface to the temperature at depth x. The weighting function is highly sensitive to the depth x. Figure 24 shows the sum of the weighting function for depths of 2, 5, and 10 meters beneath the seafloor.

When estimating the effect of changes in water temperature on the thermal gradient in the upper 10 m of sediment, it is only necessary to include the effect of variations which have occurred during the Holocene. For sediment with thermal diffusivity of 0.002 cm^2/sec, over 90% of the effect of thermal events of equal amplitude and duration is due to events which have occurred within the last 1000 years; 69% is caused by changes during the last 100 years.

2.24 Topography and Irregular Sediment Thickness

Because the sea floor is nearly an isothermal surface,

Figure 24. Cumulative weighting function for the effect of past thermal disturbances on the present temperature distribution in the sediment, computed for depths of 2, 5, and 10 m below the sea floor. For depths less than 10 m, almost all of the effect on the thermal gradient is due to climatic events within the last 1000 yrs.

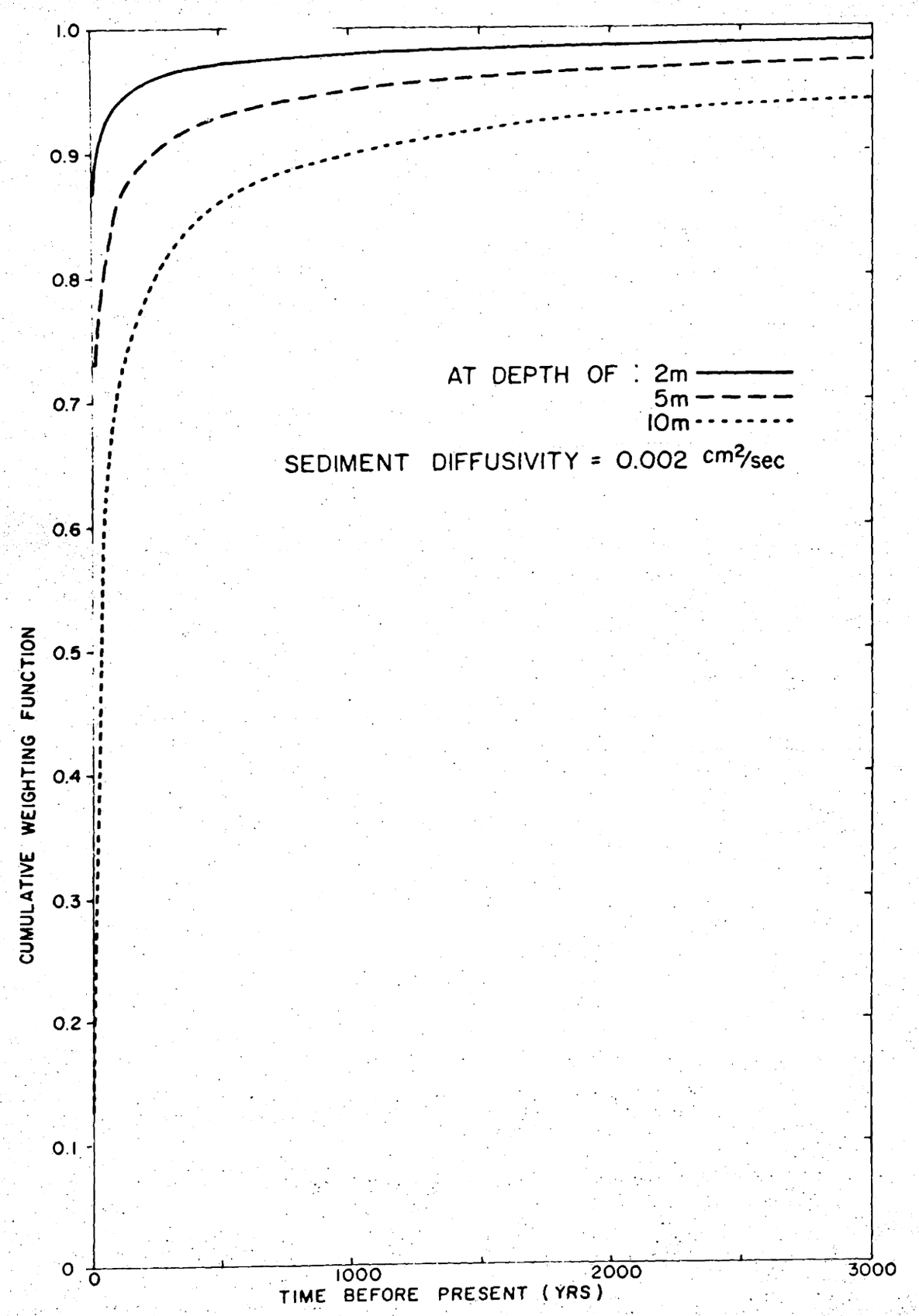
1.0
0.9
0.8
0.7
0.6
0.5
0.4
0.3
0.2
0.1
0
CUMULATIVE WEIGHTING FUNCTION
AT DEPTH OF : 2m
5m
10m
SEDIMENT DIFFUSIVITY = 0.002 cm²/sec
0
1000
2000
3000
TIME BEFORE PRESENT (YRS)

Figure 24

isotherms diverge beneath topographic highs and converge beneath depressions. Such changes in the isotherms alter the local gradient. Methods of estimating the magnitude of the effect were discussed by Lachenbruch (1968) and Jaeger (1965). The effect of topographic features on the geothermal gradient is not large as long as the height of the feature is both less than the horizontal distance to the measurement point and less than the depth of measurement (Lachenbruch, 1968).

Because most marine heat flow measurements are made over a depth interval of less than 20 m beneath the sea floor, small-scale topography can influence the observed gradient. Special survey techniques using deep-towed echo sounders are required to detect short-wavelenth topography on this scale. These techniques were applied by Sclater, Mudie, and Harrison (1970) to assist in the interpretation of heat flow measurements on the Hawaiian arch. They concluded that the observed topographic relief could not account for all of the observed scatter in the heat flow measurements. Although the small-scale topography of the Mediterranean and Black Seas is virtually unknown, very rough bottom relief was photographed at several locations on the Mediterranean ridge in areas where intense short-wavelength deformation was apparent from continuous seismic reflection data.

Deposition of the largely terrigenous sediment accumulating in the Mediterranean and Black Seas is

strongly controlled by sea floor topography. Turbidity currents and slumping off of the sides of elevated areas cause thick accumulations of sediment in topographic lows and reduced thicknesses on slopes and elevations. The thermal conductivity of ocean sediment is 2 or 3 times lower than the conductivity of the basement beneath the sediment. This contrast in thermal conductivity results in the refraction of heat through areas with little or no sediment cover, and relatively low heat flux through more thickly sedimented parts of the sea floor.

The magnitude of the refractive or topographic effects can be expressed in analytical form for a few simple geometries (see Von Herzen and Uyeda, 1963; Bullard et al., 1956; Lachenbruch and Marshall, 1966). A numerical technique was developed by Sclater et al. (unpublished manuscript, 1968) to estimate the effects of both topography and irregular sediment cover on the geothermal gradient. Although a combination of a deep sediment basin and sharp topographic relief can produce a narrow region of heat flow at the edge of the basin, the presence of even a thin layer of sediment beyond the edge of the basin causes a marked reduction in the amplitude of the positive anomaly (see Figure 25).

In conclusion, topography and irregular thicknesses of poorly-conducting sediment on the sea floor can produce locally high or low heat flow values, and, in regions of rough sub-bottom and sea floor relief, can

Figure 25. The computed relative heat flow across a sediment-filled hemi-cylindrical depression of radius R covered with sediment layers 0.1R and 0.3R thick. The thermal conductivity of the basement is assumed to be 3 times the conductivity of the sediemt, and heat flow is assumed to be uniform at depth. True-scale models of the sub-bottom topography are shown below the profiles. From Sclater, Jones, and Miller (1968).

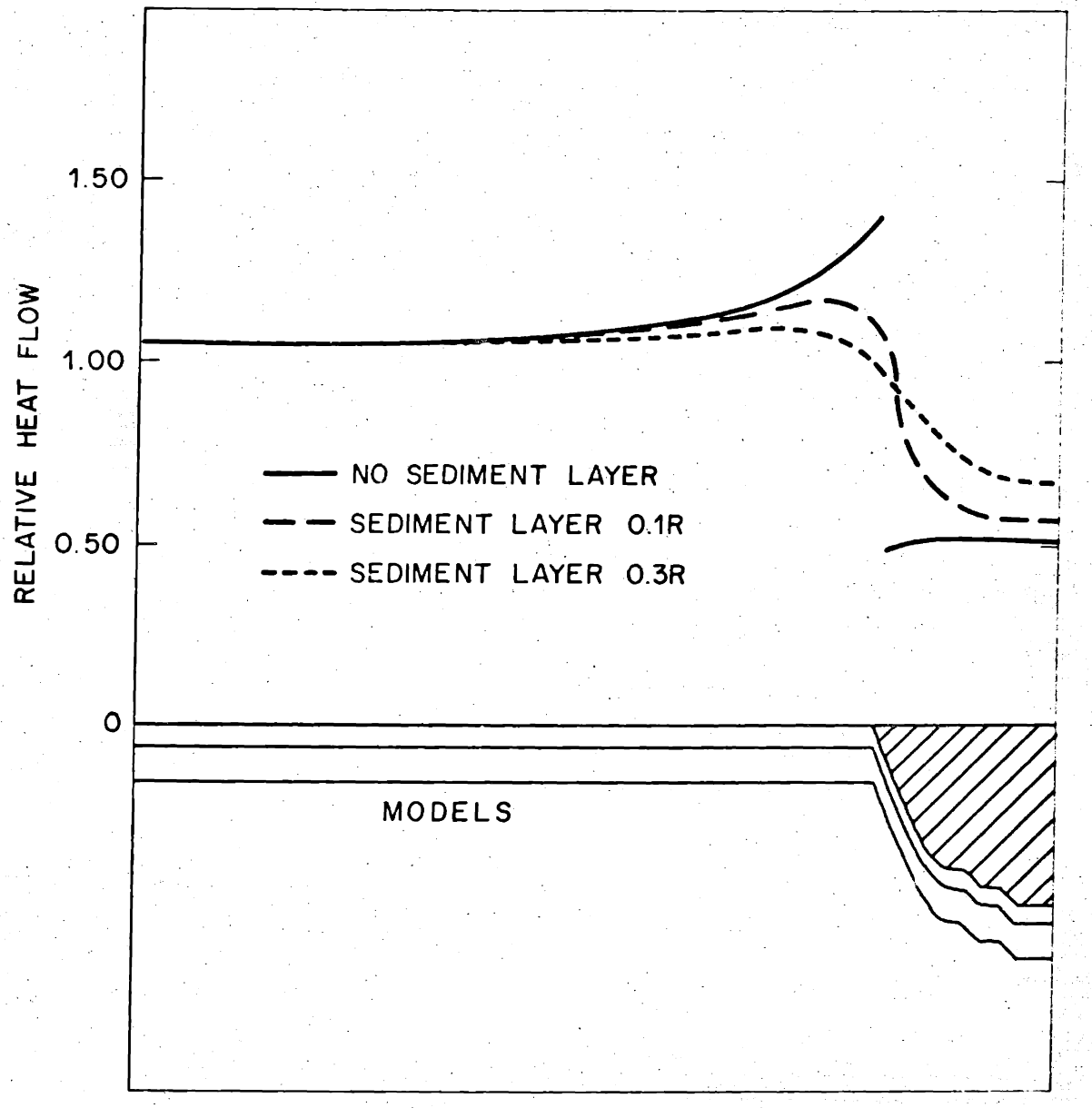
1.50
1.00
0.50
0
RELATIVE HEAT FLOW
NO SEDIMENT LAYER
SEDIMENT LAYER 0.1R
SEDIMENT LAYER 0.3R
MODELS

Figure 25

account for much or all of the observed variability. In order to make reliable corrections to the observed heat flow values it is necessary to know the sea floor and sub-bottom topography in the vicinity of the thermal gradient measurement on regional, and even more important, on local scales. This data is unavailable for most measurements discussed in this manuscript, and only qualitative estimates are possible.

2.25 Movement of Water in Sediments

Water moving through sediment can carry significant amounts of heat by mass transport. The resultant increase in the effective thermal conductivity of the sediment reduces both the thermal gradient and the heat flow value computed on the assumption that heat is flowing by conduction only. Movement of water through sediments can occur through convection of interstitial water, through migration of interstitial water during compaction and lithification, and through forced local submarine discharge.

Upward movement of interstitial water, and thus mass transport of heat, can occur from the uniform expulsion of water due to sediment compaction. Lubimova et al. (1965) concluded that very small velocities of migration of interstitial water could increase the thermal gradient near the seafloor, and that the thermal gradient

would decrease rapidly with depth to its conductive value.

The thermal gradient at the sea floor is given by

$$dT/dz\Big|_{z=0} = g_o \exp(v\rho c\ell/K)$$

where v is the velocity of migration, ρ, c, and K the density, heat capacity, and thermal conductivity of the interstitial water, respectively, ℓ the thickness of the layer through which the water is migrating, and g_o the thermal gradient unaffected by mass transport (Lubimova et al., p.85, 1965). Under steady-state conditions, the velocity with which water migrates upward cannot exceed the sedimentation rate. Sedimentation rates in the Mediterranean or Black Seas are less than 1 m/1000 yrs (Wong and Zarudzki, 1970; Ryan, 1969b). Substituting v = 0.1 cm/yr, ρ = 1 gm/cm^3, c = 1 cal/^{o}C gm, K = 1.3 mcal/^{o}C cm sec, and $\ell = 10^4$ cm, the thermal gradient at the seafloor is 1.022 g_o. If the thickness of the layer and/or the sedimentation rate is increased, the effect of the migration of interstitial water on the thermal gradient may be significant. The high sedimentation rate and great sediment thickness in the Black Sea may provide an environment where this effect is important, although it is difficult to manipulate ℓ and v so as to provide the increase in the thermal gradient observed in the upper few meters beneath the seafloor in the Black Sea and still maintain ℓ and v within realistic limits.

2.26 Biochemical Heating

The amount of heat produced or absorbed in biochemical reactions in deep-sea sediments appears to be insignificant compared to heat flowing through the sediments in almost all marine environments (Bullard et al., 1956). Zobell et al. (1953) observed abnormally high temperatures to depths of 10 m beneath the floor of Lake Mead. They attributed the high temperatures to heat released in exothermic reactions accompanying the oxidation of the organic material in the mud through bacterial action. Marked increases in the thermal gradient were observed within the upper few meters of sediment beneath many parts of the Black Sea, and are shown in Figure 26. Black Sea sediments contain as much as 35 weight percent organic material and Liston (1968) noted that surface sediments in estuarine areas of Washington and Oregon contain up to 10^6 bacteria per gram--much higher counts than are characteristic of the open ocean. These observations, plus the difficulty of explaining the gradient increase in terms of changes in water temperature (see Section 3.312), suggest that reinvestigation of the problem may be worthwhile.

Carslaw and Jaeger (p. 79, 1959) provided the solution to the problem in which heat is produced at a constant rate A in a layer of thickness ℓ beneath a surface maintained at a constant temperature. In the

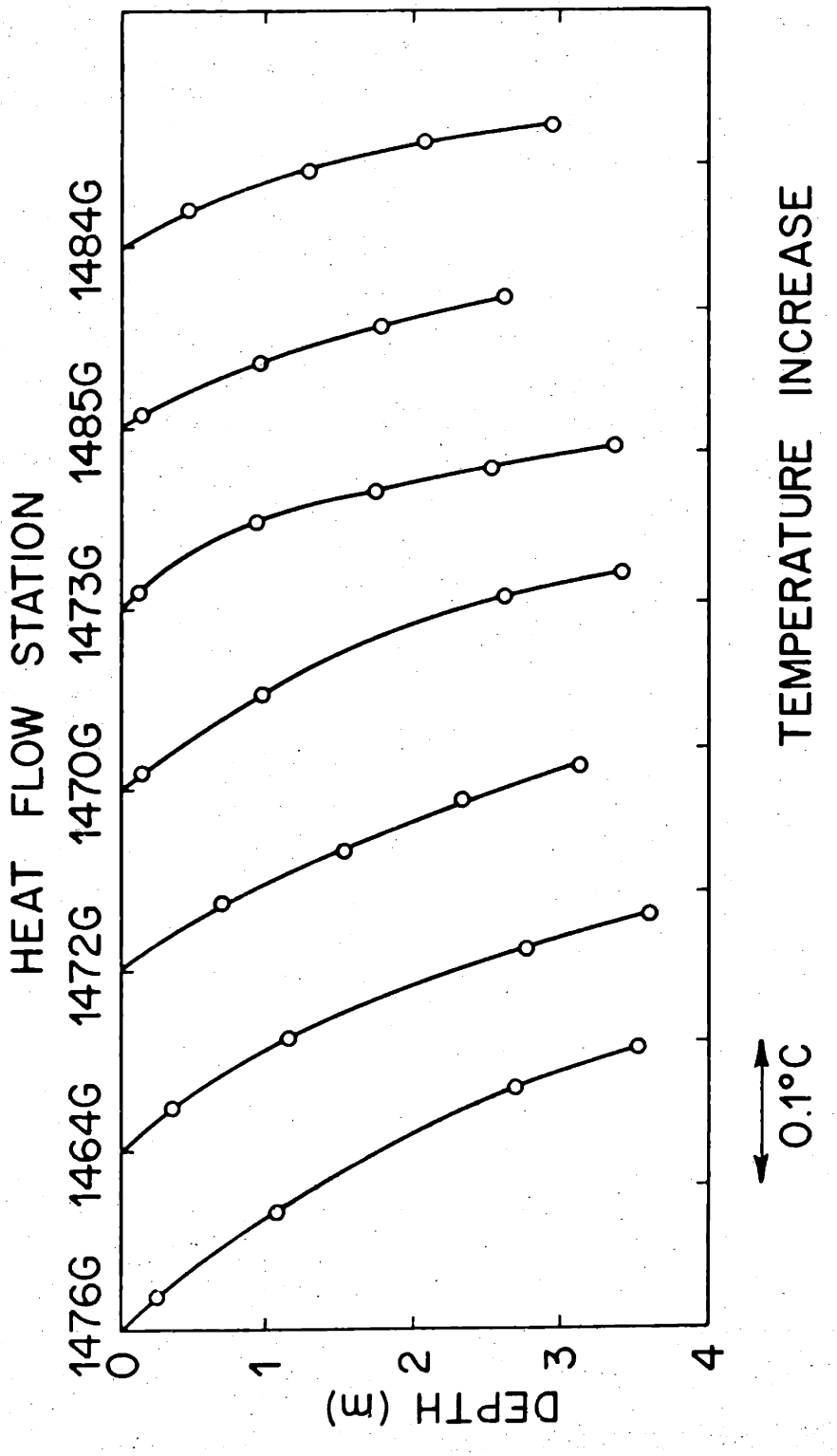

Figure 26. Typical non-linear temperature-depth profiles observed in sediment beneath the Black Sea.

steady state approximation, the temperature gradient G at the surface due to heat produced within the layer is given by Equation 1, where K is the thermal conductivity of the sediment, estimated as 2 KU.

$$G = \frac{A\ell}{K} \qquad \text{Equation 1}$$

Analysis of the shapes of the thermal gradients shown in Figure 26 suggests that the value of ℓ is between 1 and 10 m, and that the thermal gradient at the sediment surface is about 0.05 $^{o}C/m$ higher than the thermal gradient at depths below which the gradient is constant with depth. Substitution of these values into Equation 1 yields a value between 10^{-8} and 10^{-9} cal/cm^3sec for the heat production in the Black Sea sediments. In comparison, for Lake Mead sediments with a measured bacterial population of 10^6 to 10^7 per gram, a sediment density of 2 gm/cm^3, and an experimentally determined value for heat production of 8.3×10^{-15} calories per bacterial cell per second, Zobell et al. (1953) calculated that heat was being generated at a rate of 2×10^{-8} to 2×10^{-9} cal/cm^3sec in the Lake Mead mud.

The approximate agreement between the heat production rates calculated for Lake Mead and required in the Black Sea suggests that the anomalous gradients observed beneath the Black Sea could be produced if biochemical reactions analogous to those taking place beneath Lake

Mead were occurring in the Black Sea sediments.

2.3 WESTERN MEDITERRANEAN

2.31 Presentation of Data

The locations of 22 new and 3 published heat flow measurements in the western Mediterranean Sea are shown in Figure 27. Station parameters and other information for all of the new measurements are presented in Tables 3 and 4. The 3 published heat flow values were described in Table 1.

2.32 Environmental Corrections

2.321 Sedimentation

Geological and geophysical data can be interpreted as indicating a late Miocene-Early Pliocene origin for the western Mediterranean basin (DeBoov, 1969; Pannekoek, 1969). In calculating the sedimentation correction for the western Mediterranean basin, it was assumed that the most recent cycle of sedimentation began roughly 15 m.y. ago, and continued at a constant rate to the present time. The thickness of the sediment column was estimated from Fahlquist's (1963) deep water seismic refraction profiles 194, 195, 4 and 5.

The maximum estimate for the thickness of the sediment column was obtained by identifying material with a compressional velocity less than 4.53 km/sec as sediment in various stages of consolidation. This assumption lead to a value of 4.72 km for the average sediment

WESTERN MEDITERRANEAN HEAT FLOW STATIONS

Station Number	Position Lat.	Long.	Depth (corr. m)	Seafloor Description	Penetration (m)	Probes
CT-17	38°58'N	14°11'E	3504	Smooth plain at base of continental rise north of Sicily	6.8	5
CT-29	39°20'N	13°44'E	3497	Smooth plain north of Sicily	6.3	5
CT-31	39°28'N	13°20'E	3545	Smooth plain south-east of Tyrrhenian Abyssal Plain	10.3	7
CT-32	39°35'N	12°53'E	3590	Southeast tip of Tyrrhenian Abyssal Plain	16.0	8
CT-50	40°28'N	12°10'E	3416	Immediately north-west of Tyrrhenian Abyssal Plain	8.8	3
CT-53	41°30'N	11°59'E	3502	Immediately north-west of Tvrrhenian Abyssal Plain	8.4	5

Table 3-1

WESTERN MEDITERRANEAN HEAT FLOW STATIONS

Station Number	Position Lat.	Long.	Depth (corr. m)	Seafloor Description	Penetration (m)	Probes
CT-54	40°05'N	12°11'E	3617	Eastern Tyrrhenian Abyssal Plain	10.6	5
CT-55	40°21'N	11°16'E	2889	Gently sloping plain east of Sardinia	11.9	6
CT-77	39°54'N	10°35'E	2512	Gently sloping plain east of Sardinia	1.0	6
CT-78	39°24'N	10°41'E	2785	Gently sloping plain east of Sardinia	12.0	7
CT-79	39°11'N	13°00'E	3441	Gently sloping plain northwest of Sicily	9.9	5
CH61-19	35°47'N	13°09'E	1525	Horizontally stratified sediment pond south of Sicily	11.5	5
C9-131	40°19'N	12°33'E	3579	Tyrrhenian Abyssal Plain	10.0	3

Table 3-2

WESTERN MEDITERRANEAN HEAT FLOW STATIONS

Station Number	Position Lat.	Long.	Depth (corr. m)	Seafloor Description	Penetration (m)	Probes
C9-132	40°46'N	11°07'E	2338	Side of hill east of Sardinia	13.5	4
C9-133	41°33'N	08°01'E	2699	East of northern tip of Balearic Basin	10.1	4
C9-134	41°59'N	06°54'E	2703	Balearic Basin near base of Rhone Fan	11.5	4
C9-135	41°37'N	05°18'E	2395	Rhone Fan north of Balearic Abyssal Plain	6.3	2
C9-136	39°03'N	04°26'E	2332	Sediment covered slope south of Balearic Platform	11.2	4
C9-137	38°24'N	03°58'E	2659	Sediment covered escarpment south of Balearic Abyssal Plain	11.9	4

Table 3-3

WESTERN MEDITERRANEAN HEAT FLOW STATIONS

Station Number	Position Lat.	Long.	Depth (corr. m)	Seafloor Description	Penetration (m)	Probes
C9-138	37°12'N	01°58'E	2783	Southern Balearic Abyssal Plain	10.9	3
C9-139	37°50'N	00°44'E	2701	Southern Balearic Abyssal Plain	12.0	3
C9-140	36°10'N	02°01'W	1286	Rise west of Balearic Abyssal Plain	10.2	3
C9-141	35°59'N	04°02'W	1375	Alboran Abyssal Plain	11.2	3

Table 3-4

WESTERN MEDITERRANEAN HEAT FLOW DATA

STATION NUMBER	THERMAL GRADIENT ($°C/m \times 10^{-2}$)	THERMAL CONDUCTIVITY No.Meas.	Average (mcal/cm sec °C)	OBSERVED HEAT FLOW (HFU)
CT-17	15.10±0.20	19	2.20±0.17	3.32±0.33
CT-29	17.50±0.11	21	2.06±0.15	3.61±0.41
CT-31	15.20±0.40	35	2.12±0.19	3.23±0.32
CT-32	12.20±0.40	37	2.13±0.18	2.60±0.26
CT-50	18.60±2.19	13	2.22±0.16	4.14±0.70
CT-53	5.60±0.24	12	2.47±0.31	1.38±0.14
CT-54	18.20±1.80	23	2.15±0.15	3.92±0.58
CT-55	13.40±0.50	25	2.30±0.19	3.09±0.31
CT-78	12.60±0.71	24	2.41±0.18	3.04±0.32
CT-79	15.80±0.30	25	2.12±0.16	3.35±0.34
CH61-19	5.45±0.33	24	2.20±0.16	1.20±0.13
C9-131	3.22±0.55		(2.24)	0.72±0.19
C9-132	6.23±1.12		2.49	1.55±0.35

Table 4-1

WESTERN MEDITERRANEAN HEAT FLOW DATA

STATION NUMBER	THERMAL GRADIENT (°C/m x 10^{-2})	THERMAL CONDUCTIVITY* No.Meas.	Average (mcal/cm sec °C)	OBSERVED HEAT FLOW (HFU)
C9-133	6.35±0.32		3.06	1.94±0.19
C9-134	7.48±1.50		2.78	2.08±0.52
C9-135	5.61±0.56		(2.49)	1.39±0.28
C9-136	6.39±0.95		3.02	1.93±0.38
C9-137	7.20±0.36		2.91	2.10±0.21
C9-138	11.20±1.17		2.81	3.15±0.48
C9-139	4.82±0.60		(2.81)	1.35±0.24
C9-140	3.08±0.77		2.55	0.79±0.24
C9-141	9.51±0.75		(2.43)	2.22±0.40

*Conductivity values in parentheses are estimated on the basis of data from nearby stations.

Table 4-2

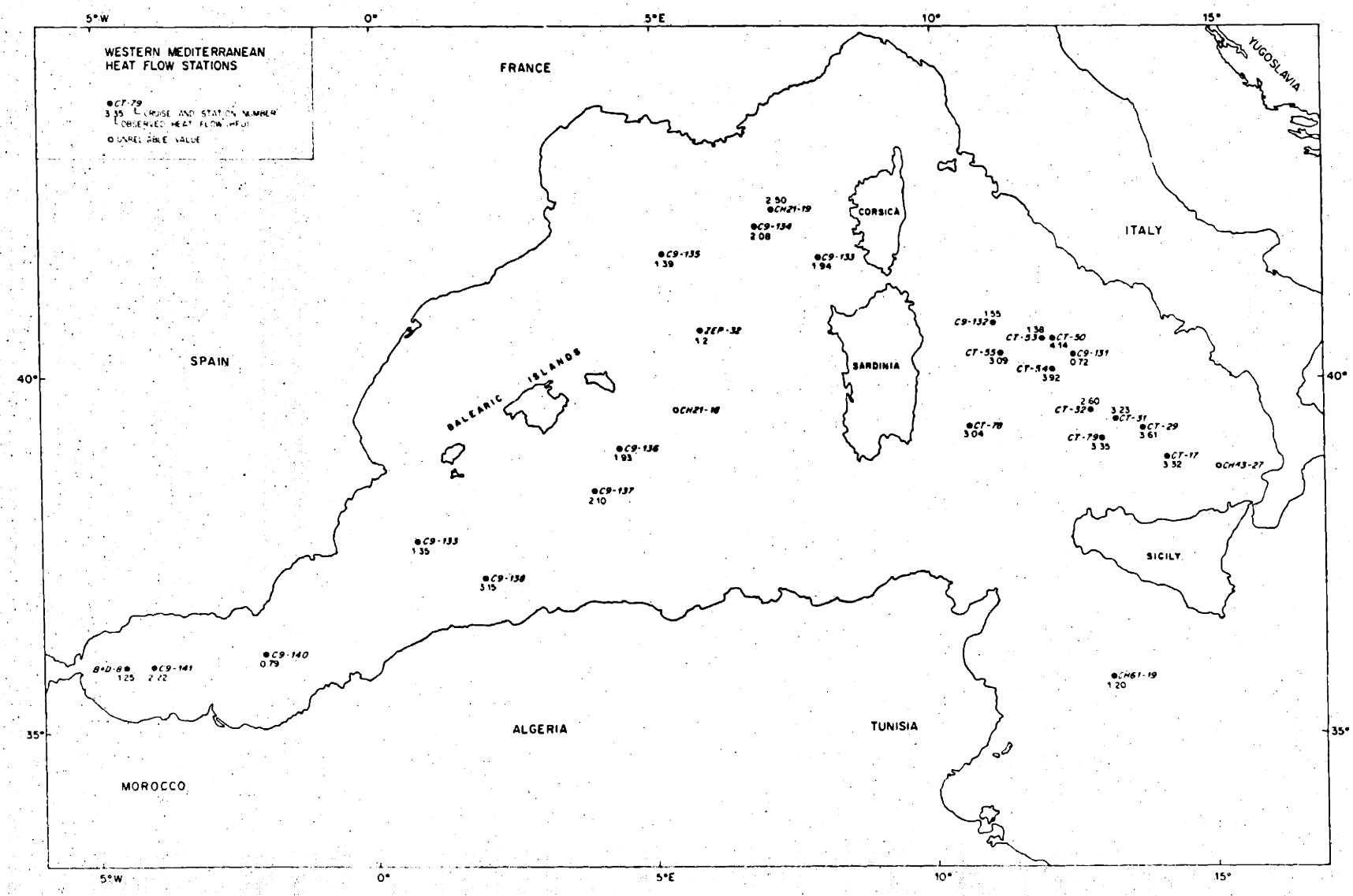

Figure 27. Locations of heat flow stations in the western Mediterranean Sea

thickness. It is unlikely that in Upper Tertiary sedimentary material compressional wave velocities exceed 4.0 km/sec. Well-lithified limestones can possess velocities this high, however the probable large terrigenous component to sedimentation from erosion of the Late Tertiary mountain ranges adjacent to the western Mediterranean would make deposition of limestones unlikely. Seismic velocities less than or equal to 4.2 km/sec were observed for Upper Cretaceous sediments on the Blake plateau, and velocities between 5.5 and 6.0 km/sec were associated with Lower Cretaceous or older material (Drake, Ewing, and Stockard, 1968). The possibility exists that these low and intermediate range velocity layers are consolidated Paleozoic or Mesozoic sediments, meta-sediments, or crystalline rocks exposed after a long erosional history, as discussed by Aubouin (1965). However, for estimation of the sedimentation correction it is still valid to define the base of the sedimentary sequence as the first sediments to be deposited in the most recent cycle of sedimentation, provided that thermal equilibrium was established in the underlying crust before sedimentation began. On the assumption that refracting material with velocities as high as 4.53 km/sec are associated with Upper Tertiary sediments, the average thickness of the sediment column in the western Mediterranean basin is 4.72 km.

Hamilton (1959) provided guidelines for determining

the original thickness of unconsolidated sediment represented by the unconsolidated, semi-consolidated, and consolidated sediment now on the sea floor. He noted that "the behavior of Globigerina ooze, or calcareous ooze, under gravitional pressure, should follow the expectable consolidation curve for sandy silt or silty sand", and that "calcareous ooze should show a faster decrease in porosity than typical quartz-particle sediments", as a result of many of the calcareous grains being hollow shells of calcium carbonate. Thus Hamilton's Globigerina ooze curve, shown in Figure 28, provides an upper limit on the unconsolidated sediment thickness. Extrapolating this curve, an unconsolidated thickness of 6.6 km is indicated.

The average sedimentation rate of 44 cm/1000 yrs, obtained by dividing this thickness by its age, estimated at 15 m.y., is comparable with the value of 35 cm/1000 yrs estimated by Ericksson (1965) for the Balearic abyssal plain. Using a value of 0.002 cm^2/sec for the thermal diffusivity of the unconsolidated sediment, the equilibrium thermal gradient should be reduced by nearly 50 %. Thus the equilibrium heat flow is twice the observed flux, and is estimated as 3.66 HFU. This average value is substantially higher than the mean heat flux through other small ocean basins or from deep ocean basins, although even higher values are associated with mid-ocean ridges and rift-like features. On the basis of the un-

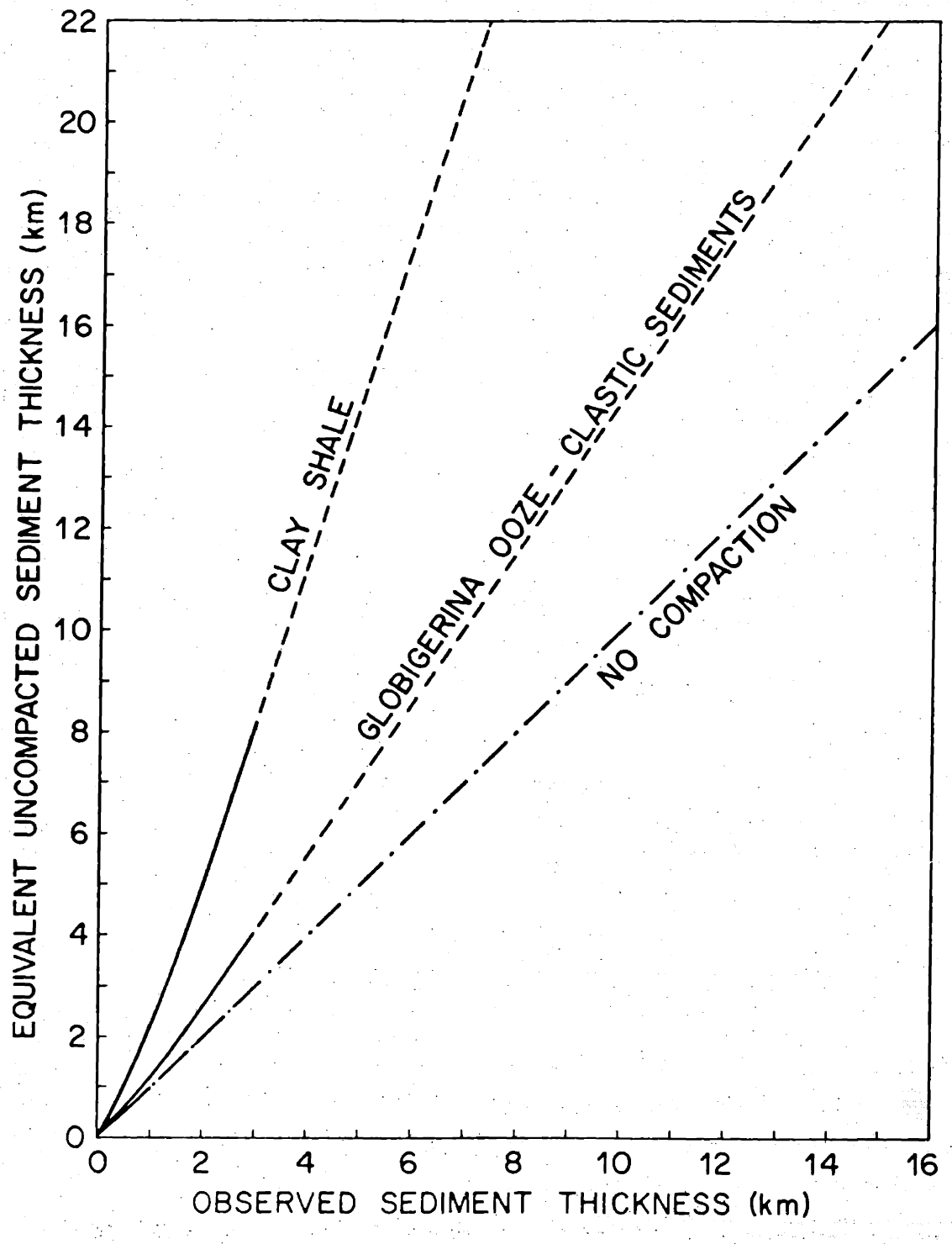

Figure 28. Thickness of uncompacted sediment equivalent to observed thicknesses of clay-shale and globigerina ooze or clastic material. Drawn from Hamilton (Table 4, 1959).

usually high seismic velocity which must be attributed to the Neocene marine sediments, the discrepancy between the observed and the computed sedimentation rates, and the unusually high equilibrium heat flow calculated from the resultant sedimentation correction, it is considered likely that material with refracting velocities greater than 4.0 km/sec should not be included in the most recent sediment column.

Recalculating the sediment thickness under this assumption, an average thickness of 2.61 km is found to overlay material with a velocity greater than 4.0 km/sec. The equivalent unconsolidated thickness is 3.45 km (Hamilton , 1959), and the resultant sedimentation rate becomes 23 cm/1000 yrs. Sedimentation at this rate for 15 m.y. would reduce the observed heat flow by about 33 ⅓, and would suggest an average heat flow of 2.73 HFU through the western Mediterranean basin.

It is necessary to assume an age for the Tyrrhenian basin in order to estimate an average sedimentation rate and duration. Although many different hypotheses have been advanced for the origin of the Tyrrhenian Sea, most have in common an Early or Middle Pliocene age for the subsidence of the land mass from which the flysch now found in the Appennines, on Sicily, Corsica, Sardinia, and in southern France, was derived. For this reason the duration of sedimentation is estimated as 10 m.y.

An average thickness of about 0.3 km of unconsolidated

sediment rests on about 2.5 km of material with a velocity of 4.0 to 6.0 km/sec beneath most of the Tyrrhenian Sea. The Tyrrhenian abyssal plain consists of a sedimentary layer with an average thickness of nearly 1 km (Ryan et al., 1965), again underlain by 4.0 to 6.0 km/sec material.

The identity of the intermediate velocity layers is uncertain. Michno (1963) and Moskalenko (1967) associated the 4.0 to 6.0 km/sec layers with well-consolidated sediment, whereas Ritsema (1969a) stated that the low-velocity crustal layers were young volcanic material. Ryan (1969a) also suggested a volcanic origin for this material, mainly on the basis of its greater thickness in regions where volcanic seamounts and ridges are located. Fahlquist noted the similarity between the crustal structure of the Tyrrhenian basin and that determined by Officer et al. (1952) for portions of the Bermuda platform, where the 4.0 to 4.5 km/sec layer material was tentatively identified as volcanics, sediments, and pyroclastics.

The heat flow measurements in the Tyrrhenian Sea are located either in the deep-water margins of the basin or on the abyssal plain; thus an average thickness of about 1.0 km of unconsolidated sediment is probably present above the 4.0 to 6.0 km/sec layer. Using Hamilton's (1959) Globigerina ooze curve (Figure 28), the uncompacted sediment thickness is about 1.20 km, leading to the conclusion that sedimentation has taken place at

the rate of 12.0 cm/1000 yrs for 10 m.y., and has reduced the equilibrium thermal gradient by about 9%.

The sedimentation rate calculated in this way is much smaller than the value of 100 cm/1000 yrs estimated from cores taken on the Tyrrhenian abyssal plain by Ryan et al. (1965), who based his estimate on the thickness of sediment above and between layers of volcanic ash tentatively identified with subareal eruptions of volcanoes of known age. This discrepancy is not a serious objection to limiting the sediment column to low-velocity material, since it is probable that the sedimentation rate has been higher during the glacial Pleistocene than during the Pliocene. Sedimentation at the rate of 100 cm/1000 yrs would account for all of the sediment in the Tyrrhenian Sea in less than 1 m.y. The widespread existence of an acoustically transparent layer, conformable to the basement topography and overlain by horiziontally stratified turbidite layers, is indicative of the rapid deposition of primarily terrigenous material which began during the Pleistocene (Ryan, 1969a).

If the 4.0 to 6.0 km/sec material is included in the sedimentary column, the total sediment thickness is 2.5 km, equivalent to 3.3 km of uncompacted sediment. Sedimentation at an average rate of 33 cm/1000 yrs for 10 m.y. is required to produce this thickness and would result in a 40 % reduction in the observed thermal gradient. The observed average heat flow would have to

then be raised to 4.72 HFU to compensate for the effect of sedimentation.

The presence of short-wavelength, high amplitude magnetic anomalies, volcanic seamounts, and abnormally high heat flow in the southern Tyrrhenian Sea makes it probable that the 4.0 to 6.0 km/sec material is of volcanic, rather than sedimentary origin. Thus a reduction of the thermal gradient of 9%, rather than 40%, is favored in the computation of the equilibrium heat flux. The regional heat flow through the floor of the Tyrrhenian Sea is estimated as 3.11 HFU.

2.322 Water Temperature Variations in the Mediterranean Sea

Western Mediterranean bottom water is produced by the cooling and consequence sinking of surface water in the vicinity of northern Corsica and the Ligurian Sea during winter storms (Miller, 1963). The primary source of eastern Mediterranean bottom water is the northern and central Adriatic Sea where water cooled to 12.6°C during the winter months sporadically spills through the Straits of Otranto and flows along the floor of the Ionian Sea (Pollack, 1951). Other sources include the cooling and sinking of water at the surface of the Ionian Sea during periods of cold, stormy weather, and the production within the Aegean Sea of dense, saline water which flows south into the Levantine basin (Ovchinnikov and Plakhin, 1965).

The change in bottom water temperature due to the displacement of the bottom water by denser water depends upon both the salinity and temperature of the water masses. Within the western Mediterranean, newly created bottom water is more saline, as well as cooler, than the former bottom water; thus only a small decrease in temperature is required to provide the additional density necessary to displace the existing bottom water. The seasonal bottom water temperature change observed by Miller (1963) was less than 0.2°C, in good agreement with values ranging from 0.05 to 0.14°C estimated from observations that 1., newly created bottom water has a temperature of 12.60 to 12.65°C (Ovchinnikov and Plakhin, 1965), and 2., that the deepest areas of the Balearic and Tyrrhenian basins are characterized by very uniform temperatures of 12.65°C and 12.74°C, respectively. (Wüst, 1961).

Aegean bottom water is 0.6 to 0.7°C warmer than the water it displaces because its excess density is largely due to its very high salinity. There is little evidence from hydrographic data that Aegean bottom water has a significant effect upon the temperature distribution in eastern Mediterranean bottom water (Pollak, 1951, Wüst, 1961).

Adriatic bottom water is formed by the mixture of Ionian Sea water from intermediate depths and fresh water entering the Adriatic Sea from rivers to the north.

The transformation of this relatively low salinity water to Adriatic bottom water denser than the Ionian Sea bottom water requires a large temperature decrease of about 0.5°C. Cold, relatively fresh Adriatic bottom water flows southward in a thin layer along the bottom of the Ionian basin and then flows eastward. Its temperature and thickness gradually increase as it passes through the Levantine Sea (Ovchinnikov and Plakhin, 1965). The effect of the sudden appearance of a layer of cold (or warm) water above the seafloor on the thermal gradient in the sediment is thus strongly dependent upon the location, water depth, time of year, and other factors peculiar to each determination.

At only a few heat flow measurements in the Ionian Sea and in the extreme eastern Mediterranean was there any indication of a thermal gradient which is not constant with depth. At these stations the gradient is high near the sediment surface and becomes constant a few meters below the surface, as though cooler water had recently replaced warmer water above the sediment. The departure of the shallow temperature from the value estimated on the basis of the deeper probes exceeds 0.1°C in only one measurement (CH61-56). It is probable that some of the increase in the thermal gradient near the sea floor is due to a decrease in thermal conductivity caused by higher water content in the near-surface sediment. However, the downward increase in thermal conductivity

actually observed rarely exceeds 5% of the mean conductivity and precludes this as an important factor in the behaviour of the thermal gradient.

In summary, yearly replenishment of Mediterranean bottom water does not present a major problem for temperature measurements made deeper than a few meters below the sea floor, particularly where a sufficient number of temperature sensors is available to detect a non-linear temperature distribution.

The long-term thermal history of the Mediterranean is poorly known. Emiliani (1955a) estimated the temperature of the oceans during the Pleistocene making use of the principle that the O^{18}/O^{16} ratio in calcium carbonate precipitated from seawater is dependent upon the temperature at which precipitation occurs. The O^{18}/O^{16} ratios in benthonic foraminifera from the Atlantic, Caribbean, and Pacific Oceans are consistent with a temperature maxima about 6000 years ago, followed by a small temperature decrease. From a more detailed study of shells buried in coastal caves in North Africa and Italy, Emiliani et al. (1963) concluded that a rapid temperature increase began about 10,000 years ago and culminated in a marked post-glacial maximum extending from 6500 to 4500 years ago. A $2^{\circ}C$ temperature decrease occurred between 4800 and 4500 years ago, followed by a $1^{\circ}C$ rise which brought temperatures to their modern values.

A sudden and substantial change in both the tem-

perature and isotopic composition of the seawater in the Mediterranean and Black Seas was hypothesized by Ryan (1969b). Ryan noted that sapropelic layers in eastern Mediterranean sediment cores occur precisely near the peak of the warming trend of all the major, faunally defined, climatic temperature oscillations. He attributed the sapropelic layers to deposition during stagnant conditions caused by the sudden appearance of a large volume of cool, light, brackish Black Sea water on the surface of the eastern Mediterranean Sea. Rapid replacement of the cold Black Sea water by denser, more saline Mediterranean water is believed to have occurred when the influx of melt-water from the rapidly receding glaciers raised sea level above the -40 m sill depth separating the Black and Mediterranean Seas.

Temperatures estimated from the O^{18}/O^{16} ratio in pelagic foraminifera are related critically to the isotopic composition of the seawater. Evaporation increases the concentration of O^{18} in the fluid phase and produces a low O^{18}/O^{16} ratio in fresh water and continental ice sheets and a high O^{18}/O^{16} ratio in ocean water. Emiliani (1955b) attempted to correct for this effect in the Mediterranean, however the influx of melt water and changes in the circulation system during periods of low sea level could cause uncertainties in the amplitude of the observed temperature variations. Ryan's hypo-

thesis makes estimation of the isotopic ratio since the last glaciation extremely difficult. In addition, flushing of the Black Sea must have produced a major change in temperature, both within the Mediterranean and Black Seas. In conclusion, the late Pleistocene thermal history of the Mediterranean is not known in sufficient detail to justify the application of a correction to the observed thermal gradient.

2.33 Interpretation

The average of 12 heat flow measurements located in the western Mediterranean basin is 1.83 HFU, with a standard deviation of 0.66 HFU or 36%. Five of the measurements at which heat flow values ranged between 1.93 and 2.50 HFU were located on the margin of the Rhone fan, the Balearic island rise, and the Balearic abyssal plain. Heat flow values of 1.35 and 3.15 HFU were measured in the western end of the Balearic abyssal plain, near the area affected by the turbidity currents associated with the Orleansville earthquake (Heezen and Ewing, 1955). Although submarine cables were not broken in the immediate vicinity of either station, the relatively low heat flow (1.35 HFU) observed at station C9-139 could be the result of the sudden deposition of a thick layer of turbidite material. The extreme non-linearity of the thermal gradient at C9-135 supports the hypothesis that

a layer of warm water and sediment was deposited on the cooler seafloor, however the excess temperature of 0.25°C registered by the uppermost probe cannot be due to this cause. The temperature T(x,t) at time t and depth x in a half-space having a uniform thermal diffusivity of 0.002 cm^2/sec and having had an initial temperature ΔT to a depth of d, below which the temperature was initially zero and above which the temperature has been maintained at zero, is given by Carslaw and Jaeger (p. 62, 1959).

$$T(x,t) = \frac{\Delta T}{2}\left\{2\,\mathrm{erf}\frac{x}{\sqrt{4\kappa t}} - \mathrm{erf}\frac{x-d}{\sqrt{4\kappa t}} - \mathrm{erf}\frac{x+d}{\sqrt{4\kappa t}}\right\} \quad \text{Equation 1}$$

If 4 m of anomalously warm material having a thermal diffusivity of 0.002 cm^2/sec was deposited on the sea floor 16 years ago, the present excess temperature 2 m below the seafloor would be less than 1% of the initial excess temperature.

One heat flow measurement just west of the Balearic abyssal plain and two others on the Alboran abyssal plain yielded values of 0.79, 2.22, and 1.25 HFU, respectively. Their proximity to the steep, earthquake-prone north African continental slope and evidence for fault tectonics in the Alboran basin suggests that some of the variability may be due to sedimentation and topographic or refractive effects. However, the variability in the heat flux may actually reflect local variations in the

thermal properties of the upper mantle and crust.

Four reliable heat flow values are available from the Rhone fan (Figure 29). Three are situated at the base of the fan, near the northern Balearic abyssal plain. Station C9-135 is located well up on the fan in an area eroded by a system of large, disrupted, leveed channels that were possibly formed during the Pleistocene when Alpine glaciation and deglaciation introduced large volumes of relatively coarse sediment into the Rhone River (Menard, 1965). An average sedimentation rate of about 100 cm/1000 yrs was estimated on the basis of a Pleistocene age for the 1.3 km thick layer of the unconsolidated sediment beneath the center of the fan (Menard, 1965), leading to a 38% reduction in the equilibrium heat flow. The gradient may have already been reduced prior to the Pleistocene by the deposition of an average of 2.1 km of sediment now present beneath the unconsolidated layer. If deposition of most of this layer occurred since the elevation of Alpine structures after the Eocene, then the sedimentation at an average rate of 7.5 cm/1000 yrs for 36 m.y. would have reduced the gradient by 19% prior to the most recent sedimentation epoch. Thus the observed gradient may be only half (0.81 x 0.62) of the equilibrium gradient. It is probable that the observed heat flow of 1.39 HFU should be increased to 2.8 HFU in order to represent the steady state heat flux.

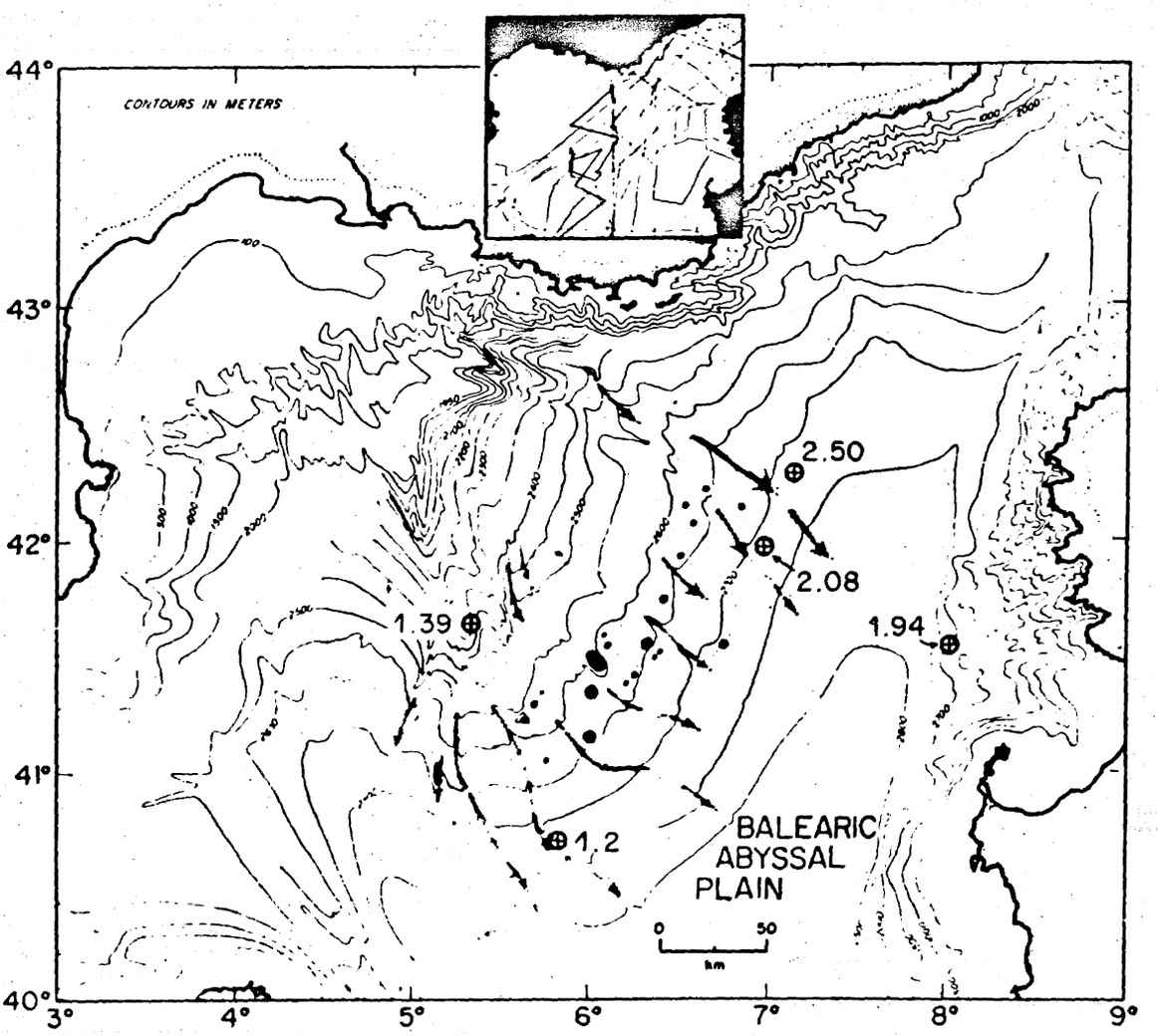

Figure 29. Bathymetric map of the Rhone fan and northern Balearic abyssal plain showing observed heat flow values in HFU. After Menard et al. (1965).

Two other reliable heat flow measurements on the northeastern margin of the fan have values of 2.50 and 2.08 HFU. The heat flow at station ZEP-32, which appears to be located either within or near a major channel at the southern edge of the fan, was reported as 1.2 HFU by Nason and Lee (1964). They noted that the measurement was of questionable value because of the effects of possible instabilities in bottom water temperature and a probable high sedimentation rate. The value of 1.2 HFU is lower than the regional average and may indeed reflect one or both of the perturbations suggested by Nason and Lee.

Twelve reliable heat flow values are available from the Tyrrhenian Sea, 10 of which were obtained by George Harlow with the cooperation of Italian scientists aboard the M. N. Bannock. Although the Tyrrhenian Sea has a relatively small abyssal plain, it is surrounded on the northeast and south by a broad, deformed, gently sloping continental slope. Heat flow values from the Tyrrhenian basin are strikingly high, with an average of 2.83 HFU and a standard deviation of 1.07 HFU, or 41%. The average of 4 measurements made in the basin southeast of the abyssal plain is 3.38 ± 0.16 HFU. The locations of heat flow values on or near the abyssal plain is shown in Figure 30. Values range from 0.72 to 3.92 HFU with a mean of 1.83 ± 0.66 HFU. The value of 0.72 HFU at station C9-131 was measured in a narrow abyssal channel connecting the

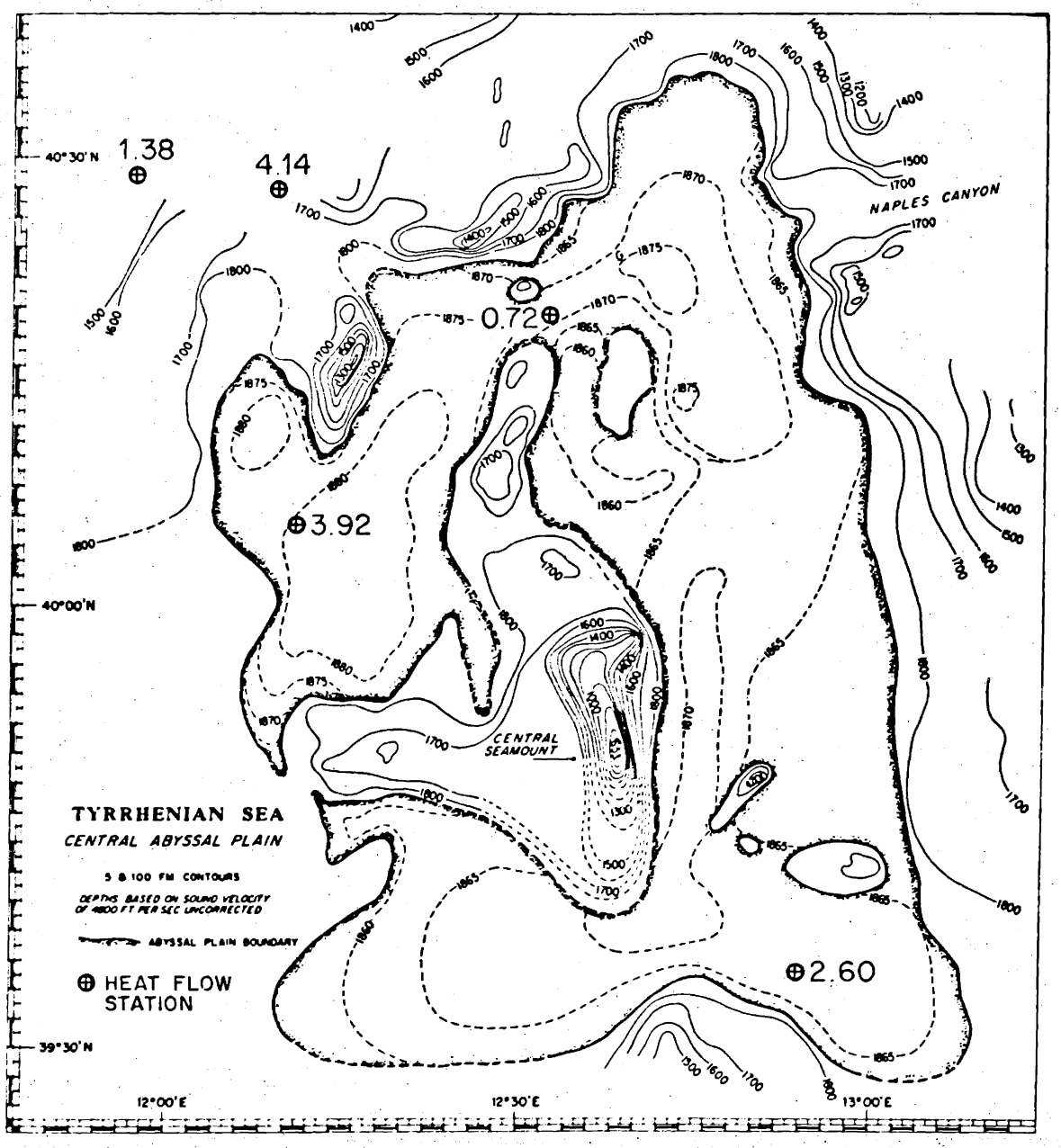

Figure 30. Bathymetric map of the Tyrhennian abyssal plain showing observed heat flow values in HFU. After Ryan et al. (1965).

slightly deeper western lobe with the eastern lobe of the Tyrrhenian abyssal plain. It is likely that the unusually low heat flow is due to sediment slumping off of the adjacent topographic highs. In addition, heat would tend to flow out through the higher thermal conductivity areas on either side of the sediment filled channel, further reducing the heat flux measured in the channel. Heat flow values of 2.60 and 3.92 HFU were found at stations CT-32, located in the southeastern corner of the abyssal plain, and CT-54, located in the western lobe, respectively. At stations CT-50 and CT-53, less than 20 km northwest of the abyssal plain, values of 4.14 and 1.38 HFU were obtained. The fact that significantly different heat flux was found at measurements only 10 km apart indicates that if the source of the variation is geophysical rather than environmental, it is located within the crust or uppermost mantle.

The average heat flow through the floor of the western Mediterranean, corrected for the effect of sedimentation, is 2.9 HFU, over twice as large as the world average heat flow of about 1.4 HFU (Langseth, 1969). Seven of the 12 heat flow values located west of the Tyrrhenian Sea exceed 1.90 HFU. All of the remaining 5 may be subject to environmental effects which could lower the observed heat flow substantially; two measurements are located on the thickly sedimented Rhone fan, two more in a topographically rough region of the Alboran basin, and one in the extreme

western Balearic basin at the base of the Balearic island rise. The average corrected heat flow in the Tyrrhenian Sea (3.1 HFU) is greater than the average corrected value for the western Mediterranean basin (2.7 HFU). In view of the large variability of the heat flow data and uncertainties in the environmental corrections, this difference may not be geophysically significant. However, the existence of a zone of uniformly high heat flow in the southeastern Tyrrhenian basin, where active volcanism is present, is in accord with higher upper mantle temperatures beneath the Tyrrhenian Sea than beneath the western Mediterranean basin.

If basalt with the same average composition as the highly radioactive products of the southern and central Italian volcanoes exists beneath the adjacent Tyrrhenian Sea, a significant fraction of the observed heat flux may originate in this material. Each kilometer of basalt having the radioactivity of the parent magma as determined by Locardi (1968) could contribute 0.4 HFU to the surface heat flow. Large magnetic anomalies in the Tyrrhenian Sea are frequently associated with seamounts or ridges from which samples of basalt have been dredged.

A layer of 4.5 km/sec material 2.0 to 2.5 km thick is present beneath the unconsolidated sediment in the central Tyrrhenian basin. A similar layer of material about 1.5 km thick with a compressional wave velocity between 4.5 and 5.5 km/sec is present beneath the sediment

in many oceanic areas (Ewing, 1969; Shor and Raitt, 1969). Igneous material believed to be representative of at least the surface of this layer was recovered from three locations beneath the Atlantic Ocean, and consisted of interbedded basaltic flows, sills, and sediment (Peterson, 1970). If the 4.5 km/sec material beneath the Tyrrhenian Sea includes basalt of the "Mediterranean" type, it could provide as much as 0.8 to 1.0 HFU to the corrected regional flux of 3.1 HFU. Thus the fact that the average corrected heat flux in the Tyrrhenian Sea is about 0.4 HFU higher than the corrected flux in the western Mediterranean basin may also reflect the presence of a layer of highly radioactive basalt over a thermally uniform upper mantle. Uniformity of the western Mediterranean upper mantle structure is consistent with Payo's (1967) observation that Rayleigh and Love wave group velocity dispersion curves appear to depend upon the fraction of the path which is continental or oceanic, rather than on the location of the path through the western Mediterranean.

The high average heat flow in the western Mediterranean Sea is consistent with other types of geophysical data which can be interpreted as indicating that the upper mantle beneath the sea is abnormally hot. Active volcanism exists along the coast of central and southern Italy and areas of extremely high heat flow are observed both on land at Larderello and Mount Amiata and in the southern Tyrrhenian Sea. Berry and Knopoff (1967) and Payo (1969)

proposed models of the shear velocity structure beneath the western Mediterranean basin in which an ultra-low velocity layer was located at an unusually shallow depth beneath the seafloor. In a series of refraction profiles in the western Mediterranean basin, Fahlquist (1963) observed arrivals from 7.7 km/sec material which he identified as low velocity mantle. The existence of material with abnormally low shear and/or compressional velocities beneath the western Mediterranean suggests, but does not demand, an abnormally high temperature upper mantle; compositional or phase changes could produce the same effect.

2.4 EASTERN MEDITERRANEAN SEA

2.41 Presentation of Data

The locations of the 31 heat flow measurements in the eastern Mediterranean Sea and a single measurement in the southern Aegean Sea are shown in Figure 31. Information relating to the new heat flow values is presented in Tables 5 and 6. The locations are spaced rather uniformly throughout the eastern two-thirds of the eastern Mediterranean and include all of the major topographic provinces.

2.42 Environmental Corrections

2.421 Sedimentation

The average crustal structure of the deep water

Figure 31. Locations of heat flow stations in the eastern Mediterranean Sea.

EASTERN MEDITERRANEAN HEAT FLOW STATIONS

Station Number	Position Lat.	Long.	Depth (corr. m)	Seafloor Description	Penetration (m)	Probes
CH61-29	34°00'N	19°39'E	3955	Sirte Abyssal Plain	12.3	5
CH61-37	35°44'N	25°17'E	1862	Sediment pond in southern Aegean Sea	5.3	2
CH61-39	34°22'N	22°32'E	2679	Region of finely fractured topography on Mediterranean Ridge	3.8	2
CH61-40	33°17'N	23°10'E	2470	Deformed floor of trench at base of African Continental Rise	6.0	3
CH61-42	34°15'N	25°01'E	3500	Gently deformed sediment pond in Hellenic Trough south of Crete	5.8	3
CH61-46	34°17'N	26°13'E	3140	Region of gently rolling hills seaward of Strabo Trench	4.6	2

Table 5-1

EASTERN MEDITERRANEAN HEAT FLOW STATIONS

Station Number	Position Lat.	Long.	Depth (corr. m)	Seafloor Description	Penetration (m)	Probes
CH61-50	35°31'N	28°12'E	2450	Steep slope amidst very rough topography southwest of Rhodes Basin	5.4	2
CH61-53	34°12'N	28°58'E	2603	Region of fractured topography on southern flank of Mediterranean Ridge south of Rhodes Basin	7.8	5
CH61-54	35°20'N	30°07'E	2017	At base of southern wall of eastern Anaximander Mountains	2.5	2
CH61-55	34°49'N	31°04'E	2466	On northern flank of Mediterranean Ridge west of Cyprus	7.0	4
CH61-56	33°00'N	31°06'E	2167	Base of Nile Cone	9.0	5
CH61-57	33°11'N	32°29'E	1926	Region of abyssal hills at base of Nile Cone	7.5	4

Table 5-2

EASTERN MEDITERRANEAN HEAT FLOW STATIONS

Station Number	Position Lat.	Long.	Depth (corr. m)	Seafloor Description	Penetration (m)	Probes
CH61-59	33°52'N	33°17'E	2301	On thickly sedimented region with "diapiric" structures east of Eratosthenes Seamount	7.4	4
CH61-62	36°01'N	31°46'E	2500	On continental rise south of Turkey	4.4	3
CH61-63	35°41'N	32°58'E	1240	Generally flat basin at western edge of Cilicia Plateau	7.3	4
CH61-64	35°56'N	34°14'E	956	Axis of broad shallow trough on eastern Cilicia Plateau	7.3	5
CH61-65	35°32'N	35°26'E	1392	Sediment pond west of Syria	7.4	4
CH61-66	34°19'N	34°42'E	1981	Northeastern end of Herodotus Basin	7.6	4

Table 5-3

EASTERN MEDITERRANEAN HEAT FLOW STATIONS

Station Number	Position Lat.	Long.	Depth (corr. m)	Seafloor Description	Penetration (m)	Probes
CH61-67	34°11'N	33°37'E	1966	At base of southern edge of Hecataeus Mountains south of Cyprus	7.4	4
CH61-68	34°53'N	34°53'E	1591	Thickly sedimented, deformed basin between Syria and Cyprus	7.8	5
C9-115	32°58'N	32°24'E	1398	Abyssal hills at base of Nile Cone	10.5	4
C9-116	33°50'N	32°16'E	2641	Herodotus Abyssal Plain west of Eratosthenes Seamount	11.5	2
C9-117	33°44'N	30°07'E	2775	Herodotus Abyssal Plain	9.1	2
C9-118	33°46'N	27°54'E	2622	Southern flank of Mediterranean Ridge southeast of Crete	8.5	2

Table 5-4

EASTERN MEDITERRANEAN HEAT FLOW STATIONS

Station Number	Position Lat.	Long.	Depth (corr. m)	Seafloor Description	Penetration (m)	Probes
C9-119	34°19'N	27°11'E	2627	Northern edge of Mediterranean Ridge southeast of Crete	9.5	1
C9-121	34°30'N	23°25'E	2690	Eastern end of Ionian Basin south of Crete	3.5	2
C9-123	34°29'N	20°04'E	2860	Southern flank of Mediterranean Ridge southwest of Greece	7.0	2
C9-124	33°57'N	19°13'E	3889	Sirte Abyssal Plain	10.5	3
C9-125	35°48'N	19°25'E	3304	Southern flank of Mediterranean Ridge	5.5	2
C9-126	36°11'N	19°31'E	3290	Central Mediterranean Ridge in Ionian Basin	6.5	2

Table 5-5

EASTERN MEDITERRANEAN HEAT FLOW STATIONS

Station Number	Position Lat.	Long.	Depth (corr. m)	Seafloor Description	Penetration (m)	Probes
C9-127	36°52'N	19°39'E	3373	Northwestern end of Mediterranean Ridge	9.0	3
C9-129	38°11'N	17°58'E	2348	Calabrian Continental Rise	12.0	3

Table 5-6

EASTERN MEDITERRANEAN HEAT FLOW DATA

STATION NUMBER	THERMAL GRADIENT (°C/m x 10^{-2})	THERMAL CONDUCTIVITY* No.Meas.	Average(mcal/cm sec °C)	OBSERVED HEAT FLOW (HFU)
CH61-29	2.73±0.38	18	2.30±0.11	0.63±0.12
CH61-37	5.21±0.38	9	2.01±0.04	1.05±0.13
CH61-39	2.74±0.47	5	2.78±0.07	0.76±0.17
CH61-40	5.70±0.14	11	2.38±0.29	1.36±0.40
CH61-42	2.50±0.73	31	2.47±0.17	0.62±0.21
CH61-46	2.30±0.90	31	2.58±0.18	0.59±0.26
CH61-50	2.88±0.39	36	2.51±0.14	0.73±0.14
CH61-53	3.02±0.46	49	2.10±0.25	0.63±0.13
CH61-54	3.81±0.61	10	2.39±0.12	0.91±0.19
CH61-55	2.67±0.61	22	2.23±0.14	0.59±0.16
CH61-56	2.31±0.63	34	2.12±0.16	0.49±0.12
CH61-57	1.60±0.31	24	2.37±0.31	0.38±0.09

Table 6-1

EASTERN MEDITERRANEAN HEAT FLOW DATA

STATION NUMBER	THERMAL GRADIENT (°C/m x 10^{-2})	THERMAL CONDUCTIVITY* No.Meas.	Average (mcal/cm sec °C)	OBSERVED HEAT FLOW (HFU)
CH61-59	3.75±0.63	26	2.19±0.19	0.82±0.18
CH61-62	2.84±0.49	13	2.71±0.18	0.77±0.14
CH61-63	2.33±0.32	24	2.62±0.11	0.61±0.11
CH61-64	2.19±0.72	21	2.52±0.70	0.55±0.21
CH61-65	2.19±0.40	12	2.23±0.15	0.49±0.11
CH61-66	3.68±0.81	12	2.32±0.58	0.85±0.23
CH61-67	1.15±0.19	13	2.23±0.08	0.25±0.05
CH61-68	3.14±0.26	17	2.13±0.04	0.67±0.09
C9-115	4.02±0.36		(2.60)	1.04±0.15
C9-116	2.87±0.48		2.09	0.60±0.13
C9-117	2.88±0.23		2.22	0.64±0.08
C9-118	1.78±0.23		2.50	0.45±0.08

Table 6-2

EASTERN MEDITERRANEAN HEAT FLOW DATA

STATION NUMBER	THERMAL GRADIENT (°C/m x 10^{-2})	THERMAL CONDUCTIVITY* No.Meas.	Average (mcal/cm sec °C)	OBSERVED HEAT FLOW (HFU)
C9-119	1.10±0.17		(2.25)	0.25±0.05
C9-121	5.38±0.88		2.26	1.22±0.26
C9-123	2.92±0.42		2.66	0.78±0.15
C9-124	3.36±0.46		2.48	0.83±0.16
C9-125	3.31±0.29		(2.65)	0.88±0.12
C9-126	6.61±1.48		2.64	1.76±0.48
C9-127	2.83±0.56		2.63	0.74±0.21
C9-129	1.30±0.24		2.49	0.32±0.07

* Conductivity values in parentheses are estimated on the basis of data from nearby stations.

Table 6-3

sections of the Ionian and Levantine Seas consists of 0.3 km of unconsolidated and semiconsolidated sediment above 1.8 to 2.0 km of 4.2 to 4.8 km/sec material which is, in turn, underlain by a 6.1 to 6.6 km/sec refracting layer. Russian investigators (Michno, 1963; Moskalenko, 1966; Kovilin, 1964) proposed that the 4.2 to 4.8 km/sec material is lithified sediment. Moskalenko (1966) tentatively assigned a Cretaceous age to the 4.7 km/sec layer observed beneath the Levantine Sea on the basis of the supposed correlation of layers of known age in northern Egypt with their proposed seaward extensions.

Gaskell and Swallow (1953), Ewing and Ewing (1959), Ludwig et al. (1965), and Ryan (1969a) acknowledged that this material could be either igneous or sedimentary. If the 4.7 km/sec material is igneous, or is sediment of pre-Tertiary age, it is difficult to explain why such a thin layer of poorly consolidated material is present, considering the present high sedimentation rate and evidence that deposition was occurring during Eocene or earlier times (Ryan, 1969a). The absence of magnetic anomalies in regions of rough relief further suggests sedimentary, rather than igneous material beneath the uncompacted sediment. The sedimentation correction is computed on the assumption that the sediment column in the eastern Mediterranean now averages 2.2 km in thickness, and that an equivalent uncompacted sediment thickness of 2.7 km has been deposited at a constant rate throughout

the Cenozoic, resulting in a reduction of the equilibrium thermal gradient by 16%. The estimated average sedimentation rate of 4.3 cm/1000 yrs agrees well with rates determined by Ryan (1969b) for sediments on the Mediterranean ridge, and with rates compiled by Wong and Zarudski (1969) and shown in Figure 32.

The applicability of one sedimentation correction to heat flow measurements made over much of the eastern Mediterranean is suggested by the conclusions of Hersey (1965) and Ryan (1969a). They proposed that the physiography of the Mediterranean sea floor has evolved through the interaction of tectonic deformation and sedimentation. In this interpretation elevated areas such as the highly deformed Mediterranean ridge were formerly areas of ponded sediments and are now in various stages of tectonic evolution.

2.422 Water Temperature Variations

The effects of short and long-term variations in bottom water temperature on the geothermal gradient beneath the Mediterranean were summarized in Section 2.322 Semidiurnal temperature fluctuations are attenuated rapidly in the sediment and are negligible for temperature measurements deeper than about 50 cm beneath the sea floor. Annual temperature variations, if they exist, can seriously affect the temperature distribution in the sediment to depths comparable to the maximum length of the interval

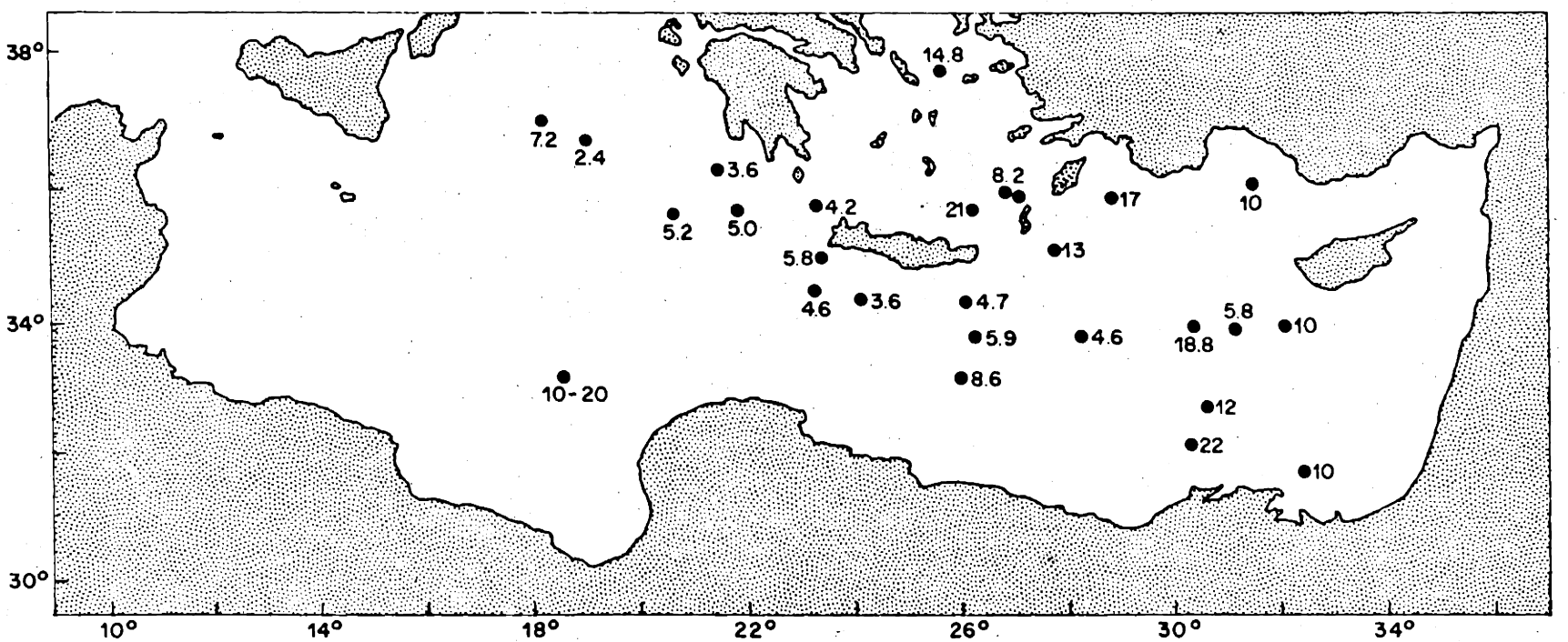

Figure 32. Compilation of modern sedimentation rates in the eastern Mediterranean in cm/1000 yrs, from various investigators as reported in Wong and Zarudzki (1969).

over which the thermal gradient was measured. In order for the effect of annual temperature variations to be significant deeper than a few meters below the seafloor, an extremely non-linear temperature-depth relation should be easily observable in the near-surface sediments. Because slightly non-linear temperature-depth distributions were observed at only a few locations, annual temperature fluctuations do not appear to be an important source of error in the eastern Mediterranean Sea.

Longer-term temperature variations associated with changes in climate or water circulation may have changed the temperature-distribution beneath the eastern Mediterranean Sea (see Section 2.322). The thermal history of the eastern Mediterranean is too poorly known to justify applying corrections for these long-term changes.

2.43 Interpretation

The most obvious characteristics of the observed heat flow in the eastern Mediterranean are its generally low average value (0.74 ± 0.30 HFU) and its small variance across different physiographic provinces. Heat flow values plotted as a profile perpendicular to the axis of the Mediterranean ridge are shown in Figure 33. This treatment of the data is justified by the basic linearity and parallelism of the major physiographic provinces of the eastern Mediterranean, as well as by the magnetic and gravitational fields and zones of tectonic activity

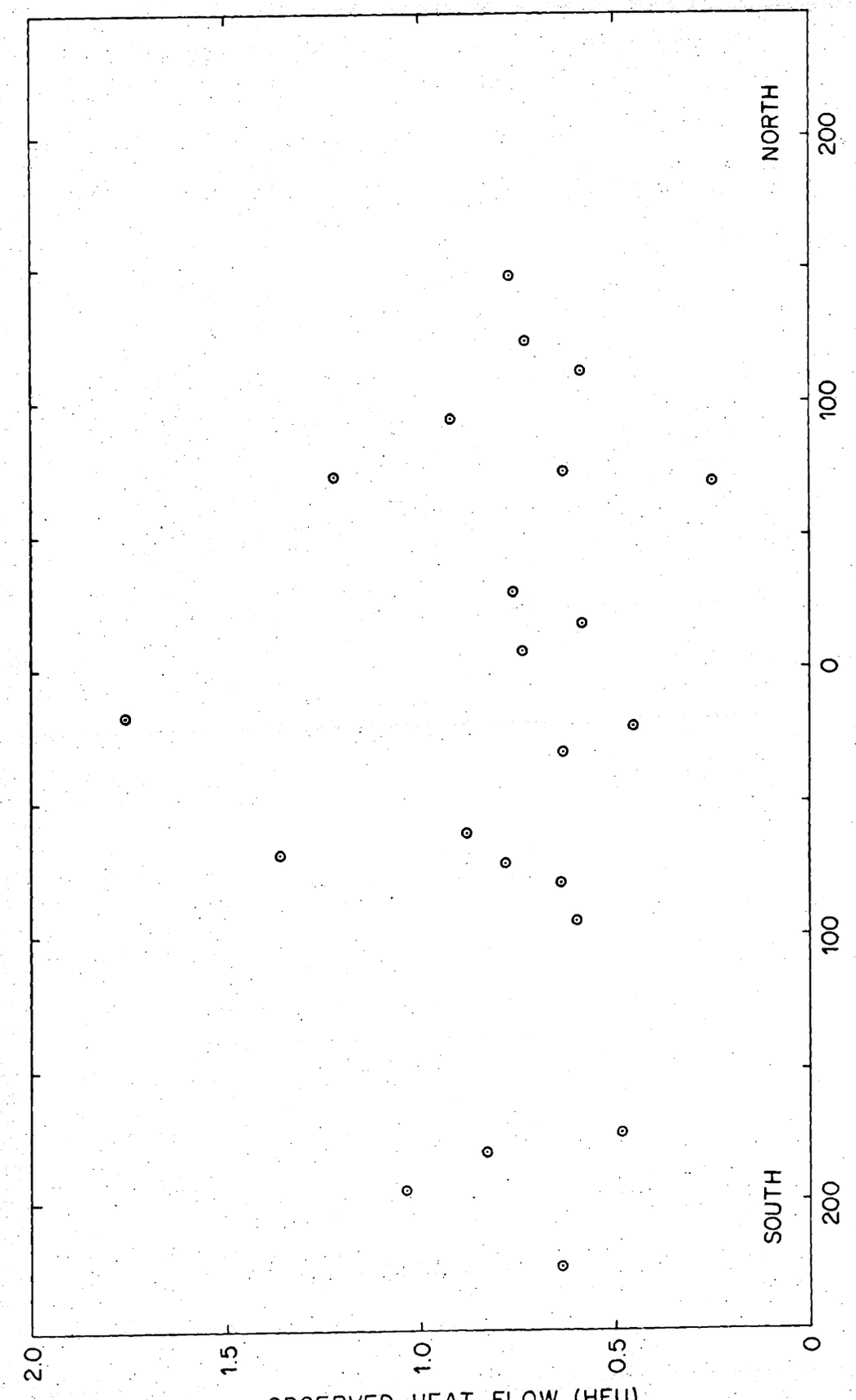

Figure 33. Eastern Mediterranean heat flow values plotted as a function of distance from the axis of the Mediterranean ridge.

which are in the form of broad, concentric bands parallel to the Cretan arc. There is no evidence for any regional heat flow anomaly associated with the Mediterranean ridge, nor with the basin and trench provinces located north and south of it.

Where individual anomalously high or low values occur, the measurement is invariably located in an area where the anomalous heat flow value, whether high or low, can be attributed to the effect of nearby extreme topography and/or sedimentation processes. Station C9-126, at which a heat flow of 1.76 HFU was measured, was located at the bottom of a narrow, steep-walled valley in a highly deformed and fractured area of the Mediterranean ridge. The effect of the local sea floor relief is to increase the heat flux through the floor of the valley. Two of the three heat flow values (CH61-56 and CH61-57) on the Nile cone are slightly below the eastern Mediterranean average, probably as a result of a locally high sedimentation rate caused by deposition of the large amount of sediment carried into the eastern Mediterranean by the Nile River.

A heat flow of 1.05 HFU was measured at station CH61-37, located in a horizontally stratified sediment pond in the southern Aegean Sea. This value is well above the average value of eastern Mediterranean heat flux, but still lower than the world average. Many more measurements are needed to estimate the regional flux in the Aegean Sea

with confidence.

In accord with the absence of regional variations in heat flux, there is no apparent relation between the observed heat flow and other types of geophysical data in the eastern Mediterranean Sea. Nor does any relation exist between the thickness of the unconsolidated sediment, as determined by Wong and Zarudski (1969), and the observed heat flow. The variability of the heat flow data is higher in areas of rough sea floor topography. The relationship between topographic roughness and variability of heat flow observed in the eastern Mediterranean is understandable in terms of the effects of topography, refraction, and sedimentation on the thermal gradient.

The absence of high heat flow values and the existence of a smooth magnetic field over the eastern Mediterranean ridge suggest that volcanic activity is not present in the crust and strengthens the conclusion that the ridge is not tectonically similar to active mid-ocean ridges.

The mere absence of volcanic activity in the eastern Mediterranean is not sufficient to reduce the observed heat flow to nearly half of its normal value. Neither can the effect of sedimentation, estimated as having reduced the heat flow by 16%, explain the low flux. "Crustal shortening", defined by Ryan (1969a) as "The process of thickening the sedimentary crustal layers by folding on decollement planes, or by piling up layers of sediments as the result of underthrusting", may be responsible for

a reduction of the heat flux over tectonically deformed areas of the eastern Mediterranean. Ryan proposed that the negative free-air gravity anomalies over and north of the Mediterranean ridge are due to sedimentary material "uplifted onto and crushed into the Mediterranean ridge southeast of Crete and Rhodes". The existence of low heat flow through relatively undeformed regions in the eastern Mediterranean south of the Mediterranean ridge and in the vicinity of Cyprus cannot be attributed to crustal shortening.

It is possible that the sub-normal heat flux in the eastern Mediterranean is due to a deficiency in radiogenic elements in the upper mantle. In this connection, it may be significant that the low velocity zone is found at shallower depth and with a lower minimum velocity beneath the western Mediterranean than beneath the eastern Mediterranean. This observation is consistent with the upper mantle east of Italy being cooler than the upper mantle beneath the western Mediterranean.

2.5 BLACK SEA HEAT FLOW DATA

2.51 Presentation of Data

Thirty heat flow measurements were made in the Black Sea with either of two different types of probes. The data are given in Tables 7 and 8 and locations are shown in Figure 34. Piston cores, typically 9 m long and

R/V ATLANTIS II CRUISE 49 BLACK SEA HEAT FLOW STATIONS

Station Number	Position Lat.	Long.	Depth (corr. m)	Seafloor Description	Penetration (m)	Probes
1431P	42°11'N	33°00'E	2113	Rolling sub-horizontally stratified topography at base of Turkish Continental Slope	9.0	7
1432G	43°01'N	34°05'E	2192	Abyssal plain in central Black Sea south of Crimea	2.2	5
1433P	44°04'N	35°00'E	2170	Horizontally stratified abyssal plain in northern Black Sea south of Crimea	10.5	8
1442P	44°40'N	31°56'E	491	Side of steep topographic feature on continental rise west of Crimea	6.0	6
1443P	44°35'N	31°55'E	1033	Base of continental rise west of Crimea	9.5	7

Table 7-1

R/V ATLANTIS II CRUISE 49 BLACK SEA HEAT FLOW STATIONS

Station Number	Position Lat.	Long.	Depth (corr. m)	Seafloor Description	Penetration (m)	Probes
1444P	43°48'N	31°45'E	1597	Abyssal plain southwest of Crimea	11.0	7
1445P	43°09'N	31°33'E	1883	Central abyssal plain in western Black Sea	10.0	7
1446P	42°11'N	31°22'E	2143	Abyssal plain in western Black Sea near Turkish Continental Rise	8.8	7
1447P	41°23'N	30°04'E	1274	Rough topography at base of Turkish Continental Rise	12.0	8
1452P	42°47'N	28°36'E	733	Rolling topography on continental slope east of Rumania	10.0	7
1460P	41°40'N	29°44'E	1888	Abyssal plain near Turkish Continental Rise adjacent to the Bosporous	10.0	7

Table 7-2

R/V ATLANTIS II CRUISE 49 BLACK SEA HEAT FLOW STATIONS

Station Number	Position Lat.	Long.	Depth (corr. m)	Seafloor Description	Penetration (m)	Probes
1462G	43°02'N	33°04'E	2179	Flat, horizontally stratified central abyssal plain south of Crimea	3.1	3
1464G	43°03'N	35°31'E	2179	Flat, horizontally stratified central abyssal plain south-east of Crimea	4.0	4
1468G	42°01'N	40°06'E	1892	Slightly deformed central abyssal plain in eastern end of Black Sea	2.5	4
1469G	41°24'N	40°40'E	1756	Very rough topography in southeastern corner of Black Sea at base of continental rise	2.5	4
1470G	42°03'N	41°18'E	906	Rough continental slope in extreme eastern Black Sea	3.3	5

Table 7-3

R/V ATLANTIS II CRUISE 49 BLACK SEA HEAT FLOW STATIONS

Station Number	Position Lat.	Long.	Depth (corr. m)	Seafloor Description	Penetration (m)	Probes
1472G	43°08'N	39°51'E	1539	Rough continental slope in extreme eastern Black Sea	5.0	5
1473G	43°49'N	38°55'E	1418	Edge of abyssal plain at base of continental slope in extreme northeastern Black Sea	3.3	5
1473P	43°52'N	38°48'E	1470	Same as 1473G, slightly further out on abyssal plain	10.0	7
1474P	42°23'N	37°37'E	2114	Horizontally stratified abyssal plain in central eastern Black Sea	13.0	7
1476G	41°37'N	37°41'E	1741	Base of Turkish Continental Rise in southeastern Black Sea	3.5	5

Table 7-4

R/V ATLANTIS II CRUISE 49 BLACK SEA HEAT FLOW STATIONS

Station Number	Position Lat.	Long.	Depth (corr. m)	Seafloor Description	Penetration (m)	Probes
1477P	41°36'N	39°04'E	1967	Edge of abyssal plain north of Turkish Continental Rise in eastern Black Sea	4.4	4
1478P	42°08'N	39°14'E	2024	Central abyssal plain in eastern Black Sea	6.0	5
1478G	42°11'N	39°15'E	2030	Same as 1478P	2.5	4
1479P	42°18'N	38°10'E	2097	Central abyssal plain in eastern Black Sea	0.0	0
1480P	43°06'N	38°26'E	2110	Abyssal plain in northeastern Black Sea	8.0	7
1481P	44°02'N	37°58'E	2035	Edge of abyssal plain immediately southwest of Georgian coast	6.5	7

Table 7-5

R/V ATLANTIS II CRUISE 49 BLACK SEA HEAT FLOW STATIONS

Station Number	Position Lat.	Long.	Depth (corr. m)	Seafloor Description	Penetration (m)	Probes
1484G	44°42'N	36°55'E	386	Smoothly sedimented base of continental rise south of Straits of Kerch	3.0	4
1485G	44°25'N	35°15'E	1758	Base of continental rise southwest of Straits of Kerch	2.5	4
1486P	43°59'N	33°45'E	1886	Base of continental rise south of Crimea	9.0	8
1486G	44°00'N	33°42'E	1992	Edge of abyssal plain just south of 1486P	3.0	5

Table 7-6

BLACK SEA HEAT FLOW DATA

STATION NUMBER	THERMAL GRADIENT (°C/m x 10^{-2})	THERMAL CONDUCTIVITY* No.Meas.	Average(mcal/cm sec °C)	OBSERVED HEAT FLOW** (HFU)
1431P	2.31±0.12	18	2.17±0.17	0.50±0.05
1432G	3.57±0.18	0	1.85±0.19	0.66±0.07
1433P	<1.10	10	2.06±0.23	(<0.23)
1442P	5.33±0.47	0	3.06±0.31	1.63±0.22
1443P	1.67±0.17	11	3.06±0.43	0.51±0.08
1444P	3.09±0.22	14	2.23±0.17	0.69±0.08
1445P	2.20±0.41	21	2.31±0.23	0.51±0.12
1446P	4.46±0.35	20	2.03±0.21	0.91±0.12
1447P	5.40±0.27	6	2.00±0.15	1.08±0.11
1452P	4.05±0.20	23	2.39±0.18	0.97±0.10
1460P	5.35±0.35	32	1.87±0.18	1.00±0.12
1462G	1.97±0.10	15	1.73±0.15	0.34±0.03

Table 8-1

BLACK SEA HEAT FLOW DATA

STATION NUMBER	THERMAL GRADIENT ($°C/m \times 10^{-2}$)	THERMAL CONDUCTIVITY* No.Meas.	Average(mcal/cm sec °C)	OBSERVED HEAT FLOW** (HFU)
1464G	<2.86	9	1.98±0.10	(<0.57)
1468G	1.00±0.10	0	2.10±0.21	(0.21±0.03)
1469G	1.18±0.08	0	2.10±0.21	(0.25±0.03)
1470G	<1.95	22	1.98±0.18	(<0.39)
1472G	3.29±0.17	7	2.03±0.07	0.67±0.07
1473P	2.65±0.13	33	2.33±0.22	0.62±0.06
1473G	1.96±0.17	8	2.03±0.17	(0.40±0.05)
1474P	3.00±0.25	0	2.33±0.23	0.70±0.09
1476G	<2.11	8	1.88±0.08	(<0.40)
1477P	4.84±0.48	10	2.23±0.52	1.08±0.16
1478G	<1.60	0	2.33±0.23	(<0.37)
1478P	4.00±0.20	18	2.33±0.27	0.93±0.09
1480P	3.57±0.18	10	2.15±0.12	0.77±0.08

Table 8-2

BLACK SEA HEAT FLOW DATA

STATION NUMBER	THERMAL GRADIENT (°C/m x 10^{-2})	THERMAL CONDUCTIVITY* No.Meas.	Average (mcal/cm sec °C)	OBSERVED HEAT FLOW** (HFU)
1481P	5.00±0.25	13	2.19±0.20	1.10±0.11
1484G	<1.20	7	2.16±0.25	(<0.26)
1485G	<2.52	6	2.30±0.19	(<0.58)
1486P	6.22±0.38	18	2.11±0.13	1.31±0.14
1486G	<3.42	0	2.11±0.21	(<0.72)

* Where no thermal conductivity measurements are available for a given station, conductivity is estimated on the basis of data from nearby stations.

** Heat flow values within parentheses are considered unreliable.

Table 8-3

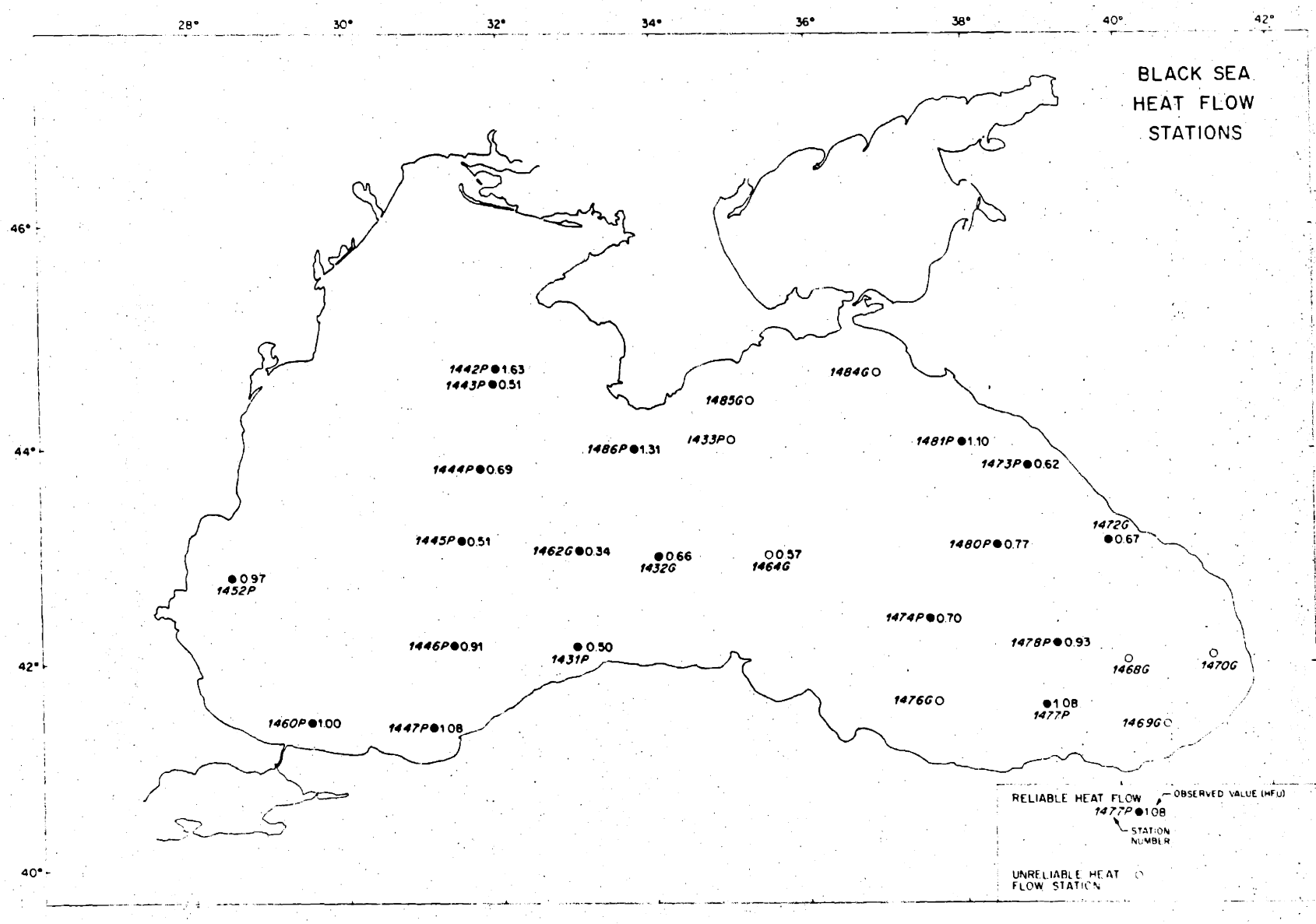

Figure 34. Locations of heat flow stations in the Black Sea.

designated by the letter "P", were instrumented with either 7 or 8 thermistor probes in an effort to detect non-linear gradients and to determine the thermal gradient below the disturbed zone. In addition, 13 heat flow measurements were made using 5 temperature sensors on a gravity ("G") corer 3.25 m long. Most measurements made with the gravity corer were unusuable for the determination of the regional heat flow because a non-linear temperature-depth distribution exists in the upper few meters of sediment. As shown in Figure 25 the thermal gradient decreases with depth at a rate which appears to depend upon conditions peculiar to each measurement.

At stations 1478G and 1486G, very closely spaced heat flow measurements were made with the 3.25 m probe by repeatedly lowering the probe into the bottom as the ship drifted. Up to 10 independent gradient determinations were obtained at intervals of approximately 100 m. The data allow an evaluation of the significance of "single determination" heat flow measurements made with the same, or similar, equipment under similar sea floor conditions.

Station 1478G was situated on the central abyssal plain in the eastern half of the Black Sea. Continuous seismic profiles and bathymetric data indicate a thick sequence of flat-lying, horizontally uniform, undisturbed layers of sediment beneath this station. Piston core 1478P was obtained nearby and contained layers of sand interleaved with calcareous mud. The presence of the sand

layers was also evident from the heat flow record at station 1478P where several of the probes underwent a large initial temperature increase, usually associated with increased frictional heating due to the coarse material. However, there is no indication from the heat flow record at station 1478G that sand layers were encountered by the shorter probe.

Station 1486G was located at a depth of 1992 m seaward of the base of the continental rise south of Crimea. Piston core 1486P was taken higher on the rise in 1886 m of water in an area of rough topography, as indicated by the presence of side-echoes and a depth change while the ship drifted during the 5 minutes that the heat probe was in the bottom.

The temperature versus depth curves for both multiple heat flow stations are shown in Figures 35 and 36. The isotherms within the sediment at both stations have been drawn on the assumptions that the corer penetrated vertically and that the temperature within the sediment at each measurement is well represented by a smoothly varying curve drawn through the temperature-depth data (see Figures 37 and 38). Although variations in the depth of the isotherms occur in both sets of measurements, the temperature-depth profiles within each set are of nearly the same shape and slope. The similarity can be greatly improved if it is assumed that the corer failed to penetrate vertically at measurements where small temperature increases

Figures 35 and 36. Temperature-depth profiles at multiple heat flow stations 1478G and 1486G, respectively. Horizontal arrows indicate probes warming or cooling during the measurement. Also shown for comparison is the temperature-depth profile inferred from the uppermost probes on nearby heat flow stations 1478P and 1486P. The thermal gradient was calculated from the slope of the solid line tangent to the base of the dashed temperature-depth profile.

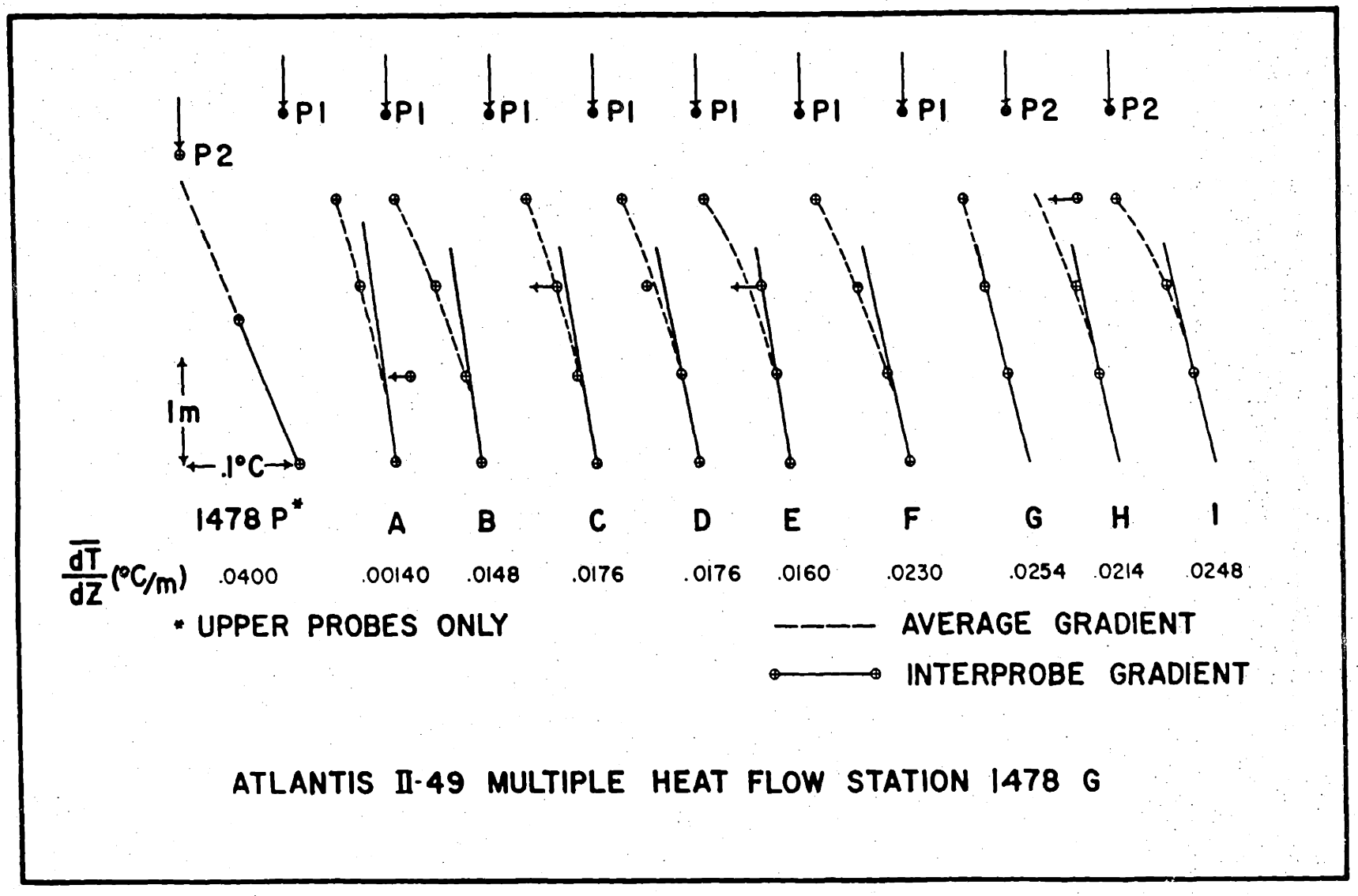
P1
P1
P1
P1
P1
P1
P1
P2
P2
P2
1m
.1°C
1478 P*
A
B
C
D
E
F
G
H
I
dT/dZ (°C/m)
.0400
.00140
.0148
.0176
.0176
.0160
.0230
.0254
.0214
.0248
* UPPER PROBES ONLY
AVERAGE GRADIENT
INTERPROBE GRADIENT
ATLANTIS II-49 MULTIPLE HEAT FLOW STATION 1478 G

Figure 35

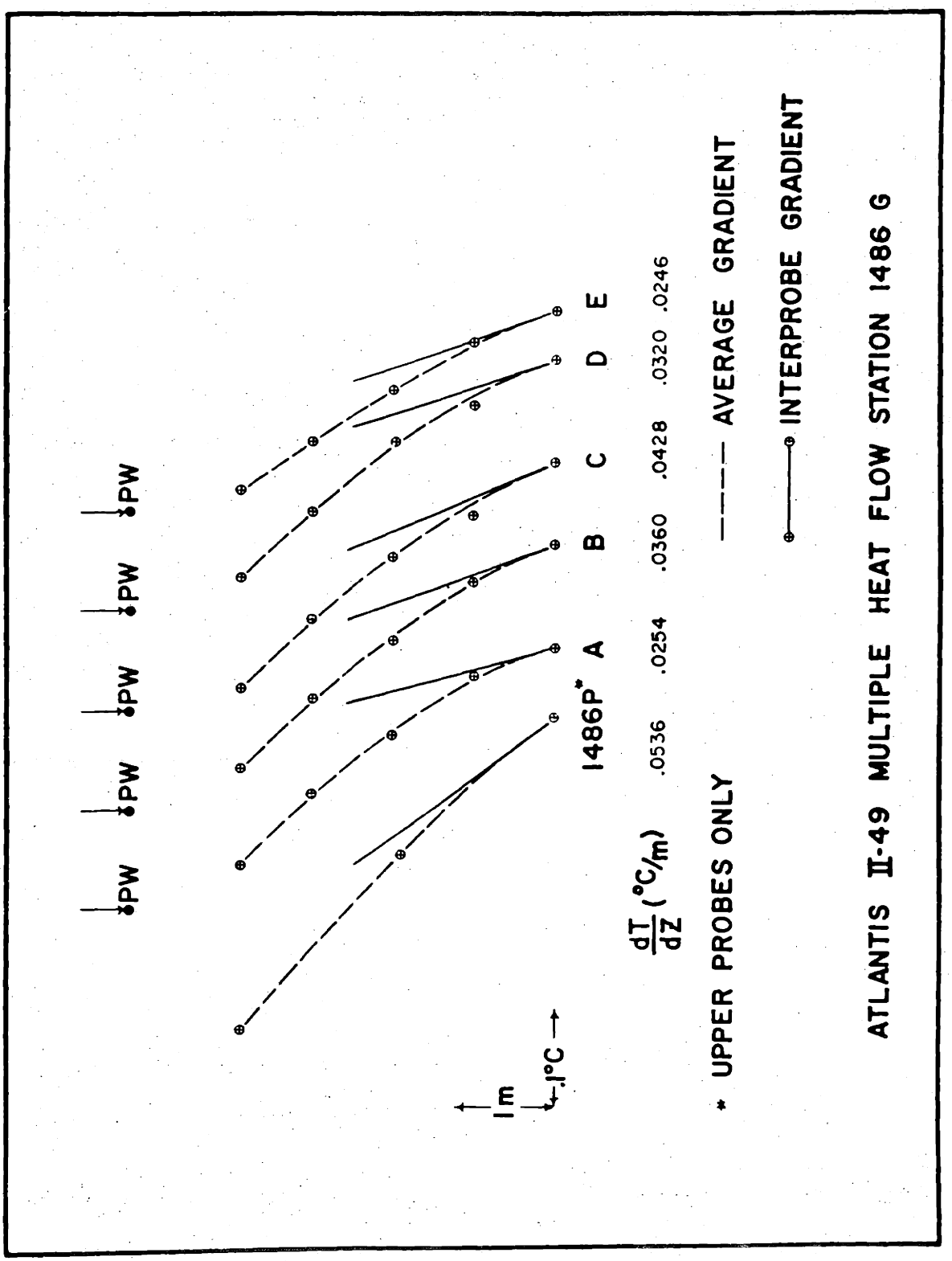
ATLANTIS II-49 MULTIPLE HEAT FLOW STATION 1486 G
INTERPROBE GRADIENT
AVERAGE GRADIENT
* UPPER PROBES ONLY
1m
.1°C
1486P* A B C D E
dT/dz (°C/m) .0536 .0254 .0360 .0428 .0320 .0246
PW PW PW PW PW PW

Figure 36

Figures 37 and 38. Isotherms in the sediment as drawn from temperature-depth data at multiple heat flow station 1478G and 1486G, respectively.

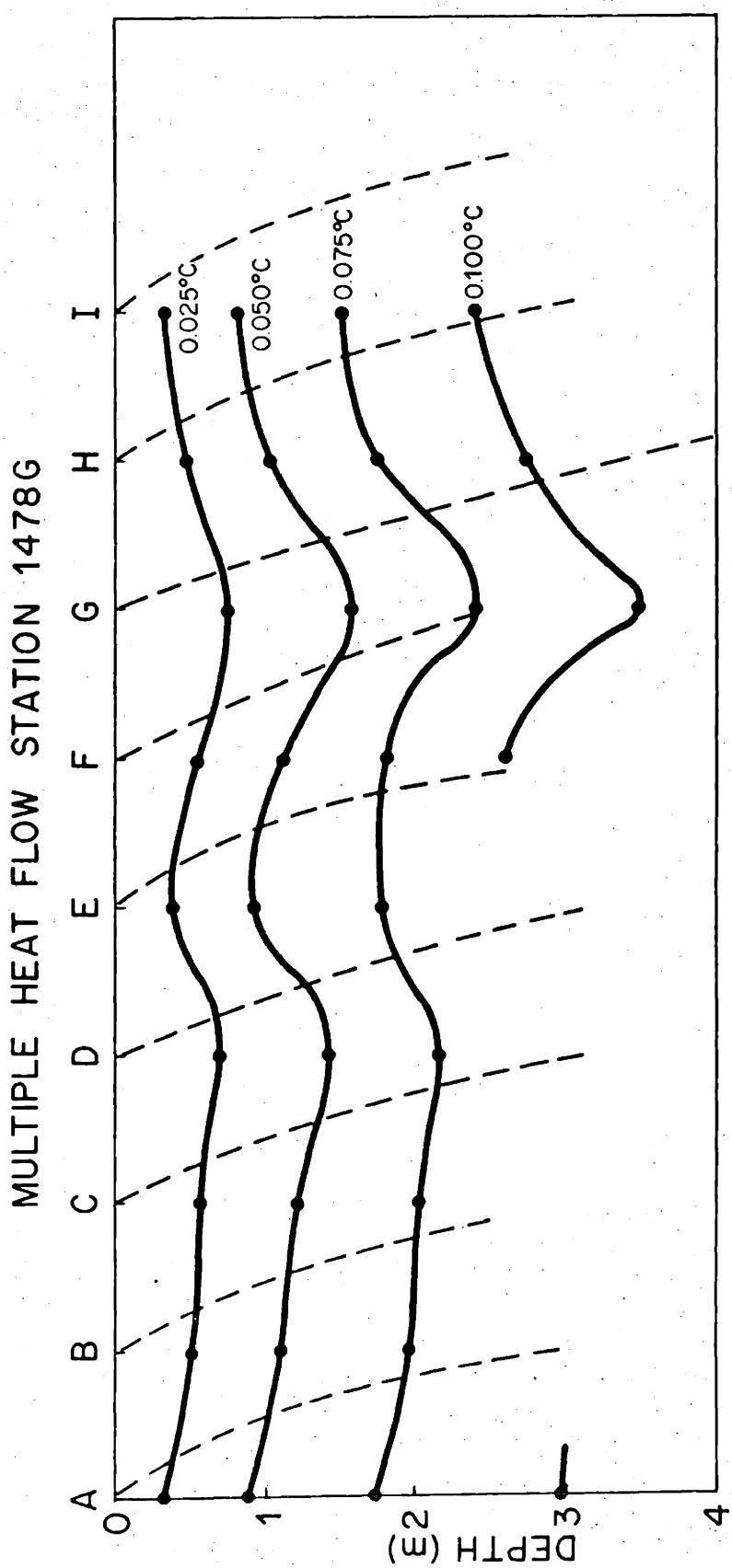
MULTIPLE HEAT FLOW STATION 1478G
A
B
C
D
E
F
G
H
I
0.025°C
0.050°C
0.075°C
0.100°C
0
1
2
3
4
DEPTH (m)

Figure 37

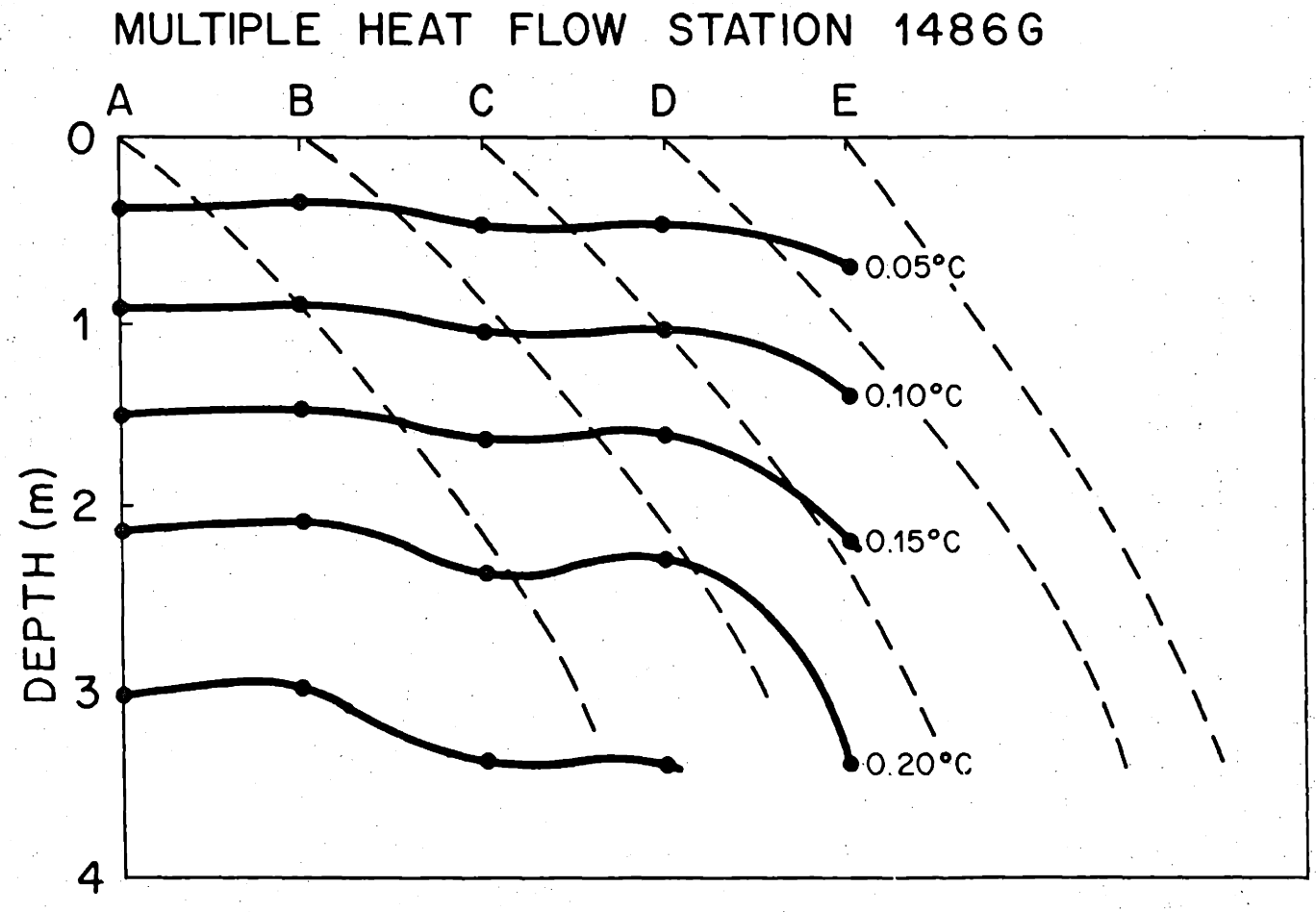
MULTIPLE HEAT FLOW STATION 1486G
A
B
C
D
E
0
1
2
3
4
DEPTH (m)
0.05°C
0.10°C
0.15°C
0.20°C

Figure 38

were observed. Correcting the isotherm plots for non-vertical penetration removes the tendency for the isotherms to show increasing departure from "normal" behavior with increasing depth (or temperature increase). No measurements of the inclination of the probe in the sea floor were made at these stations, thus the validity of the above corrections cannot be verified independently.

The observed variation in the position of the isotherms is probably due to non-vertical penetration of the probe, and, to a lesser extent, measurement error. Lateral variations in the thermal gradient are unlikely in view of seismic and bathymetric data suggesting that the sediment is horizontally uniform and undisturbed.

The tendency for the thermal gradient to decrease with depth was observed in only a few of the heat flow measurements made with the deeper penetrating piston coring apparatus. The probe spacing on the upper part of the piston core (about 3 m) was slightly larger than the interval over which the largest change in the gradient occurred. In the 19 measurements considered to be useful for the determination of heat flow, the gradient became constant at depth and was assumed to represent the thermal gradient undisturbed by whatever environmental effects have affected the shallower measurements.

2.52 Environmental Corrections

2.521 Sedimentation

The presence of up to 14 km of low velocity, horizontally stratified material, usually identified as sediment in varying stages of consolidation, and the observed average heat flow of 0.84 HFU, strongly constrain models of the sedimentation history in the Black Sea, and in particular, the minimum length of time that sediment could have been accumulating.

Hamilton (1959) calculated that for sediments over a few kilometers thick, a clay-shale section represents about two and a half times its uncompacted thickness and a predominantly calcareous layer about one and a half times its original thickness. Contemporary sedimentation in the Black Sea basin includes both types. If compaction by a factor of two is a reasonable assumption, an average thickness of 10 to 20 km of uncompacted sediment lies beneath much of the Black Sea.

Although estimates of the age of the Black Sea range from Lower Quaternary (Nalivkin, 1960) to Paleozoic or Precambrian (Milanovskiy, 1967), most investigators appear to favor an Upper Mesozoic (Brinkmann, unpublished manuscript, 1968) or Lower-Middle Cenozoic (Rezanov and Chamo, 1969); Muratov, 1962) origin. The reduction of the thermal gradient due to the deposition of a given

thickness of sediment is greatest for the highest sedimentation rate (shortest duration of sedimentation). The dependence of the reduction on the age of the Black Sea is shown in Figure 21. For ages less than about 150 m.y., the amplitude of the correction increases rapidly with decreasing age. The assignment of a Middle Eocene (50 m.y.) age implies that the thermal gradient has been reduced by 77%, and that the true heat flow is 3.6 HFU or more. Middle Cretaceous (100 m.y.) and Triassic (200 m.y.) origins imply heat flows of 2.3 and 1.7 HFU, respectively.

Contemporary sedimentation rates in the central Black Sea range from 10 to 30 cm/1000 yrs (Starik et al., 1959; Ross et al., unpublished manuscript, 1970), and agree well with the value of 9 to 30 cm/1000 yrs calculated on the assumption of a Mesozoic origin. Milanovskiy (1967) noted that throughout all of the Tertiary almost all of the sediment carried by the Danube River failed to reach the Black Sea, and was dumped into the Pannonian and Lower Danubian depressions. He suggested that the present sedimentation rates are much higher than those prevailing before the Upper Tertiary, and consequently the time required for the accumulation of the Black Sea sediments--and thus the age of the Black Sea--is Paleozoic or older. However, the creation and rejuvenation of major Alpine (Tertiary) and Kimmerian (Mesozoic) mountain ranges around the Black

Sea may have provided an almost continuously high sedimentation rate. In the following discussions, a Cretaceous age (100 m.y.) is assumed for the origin of the Black Sea.

2.522 Thermal Refraction

In addition to the reduction in the thermal gradient caused by sedimentation, the presence of a thick blanket of low thermal conductivity sediment beneath the Black Sea has further reduced the average flux through the central basin and increased the heat flow around the margins. The magnitude of the reduction can be estimated using the solution presented by Von Herzen and Uyeda (p. 4238, 1963) for thermal refraction through a sediment-filled, hemiellipsoidal depression.

The effect was computed for two geometries which bracket the actual shape of the Black Sea basin, and for contrasts in the thermal conductivity of the sediment and basement ranging from 2:1 to 4:1. Heat flow would be uniformly lower over the entire sediment-filled depression by an amount shown in Figure 39. The dotted curve was calculated for an infinitely long trough with a hemiellipsoidal cross section having major and minor axes of 95 and 14 km, respectively. The dashed curve shows the reduction due to a circular hemiellipsoidal depression with the same axes. The actual contrast in thermal conductivity is probably between 2 and 3 and a reduction of the heat flow out of

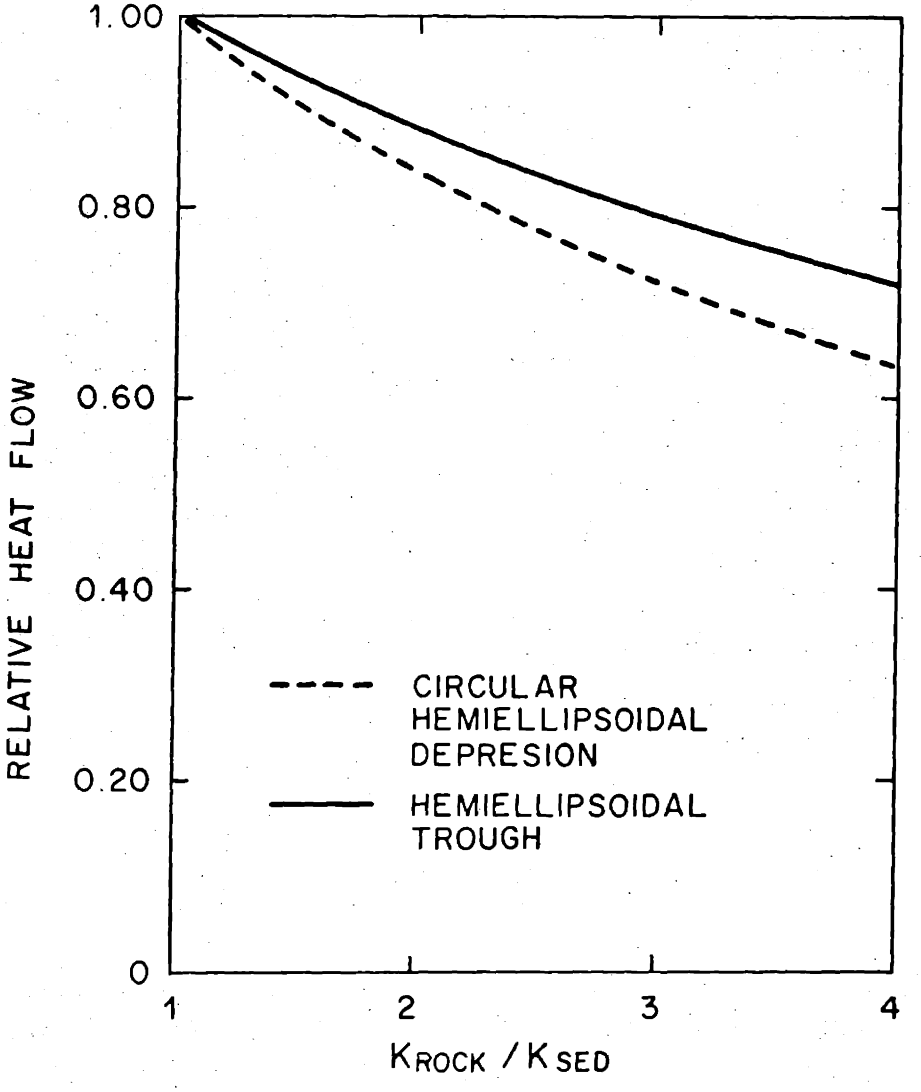

Figure 39. Reduction of the heat flux through a circular and an infinitely long sediment-filled hemiellipsoidal depression caused by various contrasts in thermal conductivity between the sediment and the basement rock. Major and minor axes are 95 and 14 km, respectively.

the basin of about 20% is likely.

A non-ellipsoidal shape of the Black Sea basin will cause the magnitude of the reduction to vary according to position, rather than being constant across the basin. A serious discrepancy between the real and idealized sediment thicknesses is that the sediment beneath the margins of the deep basin is thinner than that required by the model. The effect of this discrepancy is to reduce the refraction effect away from the center of the Black Sea - particularly near the continental rise where the sediment thins rather abruptly, as shown in Figure 19. Thus the observed heat flow should be lower in the central basin and higher near the continental rise. Evidence for the existence of just such a heat flow distribution is discussed in Section 2.53.

2.523 Water Temperature Variations

The Black Sea is divided vertically into two distinct water masses. The uppermost layer extends from the surface to a depth of about 200 m and is characterized by a rapid downward increase in density due to an increase in salinity from 1.8% at the surface to 2.2% below about 200 m (Caspers, 1957). This stabley stratified layer prevents the penetration of very cold, fresh surface water into the underlying region which extends, with only minor changes in salinity and temperature, to the seafloor.

The Black Sea is connected to the Sea of Marmora

and to the world ocean through the Bosporous, a narrow strait with a sill depth of 40 m (Caspers, 1957). It is generally accepted that a strong surface current flows southwards through the Bosporous, carrying brackish Black Sea surface water into the Sea of Marmora and on into the Aegean Sea. Beneath this southward flowing current denser, salty, and warm (13°C) Aegean water is known to flow northward over the sill into the Black Sea, although its importance to the physical oceanography of the Black Sea is not understood. Carruthers (1964) and Novitskiy (1965) suggested that the inflow exerts a significant effect on the near-Bosporous water mass and Caspers (1957) noted that an influx of Aegean water is required to replace the salt lost in the outward flowing surface current. He suggested the most likely cause for the currents observed in the Black Sea are pressure differences produced and maintained by the inflow of dense salty water through the bottom zone of the Bosporous and the continuing inflow of less saline water in the northwestern area.

Temperature and salinity data tend to minimize the possibility of the Bosporous being an important source of warm, dense bottom water. No indication of a warm, salty layer of bottom water has been observed in the Black Sea, although most hydrocasts do not sample within 100 m of the sea floor, and therefore would miss a thin layer. An even better indication of the absance of a warm water layer

on the seafloor is provided by semi-continuous water temperature measurements made with the thermal gradient recorder at each station.

On the basis of the ability of the stable density stratification in the upper 200 m of water to prevent the downward penetration of newly formed bottom water and observational evidence for the absence of anomalously warm or cool bottom water either at stations in the deepest parts of the Black Sea or at shallower depths on the continental slopes, it is concluded that there is no evidence that annual variations in bottom water temperature occur in the Black Sea. The non-linear temperature-depth distributions observed in the sediment cannot be caused by short-term changes in bottom water temperature.

Long term changes in the temperature of the Black Sea are more difficult to evaluate. The Black Sea has had a complicated hydrologic history dominated by the sporadic opening and closing of marine connections to the Sea of Marmora and to the Caspian Sea (Caspers, 1957). During the last glacial stage the level of the Black Sea fell 80 to 100 m below the present level, effectively cutting off the inflow of saline Aegean water. As sea level rose following the last glaciation, the Bosporous reopened and salinity increased, as indicated by the appearance of Mediterranean faunal species in the Black Sea (Caspers, 1957). At the time of the post glacial "climatic optimum", sea level rose in the Black Sea, as

in the oceans in general, 5 m above the present level. Ryan (1969b) suggested that the relatively light, brackish water which accumulated in the Black Sea during the glacial period was displaced by the influx of denser Aegean water. The present temperature (8.8°C) of the bottom water in the Black Sea is considerably less than the temperature (13°C) of Marmoran water. If such an overturn occurred 7000 to 9000 years ago, as proposed by Ryan, (1969b), the floor of the Black Sea very likely was warmed rather than cooled. It is not known whether the warming is continuing at present due to continued influx of Marmoran water, or whether a possible 5 m decrease in sealevel has effectively reduced the inflow and started a gradual cooling in response to the cold surface temperatures. No correction to the thermal gradient for short-term temperature changes is required, and no reliable correction for long-term changes can be estimated.

2.53 Interpretation

Nineteen heat flow measurements are believed to provide data useful for estimating the regional geothermal flux through the floor of the Black Sea. The data of Lubimova (1966) is not included in the following discussion because their reliability is uncertain.

The average of 19 heat flow measurements is 0.84 HFU, with a standard deviation of 0.32 HFU. Observed

values range from highs of 1.63 and 1.31 HFU, observed on the continental slopes west and south of Crimea, respectively, to 0.34 HFU through the deep-water abyssal plain in the central Black Sea.

A tendency for heat flow values above the regional mean to be located around the margins of the Black Sea above the 2000 m depth contour is shown in Figure 40. Very low values, on the other hand, occur about equally on either side of the 2000 m contour. This skewed distribution results in an average heat flow within the deep-water region equal to 0.72 $\pm$ 0.21 HFU, and through the shallower margins, of 0.92 $\pm$ 0.42 HFU.

Longitudinal variations in heat flux are much less obvious. The average flux through the Black Sea east and west of Crimea is almost equal. Two very low values (0.21 and 0.25 HFU) at stations 1468G and 1469G, respectively, were not used in computation of the average flux for the eastern Black Sea because the temperature-depth data and the absence of a core at these stations implied little or no penetration.

The high heat flow value at station 1442P exerts a powerful influence on the regional average and on the credibility of the hypothesis that the marginal heat flux is relatively high. Although 4 probes penetrated the sediment, only data from the upper 3 yielded a linear temperature-depth profile. The abnormally high gradient may be due to a slump having occurred relatively recently

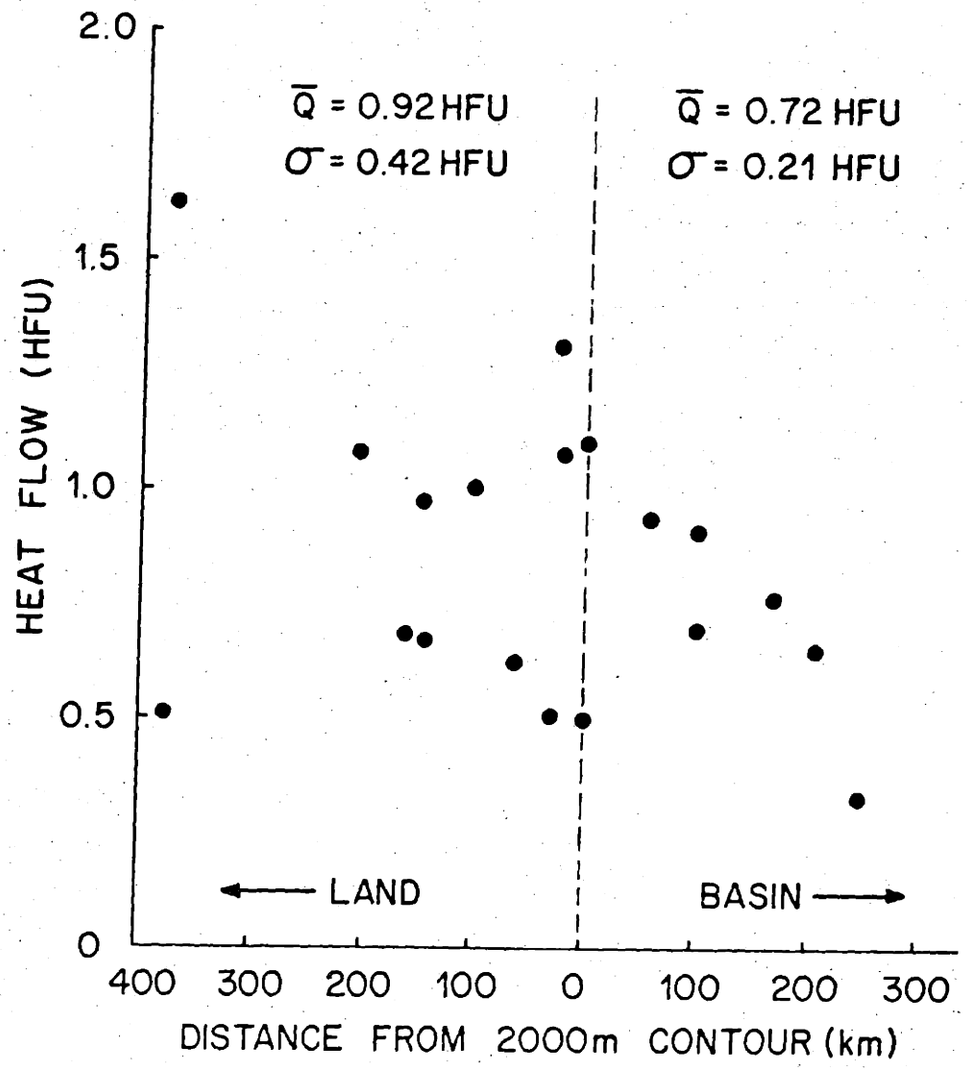

Figure 40. Heat flow values projected onto a profile perpendicular to the 2000 m depth contour around the Black Sea.

there. The thermal conductivity used for computation of the heat flow was measured in a small, sandy, disturbed segment of core and may not be representative of the average conductivity of the sediment.

Station 1486P was taken in a similar physiographic environment and thus its reliability is subject to some of the same uncertainties as 1442P. However, the temperature-depth data at 1486P are of much higher quality and do not show an abnormal temperature-depth relationship, although there is a definite decrease in the thermal gradient with depth in the top few meters.

2.531 Calculation of Flux out of the Mantle

As discussed in Sections 2.521 and 2.522, the average heat flow through the floor of the Black Sea has been reduced by factors of 0.63 and 0.2 as a result of continuous sedimentation and contrasts in the thermal conductivity of the sediment and basement rock, respectively. In order to estimate the heat flux into the base of the sedimentary column the average observed heat flow of 0.84 HFU should be corrected for these effects and flow which originates in the sediment must be removed. The thick sediment in the Black Sea may provide a significant fraction of the observed heat flux if enough time has elapsed for the radiogenic heat to warm the sediment layer, and if the radioactivity of the sediment is sufficiently high.

Carslaw and Jaeger (p. 80, 1959) derived an expression for the temperature gradient G after time t at the surface of a layer of thickness l, thermal diffusivity k, thermal conductivity K, and heat production A.

$$G = \frac{2A\sqrt{Kt}}{K}\left\{\frac{1}{\pi} - i\,\mathrm{erfc}\left(\frac{l}{\sqrt{4Kt}}\right)\right\} \qquad \text{Equation 1}$$

Values of k and K were estimated as 0.004 cm^2/sec and 4 KU, respectively; intermediate between the diffusivity and conductivity values characteristic of unconsolidated and lithified sediment. The content of U, Th, and K in the sediment was estimated as the arithmetic mean of the concentrations of radiogenic material in Black Sea sediments, Russian platform shales and carbonates, and in Mesozoic graywakes from the northern Coast Ranges of California (Table 9). The rate of energy release for the radiogenic materials was calculated using decay energies given by Birch (1954). An average density of 2.3 gm/cm^3 compatible with the gravity data was assumed and the heat production of the sediment was estimated at 2.83×10^{-13} $cal/cm^3 sec$. Heat production at this rate, under steady state conditions, would provide 0.028 HFU per kilometer of sediment; thus the contribution to the observed heat flux from up to 14 km of sediment could be as large as 0.40 HFU.

Figure 41 provides some insight into the length of

U, Th, and K CONTENT OF BLACK SEA SEDIMENTS

Material	U(ppm)	Th(ppm)	K(%)	Reference
Black Sea Sediments	3.9	7.3	2.5	Clark, et al. (1966)
Russian Platform Shales	4.1	10.2	2.1*	Adams and Weaver (1958)
Russian Platform Carbonates	2.3	2.7	0.3*	Adams and Weaver (1958)
Coast Range Graywacke	1.8	6.3	1.3	Wollenberg, Smith and Bailey (1967)

*Estimated from Table 24-8 of Clark, et al. (1966)

Table 9

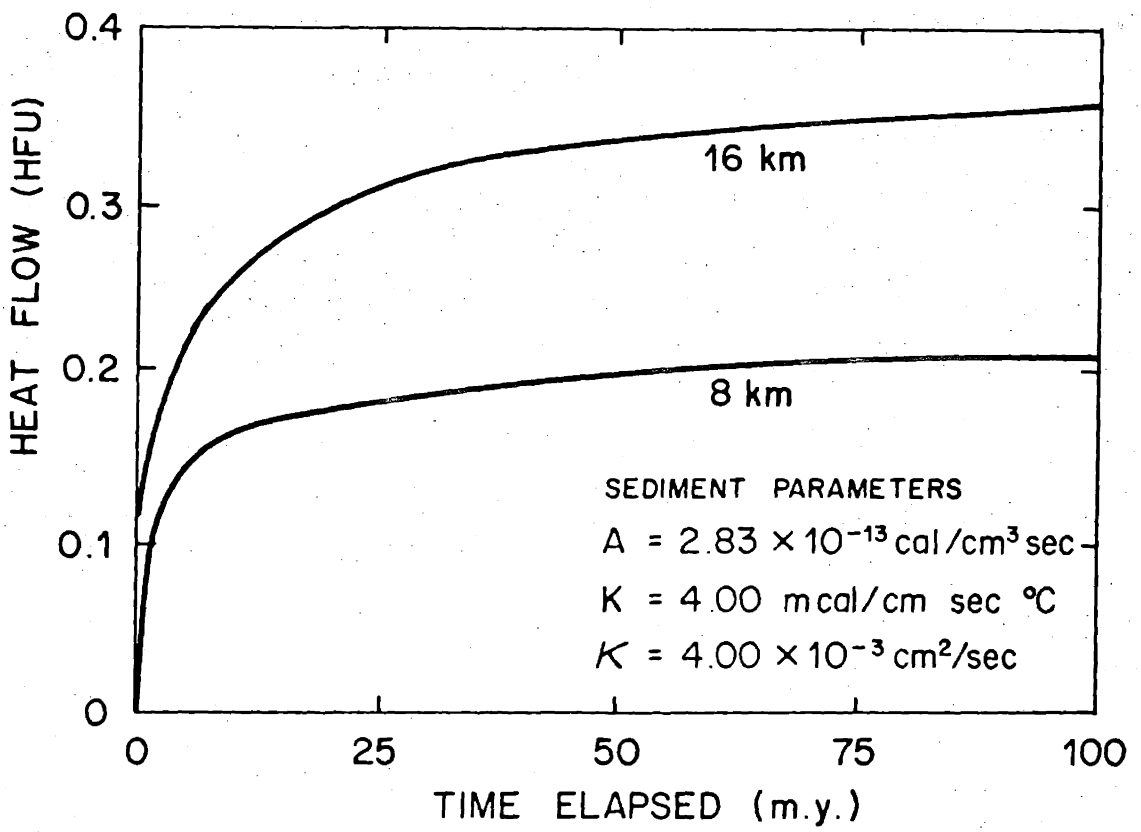

Figure 41. Radiogenic heat flow out of the surface of a layer of sediment 8 and 16 km thick having thermal properties as shown, assuming that the entire layer was deposited at constant temperature at time zero, and that no heat is flowing into the base of the sediment from the mantle.

time required for steady-state thermal conditions to be established in the sediment. It can be seen that the heat flux out of the upper surface of a sediment layer as thick as 16 km is within about 10% of the equilibrium value after 50 m.y., a period of time which is probably considerably shorter than the age of the Black Sea.

If Q is defined as the sum of the heat flux into the base of the sediments Q_B and the heat produced within the sediment layer Q_{SED}, then the observed heat flow Q_{OBS} can be written

$$Q_{OBS} = (Q_B + Q_{SED}^0 (1 - \alpha)(1 - \beta) \qquad \text{Equation 2}$$

where α and β are the fractional reductions of the heat flow due to sedimentation at a constant rate and thermal conductivity contrasts, respectively. Solving Equation 2 for Q_B,

$$Q_B = \frac{Q_{OBS}}{(1 - \alpha)(1 - \beta)} - Q_{SED} \qquad \text{Equation 3}$$

and substituting values for Q_{OBS} = 0.84 HFU, Q_{SED} = 0.28 HFU (for a 10 km thick sediment layer) and for α and β (0.63 and 0.2, respectively), the heat flux into the base of the sediment is about 2.4 HFU.

The temperature T at the base of a sediment layer of

thickness l , thermal conductivity K, diffusivity k , and volume heat production A is given by Carslaw and Jaeger (p. 80, 1959). For the case where l is small compared to $\sqrt{4Kt}$,

$$T = Gl + \frac{Al^2}{2K} \operatorname{erfc}\left(\frac{l}{\sqrt{4Kt}}\right) \qquad \text{Equation 4}$$

where G is the thermal gradient in the sediment due to heat flowing out of the mantle. G can be rewritten

$$G = Q_B / K \qquad \text{Equation 5}$$

Under steady state conditions, Equation 4 can be rewritten as

$$T = \frac{Q_B l}{K} + \frac{Al^2}{2K} \qquad \text{Equation 6}$$

Substituting values for Q_B, l , A, and K used in the computation of Q_B, the temperature at the base of the sediment column is estimated at 680°C. At a depth of 14 km the temperature in the sediment is 980°C.

Even allowing for an increase in thermal conductivity

resulting from metamorphism, it is certain that the minimum temperature at which metamorphism can proceed is exceeded by a wide margin. Fyfe and Verhoogen (1958), Winkler (1965), and Turner and Verhoogen (1960) estimated that metamorphism is likely if a temperature of 300°C or more is maintained for a geologically long period. Beneath thinner layers of sediment the temperature will be lower, however on this basis it is likely that metamorphic reactions are occurring at depths greater than about 5 km.

2.532 Explanation of Regional Heat Flow Variations

Although exothermic metamorphic reactions involving the hydration of water-poor sediments in low-grade metamorphic zones are possible, Fyfe and Verhoogen (1958) suggested that the most important reactions will be endothermic. The extent to which the heat flow is affected by metamorphism is determined by the nature and rate of the reactions-neither of which are known for the Black Sea. Metamorphism is most likely to be important in areas of thick sediment. This fact, coupled with the probable endothermic nature of the reactions, may be a cause of slightly lower heat flow in the central basin, where maximum sediment thicknesses occur, than in marginal areas with thinner sediment accumulations.

Areas now covered with great thicknesses of sediment must be regions where deposition has been in progress for

a geologically long period of time. Peripheral areas with thinner sediment thicknesses are younger areas which have subsided since the Miocene. The magnitude of the reduction in the thermal gradient due to sedimentation is a function of both sedimentation rate and duration; thus a higher observed gradient and heat flow would be expected through thinly sedimented areas marginal to the older Black Sea basin. The effect of contrasts in thermal conductivity between sediment and basement rock was discussed in Section 3.322, where it was concluded that the distribution of sediment in the Black Sea would be expected to cause high heat flow around the relatively thinly-sedimented margins and lower heat flow in the central basin.

Still another possible explanation of the slightly higher heat flux around the margins of the Black Sea is based upon the observation that the layer of 5.8 to 6.4 km/sec material present around the margins of the Black Sea thins or disappears beneath the central basin. This "granitic" material was identified as metamorphosed sedimentary rocks or of "intermediate" composition by Neprochnov et al. (1967). If it is characterized by a markedly higher concentration of radiogenic materials than either the 6.4 to 7.0 km/sec "basaltic" or 3.0 to 5.0 km/sec sediment layer, heat flow will be higher through portions of the sea floor above the "granitic" material than through areas underlain by "basaltic"

material. Although the crustal structure is well known south of Crimea, too little is known of the structure and composition of the crust beneath other areas of the Black Sea to evaluate the importance of this effect.

DISCUSSION

3.1 The Origin of Small Ocean Basins

Hypotheses for the origin of small ocean basins include almost every conceivable mechanism through which an area with crustal characteristics intermediate between those of oceans and continents can be formed. The geophysical properties of transitional areas were summarized by Menard (1967). He concluded that small ocean basins may be regions of crustal transition from typical oceanic to typical continental crust, or more infrequently, from continental to oceanic crust.

The former existence of continental crust in parts of the Mediterranean and Black Seas is strongly suggested by the abrupt termination of Tertiary and older tectonic trends by areas now covered by several kilometers of water. The Caucasus, Alps, Atlas mountains, Betic cordillera, and Apennine chains all strike into or appear to have been continuous across areas of submerged, transitional crust. Geological evidence exists for the movement of nappes and sediment from the present sea towards their present locations on land in the Apennines, Sicily, north Africa, and southern Spain (Pannekoek, 1969) and paleocurrent studies suggest a former drainage pattern inland from the Ligurian coast (Stanley and Mutti, 1968). Similar, although less abundant, evidence exists from the Black Sea region (Brinkmann, unpublished manuscript, 1968) and the eastern Mediterranean (Aubouin,

1965). A close relationship between the structural geology of the northern part of the eastern Mediterranean and the adjacent continental areas was noted by Emery et al. (1966) as suggesting that a typical oceanic crustal structure is not present beneath the eastern Mediterranean. Aeromagnetic data support the continuity of tectonic trends in Cyprus with Alpine tectonic trends on Turkey (Vogt and Higgs, 1969) and the former existence of continental crust in this area.

Hypotheses which attempt to explain the transitional crustal structure in an area formerly occupied by continental crust are of three main types. The first set of hypotheses deals with the processes responsible for the conversion of thick, light, continental crust into thinner, denser, more nearly oceanic crust. Models which have been proposed include subaerial erosion in response to uplift caused by density decrease in the mantle (Hsu, 1965), subcrustal erosion (Van Bemmelen, 1969), or both (Schuiling, 1969). Beloussov (1966) proposed a variety of geochemical subcrustal erosion by the intrusion of basic and ultrabasic magmas into the base of the continental crust, thereby causing fragments of the crust to sink into the mantle through density increases associated with largely unspecified metamorphic reactions and phase changes. Schuiling (1969) noted the inability of known geochemical processes to melt, assimilate, or react with continental crust at shallow

depths. The transformation at pressures of a few kilobars of continental material of acidic composition to mineral assemblages dense enough to sink into the mantle also appears to be a difficult problem.

The second class of oceanization hypotheses largely avoids the difficult mechanical and geochemical problems associated with thinning and increasing the density of the continental crust. Thick, light, continental crust can be replaced with dense, thin, oceanic crust if the continental crust is split apart and replaced with upwelling mantle material, as was suggested for the crust beneath the axial trough of the Red Sea (Girdler, 1969; Tramontini and Davies, 1969).

Rifting and separation of the earth's crust in the Mediterranean region may have occurred on both regional and local scales. Paleomagnetic data supports extensive relative movement between Africa and Eurasia during the Paleozoic and Lower Mesozoic, and smaller movement during the Cenozoic (Van Hilten, 1964). Further support for, as well as the details of, Mesozoic and Cenozoic movements can be obtained by studying the global pattern of marine magnetic anomalies and fracture zones and interpreting them in terms of plate tectonics (Le Pichon, 1968). Three main episodes of sea floor spreading were recognized - late Mesozoic, early Cenozoic, and late Cenozoic. Each phase of spreading occurred in response to the reorganization of the global pattern of motion.

According to the reconstruction proposed by Le Pichon, either a large "Tethys" sea existed during the Paleocene or a minimum amount of crustal shortening of 500 km has occurred since that time. The separation of Greenland and Europe began during the Paleocene and was completed during the Eocene. The resultant southeastward movement of Eurasia relative to Africa must have created a zone of shear between Eurasia and Africa. Le Pichon noted that the inversion of tectonic forces from extensional shear during the Mesozoic to compressional shear during the Cenozoic may explain some of the complexity of the Mediterranean area.

Within the large extensional (or compressive) zone opened (or closed) by relative movement between Africa and Eurasia, individual blocks appear to have undergone both translation and rotation. The counterclockwise rotation of the Iberian peninsula is well documented on paleomagnetic (Van der Voo, 1969), geophysical (Matthews and Williams, 1968), and geological (Jones and Ewing, 1969) evidence. Similar counterclockwise rotations were proposed for Corsica and Sardinia by Ashworth and Nairn (1965) and Nairn and Westphal (1967), and for the southern Alps (Van der Voo and Zijderveld, 1969).

A third model for the origin of the transitional crust may be applicable in areas where evidence for a former continental crust is weak. The crust beneath these areas may consist of a remanent of oceanic crust

buried beneath an unusually large accumulation of sediment. Reconstructions of the positions of Eurasia and Africa based on paleomagnetic data (Van Hilten, 1964) and analysis of sea floor spreading patterns (Le Pichon, 1968) indicate that the African continent has both moved nearer and rotated relative to Eurasia. If the broad region between the two land masses was oceanic, as seems most probable, then the presence of relict ocean crust in the Alpine zone is not difficult to understand.

In the following sections the applicability of these models to the Mediterranean and Black Seas will be examined. Particular attention will be given to a comparison of the observed geophysical characteristics of the various basins with the geophysical properties which would be expected for different models of formation. Although the new heat flow data provides a valuable constraint on possible origins, additional data of all types, as well as a better understanding of thermal processes in the earth, will be required before the origin of small ocean basins is understood.

3.11 The Western Mediterranean

Seismic refraction results indicate the presence of a thin crust 10 to 12 km thick beneath the western Mediterranean Sea. In most places the velocity structure includes 3 to 5 km of material with a velocity between

6.5 and 6.8 km/sec, similar to the oceanic layer characteristic of oceanic basins. In other areas material with velocities in this range is absent. In the Balearic basin west of Sardinia and in the central Tyrrhenian Sea crustal material with unusually high apparent velocities (7.0 to 7.3 km/sec) is present. Material with a shear velocity of 4.1 to 4.3 km/sec occurs only 5.0 km beneath the sea floor; thus the upper mantle beneath the western Mediterranean is more nearly typical of oceanic regions than continents.

The hypothesis that the nearly oceanic crust beneath the western Mediterranean is a piece of sea floor enclosed between Europe and Africa faces severe difficulties if the geologic evidence from the adjacent land areas has been correctly interpreted as inferring a former land mass in the Tyrrhenian Sea and western Mediterranean basin. Additional strong arguments against a relict ocean crust can be advanced based upon geophysical data (low P_n and mantle shear velocities, high heat flow, and volcanism) implying high upper mantle temperatures. The observed heat flow is much higher than can be explained by the heat produced in terrigeous sediments added to normal oceanic lithosphere, and requires high heat flux out of the mantle.

The creation of the floor of the western Mediterranean by a variety of continental rifting, either due to the relative movement of continental fragments or of extension

between the African and Eurasian plates, is in accord with most types of geophysical evidence. The ability of rifting to produce a nearly typical oceanic crust in the Red Sea was discussed by Tramontini and Davies (1969) and Girdler(1969). Material with velocities ranging from 6.7 to 7.3 km/sec is present at depths ranging from 4 to 7 km beneath the sea floor in the central Red Sea (Girdler, 1969).

Paleomagnetic data from Africa and Eurasia can be interpreted as indicating extensive dextral shearing in the Mediterranean area (Van Hilten, 1964). Le Pichon's (figure 8, 1968) reconstruction of the former positions of Africa and Eurasia shows a northwestward translation and counterclockwise rotation of Africa relative to Eurasia since the Paleocene. According to theories of plate tectonics, the relative movement of Africa and Eurasia is intimately connected with the global pattern of lithospheric sources and sinks. If the complex history of sea floor spreading in the north and south Atlantic Oceans since the Urassic involves at least three active phases of drift, as well as the opening of the Labrador and Norwegian Seas (Le Pichon, 1968), then these movements must be reflected in the tectonic history of the entire Alpine -Mediterranean region. Ryan (1969a) suggested that "the episodic nature of the spreading on either side of the Azores-Gibraltar ridge has implied alternate periods of extension, shear, and compression

within the Tethys domain between Europe and Africa."

Paleomagnetic data from the Alpine area suggests that the effect of large-scale movements of lithospheric plates has been both absorbed and modified by local translation and rotation of smaller lithospheric slabs (Iberian peninsula, Sardinia, Corsica, Italy). The movement of these blocks may have occurred solely in response to regional stresses set up by the movement of the larger African and Eurasian plates, or it may reflect dynamic conditions in the upper mantle consistent with the observed high heat flow, volcanism, low mantle velocities, and highly developed low shear velocity channel. The crust beneath the central Tyrrhenian Sea consists of 4.0 to 5.0 km/sec material underlain by a layer of 7.2 km/sec material, similar to that observed beneath active mid-ocean ridges. However, the existence of intermediate depth earthquakes beneath the Tyrrhenian Sea is not in accord with the location of an ocean ridge in the area. In addition, strike-slip movement along the Gibraltar-Azores ridge (Ritsema, 1969a), the absence of seismic activity in the western Mediterranean and Ionian Seas, and the measurement of low heat flow throughout the eastern Mediterranean Sea, preclude the extension of an active mid-oceanic ridge from the Tyrrhenian Sea into the adjacent ocean basins. Thus if crustal rifting in the Tyrrhenian Sea or western Mediterranean basin is driven by large-scale upwelling of upper mantle material, the zone of

upwelling is nearly equidimensional.

If conversion of continental crust to oceanic crust is in progress in the western Mediterranean, the process appears to be nearly completed. Transformation of continental crust through mechanical and thermal erosion at the base of the crust is in accord with geophysical data suggestive of high temperatures in the upper mantle. Although subcrustal erosion caused by differential movement between the crust and mantle would appear capable of thinning and mobilizing material at the base of the crust, it would remove the high velocity basic and intermediate material at the base of the crust which is seismically equivalent to the oceanic layer now present beneath much of the western Mediterranean Sea, and leave the low velocity material characteristic of rocks of granitic composition. If subcrustal erosion of the entire crust occurs, the effect of the erosional mechanism differs little from the sea floor spreading concepts already discussed.

An additional difficulty faced by advocates of subcrustal erosion is the present location of the enormous volume of sialic material eroded from the base of the crust. Lastly, the way in which differential movement can occur between the mantle and crust is not understood. Current concepts of plate tectonics involve the relative movement of a strong lithospheric slab 50 km (McKenzie,

1969) to 200 km (Minear and Toksöz, 1970) thick over the underlying mantle. In this view, the continental and oceanic crust are carried passively on top of the slab. In order for subcrustal erosion to thin the crust, it must first remove 50 km or more of lithosphere. Although this requirement is compatible with disruptions in the lithosphere inferred from the failure of S_n waves to travel through the western Mediterranean, other explanations appear more plausible. The absence of shallow earthquakes beneath the sea floor in the western Mediterranean also suggests that mechanical erosion of the crust is not in progress. In addition, it is unlikely that a slab of continental crust can withstand the drag caused by the horizontal movement of the lithosphere beneath it. Depending upon the geometry of the crust and surrounding lithospheric plates and the flow pattern in the mantle, either rifting or crustal thickening would be expected. As already discussed, an origin by rifting is compatible with the available geophysical data; thickening of the crust through crustal shortening obviously will not result in the creation of oceanic crust.

Crustal thinning can occur at the surface, as well as the base of the continental crust, if reversable changes in the density of the upper mantle are possible. Evidence from seismic data for regional lateral as well as vertical variations in temperature, velocity, and density of the upper mantle was presented by Toksöz et al..

(1969), Brune (1969), and Toksöz et al. (1967).

The ability of the basalt-eclogite transition or phase changes in a pyrolitic upper mantle to cause a sequence of crustal uplift, erosion, and subsidence has been suggested by Hsu (1965), Schuiling (1969), Ringwood (1969), and studied by Joyner (1967). In these models, thermal blanketing and the radiogenic heat released by the continental crust increase the temperature in the upper mantle, thereby driving the basalt-eclogite boundary deeper into the mantle and causing additional crustal uplift. Subsequent erosion of the crust reduces the pressure in the mantle, and causes additional eclogite to transform into basalt. The erosion of the upper crust, containing much of the radiogenic material, and the absorption of heat in the eclogite-basalt transition will eventually cool the upper mantle and cause a reversal in the phase transition; basalt will begin to revert back to its high pressure - low temperature state. The crust will begin to subside as the mantle continues to cool and eventually the deeply eroded surface of the former continental crust, greatly reduced in thickness and with density and velocity parameters more similar to oceanic crust than to continental crust, will sink beneath sea level. Sedimentation will increase the pressure at the base of the crust, causing additional basalt to transform to eclogite and additional subsidence, followed by still more sedimentation. The addition of a thick

blanket of low thermal conductivity sediment, radiogenic heat released in the thickening crust, and heat released in the basalt-eclogite transition will eventually cause a warming of the upper mantle and the entire cycle can repeat itself.

The results of a detailed experimental investigation of the basalt-eclogite transformation by Ringwood and Green (1967) strongly indicate that eclogite is stable relative to material of basaltic composition throughout large regions of normal continental crust. Ringwood and Green concluded that the hypothesis that the continental Moho is caused by an isochemical transformation from gabbro to eclogite must be rejected, but that this transformation may be of major importance in tectonically active areas where the Moho is not clearly defined. As examples of such areas, they cite the mid-ocean ridges, island arcs and regions of recent orogenesis; it is likely that at least parts of the western Mediterranean fall in this category. In particular, the southern Tyrrhenian Sea and the central Balearic basin are characterized by high heat flow, anomalous velocity structure, and marginal structural features suggestive of recent "fault subsidence" (Aubouin, 1965). These areas may indicate the former position of a recently submerged continental crust which is now undergoing sedimentation and rapid cooling.

3.12 The Eastern Mediterranean

The western part of the eastern Mediterranean Sea (the Ionian Sea)resembles the Tyrrhenian Sea in being enclosed on all sides by fault structures indicative of fault subsidence and in having positive Bouguer gravity anomalies as large as 266 mgal (De Bruyn, 1955). A major difference is the regionally low heat flow (0.88 HFU) in the Ionian Sea, contrasted with the high heat flow (3.11 HFU) and volcanic activity observed in the Tyrrhenian Sea.

Gravity (Woodside and Bowin, 1970) and magnetic (Vogt and Higgs, 1969) data are in accord with the extension of structural trends on Cyprus beneath the sea floor toward Alpine tectonic features in Turkey. Aubouin (1965) suggested that the outer tectonic lineaments of the Hellenies once occupied an arc parallel to and slightly south of the Hellenic arc. Geologic evidence for the former existence of continental crust elsewhere in the eastern Mediterranean is scarce, and the requirement that models of the origin of the eastern Mediterranean must be capable of converting, or at least removing, continental crust, is greatly relaxed.

Despite geophysical evidence for very different upper mantle temperatures beneath the Tyrrhenian and Ionian Seas it is possible that the transitional structure of the crust and upper mantle beneath both seas

is representative of different stages of the same subcrustal process. Analyses of surface wave dispersion data for paths through the eastern Mediterranean east of 23°E by Papazachos (1969) and Payo (1967, 1969) indicated that a thick, low-velocity crust exists beneath that area. The existence of large, positive Bouguer gravity anomalies (de Bruyn, 1955) in the Ionian Sea west of 23°E, and the abrupt decrease in gravity west of 23°E, strongly suggest a significant difference in the crustal structure of the Ionian and Levantine Seas.

The uniformly low heat flow in the Ionian Sea is consistent with that area being in a later stage of the oceanization process outlined in the last section. The lower heat flow and greater water depth in the Ionian Sea compared to the Tyrrhenian Sea are consistent with a hypothesis in which the upper mantle has already cooled due to the removal of a thick insulating and radiogenic continental or sedimentary cover, and has sunk isostatically beneath the sea in response to phase changes in the upper mantle.

Earthquake mechanisms for crustal and mantle earthquakes beneath southwestern Greece (Ritsema, 1969b) are not in accord with this hypothesis. Sinistral strike-slip faulting is typical of crustal earthquakes, and mantle earthquakes are characterized by reverse, rather than normal faulting associated with the expected graben-type subsidence.

Fragments or splinters of continental crust, equivalent to Sardinia, Corsica, Italy and Sicily in the western Mediterranean, are absent in the eastern Mediterranean Sea. Arguments that the island of Cyprus is a fragment of the former Tethys sea floor, or of a mid-Tethyan ocean rise, were presented by Gass and Masson-Smith (1963) and Gass (1968). The absence of areas of continental crust in the eastern Mediterranean further reduces the necessity to postulate the former existence of a continental mass, and precludes an origin for the Ionian Sea similar to that proposed for the Ligurian and Tyrrhenian Seas by Carey (1958), in which areas of oceanic crust were formed by the rifting and separation of the sialic crust accompanying the translation and rotation of the Sardino-Corsican and Italian lithospheric blocks.

The structural and tectonic features of the eastern Mediterranean east of 23°E are significantly different from those of the Ionian and western Mediterranean Seas. The presence of a thicker, lower-velocity crust in the eastern Mediterranean is in accord with crustal models based on gravity (Woodside and Bowin, 1970; Ryan, 1969a) and surface wave dispersion data (Papazachos, 1969; Payo, 1967, 1969). Estimates of crustal thickness along a north-south section between the Nile cone and Turkey range from a minimum of 18 km (Ryan, 1969a) to over 30 km (Woodside and Bowin, 1970). Ryan's preferred crustal model accounts for most of the gravity minimum above and

north of the Mediterranean ridge by a northward thickening of the upper crustal layers with an assumed density of 2.3 gm/cm^3. This material is seismically equivalent to material with a compressional wave velocity of 4 to 5 km/sec, according to the velocity-density curves of Woollard (p.111-72, 1962). A refracting layer having velocities in this range is present throughout the eastern Mediterranean. Refraction profiles in areas of deep water have generally been too short to determine the thickness of the 4 to 5 km/sec layer, but minimum estimates by Gaskell and Swallow (1953) range from 0.6 to 2.4 km, on the assumption that a layer of 6.4 km/sec material is present beneath the 4 to 5 km/sec material. Gaskell and Swallow also suggested that the 4 to 5 km/sec material may be a comparatively thin layer (> 100 m) underlain by lower velocity material. If so, the crustal thickness may be thinner than 18 km. Explanation of the gravity anomalies in terms of variations in crustal density eliminates the need to postulate the large and rapid lateral variations in crustal thickness preferred by Woodside and Bowin (1970).

Interpretations of the gravity minimum in the eastern Mediterranean by Woodside and Bowin (1970), Ryan (1969a), and Harrison (1955) all involve a northward thickening of the crust and/or upper sedimentary layers caused by north-south compression and underthrusting of the European continent by the Mediterranean crust. Thus,

the original thickness of the crust was probably more similar to oceanic than to continental thickness. As discussed earlier, paleomagnetic data and implications drawn from sea floor spreading and plate theory (Le Pichon, 1968) are in accord with the existence of oceanic crust between the African and Eurasian continents into the Cenozoic. Geological and geophysical evidence from Cyprus suggests that the Troodos massif evolved as an oceanic volcanic pile situated between the then more widely separated masses of African and Eurasia (Gass and Masson-Smith, 1963). As these plates converged both the volcanic pile and the oceanic crust were underthrust by the leading edge of the African continent, and uplifted above sea level. Similarities between the mode of emplacement of the extensive, basic dyke swarm and proposed models for the injection of basalt magma at spreading ocean ridges were discussed in a more recent paper (Gass, 1968). In addition, Gass noted that the bulk chemical composition of the Troodos volcanic rocks, while poorly known, seems equivalent to oceanic tholeitic basalts associated with mid-ocean ridges.

The hypothesis that the eastern Mediterranean is a piece of thickly sedimented former oceanic crust--perhaps the last remaining piece of a more extensive Tethyan sea floor - appears to be consistent with the existing geophysical data. The absence of a pattern of linear magnetic anomalies characteristic of other ocean basins

may indicate that no geomagnetic reversals occurred while the crust was generated or that the crust was generated in low geomagnetic latitudes by a north-trending ridge (Vogt and Higgs, 1969). Magnetically quiet zones are present on both sides of the North Atlantic Ocean and are believed to reflect creation of the oceanic crust during a long period of no magnetic reversals during the late Paleozoic (Heirtzler and Hayes, 1967). A similar magnetically quiet zone is situated seaward of the Aleutian trench and may result from a change in the magnetic properties of the crustal rocks brought about by the tectonic processes associated with the formation of the trench (Hayes and Heirtzler, 1968).

The corrected heat flow of 0.88 HFU is surprisingly low if oceanic crust and lithosphere are present beneath the eastern Mediterranean. The additional heat produced in the sediments deposited on the sea floor would be expected to result in a small increase, rather than a decrease in the heat flow. If the low heat flow is caused by low upper mantle temperatures, rather than by crustal shortening or environmental effects, it may indicate either a downward component of movement of the mantle material relative to the sea floor, a deficiency in radiogenic material in the upper mantle beneath the sea floor, or both. One explanation for the observed equality of oceanic and continental heat flow, despite

the higher concentrations of radiogenic elements in the continental crust, is that the oceanic mantle contains a greater concentration of radioactive elements than the mantle beneath the continent (Von Herzen, 1967). The subcrustal erosion, displacement, or replacement of the oceanic asthenosphere or lithosphere by less radioactive material formerly situated beneath the African continent could account for the low heat flow. A necessary consequence of this mechanism would be the removal of the less radiogenic mantle material beneath the southern edge of Europe and its replacement with more radiogenic oceanic mantle material. The abnormally high concentration of radioactive material beneath the Alpine region of southern Eurasia could cause or at least contribute to the energy required for the Alpine orogeny.

3.13 The Black Sea

Geologic and geophysical data from the Black Sea and adjacent areas indicate the former presence of a land mass on the area now covered by up to 14 km of sediment and 2 km of water. Sediment deposited in northwestern Anatolia during the Paleozoic appears to have been derived from an elevated source area in the Black Sea (Brinkmann, 1960). The appearance and outward thickening of intermediate velocity "granitic" material away from the central Black Sea is in accord with erosion of the

uppermost layers of continental crust during a long period of uplift (Rezanov and Chamo, 1969). Residual magnetic anomalies in the eastern half of the Black Sea are parallel to and may represent the extension of structural trends of the Caucasus. Large parts of continental structures of the Caucasus, Crimea, and Anatolia are partly or completely submerged beneath the Black Sea.

It is therefore probable that models for the origin of the Black Sea must be capable of either transforming continental crust or replacing it with the crustal structure observed in the Black Sea. An origin based upon the entrapment of a block of oceanic crust, as proposed by Milanovskiy (1967), does not meet this requirement. Although the crustal structure of the western Black Sea is similar to that which would be created by the deposition of a thick sediment layer on normal oceanic crust (and thus similar to the crustal structure beneath the abyssal region of the Gulf of Mexico as determined by Ewing et al.,(1962), the thickness of the 6.8-7.0 km/sec layer beneath the central and eastern Black Sea is much greater than is characteristic of normal oceanic crust.

An origin of the Black Sea by rifting of the continental crust and its replacement by mantle material is incompatible with the observed continuity of the geologic structures surrounding the Black Sea. The

crustal structure of the transition zone between the central Black Sea and surrounding continental areas appears to be gradual and smooth (Neprochnov, 1968), and not in accord with subsidence by faulting. In addition, the continuity of magnetic anomalies associated with tectonic trends in the Caucasus and Pontic mountains beneath the sea floor further argues against an origin by rifting. The possibility that the observed magnetic anomalies were created by magnetic reversals during a period of sea floor spreading seems remote in view of the shift in the direction of the magnetic trends in the central Black Sea.

Once again, the nature and feasibility of a process which could cause uplift of the continental crust so as to expose it to erosion, followed by subsidence of nearly 20 km, is in question. Mantle velocities beneath the Black Sea are normal (8.2 ± 0.2 km/sec) and a sub-Moho layer with velocities of 8.8 km/sec may be situated at a depth of 30 km beneath the western Black Sea (Neprochnov, 1968). The existence of unusually high velocities in the mantle are in accord with the discrepancy between the observed and computed free-air gravity anomalies, first noted by Menard (1967). The gravity anomaly predicted by assigning densities to crustal layers on the basis of empirical velocity-density relationships are several hundred milligals lower than the observed free-air anomaly. This implies either that

the densities assigned to the crustal layers are too low, or that the mantle is anomalously dense. Evidence for Late Tertiary and Pleistocene subsidence in and around the Black Sea (Chekunov, 1966; Nalivkin, 1960) is in accord with a dense upper mantle causing isostatic subsidence of the sea floor. The high heat flow calculated for the Black Sea is difficult to understand if the mantle is dense and rigid, as implied by the gravity and seismic refraction data. High upper mantle temperatures would be expected to reduce the density and seismic velocity both due to thermal effects and/or phase changes (garnet pyrolite → plagioclase pyrolite, eclogite → basalt).

The inclusion of volcanic material in the sedimentary layer is a possible, though unlikely cause of the lack of agreement between the expected and observed mantle properties. In many places in the crust beneath the Black Sea, refracting layers with velocities up to 4.5 km/sec are present within material with an average velocity of 3.0 to 3.5 km/sec (Neprochnov, 1968). If these layers are volcanic material with a density of 2.8 - 3.0 gr/cc, their presence in the sediment column would increase the average density of the crust, decrease the amplitude of the sedimentation correction and thus the calculated heat flow, and lastly provide a crustal source for at least some of the observed heat flow, thereby reducing the heat flow out of, and temperatures within, the upper mantle. Menard (1964) noted that some submarine volcanoes

have densities in the range 2.3 to 2.5 gm/cc and seismic velocities as low as 3 km/sec. In order to increase the density of the sedimentary column by about 0.4 gm/cc as is necessary to meet gravity requirements, almost all of the low velocity material would have to be volcanic material having density greater than about 2.7 gm/cc. This seems unlikely on the basis of seismic reflection and refraction data, the high sedimentation rate, gravity data in the western Black Sea, and calculations by Bowin (unpublished manuscript, 1970) of the depth to bodies causing the residual magnetic anomalies in the Black Sea.

3.2 Relation of Plate Theory to the Mediterranean

Almost all small ocean basins with intermediate crustal structure are located behind (on the concave side of) island arc systems. Island arcs, along with active continental margins, appear to delineate areas where large, aseismic plates of lithosphere are descending into the upper mantle (McKenzie, 1969; Isacks et al., 1968). Areas in which the rate of movement of the down-going slab exceeds 5 to 6 cm/yr appear to be associated with primarily tensional crustal features, as exemplified by oceanic trenches. Where rates are lower, compressional stresses prevail and result in the creation of chains of mountains (Le Pichon, 1968) or sedimentary ridges on the sea floor (Chase and Bunce, 1969). Most island arcs are situated either between two oceanic plates or between

oceanic and continental plates. If the Mediterranean is an area in which lithosphere is being consumed (McKenzie, 1969; Le Pichon, 1968; Morgan, 1968; Ryan, 1969a), it is unique in its present position between two continental plates. McKenzie (1969) noted the impossibility of sinking light continental crust beneath denser mantle material, and suggested that attempted assimilation of continental crust can produce fold mountains and changes in the flow pattern in the asthenosphere.

The distribution of intermediate and deep earthquakes along a planar surface dipping beneath a continent or marginal sea appears to be a diagnostic feature of island arcs and active continental margins. Intermediate and deep focus earthquakes occur beneath the Tyrrhenian Sea along a broad, poorly defined zone which intersects the crust along the Calabrian arc and dips to 450 km beneath the sea. A broad zone of intermediate depth earthquake hypocenters also exists in the eastern Mediterranean, principally north of the Cretan arc. The distribution of foci is limited to depths shallower than 200 km and does not define a plane dipping beneath the Aegean Sea. Intermediate depth activity is concentrated beneath the southern Aegean and ends abruptly at the arcuate zone of active volcanoes about 200 km behind the Cretan arc. An eastward increase in the maximum depth of mantle earthquakes in the southern Aegean was noted by Delibasis and Galanopoulos (1968). Additional intermediate

depth earthquakes occur in southwestern Turkey, in the northeastern Mediterranean near Cyprus, and beneath the Carpathian and Caucusus mountains.

The distribution of seismicity in the Mediterranean area can be used to draw an analogy between the Mediterranean arcs and circum-Pacific island arcs. The Aegean and Tyrrhenian Seas appear to be equivalent to marginal seas behind the Cretan and Calabrian arcs, respectively. Other geophysical data which are in accord with this hypothesis are presented below.

Short-period seismic shear waves (S_n) propagate in the lithosphere above the low-velocity zone. The failure of S_n waves to propagate across mid-ocean ridges or island arcs was interpreted as indicating a discontinuity in the lithosphere beneath these structures (Molnar and Oliver, 1969). Although S_n waves propagate efficiently across stable regions of Europe north of the Alps, they are not transmitted along paths which include "an island arc in southern Italy". S_n waves are transmitted efficiently across the eastern-most Mediterranean, but no S_n waves are observed for paths which cross the Cretan arc or western Turkey. If the interpretation proposed by Molnar and Sykes is correct, then the discontinuities in the lithosphere which are required if the Calabrian and Aegean arcs are tectonically equivalent to Pacific island arcs, do in fact exist.

The distribution of Cenozoic volcanic activity along the Tyrrhenian coast of the Apennine peninsula and northern Sicily, and in an arcuate zone in the southern Aegean behind the Cretan arc, is similar to the distribution of volcanic products usually associated with Pacific island arcs. The highly potassic lavas of southern Italy contain extraordinary concentrations of radioactive elements and are characterized by a high $^{87}Sr/^{86}Sr$ ratio. The Sr isotope evidence was interpreted by Hurley et al. (1966) as suggesting that the magmas were derived from the refusion or anatexis of ancient continental sialic rocks at depths of 50 km or more.

Geophysical similarities between the Calabrian and Cretan areas and the Japan arc are striking. A zone of high heat flow and Cenozoic volcanism is present along the inner edge of Japan (Uyeda and Vacquier, 1968; Yasui et al. 1968).

The average heat flux in the Sea of Japan is 2.22$\pm$ 0.53 HFU, with an average of over 2.5 HFU for measurements in the deeper, northern basin. An average flux of 2.23$\pm$0.28 was observed through the deep-water portion of the Sea of Okhotsk; in the region where the water depth is less than 2000 m heat flow averaged only 1.67$\pm$0.44 HFU. Heat flow is subnormal on the seaward side of the Japanese island arc and over the Japan trench.

The existence of high heat flow behind an island arc and of low heat flow ahead of the arc over the ocean trench

area are common, if not diagnostic features of active island arcs. Sinking of a cool slab of lithosphere into the upper mantle should depress the isotherms behind an island arc and result in low, rather than high, regional heat flux. Turcotte and Oxburgh (1968) and Oxburgh and Turcotte (1968) suggested that the high heat flux is a consequence of heat generated by viscous dissipation of the kinetic energy associated with a downward moving slab. They avoided the difficulty of the prohibitively long time required for the conduction of heat generated deep in the mantle to the surface by invoking mass transport of heat through the upward movement of magma. McKenzie (1969) also cited viscous dissipation as a means of heat production and suggested that a zone of shallow stress heating will occur behind the island arc, as well as the deeper zone proposed by Oxburgh and Turcotte.

It is interesting to speculate that the high heat flow in the western Mediterranean and low heat flow in the Ionian Sea may be a consequence of the thrusting or dragging of the Ionian Sea lithosphere in a northwesterly direction beneath the Tyrrhenian Sea. In this model, the Ionian Sea would be equivalent to oceanic crust, characterized by subnormal heat flow, present ahead of and over the trench area.

The analogy between the Calabrian arc and Pacific island arcs can be extended to include the Cretan arc.

The presence of active volcanism in the Aegean Sea suggests that the upper mantle is at abnormally high temperature behind the Cretan arc, and the unusually low heat flow south of the arc has already been discussed. The observations that phase velocities of Rayleigh waves are higher for waves traveling south from Athens to Helwan than for waves traveling the opposite path and the northward decrease in free-air gravity from Egypt to Turkey was interpreted as being due to a northward dipping Moho. If the floor of theeastern Mediterranean is sliding down beneath the Alpine zone of southern Europe, its velocity vector must contain a downward component. Using Le Pichon's (1968) estimate of about 2 cm/yr for the rate of closure between Europe and North Africa, and estimating the regional northward dip of the Moho as about 1.5° from a gravity model presented by Woodside and Bowin (1970), the mantle material would be moving downward relative to the sea floor at 50 cm/1000 yrs, a velocity more than sufficient to depress the isotherms in the mantle and thus the heat flow into the crust. A similar process may be occurring beneath the Ionian Sea.

McKenzie (1970) proposed a model of plate tectonics in the Mediterranean region purported to be in agreement with the distribution and fault plane mechanisms of earthquakes. His model is generally compatible with the foregoing speculations with the possible exception of the Calabrian arc. Better agreement with Ritsema's (1969b)

fault plane solutions are obtained by postulating northwestward, rather than northward movement, of his Africa block (McKenzie, figure 4, 1970) relative to the Eurasian plate. McKenzie's rejection of the concept of sinking lithospheric material behind the Calabrian arc on the basis of the clustering of earthquake foci along a westward dipping slab beneath the Tyrrhenian Sea seems unsupportable in view of the difficulty in determining the dip of the plane (Peterschmitt, 1956) and the important fact that such a plane does exist in conjunction with other geophysical features usually associated with Pacific island arc structures.

3.3 SUMMARY OF RESULTS

The principle results of heat flow measurements in the Mediterranean and Black Seas are summarized in Table 10 and Figure 42. Unless otherwise stated, the heat flow values presented in this section have been corrected for environmental factors peculiar to each area as discussed in Sections 2.32, 2.42, and 2.52.

3.31 Western Mediterranean Sea

The observed average heat flow in the Tyrrhenian basin is 2.83 HFU, 1.00 HFU greater than the observed average flux through the western Mediterranean basin. The heat flow in both areas has been reduced by sedimentation, and the reduction has been larger in the older, more

SUMMARY OF HEAT FLOW DATA

REGION	SEDIMENTATION PARAMETERS			AVERAGE HEAT FLOW	
	RATE (cm/1000 yr)	DURATION (m.y.)	REDUCTION (%)	OBSERVED (HFU)	CORRECTED (HFU)
Western Mediterranean Basin	23	15	33	1.83	2.73
Tyrrhenian Basin	12	10	9	2.83	3.11
Eastern Mediterranean Sea	4.3	67	16	0.74	0.88
Black Sea	20	100	70*	0.84	2.73

* Includes estimated 20% reduction due to thermal refraction, as discussed in Section 2.531.

TABLE 10. Summary of observed and corrected heat flow data

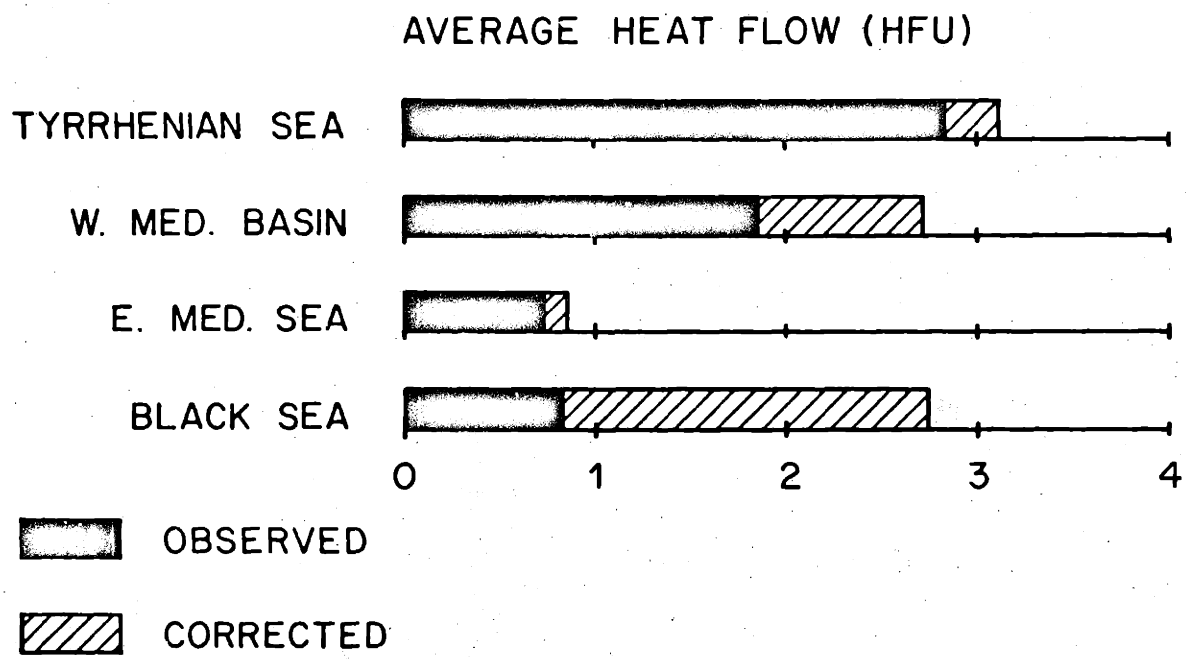

Figure 42. Summary of observed and corrected heat flow averages in the Mediterranean and Black Seas.

thickly sedimented western Mediterranean basin than in the Tyrrhenian basin. However the corrected heat flow for the Tyrrhenian basin (3.11 HFU) remains greater than the corrected western Mediterranean basin average (2.73 HFU). This observation is in accord with the presence of active volcanism in and around the southern Tyrrhenian Sea, and the absence of volcanic activity further to the west. The average heat flow out of the entire western Mediterranean Sea is 2.92 HFU. This rate is over twice the world average and distinguishes the western Mediterranean as an area of anomalously high heat flow. The existence of low P_n velocities and an ultra-low shear velocity channel at an unusually shallow depth beneath the western Mediterranean is in accord with the heat flow data indicating high upper mantle temperatures.

3.32 Eastern Mediterranean Sea

The observed heat flow values in the eastern Mediterranean are strikingly low and uniform compared to the observed heat flow through the western Mediterranean (Figure 43 and 44). The observed average flux of 0.74 HFU, even when corrected for sedimentation to 0.88 HFU, emains substantially lower than the world average heat flow (1.40 HFU) and is less than a third of the heat flow through the western Mediterranean. With only a few exceptions, heat flow values are uniformly low throughout the entire eastern Mediterranean. Significant deviations

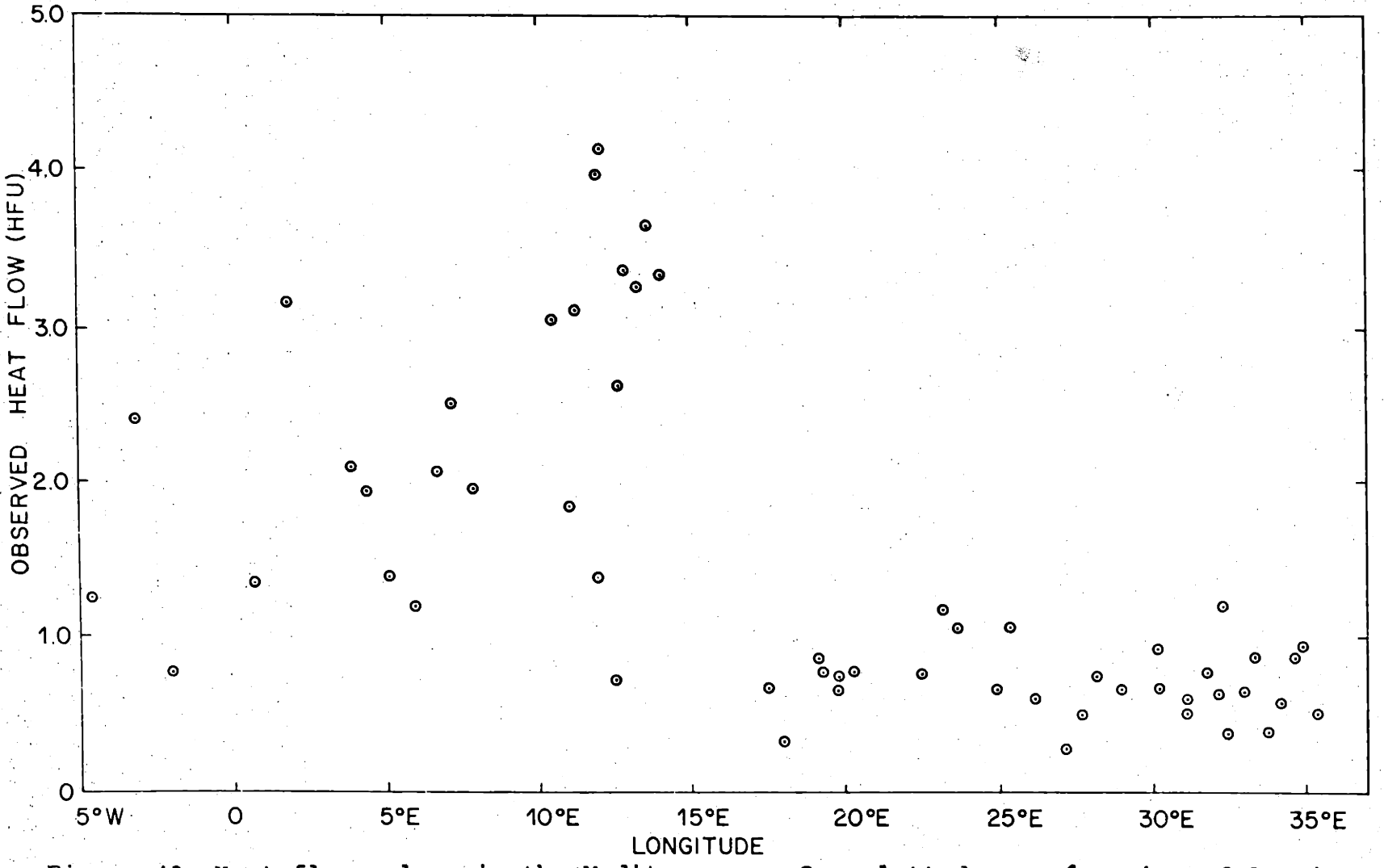

Figure 43. Heat flow values in the Mediterranean Sea plotted as a function of longitude. Boundaries between the eastern and western Mediterranean Seas and between the Tyrhennian and western Mediterranean basin are located at about 15°E and 9°E, respectively.

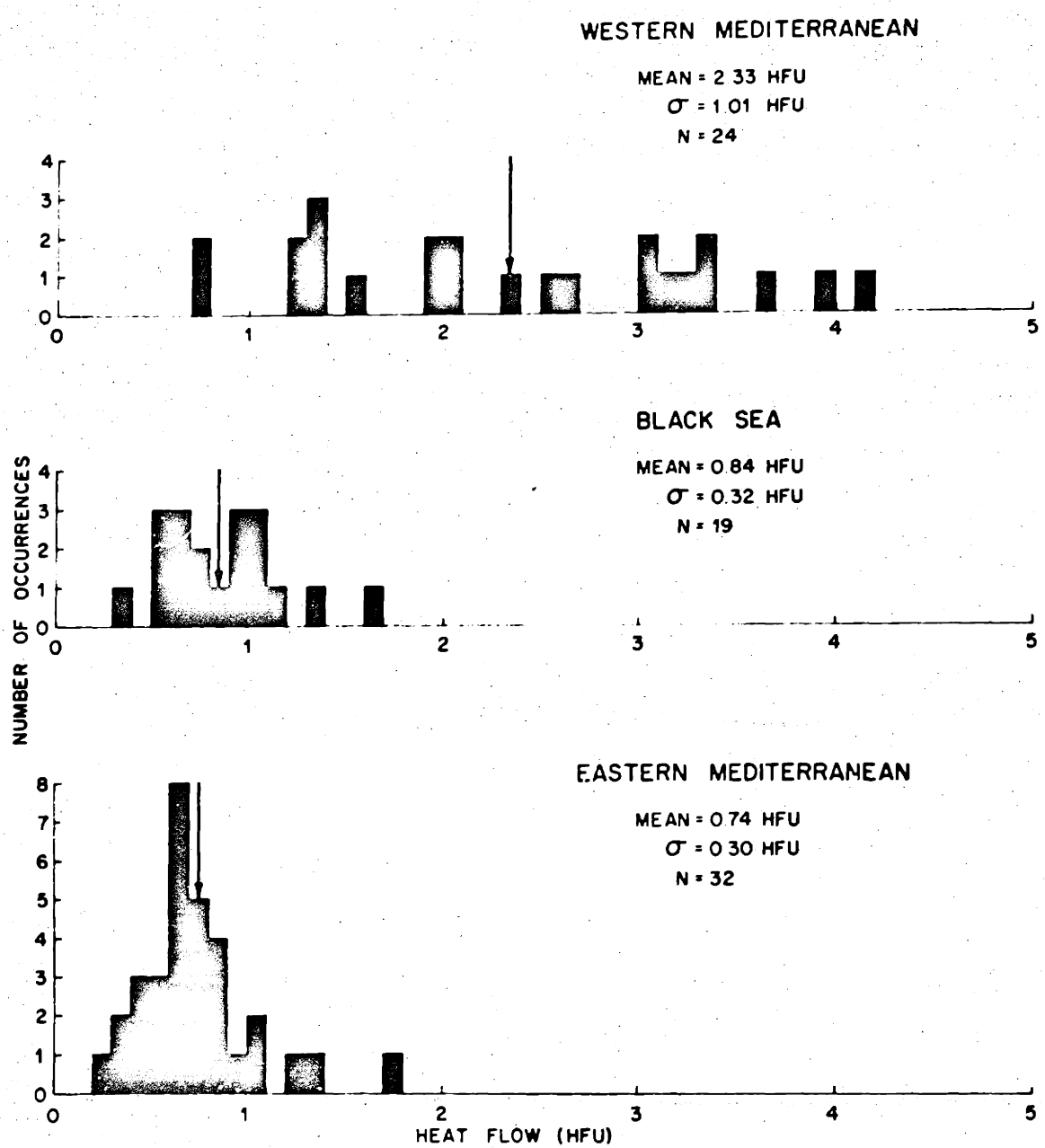

Figure 44. Histograms of observed heat flow values in the Mediterranean and Black Seas. Average heat flow in each area is shown by the position of the vertical arrows.

of individual heat flow values from the regional mean are believed to be due to localized environmental disturbances ratner than to thermal disturbances in the crust or upper mantle.

3.33 Black Sea

Although the average observed heat flow (0.84 HFU) in the Black Sea is nearly equal to that in the eastern Mediterranean, the deposition of a greater thickness of sediment in the Black Sea has preferentially reduced the flux through that sea floor relative to the heat flow in the eastern Mediterranean (see Figure 42). After correcting for sedimentation and refraction, the average flux through the floor of the Black Sea becomes 2.7 HFU, of which about 0.3 HFU is produced in the sediment column.

The eastern and western halves of the Black Sea possess nearly equal heat flux. Although the tendency for higher values to occur around the margins of the basin may be caused by subnormal heat flow out of the uppermost mantle beneath the central Black Sea, it more likely reflects the presence of thicker sediment in the central basin than around the margins. As discussed in Section 2.21, sedimentation is capable of reducing the geothermal gradient in proportion to the sedimentation rate and/or duration--thus the thickly covered deep-water areas should posssess the lowest observed heat flux. In addition the contrast in thermal conductivity between the

poorly conducting marine sediments and the crystalline rock present beneath marginal areas of the Black Sea will result in thermal refraction and further reduction of the heat flux through the floor of the central basin. Endothermic metamorphic reactions and low radiogenic heat production beneath the central basin where the intermediate velocity "granitic" layer is thin or absent also may contribute to the presence of lower heat flux through the central basin relative to the margins.

3.4 FUTURE WORK

A more definitive explanation of the origins of the Mediterranean and Black Seas must await additional geophysical data of all types, as well as a better understanding of the ability, or inability, of thermally driven upper mantle processes to directly or indirectly transform crustal structure typical of oceans and continents to an intermediate type.

The results of investigations planned as part of the JOIDES deep-drilling program in the Mediterranean Sea this summer will be of particular importance. Stratigraphic and temperature data from holes several hundred meters below the sea floor will allow more accurate calculations of the long-term climatic and sedimentation corrections to the observed heat flow and thus a more reliable estimate of the absolute value of the heat flow

characteristic of each basin. In addition, reliable heat flow measurements will be possible in relatively shallow, thermally-unstable areas of the Aegean and Adriatic Seas and Sicilian continental shelf. Terrestrial heat flow data is almost totally absent around the Mediterranean Sea and is essential for any regional mapping and understanding of upper mantle properties.

Because the interpretation of any piece of geophysical data is so dependent upon the results of all other types of investigations, it is difficult to single out a particular type of data which is more important than others. Severe limitations are placed on the interpretation of the extensive gravity data available from the Mediterranean by the absence of long refraction profiles in the Tyrrhenian and eastern Mediterranean Seas.

Seismological investigations similar to those carried out to investigate the upper mantle beneath the Tonga-Kermadec and Japan arcs by Sykes (1966), Oliver and Isacks (1967) and Kanamori (1968), respectively, may be useful to resolve the relevance of plate tectonics to the Mediterranean area.

The major contribution made by Ryan (1969a, 1969b) towards understanding the sedimentary and tectonic history of the Mediterranean suggests that the further application and combination of marine geological and geophysical techniques will yield additional important results relating to the origin and history of the sea floor. The

relevance of the JOIDES program to this type of investigation cannot be overstressed.

Evidence has been presented which is suggestive of the impermanence, on a rather short geologic time scale, of oceanic and continental areas, and underscores the necessity for additional geophysical and geological investigations on the surrounding land areas and their extension to the edge of, or preferably beneath, the adjacent sea floor.

ACKNOWLEDGEMENTS

The marine heat flow measurements discussed in this thesis were made possible through the cooperation of the Department of Earth and Planetary Sciences of the Massachusetts Institute of Technology, the Geophysics and Geochemistry Departments of the the Woods Hole Oceanographic Institution, the Lamont-Doherty Geological Observatory, and the Osservatorio Geofisico Sperimentale-Trieste. Heat flow data was obtained by the author in the eastern Mediterranean and in the Black Sea aboard the Woods Hole Oceanographic Institution research vessels CHAIN and ATLANTIS II, respectively. The author wishes to express his appreciation to the officers and crew, and to all those who assisted in the measurements - particularly Frank B. Wooding and Earl Young. Edward Zarudzki and Doctors David A. Ross and Egen Degens, as Chief Scientists aboard the R.V. CHAIN and R.V. ATLANTIS II, were extremely generous in providing ship time for the heat flow measurements.

Through the cooperation of Dr. Carlo Morelli of O.G.S.T. and Edward Zarudzki, heat flow measurements were made in the Tyrrhenian Sea aboard the M.N. BANNOCK by George Harlow, assisted by Dr. H.K. Wong of Woods Hole.

I am deeply appreciative of the assistance provided by Dr. William Ryan of the Lamot-Doherty Geological Observatory, who allowed the use of his unpublished Mediterranean heat flow data in this thesis. In addition,

I benefitted greatly from discussions with Dr. Ryan, as well as Dr. Carl Bowin.

Mrs. Mary Chessman, Anne Erickson, and Dr. James Combs provided invaluable assistance in building, testing and calibrating the heat flow equipment.

I am particularly indebted to my thesis advisor Dr. Gene Simmons and the Department of Earth and Planetary Sciences of M.I.T. for providing the opportunity, support, and incentive to establish a marine heat flow program at M.I.T. Dr. Simmons, as well as Dr. Richard P. Von Herzen of W.H.O.I. and Dr. Shawn Biehler of M.I.T., reviewed this thesis and made valuable suggestions. This work was supported by the Office of Naval Research under Nonr 1841 (74).

REFERENCES

Adams, J.A.S., and C.E. Weaver, Thorium-to-uranium ratios as indicators of sedimentary processes: example of concept of geochemical facies, Bull. Am. Assoc. Petrol. Geologists, 42(2), 387-430, 1958.

Anonymous, Karadenizde Jeofizik Arastirmalar, I Jeomagnetik, Maliye Malidir, D515-F/FS, Deniz Kuvvetleri Komutanligi Hidrografi Nesriyatai, 6 p., 26 pls., 1965.

Ashworth, T.P., and A.E.M. Nairn, An anomalous Permian pole from Corsica, Paleogeography, Paleoclimatology, Paleoecology, 1, 119-125, 1965.

Aubouin, J., Geosynclines: Volume 1 of Developments in Geotectoniques, 335 pp., Elsevier Publishing Co., Amsterdam, 1965.

Balavadze, B.K., and P.Sh. Mindeli, Earth's crust structure of Black Sea basin from geophysical evidence, Studia geophys. et geod., 9, 75-80, 1965.

Beloussov,V.V., Modern concepts of the structure and development of the Earth's crust and the upper mantle of continents, Quart. J. Geol. Soc. London, 122, 293-314, 1966.

Berry, M.H., and L. Knopoff, Structure of the upper mantle under the western Mediterranean basin, J. Geophys. Res., 72(14), 3613-3626, 1967.

Birch, F., Heat from radioactivity, Chapter 5 in Nuclear Geology, edited by H. Faul, 148-174, John Wiley and

Sons, New York, N.Y., 1954.

Birch, F., The effects of Pleistocene climatic variations upon geothermal gradients, Am. J. Sci., 246, 729-760, 1948.

Birch, F.S., and A.J. Halunen, Jr., Heat-flow measurements in the Atlantic Ocean, Indian Ocean, Mediterranean Sea, and Red Sea, J. Geophys. Res., 71(2), 583-586, 1966.

Blumenthal, M.M., and G. van der Kaaden, Catalogue of the Active Volcanoes of the World including Solfatara Fields, Part XVII, Turkey, 13 pp., Intern. Assoc. of Volcanol., Rome, 1964.

Boldizsár, T., Geothermal data from the Vienna basin, J. Geophys. Res., 73(2), 613-618, 1968.

Boldizsár, T., Terrestrial heat and geothermal resources in Hungary, Bull. Volcanol., 30, 221-227, 1967a.

Boldizsár, T., Terrestrial heat flow in Hungarian Permian strata, Pure and Applied Geophysics, 67, 128-132, 1967b.

Boldizsár, T., Terrestrial heat flow in the Carpathians, J. Geophys. Res., 69(24), 5269-5275, 1964.

Boldizsár, T., Terrestrial heat flow in the natural steam field at Larderello, Geofis. Pura Appl., 56, 115-122, 1963.

Bott, M.H.P., The upper mantle in relation to the origin of vertical movements at the Earth's surface, reported at The Upper Mantle Symposium, New Delhi, 1964, Proceedings of the Twenty-first International Geologic

Congress, edited by C. Smith and T. Sorgenfrei, 20-28, Det Berlingske Bogtrykkeri, Copenhagen, 1965.

Bowin, C., Gravity anomalies of the Black Sea, unpublished manuscript, 1970.

Briden, J.C., Paleomagnetism of the Ntonya ring structure, Malawi, J. Geophys. Res., 73(2), 725-733, 1968.

Brinkmann, R., Geologic history of the Black Sea region, unpublished manuscript, 1968.

Brinkmann, R., Geologic Evolution of Europe, 161 pp., Hafner Publishing Company, New York, 1960.

Brune, J.N., Surface waves and crustal structure, in The Earth's Crust and Upper Mantle, Geophysical Monograph 13, edited by P. Hart, 230-242, American Geophysical Union, Washington, D.C., 1969.

Bullard, E.C., and A. Day, The flow of heat through the floor of the Atlantic Ocean, Geophys. J., 4, 282-292, 1961.

Bullard, E.C., A.E. Maxwell, and R. Revelle, Heat flow through the deep sea floor, Advan. Geophys., 3, 153-181, 1956.

Burakovskiy, V. Ye., Some results of a study of the deep-seated structure of the Earth's crust in the Black Sea depression and adjacent areas, in The Structure of the Black Sea Depression, 22-26, "Nauka" Publishing House, Moscow, 1966.

Canitez, N., and S.B. Üçer, Computer determinations for the fault-plane solutions in and near Anatolia, Tectonophysics, 4(3), 235-244, 1967.

Carey, S.W., A tectonic approach to continental drift, Continental Drift Symposium, 177-355, Hobart, Tasmania, 1958.

Carruthers, J.N., The Bosporus undercurrent: some bed measurements, Nature, 201, 363-365, 1964.

Carslaw, H.S., and J.C. Jaeger, Conduction of Heat in Solids, 2nd Ed., 510 pp., Oxford University Press, New York, 1959.

Caspers, H., Black Sea and Sea of Azov, Treatise on Marine Ecology and Paleoecology, Geol. Soc. Am. Mem. 67 (1), edited by J.W. Hedgepeth, 801-890, Geol. Soc. Am., New York, 1957.

Cataldi, R., Remarks on the geothermal research in the region of Monte Amiata (Tuscany-Italy), Bull. Volcanol., 30, 243-255, 1967.

Cermák, V., Correlation of heat flow values with the tectonic structure of Czechoslovakia, Nature, 218, 556-557, 1968a.

Cermák, V., Terrestrial heat flow in the Alpine-Carpathian foredeep in Southern Moravia, J. Geophys. Res., 73(2), 820-821, 1968b.

Cermák, V., Heat flow near Teplice in North Bohemia, Geophys. J. Roy. Astron. Soc., 13, 547-549, 1967.

Chase, R.L., and E.T. Bunce, Underthrusting of the eastern margin of the Antilles by the floor of the western North Atlantic Ocean, and origin of the Barbados Ridge, J. Geophys. Res., 74(6), 1413-1420, 1969.

Chekunov, A.V., Neogene tectonics of the northwestern part of the Black Sea, Doklady Akad. Nauk. SSSR (English transl.), 168, 32-34, 1966.

Clark, S.P., Heat flow in the Austrian Alps, Geophys. J., 6, 54-63, 1961.

Clark, S.P., and E. Jäger, Denudation rate in the Alps from geochronologic and heat flow data, Am. J. Sci., 267, 1143-1160, 1969.

Clark, S.P., and E.R. Niblett, Terrestrial heat flow in the Swiss Alps, Monthly Notices Roy. Astron. Soc. Geophys. Suppl., 7, 176-195, 1956.

Clark, S.P., Jr., Z.E. Peterman, and K.S. Heier, Abundances of uranium, thorium, and potassium, in Handbook of Physical Constants, Geol. Soc. Am. Mem. 97, edited by S.P. Clark, 521-541, Geol. Soc. Am., New York, 1966.

Coster, H.P., Terrestrial heat flow in Persia, Monthly Notices Roy. Astron. Soc., Geophys. Suppl., 5, 131-145, 1947,

Cox, A., and R.R. Doell, Review of paleomagnetism, Bull. Geol. Soc. Am., 71, 645-768, 1960.

Creer, K.M., Arrangement of the continents during the Palaeozoic era, Nature, 219, 41-44, 1968.

De Boer, J., Paleomagnetic indications of megatectonic movements in the Tethys, J. Geophys. Res., 70(4), 931-943, 1965.

De Booy, T., Repeated disappearance of continental crust during the geologic development of the western Mediterranean area, Verhandelingen Kon. Ned.

Geol. Mijnbouwk, Gen., 26, 79-104, 1969.

De Bruyn, J.W., Isogam maps of Europe and North Africa, Geophys. Prospecting, 3(1), 1-14, 1955.

Delibasis, N., and A.G. Galanopoulos, Space and time variations of strain release in the Greek area, in Proceedings of the Eighth Assembly of the European Seismological Commission, edited by E. Bisztricany, 49-58, Akademiai Kiado, Budapest, 1968.

Drake, C.L., J.I. Ewing, and H. Stockard, The continental margin of the eastern United States, Can. J. Earth. Sci., 5, 993-1010, 1968.

El-Hinnawi, E.E., Petrographical and geochemical studies on Egyptian (U.A.R.) basalts, Bull. Volcanol. 28, 282-292, 1965.

Emiliani, C., Pleistocene temperature variations in the Mediterranean, Quaternaria, 2, 89-98, 1955b.

Emiliani, C., Pleistocene temperatures, J. Geol.,63(6), 538-578, 1955a.

Emiliani, C., L. Cardini, T. Mayeda, C.B.M. McBurney, and E. Tongiorgi, Paleotemperature analysis of fossil shells of marine mollusks (food refuse) from the Arene Candide Cave, Italy, and the Haua Fteah Cave, Cyrenaica, in Isotopic and Cosmic Chemistry, edited by H. Craig, S.L. Miller, and G.J. Wasserburg, 133-156, North-Holland Pub. Co., Amsterdam, 1963.

Ericksson, K.G., The sediment core No. 210 from the western Mediterranean Sea, Swedish Deep-Sea Expedition, 1947-48, Rept. 8, fasc. 5(7), 393-594, 1965.

Ewing, J., Seismic model of the Atlantic Ocean, in The

Earth's Crust and Upper Mantle, Geophysical Monograph 13, edited by P. Hart, 220-225, American Geophysical Union, Washington, D.C., 1969.

Ewing, J.I., J.L. Worzel, and M. Ewing, Sediments and oceanic structural history of the Gulf of Mexico, J. Geophys. Res., 67(6), 2509-2527, 1962.

Ewing, J., and M. Ewing, Seismic refraction measurements in the Atlantic Ocean basins, in the Mediterranean Sea, on the mid-Atlantic ridge, and in the Norwegian Sea, Bull. Geol. Soc. Am., 70, 303-305, 1959.

Ez, V.V., Tectonic conditions for the occurrence of violent earthquakes in the Czechoslovak Carpathians, Izv. Geophys. Ser., English Trans., 2, 161-173, 1964.

Fahlquist, D.A., Seismic refraction measurements in the western Mediterranean Sea, Ph.D. Thesis, MIT, Cambridge, Mass., 1963.

Fyfe, W.S., and J. Verhoogen, Water and heat in metamorphism, in Metamorphic Reactions and Metamorphic Facies, Geol. Soc. Am. Mem. 73, edited by W.S. Fyfe, F.J. Turner, and J. Verhoogen, 187-198, Geol. Soc. Am., New York, 1958.

Galanopoulos, A.G., On mapping of seismic activity in Greece, Ann. Geofis. Rome, 16(1), 37-100, 1963.

Gansser, A., Catalogue of the Active Volcanoes of the World including Solfatara Fields, Part XVII, Iran, 20 pp., Intern. Assoc. of Volcanol., Rome, 1966.

Gaskell, T.F., and J.C. Swallow, Seismic refraction experiments in the Indian Ocean and in the Mediterranean Sea, Nature, 172, 535-537, 1953.

Gasparini, P., and J.A.S. Adams, K-Ar dating of Italian Plio-Pleistocene volcanic rocks, Earth Planet. Sci. Let., 6, 225-230, 1969.

Gass, I.G., Is the Troodos Massif of Cyprus a fragment of Mesozoic ocean floor?, Nature, 220, 39-42, 1968.

Gass, I.G., and D. Masson-Smith, The geology and gravity anomalies of the Troodos Massif, Cyprus, Phil. Trans. Roy. Soc. London, A, 255, 417-467, 1963.

Girdler, R.W., The Red Sea - a geophysical background in Hot Brines and Recent Heavy Metal Deposits in the Red Sea, edited by E.T. Degens and D.A. Ross, 38-58, Springer-Verlag, New York, 1969.

Girdler, R.W., Drifting and rifting of Africa, Nature, 217, 1102-1105, 1968.

Goncharov, V.P., and Yu.P. Neprochnov, Geomorphology of the bottom and tectonic prlbmes in the Black Sea, in International Dictionary of Geophysics, edited by S.K. Runcorn, 650-656, Pergamon Press, New York, 1967.

Gordon, A.L., P.J. Grim, and M. Langseth, Layer of abnormally cold bottom water over southern Aves ridge, Science, 151, 1525-1526, 1966.

Gregor, C.B., and J.D.A. Zijderveld, Paleomagnetism and the Alpine tectonics of Eurasia I: The magnetism of some Permian red sandstones from Northwestern Turkey, Tectonophysics, 1(4), 289-306, 1964.

Gretener, P.E., and G. Simmons, Short-time temperature variations in the waters of the Gulf of Mexico, J. Geophys. Res., 72(8), 2263-2266, 1967.

Hamilton, E.L., Thickness and consolidation of deep-sea sediments, Bull. Geol. Soc. Am., 70, 1399-1424, 1959.

Harrison, J.C., An interpretation of gravity anomalies in the eastern Mediterranean, Phil. Trans. Roy. Soc. London, A, 248, 283-325, 1955.

Hayes, D.E., and J.R. Heirtzler, Magnetic anomalies and their relation to the Aleutian island arc, J. Geophys. Res., 73(14), 4637-4646, 1968.

Heezen, B.C., and M. Ewing, Orleansville earthquake and turbidity currents, Bull. Am. Assoc. Petrol. Geologists, 39(2), 2505-2514, 1955.

Heirtzler, J.R., and D.E. Hayes, Magnetic boundaries in the North Atlantic Ocean, Science, 157(3785), 185-187, 1967.

Helsey, C.E., and A.Nur, The paleomagnetism of Cretaceous rocks from Israel, unpublished manuscript, 1969.

Hersey, J.B., Sedimentary basins of the Mediterranean Sea, in Vol. XVII of the Colston Papers, edited by W.F. Whittard and R. Bradshaw, 75-91, Butterworths Scientific Publications, London, 1965.

Holmes, Arthur, Principles of Physical Geology, 1288 pp., Ronald Press, New York, 1965.

Horai, K., and G. Simmons, Spherical harmonic analysis of terrestrial heat flow, Earth Planet. Sci. Let. 6, 386-394, 1969.

Hsu, K.J., Isostasy, crustal thinning, mantle changes, and the disappearance of ancient land masses, Am. J.

Sci., 263, 97-109, 1965.

Hurley, P.M., H.W. Fairbairn, and W.H. Pinson Jr., Rb-Sr isotopic evidence in the origin of potash-rich lavas of western Italy, Earth Planet. Sci. Let. 5, 301-306, 1966.

Imbo, G., Catalogue of the Active Volcanoes of the World including Solfatara Fields, Part XVIII, Italy, 70 pp., Intern. Assoc. of Volcanol., Rome, 1965.

Imbo, G., P. Gasparini, G. Luongo, and A. Rapolla, Contributions to the volcanological researches by determination of the radioactivity of eruptive products, Bull. Volcanol., 32, 1-25, 1968.

Isacks, B., J. Oliver, and L.R. Sykes, Seismology and the new global tectonics, J. Geophys. Res., 73(18), 5855-5899, 1968.

Jaeger, J.C., Application of the theory of heat conduction to geothermal measurements, in Terrestrial Heat Flow, Geophys. Monograph 8, edited by W.H. K. Lee, 7-23, American Geophysical Union, Washington, D.C., 1965.

Jones, E.J.W., and J.I. Ewing, Age of the Bay of Biscay: evidence from seismic profiles and bottom samples, Science, 166, 102-105, 1969.

Jones, E.J.W., and B.M. Funnell, Association of a seismic reflector and Upper Cretaceous sediment in the Bay of Biscay, Deep-Sea Res., 15, 701-709, 1968.

Joyner, W.B., Basalt-eclogite transition as a cause for subsidence and uplift, J. Geophys. Res., 72(20),

4977-4998, 1967.

Kanamori, H., Travel times to Japanese stations from long-shot and their geophysical implications, Bull. Earthquake Res. Inst., Tokyo Univ., 46, 1968.

Kárník, V., Crustal and upper mantle seismic activity in the European area, Studia geoph. et geod., 11, 324-334, 1967.

Kárník, V., Magnitude-frequency relation and seismic activity in different regions of the European area, Bull. Intern. Inst. Seismol. Earthquake Eng., 1, 9-32, 1964.

Ketin, I., The Northern Anatolian Fault, Istanbul Tek. Univ. Bull., 15(2), 49-52, 1957.

Klemme, H.D., Regional geology of circum-Mediterranean region, Bull. Am. Assoc. Petrol. Geologists, 42(3), 477-510, 1958.

Kotásek, J., and M. Krs, Paleomagnetic study of tectonic rotations in the Carpathian mountains of Czechoslovakia, Paleogeography, Paleoclimatology, Paleoecology, 1(1), 39-49, 1965.

Kovilin, B.M., Investigation of the sediment thickness in the Mediterranean Sea, Oceanology, 4(1), 81-85, 1964.

Lachenbruch, A.H., Rapid estimation of the topographic disturbance to superficial thermal gradients, Reviews of Geophysics, 6(3), 365-400, 1968.

Lachenbruch, A.H., and B.V. Marshall, Heat flow through the Arctic ocean floor: the Canada basin-Alpha rise boundary, J. Geophys. Res., 71(4), 1223-1248, 1966.

Lahn, E., Seismological investigations in Turkey, Bull. Seismol. Soc. Am., 39(2), 67-70, 1949.

Langseth, M.C., The flow of heat from the Earth and its global distribution at the surface, paper given at AIAA 4th Thermophysics Conference, San Francisco, California, June 16-18, 1969.

Langseth, M.G., Techniques of measuring heat flow through the ocean floor, in Terrestrial Heat Flow, Geophys. Monograph 8, edited by W.H.K. Lee, 58-77, American Geophysical Union, Washington, D.C., 1965.

Lavenia, A., Heat flow measurements through bottom sediments in the southern Adriatic Sea, Bolletino di Geofisica Teorica ed Applicata, 9(36), 323-332, 1967.

Lebedev, T.S., R.I. Kutas, and V.V. Gordiyenki, Geothermal investigations in the southern and southwestern areas of the Ukrainian SSR (The Crimea and Soviet Eastern Carpathians), Bollettino di Geofisica Teorica ed Applicata, 9(36), 333-343, 1967.

Lee, W.H.K., and C.S. Cox, Time variation of ocean temperatures and its relation to internal waves and oceanic heat flow measurements, J. Geophys. Res., 71(8), 2101-2111, 1966.

Le Pichon, X., Sea-floor spreading and continental drift, J. Geophys. Res., 73(12), 3661-3697, 1968.

Levitskaya, A.Ya., The seismicity of the Crimea, Chapter IX in Earthquakes of the U.S.S.R., edited by E.F. Savarenskii, I.E. Gubin, and D.A. Kharin, 271-276, Publishing House of the Academy of Sciences of the USSR, Moscow, 1961.

Lister, C.R.B., Geothermal gradient measurement using a deep-sea corer, Geophys. J. Roy. Astron. Soc., 7(5), 571-583, 1963.

Liston, J., Distribution, taxonomy and function of heterotrophic bacteria on the sea floor, Kyoto Univ. Misaki Marine Bio. Inst. Bull., 12, 97-104, 1968.

Locardi, E., Uranium and thorium in the volcanic processes, Bull. Volcanol., 31, 235-260, 1968.

Lubimova, E.A., Marine geothermal investigations and some data on heat flow in the Black Sea basin, in The Structure of the Black Sea Depression, 88-93, "Nauka" Publishing House, Moscow, 1966.

Lubimova, E.A., Heat flow in the Ukrainian shield in relation to recent tectonic movements, J. Geophys. Res., 69(24), 5277-5284, 1964.

Lubimova, E.A., R.P. Von Herzen, C. Udintsev, On heat transfer through the ocean floor, in Terrestrial Heat Flow, Geophys. Monograph 8, edited by W.H.K. Lee, 78-86, American Geophysical Union, Washington, D.C., 1965.

Ludwig, W.J., B. Gunturi, and M. Ewing, Sub-bottom reflection measurements in the Tyrrhenian and Ionian

Seas, J. Geophys. Res., 70(18), 4719-4728, 1965.

Makarenko, F.A., Ya.B. Smirnov, and S.I. Sergiyenko, Subsurface heat flow and tectonics of Ciscaucasia, Doklady Akademii Nauk SSSR (English transl.), 183(4), 901-904, 1968.

Makarenko, F.A., B.G. Polak, and Ya.B. Smirnov, Geothermal field on the U.S.S.R. territory, in The Proceedings of the Twenty-third International Geologic Congress, Volume 5, 67-73, edited by M. Malkovsky and J. Masin, Academia, Prague, 1968.

Malovitskiy, Ya.P., and Yu.P. Neprochnov, Correlation of seismic and gravimetric data on the structure of the Earth's crust in the Black Sea depression, (in Russian) in The Structure of the Black Sea Depression, 1-16, Nauka Publishing House, Moscow, 1966.

Matthews, D.H., and C.A. Williams, Linear magnetic anomalies in the Bay of Biscay: A qualitative interpretation, Earth Planet. Sci. Let. 4, 315-320, 1968.

Mazor, E., Compositional similarities between hot mineral springs in the Jordan and Suez rift valleys, Nature, 219, 477-478, 1968.

McElhinny, M.W., J.C. Briden, D.L. Jones, and A. Brock, Geological and geophysical implications of paleomagnetic results from Africa, J. Geophys. Res., 6(2), 201-238, 1968.

McElhinny, M.W., and P. Wellman, Polar wandering and sea-

floor spreading in the southern Indian Ocean, Earth Planet. Sci. Let. 6, 198-204, 1969.

McKenzie, D.P., Plate tectonics of the Mediterranean region, Nature, 220, 239-243, 1970.

McKenzie, D.P., Speculations on the consequences and causes of plate motions, Geophys. J. Roy. Astron. Soc., 18, 1-32, 1969.

Menard, H.W., Transitional types of crust under small ocean basins, J. Geophys. Res., 72(12), 3061-3073, 1967.

Menard, H.W., Marine Geology of the Pacific, 271 pp., McGraw-Hill Book Company, New York, 1964.

Menard, H.W., and T.E. Chase, Tectonic effects of upper mantle motion, reported at The Upper Mantle Symposium, New Delhi, 1964, ed. by C. Smith and T. Sorgenfrei, 29-36, Det Berlingske Bogtrykkeri, Copenhagen, 1965.

Menard, H.W., S.M. Smith, and R.M. Pratt, The Rhone deep sea fan, in Vol. XVII of the Colston Papers, edited by W.F. Whittard and R. Bradshaw, 271-285, Butterworths Scientific Publications, London, 1965.

Michno, M.F., Investigation of the thickness of sediment in the Tyrrhenian and Ionian Seas using the seismic method (in Russian), Okeanologiya, 3(5), 853-860, 1963.

Milanovskiy, Ye.Ye., Problem of the origin of the Black Sea depression and its position in the structure of the Alpine belt, Intern. Geol. Rev.,(English Transl.), 9(9), 1237-1249, 1967.

Miller, A.R., Physical oceanography of the Mediterranean Sea: A discourse, Extrait des Rapports et Proces-verbaux des reunions de la C.I.E.S.M.M., 17(3), 857-872, 1963.

Minear, J.W., and M.N. Toksöz, Thermal regime of a down-going slab and new global tectonics, J. Geophys. Res., 75(8), 1397-1419, 1970.

Molnar, P., and J. Oliver, Lateral variations of attenuation in the upper mantle and discontinuities in the lithosphere, J. Geophys. Res., 74(10), 2648-2582, 1969.

Morgan, J.W., Rises, trenches, great faults, and crustal blocks, J. Geophys. Res., 73(6), 1959-1982, 1968.

Moskalenko, V.N., The structure of the sedimentary strata in the Tyrrhenian Sea from seismic data (in Russian), Izv. Akad. Nauk SSSR, Ser. Geol., 6, 49-56, 1967.

Moskalenko, V.N., New data on the structure of the sedimentary strata and basement in the Levant Sea, Oceanology, 6, 828-836, 1966.

Muratov, M.V., History of the tectonic development of the Alpine folded region of southeastern Europe and Asia Minor-new data on the tectonic structure and history of development of the Alpine zone of Europe, International Geol. Rev., 6(1), 99-118, 1962.

Nairn, A.E.M., Paleomagnetic measurements on Karroo and Post-Karroo rocks, A second progress report, Overseas Geology and Mineral Resources, 9(3), 302-320, 1964.

Nairn, A.E.M., Paleomagnetic results from Europe, J. Geol., 68(3), 285-306, 1960.

Nairn, A.E.M., and M. Westphal, A second virtual pole from Corsica, the Ota gabbrodiorite, Palaeogeography, Palaeoclimatology, Palaeoecology, 3, 277-287, 1967.

Nalivkin, D.V., The Geology of the U.S.S.R. (English transl.), 170 pp., Pergamon Press, New York, 1960.

Nason, R.D., and W.H.K. Lee, Heat flow measurements in the North Atlantic, Caribbean, and Mediterranean, J. Geophys. Res., 69, 4875-4883, 1964.

Neprochnov, Yu.P., Structure of the earth's crust of epi-continental seas: Caspian, Black, and Mediterranean, Can. J. Earth Sci., 5, 1037-1043, 1968.

Neprochnov, Yu.P., A.P. Neprochnova, S.M. Zverev, and V.I. Mironova, Deep seismic sounding of the Earth's crust in the central part of the Black Sea depression, in Problems in Deep Seismic Sounding, edited by S.M. Zverev, 49-78, Plenum Publishing Corp., New York, N.Y., 1967.

Neprochnov, Yu.P., and L.N. Rykunov, Experimental data about high velocity layer in the upper mantle of the earth, paper presented at the General Assembly of the International Association of Seismology and Physics of the Earth's Interior and International Association of Geomagnetism and Aeronomy, Madrid, September 4-6, 1969.

Neuman Van Padang, M., Catalogue of the Active Volcanoes

of the World including Solfatara Fields, Part XVI, Arabia and the Indian Ocean, 64 pp., Intern. Assoc. of Volcanol., Rome, 1963.

Novitskiy, V.P., The dynamics of waters of the Sea of Marmara in the near-Bosporan shelf area of the Black Sea, Oceanology, 5, 61-66, 1965.

Officer, C.B., M. Ewing, and P.C. Wuenschel, Seismic refraction measurements in the Atlantic Ocean. Part IV: Bermuda, Bermuda rise, and Nares basin, Bull. Geol. Soc. Am., 63, 777-808, 1952.

Oliver, J., and B. Isacks, Earthquake zones, anomalous structures in the upper mantle, and the lithosphere, J. Geophys. Res., 72(16), 4259-4275, 1967.

Ovchinnikov, I.M., and Ye.A. Plakhin, Formation of Mediterranean deep water masses, Oceanology, 5, 40-47, 1965.

Oxburgh, E.R., and D.L. Turcotte, Problem of high heat flow and volcanism associated with zones of descending mantle convective flow, Nature, 218, 1041-1043, 1968.

Pannekoek, A.J., Uplift and subsidence in and around the western Mediterranean since the Oligocene: a review, Verhandelingen Kon. Ned. Geol. Mijnbouwk. Gen., 26, 53-78, 1969.

Papazachos, B.C., Phase velocities of Rayleigh waves in Southeastern Europe and Eastern Mediterranean Sea, Pure and Applied Geophysics, 75(4), 47-55, 1969.

Papazachos, B.C., and N.D. Delibasis, Tectonic stress field and seismic faulting in the area of Greece, Tectonophysics, 7(3), 231-255, 1969.

Payo, G., Crustal structure of the Mediterranean Sea. Part II. Phase velocity and travel times, Bull. Seismol. Soc. Am., 59(1), 23-42, 1969.

Payo, G., Crustal structure of the Mediterranean Sea. Part I: Group velocity, Bull. Seismol. Soc. Am., 57(2), 151-172, 1967.

Payo, G., Iberian peninsula crustal structure from surface waves dispersion, Bull. Seismol. Soc. Am., 55(4), 727-743, 1965.

Peterson, M.N.A., N.T. Edgar, C.C. von der Borch, and R.W. Rex, Cruise leg summary and discussion, in Peterson, M.N.A., et al., Initial Reports of the Deep Sea Drilling Project, Volume II, U.S. Government Printing Office, Washington, D.C., 413-427, 1970.

Pollack, M.H., The sources of the deep water of the eastern Mediterranean Sea, J. Marine Res., 10(1), 128-151, 1951.

Radu, C., and G. Purcaru, Considerations upon intermediate earthquake-generating stress systems in Vrancea, Bull. Seismol. Soc. Am., 54(1), 79-85, 1964.

Raja, P.K.S., T.A. Reilly, and A.E. Mussett, The paleomagnetism of the Turkana lavas, J. Geophys. Res., 71(4), 1217-1222, 1966.

Ratcliffe, E.H., The thermal conductivity of ocean sediments,

J. Geophys. Res., 65, 1535-1541, 1960.

Raven, T., Alpine folding as related to continental drift, Eclogae geol. Helv., 53(1), 161-168, 1960.

Rezanov, I.A., and S.S. Chamo, Reasons for absence of a 'granitic' layer in basins of the south Caspian and Black Sea type, Can. J. Earth Sci., 6, 671-678, 1960.

Richard, J.J., and M. Neuman Van Padang, Catalogue of the Active Volcanoes of the World including Solfatara Fields, Part IV, Africa and the Red Sea, 119 pp., Intern. Assoc. of Volcanol., Rome, 1957.

Ringwood, A.E., Composition and evolution of the upper mantle, in The Earth's Crust and Upper Mantle, Geophysical Monograph 13, edited by P.J. Hart, 1-17, American Geophysical Union, Washington, D.C., 1969.

Ringwood, A.E., and D.H. Green, An experimental investigation of the gabbro-eclogite transformation and some geophysical implications, Tectonophysics, 3(5), 383-427, 1966.

Ritsema, A.R., Seismo-tectonic implications of a review of European earthquake mechanisms, Geologische Rundschau, 59(1), 36-56, 1969a.

Ritsema, A.R., Seismic data of the western Mediterranean and the problem of oceanization, Verhandelingen Kon. Ned. Geol. Mijnbouwk, Gen., 26, 105-121, 1969b.

Rosenthal, E., and Y. Eckstein, Temperature gradients in the subsurface of the Dead Sea area, Israel, Israel J. Earth Sci., 17, 131-136, 1968.

Ross, D.A., E.T. Degens, and J. MacIlvaine, Black Sea-recent sedimentary history, manuscript submitted to Science, 1970.

Ryan, W.B.F., The floor of the Mediterranean Sea. Part I: The structure and evolution of the basins, Ph.D. thesis, Columbia University, New York, N.Y., 1969a.

Ryan, W.B.F., Crustal motion and crustal shortening in the Mediterranean Sea, paper presented at the General Assembly of the International Association of Seismology and Physics of the Earth's Interior and International Association of Geomagnetism and aeronomy, Madrid, September 4-6, 1969b.

Ryan, W.B.F., F. Workum, Jr., and J.B. Hersey, Sediments on the Tyrrhenian abyssal plain, Bull. Geol. Soc. Am., 76, 1261-1282, 1965.

Scheffer, V., The European values of terrestrial heat flow, Geofisica e Meteorologia, 13, 99-103, 1964.

Schuiling, R.D., A geothermal model of oceanization, Verhandelingen Kon. Ned. Geol. Mijnbouwk. Gen., 26, 143-148, 1969.

Schwarz, E.J., A paleomagnetic investigation of Permo-Triassic red beds and andesites from the Spanish Pyrenees, J. Geophys. Res., 68(10), 3265-3271, 1963.

Sclater, J.G., C.E. Corry, and V. Vacquier, In situ measurement of the thermal conductivity of ocean-

floor sediments, J. Geophys. Res., 74(4), 1070-1081, 1969.

Sclater, J.G., E.J.W. Jones, and S.P. Miller, The relationship of heat flow, bottom topography, and basement relief in Peake and Freen deeps, northeast Atlantic, unpublished manuscript, 1968.

Sclater, J.G., J.D. Mudie, and C.G.A. Harrison, Detailed geophysical studies on the Hawaiian Arch near 24°25'N, 157°40'W: a closely spaced suite of heat-flow stations, J. Geophys. Res., 75(2), 333-348, 1970.

Shimazu, Y., Thermodynamics of the upper mantle, Geophys. J. Roy. Astron. Soc., 14, 429-431, 1967.

Shirokova, E.I., General features in the orientation of principal stresses in earthquake foci in the Mediterranean-Asia seismic belt, Izv. Akad. Nauk SSSR, Ser. Earth Physics, 1, 22-36, 1967.

Shor, G.G., and R.W. Raitt, Explosion seismic refraction studies of the crust and upper mantle in the Pacific and Indian Oceans, in The Earth's Crust and Upper Mantle, Geophys. Monograph 13, edited by P. Hart, 225-230, American Geophysical Union, Washington, D.C., 1969.

Solov'ev, S.L., General review of the seismicity of the USSR, in Earthquakes in the USSR, 203-262, Office of Technical Services, Department of Commerce, Washington, D.C., 1961.

Stanley, D.J., and E. Mutti, Sedimentological evidence for an emerged land mass in the Ligurian Sea during the Palaeogene, Nature, 218, 32-36, 1968.

Starik, I.Ye., Yu.V. Kuznetsov, D.W. Nikolayev, V.K. Legin, K.F. Lazarev, S.M. Grashenko, and L.B. Kolyadin, The distribution of radioelements in the sediments of the Black Sea, Doklady Akademii Nauk SSR, English Transl., 129(5), 1043-1045, 1969.

Subbotin, S.I., V.B. Sollogub, D. Prosen, T. Dragesevic, E. Mituch, and K. Posgay, Junction of deep structures of the Carpatho-Balkan region with those of the Black and Adriatic Seas, Can. J. Earth. Sci., 5, 1027-1035, 1968.

Sykes, L.R., The seismicity and deep structure of island arcs, J. Geophys. Res., 71(12), 2981-3006, 1966.

Sysoyev, N.N., Geothermic measurements in the sediments on the floors of seas and oceans, Deep-Sea Res., 10, 325, 1963.

Texas Instruments, Inc., United States Naval Oceanographic Office Marine Geophysical Survey Program, 1965-1967, North Atlantic Ocean, Norwegian Sea, and Mediterranean Sea, Area 6, Volume 5, Geology and Geophysics, 42 pg., U.S. Naval Oceanographic Office, Washington, D.C., 1967.

Toksöz, M.N., J. Arkani-Hamed, and C.A. Knight, Geophysical data and long-wave heterogeneities of the Earth's

mantle, J. Geophys. Res., 74(15), 3751-3770, 1969.

Toksöz, M.N., M.A. Chinnery, and D.L. Anderson, Inhomogeneities in the Earth's mantle, Geophys. J. Roy. Astron. Soc., 13, 31-59, 1967.

Tramontini, C., and D. Davies, A seismic refraction survey in the Red Sea, Geophys. J. Roy. Astron. Soc., 17, 225-241, 1969.

Tskhakaya, A.D., Seismicity of the Dzhavakhet (Alkhalkalaki) Highlands, in Earthquakes in the USSR, 200-313, Office of Technical Services, Department of Commerce, Washington, D.C., 1961.

Turcotte, D.L., and E.R. Oxburgh, A fluid theory for the deep structure of dip-slip fault zones, Phys. Earth Planet. Interiors, 1, 381-386, 1968.

Turner, F.J., and J. Verhoogen, Igneous and Metamorphic Petrology, 472 pp., McGraw-Hill Book Co., Inc., New York, 1960.

Uyeda, S., and V.Vacquier, Geothermal and geomagnetic data in and around the island arc of Japan, in The Crust and Upper Mantle of the Pacific Area, Geophysical Monograph 12, edited by Leon Knopoff, Charles L. Drake, and Pembroke J. Hart, 349-366, American Geophysical Union, Washington, D.C., 1968.

Van Bemmelen, R.W., Origin of the western Mediterranean Sea, Verhandelingen Kon. Ned. Geol. Mijnbouwk, Gen., 26, 13-51, 1969.

Van der Voo, R., Paleomagnetic evidence for the rotation

of the Iberian peninsula, Tectonophysics, 7(1), 5-56, 1969.

Van der Voo, R., Jurassic, Cretaceous and Eocene pole positions from northeastern Turkey, Tectonophysics, 6(3), 251-269, 1968.

Van der Voo, R., The rotation of Spain: paleomagnetic evidence from the Spanish meseta, Paleogeography, Paleoclimatology, Paleoecology, 3, 393-416, 1967.

Van der Voo, R., and J.D.A. Zijderveld, Paleomagnetism in the western Mediterranean, Verhandelingen Kon. Ned. Geol. Mijnbouwk. Gen., 26, 121-138, 1969.

Van Dongen, P.G., R. Van der Voo, and Th. Raven, Paleomagnetic research in central Lebanon mountains and in the Tartous area (Syria), Tectonophysics, 4(1), 35-53, 1967.

Van Hilten, D., Evaluation of some geotectonic hypothesis by paleomagnetism, Tectonophysics, 1, 3-71, 1964.

Van Hilten, D., A deviating Permian pole from rocks in northern Italy, Geophys. J., 6(3), 377-390, 1962.

Van Hilten, D., and J.D.A. Zijderveld, The magnetism of the Permian porphyries near Lugano (Northern Italy, Switzerland), Tectonophysics, 3(5), 429-446, 1966.

Visscher, H., Permian and Triassic palynology and the concept of the "Tethys twist", Palaeogeography, Palaeclimatology, Palaeoecology, 3, 151-166, 1967.

Vogt, P.R., and R.H. Higgs, An aeromagnetic survey of the

eastern Mediterranean Sea and its interpretation, Earth Planet. Sci. Let., 5, 439-448, 1969.

Vogt, P.R., and R.H. Higgs, Magnetic survey of the western Mediterranean (abstract), Trans. Am. Geophys. Union, 49(1), 157, 1968.

Von Herzen,R.P., Surface heat flow and some implications, in The Earth's Mantle, edited by T.F. Gaskell, 197-230, Academic Press, Inc., New York, N.Y., 1967.

Von Herzen, R.P., and A.E. Maxwell, The measurement of thermal conductivity of deep-sea sediments by a needle-probe method, J. Geophys. Res., 64(10), 1557-1563, 1959.

Von Herzen, R.P., and S. Uyeda, Heat flow through the eastern Pacific Ocean floor, J. Geophys. Res., 68 (14), 4234-4238, 1963.

Watkins, N.D., and A. Richardson, Paleomagnetism of the Lisbon volcanics, Geophys. J. Roy. Astron. Soc., 15, 287-304, 1968.

Westphal, N., Etude paleomagnetique de formations volcaniques primaires de Corse. Rapports avec la tectonique du domaines Ligurien, Thesis, Strassburg University, 1967.

Winkler, H.G.F., Petrogenesis of Metamorphic Rocks, 220 pp., Springer-Verlag, New York, 1965.

Wollenberg, H.A., and A.R. Smith, Radioactivity of Upper Mesozoic graywackes in the northern Coast Ranges, California, J. Geophys. Res., 72(16), 4139-4150, 1967.

Wong, H.K., and E.F.K. Zarudzki, Thickness of unconsolidated sediments in the eastern Mediterranean Sea, Bull. Geol. Soc. Am., 80, 2611-2614, 1969.

Woodside, J., and C. Bowin, Gravity anomalies and inferred crustal structure in the eastern Mediterranean Sea, Bull. Geol. Soc. Am., 81(4), 1107-1122, 1970.

Woollard, G.P., The Relation of Gravity Anomalies to Surface Elevation, Crustal Structure and Geology, 225 pp., Research Report Series, Number 62-9, The University of Wisconsin, Madison, 1962.

Wüst, G., On the vertical circulation of the Mediterranean Sea, J. Geophys. Res., 66(10), 3261-3271, 1961.

Yasui, M., K. Toshiro, T. Watanabe and S. Uyeda, Heat flow in the Sea of Japan, in The Crust and Upper Mantle of the Pacific Area, Geophysical Monograph 12, edited by L. Knopoff, C.L. Drake, and P.J. Hart, 3-16, American Geophysical Union, Washington, D.C., 1968.

Zarudzki, E.F.K., H.K. Wong, J.D. Phillips, and G.K.R. Giermann, Structure of the Mediterranean east of 22°E, paper presented at the General Assembly of the International Association of Seismology and Physics of the Earth's interior and International Association of Geomagnetism and Aeronomy, Madrid, September 4-6, 1969.

Zarudzki, E.F.K., The Strait of Sicily, unpublished manuscript, 1968.

Zijderveld, J.D.A., G.J.A. Hazeu, M. Nardin, R. Van der Voo,

Shear in the Tethys and the Permian paleomagnetism in the southern Alps, including new results, to be published in Tectonophysics, 1970.

Zobell, C.E., F.D. Sisler, and C.H. Oppenheimer, Evidence of biochemical heating in Lake Mead mud, J. Sediment. Petrol., 23(1), 13-17, 1953.

Zverev, S.M., and V.I. Mironova, Results from records obtained by regional seismic stations during deep seismic sounding in the Black Sea, in Problms in Deep Seismic Sounding, edited by S.M. Zverev, 79-91, Plenum Publishing Corp., New York, N.Y., 1967.

BIOGRAPHICAL NOTE

The author, Albert Joseph Erickson, was born in Teaneck, New Jersey on March 1, 1942. He attended grammar schools in New Jersey and Connecticut, and graduated from Ridgefield High School, Ridgefield, Connecticut in June 1960. In September, 1960 he entered Brown University in Providence, Rhode Island and graduated with a Bachelor of Science Degree in Physics four years later in June, 1964.

During the summer following graduation from Brown University, the author was employed by the Woods Hole Oceanographic Institution as a research assistant. The author entered the Department of Earth and Planetary Sciences of the Massachusetts Institute of Technology in September, 1964, as a candidate for the degree of Ph.D. in Marine Geophysics. In 1966 he set up and has since maintained a marine heat flow program with the support of Gene Simmons. During that time he obtained and interpreted the heat flow data presented in this thesis, as well as data from the Red Sea, the Caribbean Sea, the Gulf of Mexico, and the Atlantic and Pacific Oceans.

In June, 1968, the author married Anne Elizabeth Crowley of West Roxbury, Massachusetts; the couple have no children. He is a member of the American Geophysical Union and has given several papers and made the following contributions to geophysical literature.

Erickson, A.J., and G.Simmons, Heat Flow in the Mediterranean Sea (abstract), Eos, 51(4), 426, 1970.

Erickson, A.J., and G. Simmons, Thermal measurements in the Red Sea hot brine pools, in Hot Brines and Recent Iron Formations in the Red Sea, edited by E.T. Degens and D.A. Ross, 114-121, Springer-Verlag, New York, 1969.

Erickson, A.J., and G. Simmons, Geothermal flux in the Red Sea hot brine pools (abstract), Trans. Am. Geophys. Union, 49(1), 192, 1968.

Erickson, A.J., and G. Simmons, A Geothermal investigation of the eastern Mediterranean (abstract), Trans. Am. Geophys. Union, 49(1), 323, 1968.

Erickson, A.J., and J. Woodside, Geological and geophysical investigation of the proposed site for Project Seaspider, Woods Hole Oceanographic Institution Ref. 66-6, Woods Hole, 1966.

Appendices to

THE MEASUREMENT AND INTERPRETATION OF HEAT FLOW IN THE MEDITERRANEAN AND BLACK SEAS

by

Albert Joseph Erickson

PhD Thesis

Massachusetts Institute of Technology

June 1970

APPENDIX I

Thermal Gradient Data

The temperature increase observed at various distances from the bottom of the core are presented in the following tables. The absence of a temperature increase ($\Delta T = 0.000$) at a particular probe indicates that the probe failed to penetrate the sediment. Dashed lines are present in the Tables where reliable measurements of the temperature increase were not possible. Positions given are relative to the core barrel, rather than to the maximum depth of penetration.

THERMAL GRADIENT DATA

CH61-19		CH61-29		CH61-37		CH61-39	
Pos(cm)	ΔT(°C)	Pos(cm)	ΔT(°C)	Pos(cm)	ΔT(°C)	Pos(cm)	ΔT(°C)
28.3	0.786	22.0	0.394	24.0	0.261	24.0	0.098
233.3	0.680	249.0	0.336	258.5	0.147	235.6	0.040
498.0	0.527	497.0	0.273	526.5	0.000	486.2	0.000
775.8	0.323	768.0	0.164				
1084.0	0.138	1064.4	0.050				

THERMAL GRADIENT DATA

CH61-40		CH61-42		CH61-46		CH61-50	
Pos(cm)	ΔT(°C)	Pos(cm)	ΔT(°C)	Pos(cm)	ΔT(°C)	Pos(cm)	ΔT(°C)
23.5	0.340	30.0	0.174	28.0	0.115	28.0	0.188
234.5	0.216	244.0	0.099	207.5	--	206.0	--
464.0	0.079	446.0	0.087	351.0	0.082	378.5	0.087
728.0	0.000	628.0	0.000	555.5	0.000	553.0	0.000

THERMAL GRADIENT DATA

CH61-53		CH61-54		CH61-55		CH61-56	
Pos(cm)	ΔT(°C)	Pos(cm)	ΔT(°C)	Pos(cm)	ΔT(°C)	Pos(cm)	ΔT(°C)
27.0	0.374	22.0	0.190	22.5	0.134	22.0	0.286
212.0	0.268	195.5	0.043	191.0	0.090	198.5	0.245
383.5	0.153	359.0	0.000	363.5	0.080	377.0	0.196
550.0	0.111			538.5	0.043	543.5	0.120
747.0	0.024			730.0	0.000	739.0	0.033

THERMAL GRADIENT DATA

CH61-57		CH61-59		CH61-62		CH61-63	
Pos(cm)	ΔT(°C)	Pos(cm)	ΔT(°C)	Pos(cm)	ΔT(°C)	Pos(cm)	ΔT(°C)
22.5	0.159	24.5	0.272	23.5	0.122	22.5	0.197
207.0	0.124	208.0	0.258	206.5	0.128	190.5	0.154
365.0	0.107	374.5	0.235	357.5	0.052	346.0	0.145
541.0	0.048	522.5	0.104	533.5	0.000	508.5	0.064
746.0	0.000	747.5	0.000			728.5	0.000

THERMAL GRADIENT DATA

CH61-64		CH61-65		CH61-66		CH61-67	
Pos(cm)	ΔT(°C)	Pos(cm)	ΔT(°C)	Pos(cm)	ΔT(°C)	Pos(cm)	ΔT(°C)
24.5	0.158	22.5	0.253	29.5	0.307	25.0	0.217
192.5	0.104	204.5	0.218	195.0	0.222	207.0	0.204
361.5	0.065	383.0	0.180	369.5	0.186	375.5	0.179
536.0	0.047	553.0	0.079	536.0	0.113	555.0	0.076
728.5	0.009	738.5	0.000	741.5	0.000	738.5	0.000

THERMAL GRADIENT DATA

CH61-68		C9-115		C9-116		C9-117	
Pos(cm)	ΔT(°C)	Pos(cm)	ΔT(°C)	Pos(cm)	ΔT(°C)	Pos(cm)	ΔT(°C)
23.5	0.264	56.0	0.443	54.0	0.319	55.0	0.279
211.5	0.202	374.0	0.286	500.0	--	371.0	0.188
378.5	0.149	711.0	0.168	750.0	--	717.0	--
557.5	0.084	1061.0	0.039	1100.0	0.020	1070.0	0.010
748.0	0.010						

THERMAL GRADIENT DATA

C9-118		C9-119		C9-121		C9-123	
Pos(cm)	ΔT(°C)	Pos(cm)	ΔT(°C)	Pos(cm)	ΔT(°C)	Pos(cm)	ΔT(°C)
52.0	0.152	54.0	0.096	55.0	--	55.0	--
406.0	0.096	368.0	--	327.0	--	424.0	0.205
672.0	--	715.0	--	713.0	0.190	721.0	0.098
964.0	0.000	1061.0	0.000	1003.0	0.034	1008.0	--

THERMAL GRADIENT DATA

C9-124		C9-125		C9-126		C9-127	
Pos(cm)	ΔT(°C)	Pos(cm)	ΔT(°C)	Pos(cm)	ΔT(°C)	Pos(cm)	ΔT(°C)
52.0	0.351	52.0	0.211	52.0	0.447	53.0	0.304
421.0	0.202	449.0	0.078	448.0	0.124	449.0	0.167
715.0	0.185	702.0	0.000	701.0	0.000	707.0	0.102
1064.0	0.000					993.0	0.000

THERMAL GRADIENT DATA

C9-129		C9-131		C9-132		C9-133	
Pos(cm)	ΔT(°C)	Pos(cm)	ΔT(°C)	Pos(cm)	ΔT(°C)	Pos(cm)	ΔT(°C)
52.0	0.213	52.0	0.271	52.0	0.841	53.0	0.682
440.0	0.167	440.0	0.175	434.0	0.609	441.0	0.431
660.0	--	770.0	0.057	707.0	0.486	713.0	0.272
940.0	0.079	1065.0	0.000	1004.0	0.238	1001.0	0.044

THERMAL GRADIENT DATA

C9-134		C9-135		C9-136		C9-137	
Pos(cm)	ΔT(°C)	Pos(cm)	ΔT(°C)	Pos(cm)	ΔT(°C)	Pos(cm)	ΔT(°C)
51.0	0.821	51.0	0.323	56.0	0.762	52.0	0.970
440.0	0.480	434.0	0.110	439.0	0.489	440.0	0.682
717.0	0.326	755.0	0.000	689.0	0.363	725.0	0.497
998.0	0.214			993.0	0.164	1010.0	0.179

THERMAL GRADIENT DATA

C9-138		C9-139		C9-140		C9-141(a)	
Pos(cm)	ΔT(°C)	Pos(cm)	ΔT(°C)	Pos(cm)	ΔT(°C)	Pos(cm)	ΔT(°C)
70.0	--	21.0	--	71.0	--	70.0	--
420.0	0.753	434.0	0.366	437.0	0.193	429.0	0.679
718.0	0.464	695.0	0.219	710.0	0.127	689.0	0.455
1016.0	0.083	1025.0	0.321	987.0	0.010	938.0	0.203

THERMAL GRADIENT DATA

C9-141(b)		AII49-1431P		AII49-1432G		AII49-1433P	
Pos(cm)	ΔT(°C)	Pos(cm)	ΔT(°C)	Pos(cm)	ΔT(°C)	Pos(cm)	ΔT(°C)
70.0	--	0.0	0.415	0.0	0.075	0.0	0.347
429.0	0.337	99.0	0.398	47.0	0.081	99.0	0.338
689.0	0.117	227.5	0.363	77.0	0.053	228.0	0.337
938.0	0.000	345.0	0.334	148.0	0.025	345.0	0.304
		486.5	0.226	199.0	0.009	487.0	0.286
		628.5	0.143			628.5	0.299
		781.0	0.080			781.5	0.145

THERMAL GRADIENT DATA

AII49-1442P		AII49-1443P	
Pos (cm)	ΔT (°C)	Pos (cm)	ΔT (°C)
0.0	--	0.0	0.263
114.0	--	110.5	0.287
224.0	0.247	223.5	0.277
363.0	0.205	347.5	0.197
363.0	0.337	478.0	0.171
478.0	0.223	633.0	0.145
633.0	0.139	790.0	0.089
790.0	0.046		

THERMAL GRADIENT DATA

AII49-1444P		AII49-1445P		AII49- 1446P		AII49-1447P	
Pos(cm)	ΔT(°C)	Pos(cm)	ΔT(°C)	Pos(cm)	ΔT(°C)	Pos(cm)	ΔT(°C)
0.0	0.346	0.0	0.187	0.0	0.406	0.0	0.589
110.5	0.308	110.0	0.194	110.0	0.333	108.0	0.565
223.5	0.291	223.0	0.186	223.5	0.308	220.0	0.548
343.0	0.217	347.5	0.124	348.0	0.235	345.0	0.406
477.5	0.188	477.0	0.106	478.0	0.278	474.5	0.343
633.0	0.159	632.5	0.095	633.0	0.128	630.0	0.273
790.0	0.102	790.5	0.066	790.5	0.029	787.0	0.189

THERMAL GRADIENT DATA

AII49-1452P		AII49-1460P		AII49-1462G		AII49-1464G	
Pos(cm)	ΔT(°C)	Pos(cm)	ΔT(°C)	Pos(cm)	ΔT(°C)	Pos(cm)	ΔT(°C)
0.0	0.474	0.0	0.500	0.0	0.062	0.0	0.167
107.0	0.477	108.5	0.483	82.0	0.045	82.0	0.141
219.5	0.387	220.0	0.488	163.5	--	164.0	--
344.5	0.312	344.5	0.335	245.0	0.013	245.0	0.083
474.0	0.290	474.0	0.271	323.0	0.000	325.0	0.036
629.5	0.209	629.5	0.201				
786.5	0.154	786.5	0.118				

THERMAL GRADIENT DATA

AII49-1468G		AII49-1469G		AII49-1470G		AII49-1472G	
Pos(cm)	ΔT(°C)	Pos(cm)	ΔT(°C)	Pos(cm)	ΔT(°C)	Pos(cm)	ΔT(°C)
0.0	0.028	0.0	0.034	0.0	0.151	0.0	0.165
82.0	0.014	82.0	0.018	82.0	0.135	82.0	0.141
163.5	0.012	164.0	0.013	164.0	0.135	164.0	0.120
245.0	0.002	245.0	0.005	245.0	0.066	245.0	0.084
324.0	0.003	325.0	-0.002	325.0	0.013	325.0	0.048

THERMAL GRADIENT DATA

AII49-1473G		AII49-1473P		AII49-1474P		AII49-1476G	
Pos (cm)	ΔT (°C)	Pos (cm)	ΔT (°C)	Pos (cm)	ΔT (°C)	Pos (cm)	ΔT (°C)
0.0	0.113	0.0	0.247	0.0	0.10	0.0	0.190
82.0	0.099	108.0	0.241	310.0	0.19	82.0	0.170
164.0	0.081	221.0	0.280	523.0	0.21	164.0	0.138
245.0	0.062	345.5	0.159	647.5	0.20	245.0	0.081
325.0	0.013	475.0	0.127	777.0	0.27	325.0	0.024
		630.5	0.113	932.0	0.35		
		787.5	0.052	1088.0	0.43		

THERMAL GRADIENT DATA

AII49-1477P		AII49-1478P	
Pos(cm)	ΔT(°C)	Pos(cm)	ΔT(°C)
0.0	0.344	0.0	0.438
101.0	0.198	98.0	0.623
212.0	0.106	210.0	0.292
338.0	0.042	335.5	0.118
468.0	0.000	465.0	0.056
		620.5	0.000

THERMAL GRADIENT DATA

MULTIPLE HEAT FLOW STATION 1478G

PROBE	1	2	3	4	5
POSITION (cm)	0.0	82.0	164.0	245.0	325.0
ΔT(°C) AT STATION					
A	0.106	0.120	0.073	0.051	0.001
B	0.090	0.075	0.047	0.006	0.001
C	0.101	0.083	0.065	0.034	0.000
D	0.101	0.082	0.061	0.028	0.000
E	0.087	0.073	0.059	0.005	0.000
F	0.105	0.083	0.063	0.016	0.000
G	0.100	0.078	0.059	0.000	0.000
H	0.098	0.067	0.067	0.000	0.000
I	0.080	0.055	0.005	0.000	0.000

THERMAL GRADIENT DATA

AII49-1480P		AII49-1481P		AII49-1484G		AII49-1485G	
Pos(cm)	ΔT(°C)	Pos(cm)	ΔT(°C)	Pos(cm)	ΔT(°C)	Pos(cm)	ΔT(°C)
0.0	0.327	0.0	0.409	0.0	0.084	0.0	0.090
0.0	0.320	0.0	0.486	82.0	0.073	82.0	0.070
110.0	0.201	112.5	0.269	164.0	0.053	164.0	0.048
224.0	0.259	226.5	0.201	245.0	0.028	245.0	0.008
350.0	0.118	352.5	0.153	325.0	0.000	325.0	0.000
479.5	0.052	482.0	0.074				
635.0	0.006	637.5	0.014				
791.0	--	793.5	0.000				

THERMAL GRADIENT DATA

MULTIPLE HEAT FLOW STATION 1486G

PROBE	1	2	3	4	5
POSITION (cm)	0.0	82.0	164.0	245.0	325.0
ΔT (°C) AT STATION					
A	0.260	0.234	0.173	0.116	0.045
B	0.265	0.230	0.170	0.111	0.043
C	0.249	0.196	0.155	0.090	0.024
D	0.250	0.207	0.170	0.100	0.032
E	0.203	0.170	0.121	0.070	0.022

THERMAL GRADIENT DATA

AII49-1486P		CT69-17		CT69-29		CT69-31	
Pos(cm)	ΔT(°C)	Pos(cm)	ΔT(°C)	Pos(cm)	ΔT(°C)	Pos(cm)	ΔT(°C)
0.0	0.803	47.0	0.97	47.0	1.11	47.0	1.63
0.0	0.804	209.0	0.71	209.0	0.81	180.0	1.44
110.0	0.720	377.0	0.46	377.0	0.52	314.0	1.22
224.0	0.674	543.0	0.21	543.0	0.25	459.0	1.00
350.0	0.574	710.0	0.00	710.0	0.00	578.0	0.82
479.0	0.485	871.0	0.00	871.0	0.00	710.0	0.66
634.5	0.358	1040.0	0.00	1040.0	0.00	871.0	--
791.5	0.178	1189.0	0.00	1189.0	0.00	1040.0	0.12

THERMAL GRADIENT DATA

CT69-32		CT69-50		CT69-53		CT69-54	
Pos (cm)	ΔT (°C)	Pos (cm)	ΔT (°C)	Pos (cm)	ΔT (°C)	Pos (cm)	ΔT (°C)
47.0	1.47	52.0	--	52.0	0.43	53.0	--
180.0	1.32	180.0	--	180.0	0.35	180.0	1.55
314.0	1.12	315.0	1.05	315.0	0.29	315.0	1.41
459.0	0.99	462.0	0.71	462.0	0.20	462.0	1.09
578.0	0.86	579.0	0.48	579.0	0.14	579.0	0.83
710.0	0.69	710.0	--	710.0	--	710.0	--
871.0	--	871.0	--	871.0	0.00	871.0	--
1040.0	0.27	1040.0	0.00	1040.0	0.00	1040.0	0.04

THERMAL GRADIENT DATA

CT69-55		CT69-78		CT69-79	
Pos (cm)	ΔT (°C)	Pos (cm)	ΔT (°C)	Pos (cm)	ΔT (°C)
54.0	--	46.0	--	46.0	--
181.0	1.31	179.0	1.28	179.0	--
321.0	--	316.0	1.14	316.0	1.16
463.0	1.01	463.0	0.93	463.0	0.93
579.0	0.84	579.0	0.79	579.0	0.76
710.0	0.67	710.0	0.73	710.0	0.51
871.0	0.46	871.0	0.44	871.0	0.30
1090.0	0.00	1190.0	0.00	1190.0	0.00

APPENDIX II

Temperature versus depth profiles for all new heat flow measurements presented in this thesis. The solid line represents the best estimate of the equilibrium thermal gradient; the dashed curved line is the probable temperature distribution in the sediment. The horizontal arrows at some temperature-depth data points are due to failure of the probe to achieve thermal equilibrium. Their direction indicates whether the probe was cooling or warming during the measurement. The large vertical arrows near the top of the profile designate the maximum possible penetrations of the corer. Their location is based on the observation that the next higher probe showed no temperature increase. The thermal conductivity values measured on the core are also plotted. At stations where no core was obtained, the mean conductivity value used in the calculation of the heat flow has been estimated from values at surrounding stations.

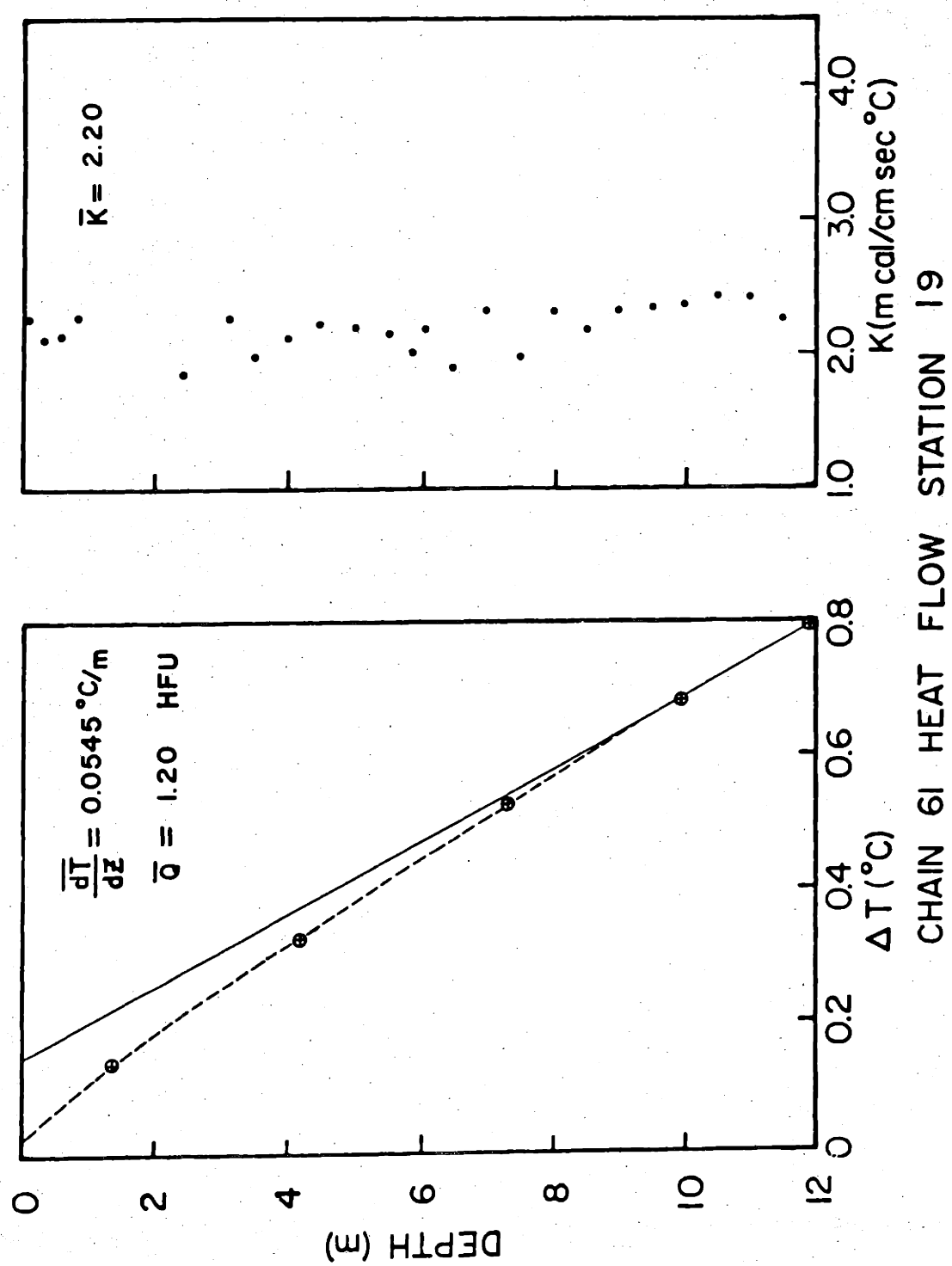

CHAIN 61 HEAT FLOW STATION 19

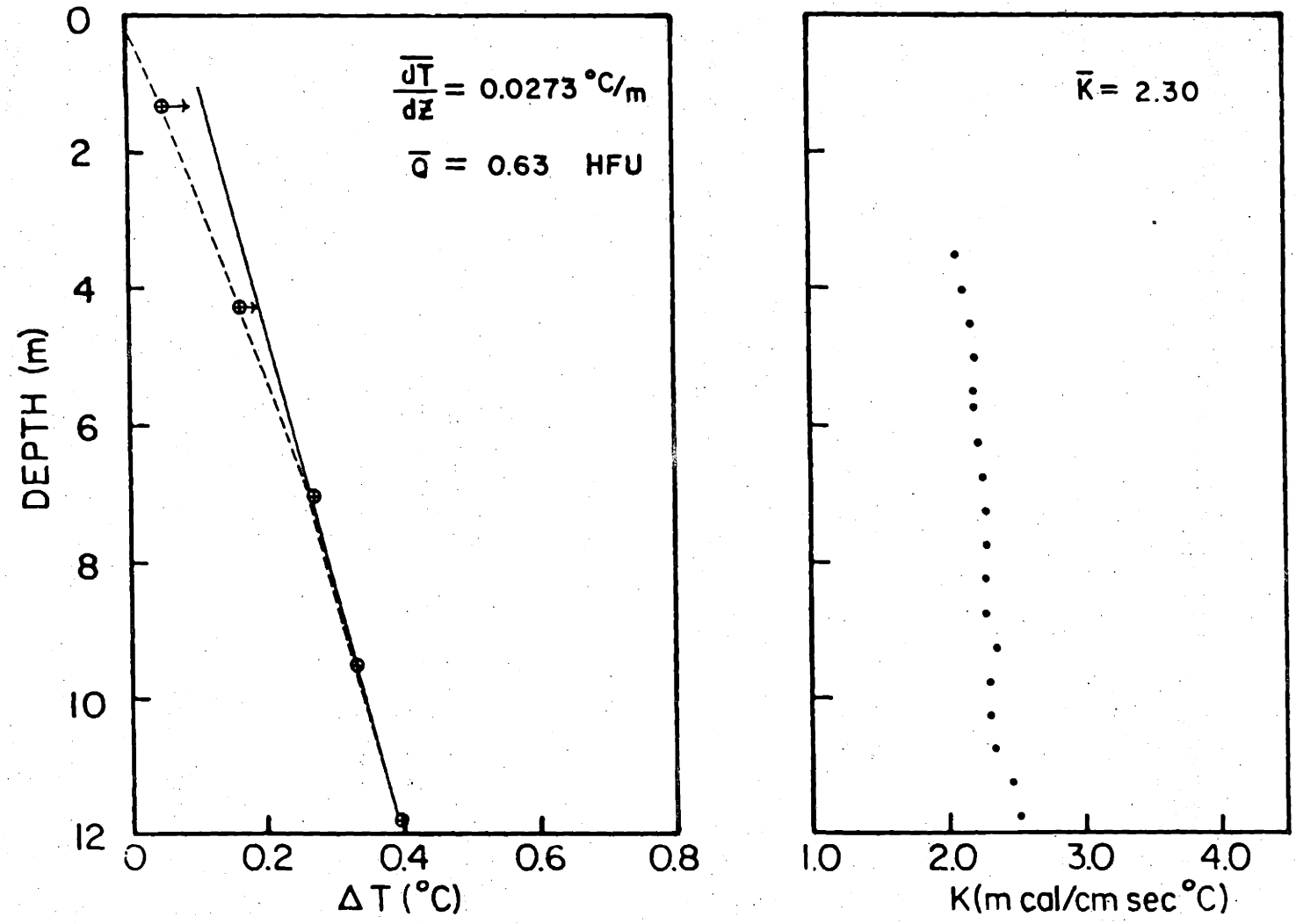

CHAIN 61 HEAT FLOW STATION 29

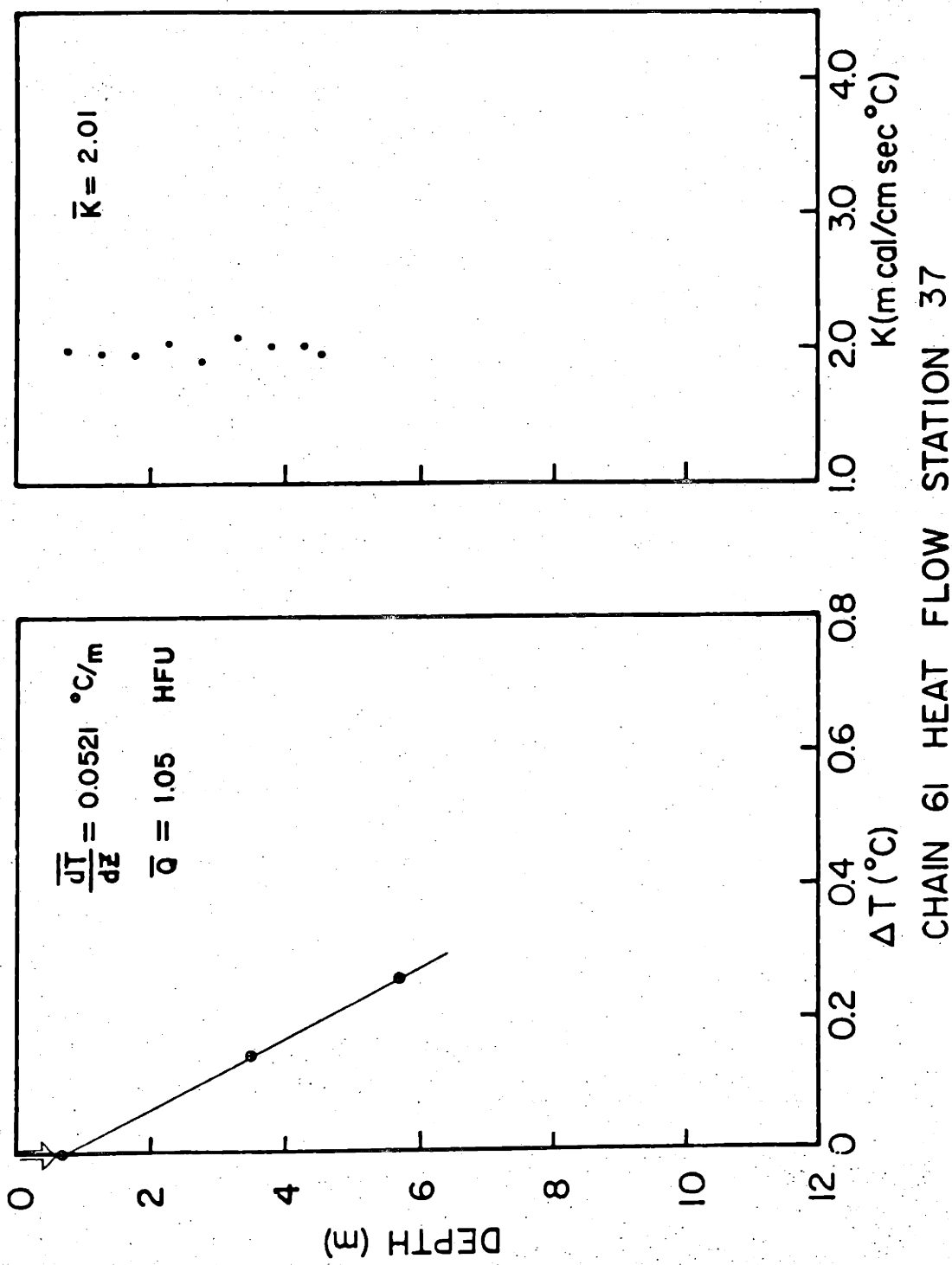

CHAIN 61 HEAT FLOW STATION 37

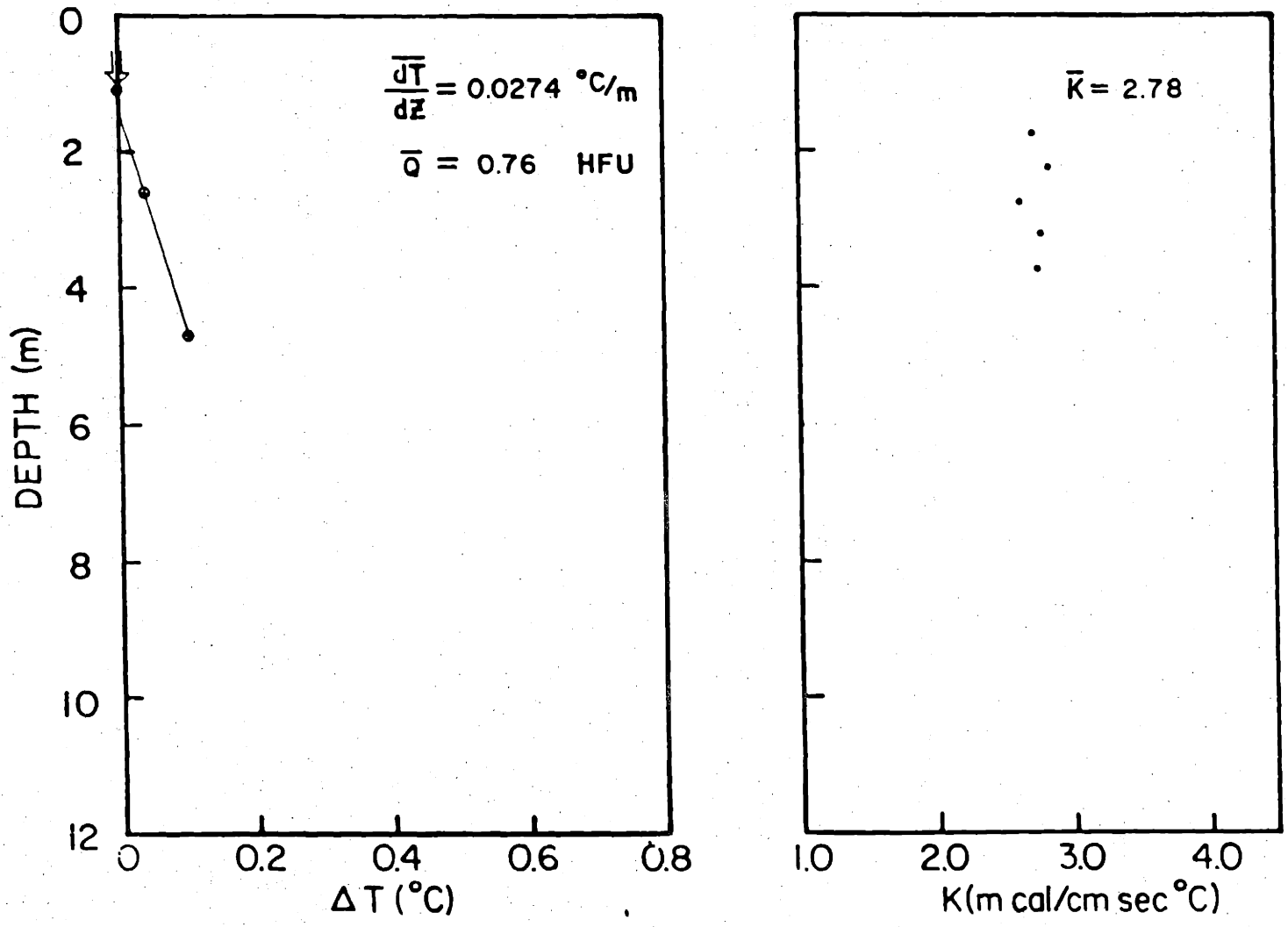

CHAIN 61 HEAT FLOW STATION 39

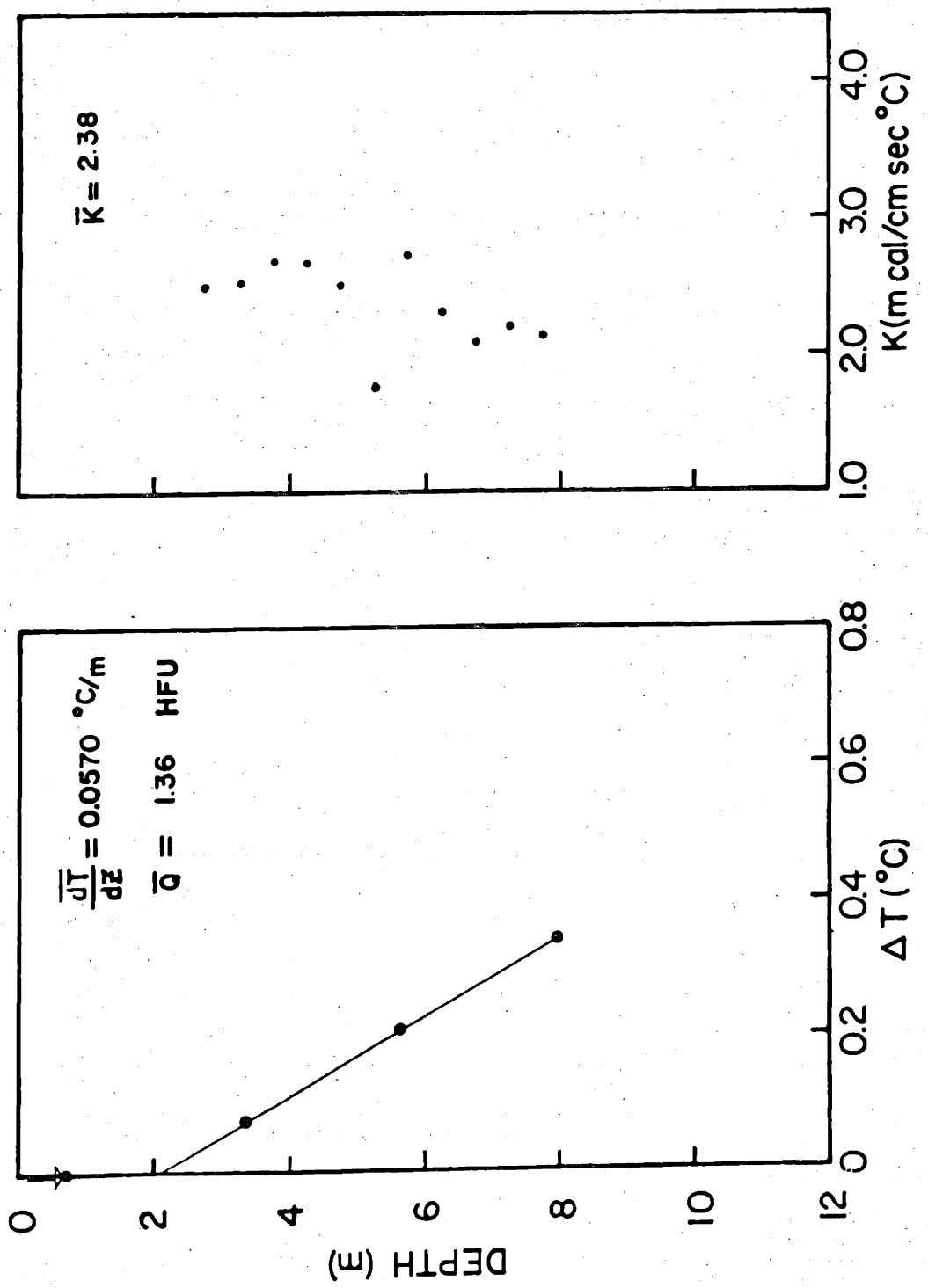

CHAIN 61 HEAT FLOW STATION 40

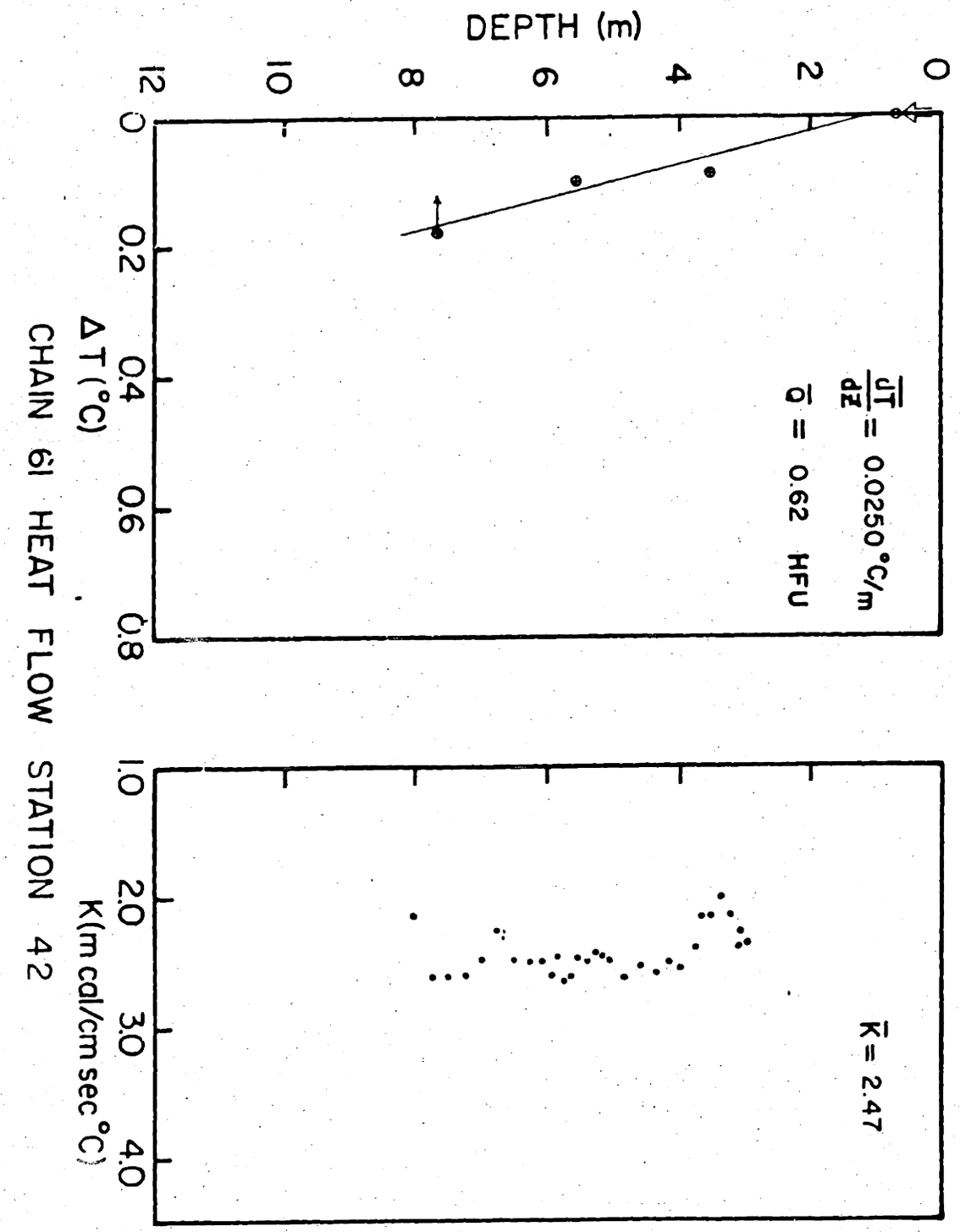

CHAIN 61 HEAT FLOW STATION 42

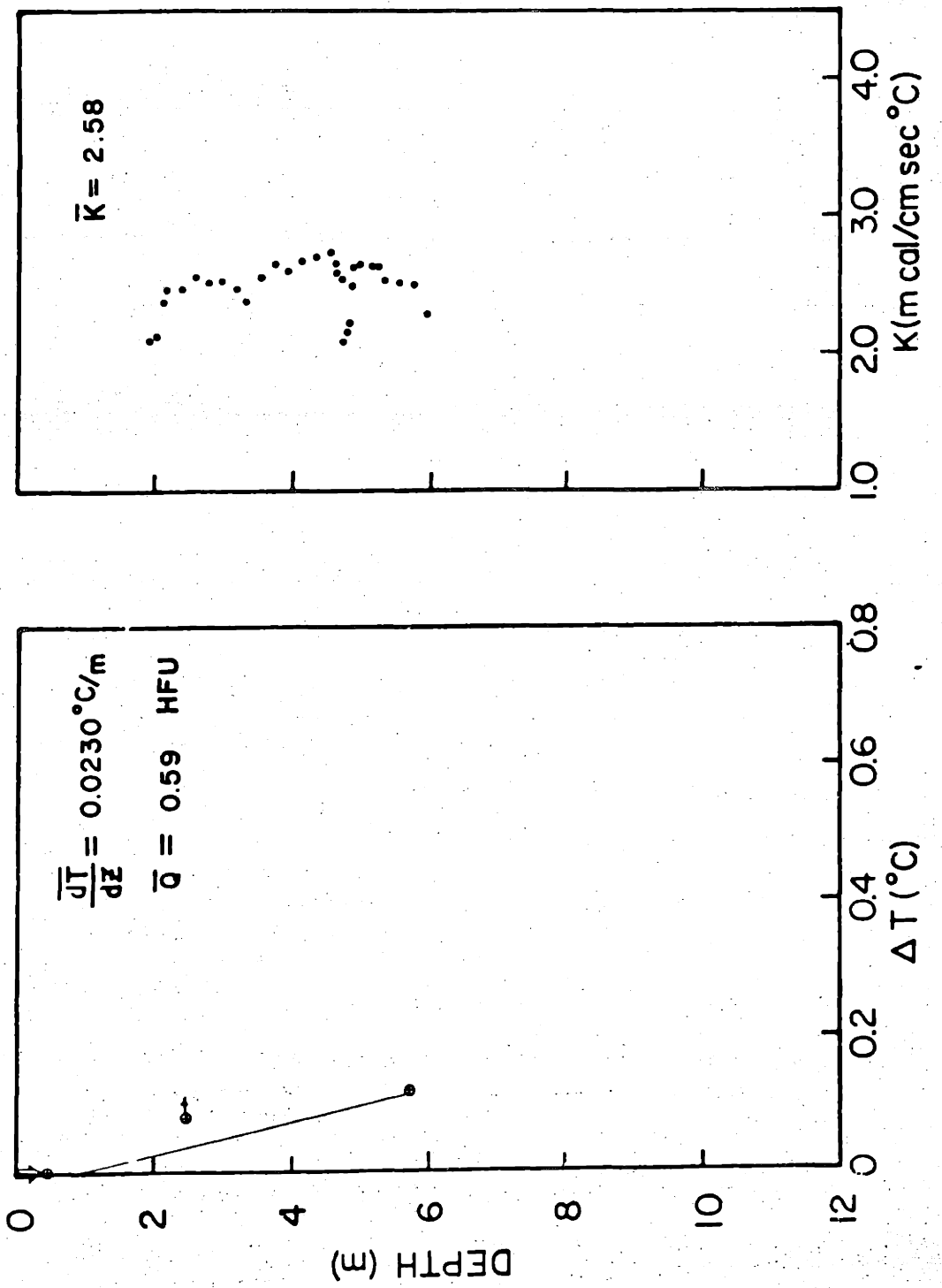

CHAIN 61 HEAT FLOW STATION 46

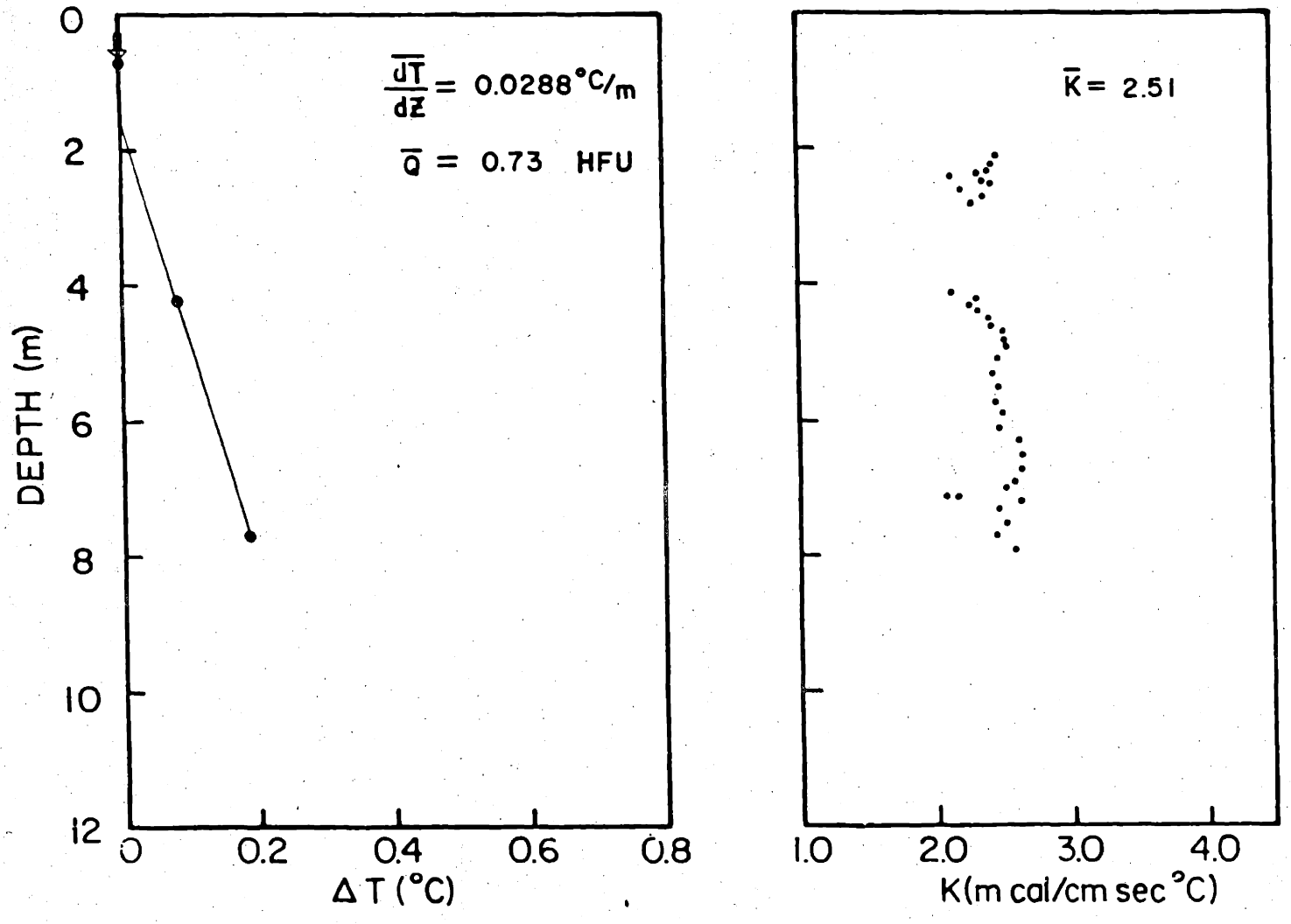

CHAIN 61 HEAT FLOW STATION 50

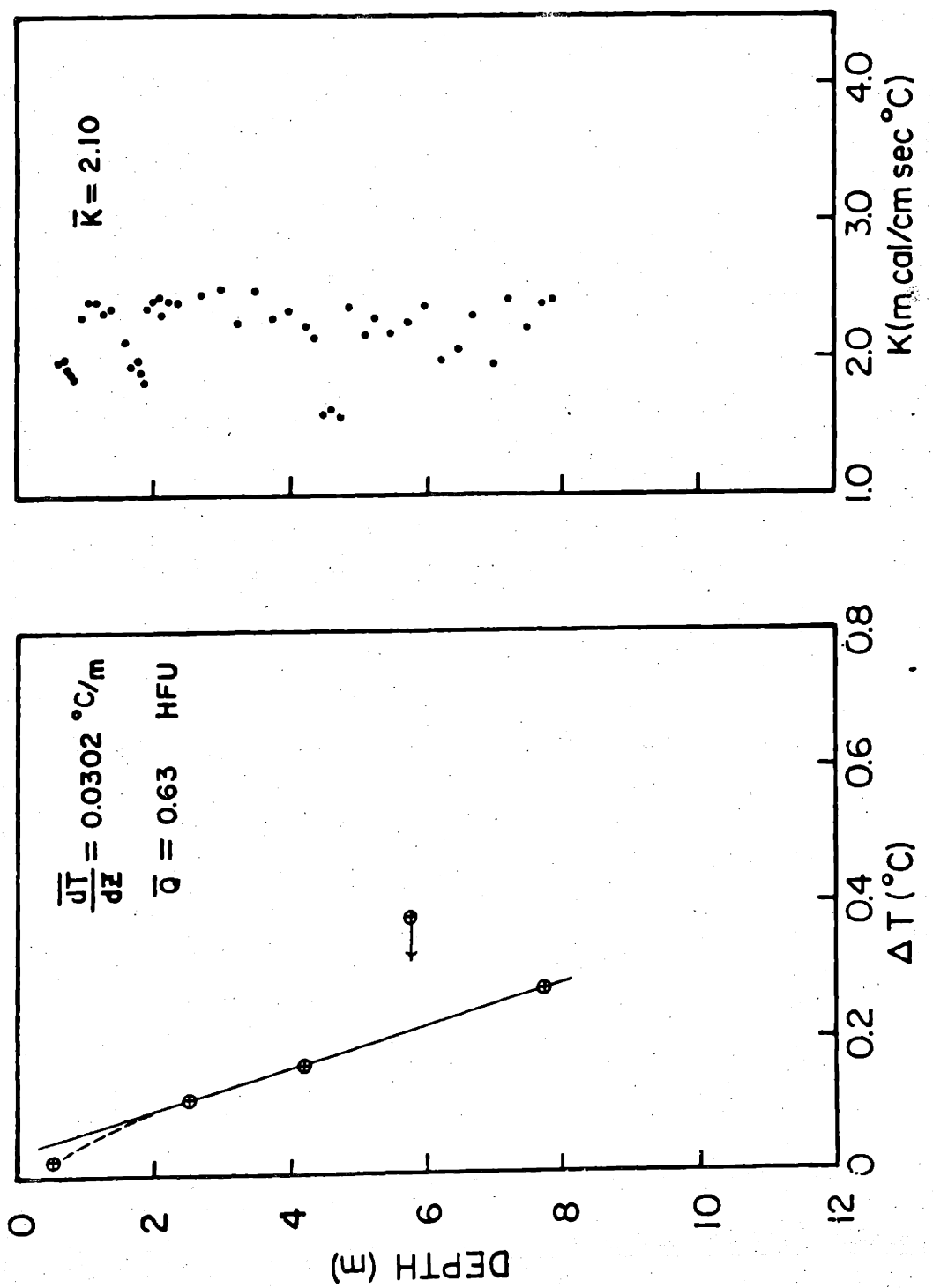

CHAIN 61 HEAT FLOW STATION 53

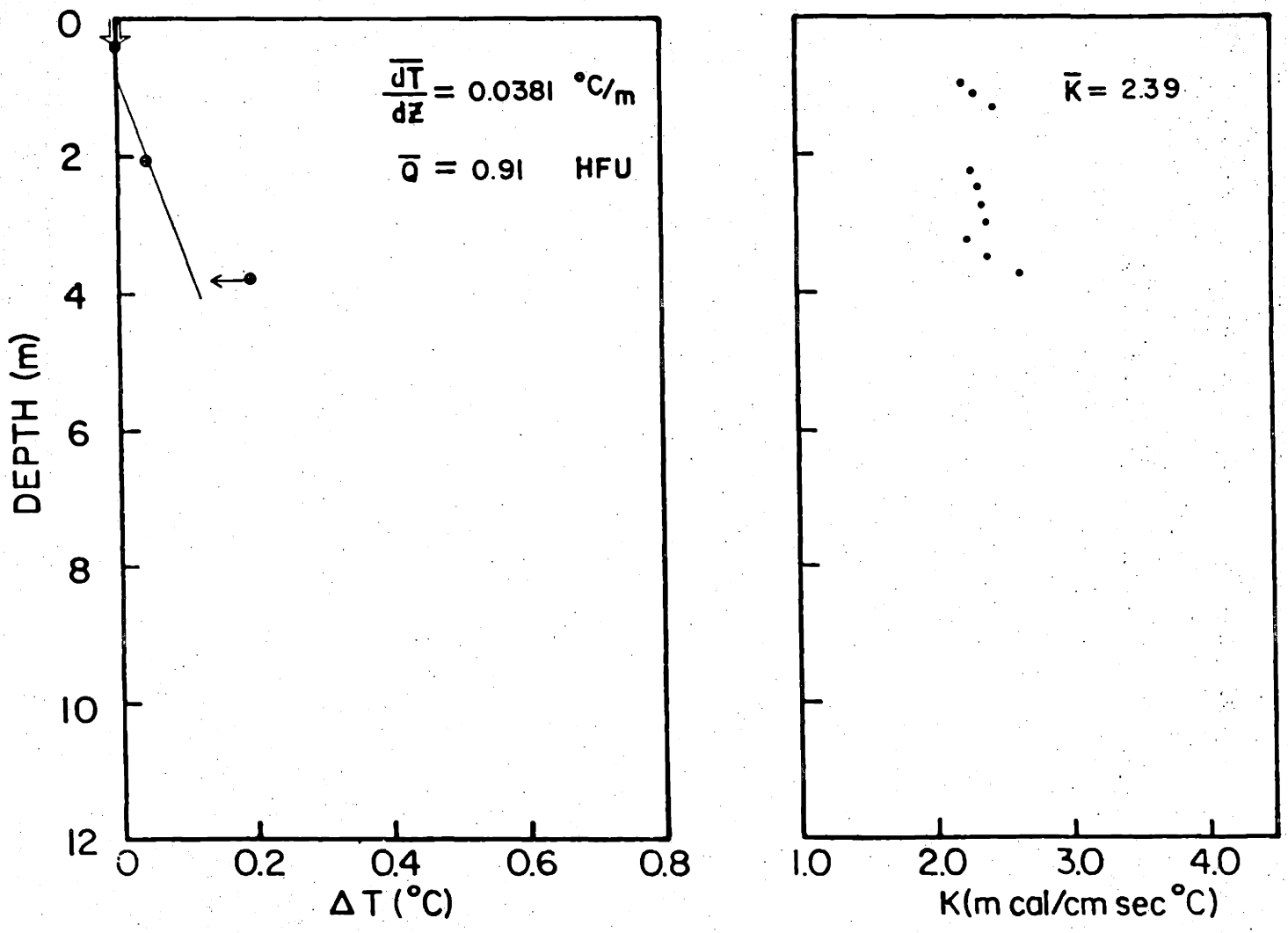

CHAIN 61 HEAT FLOW STATION 54

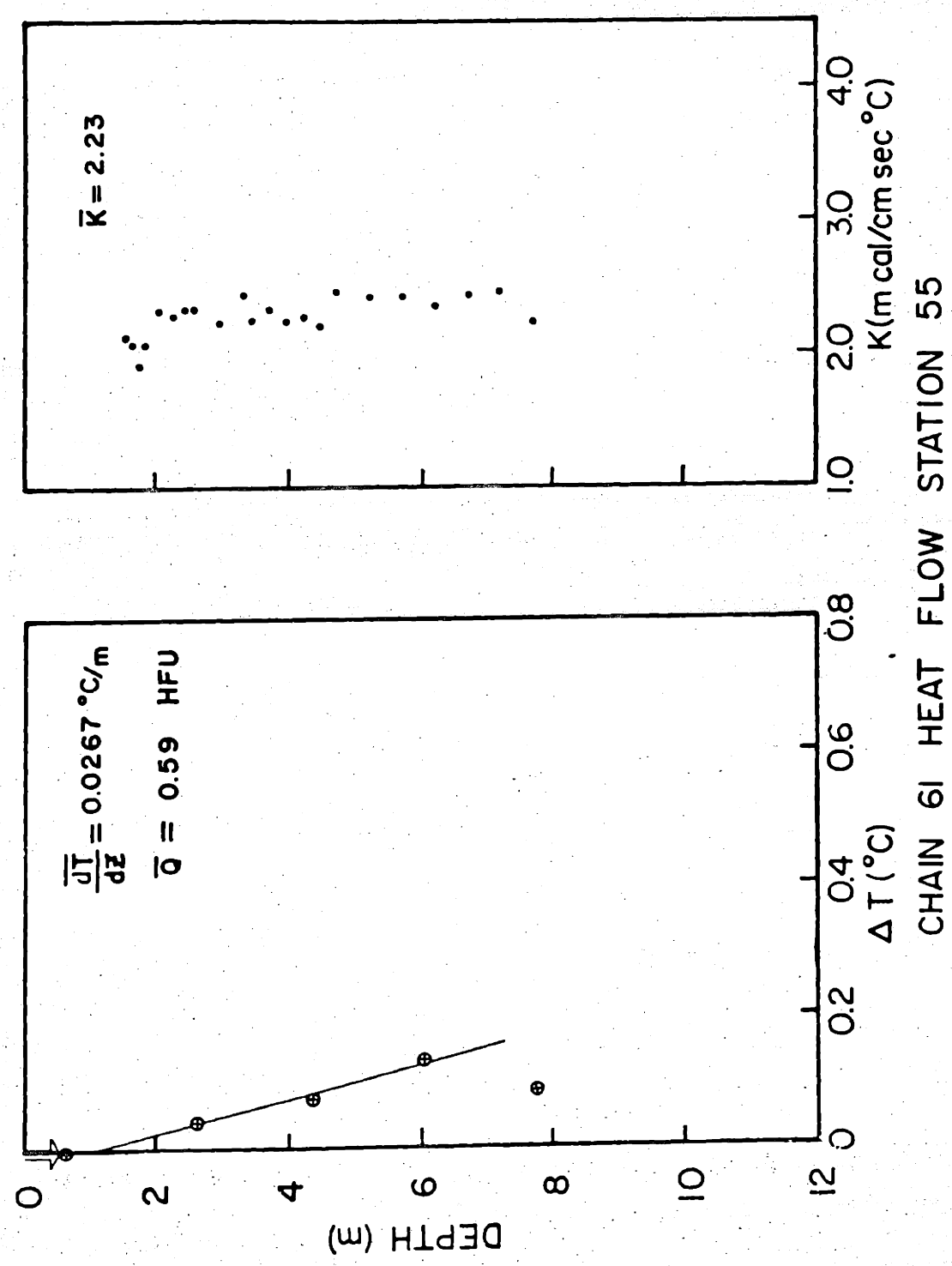

CHAIN 61 HEAT FLOW STATION 55

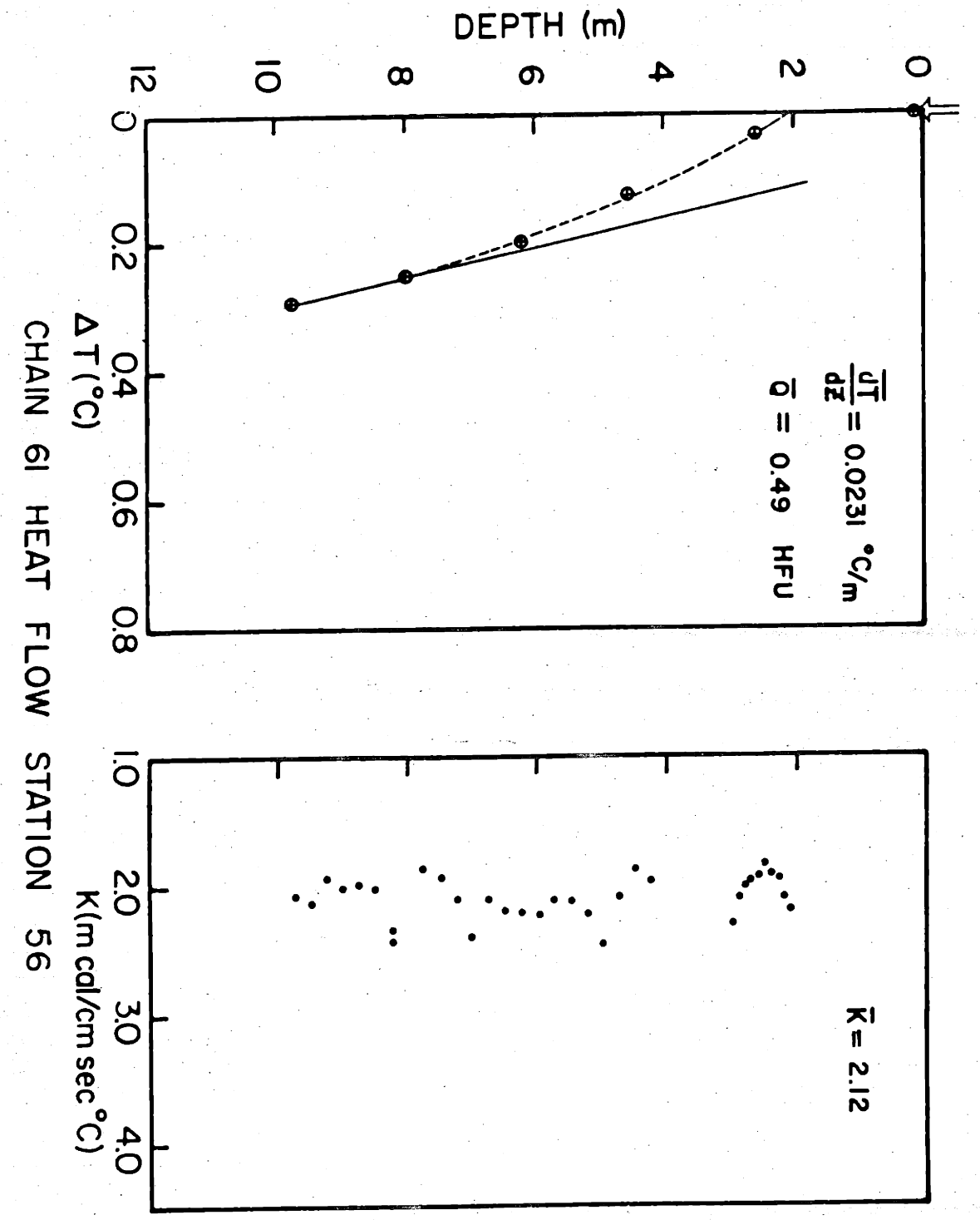

CHAIN 61 HEAT FLOW STATION 56

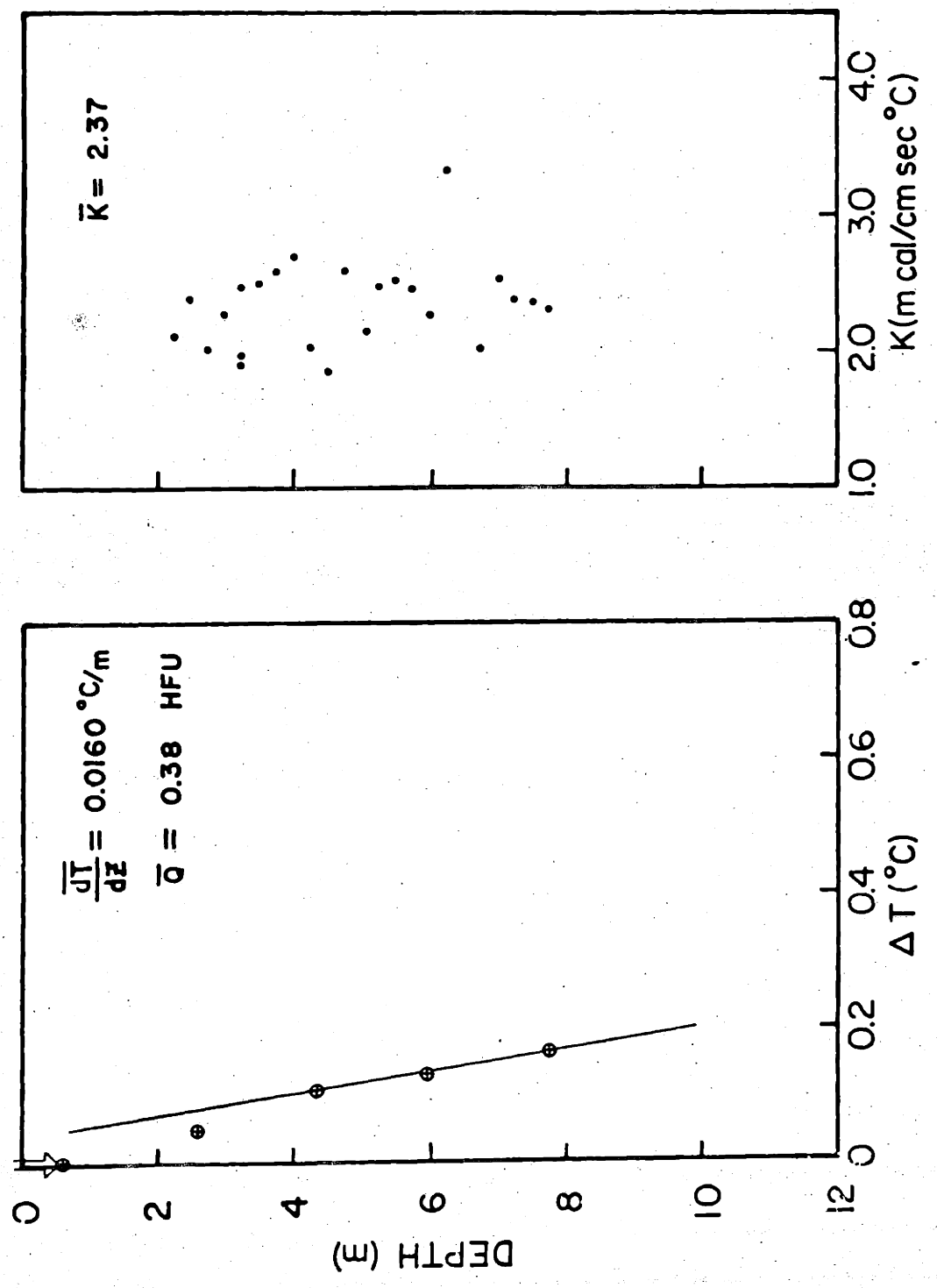

CHAIN 61 HEAT FLOW STATION 57

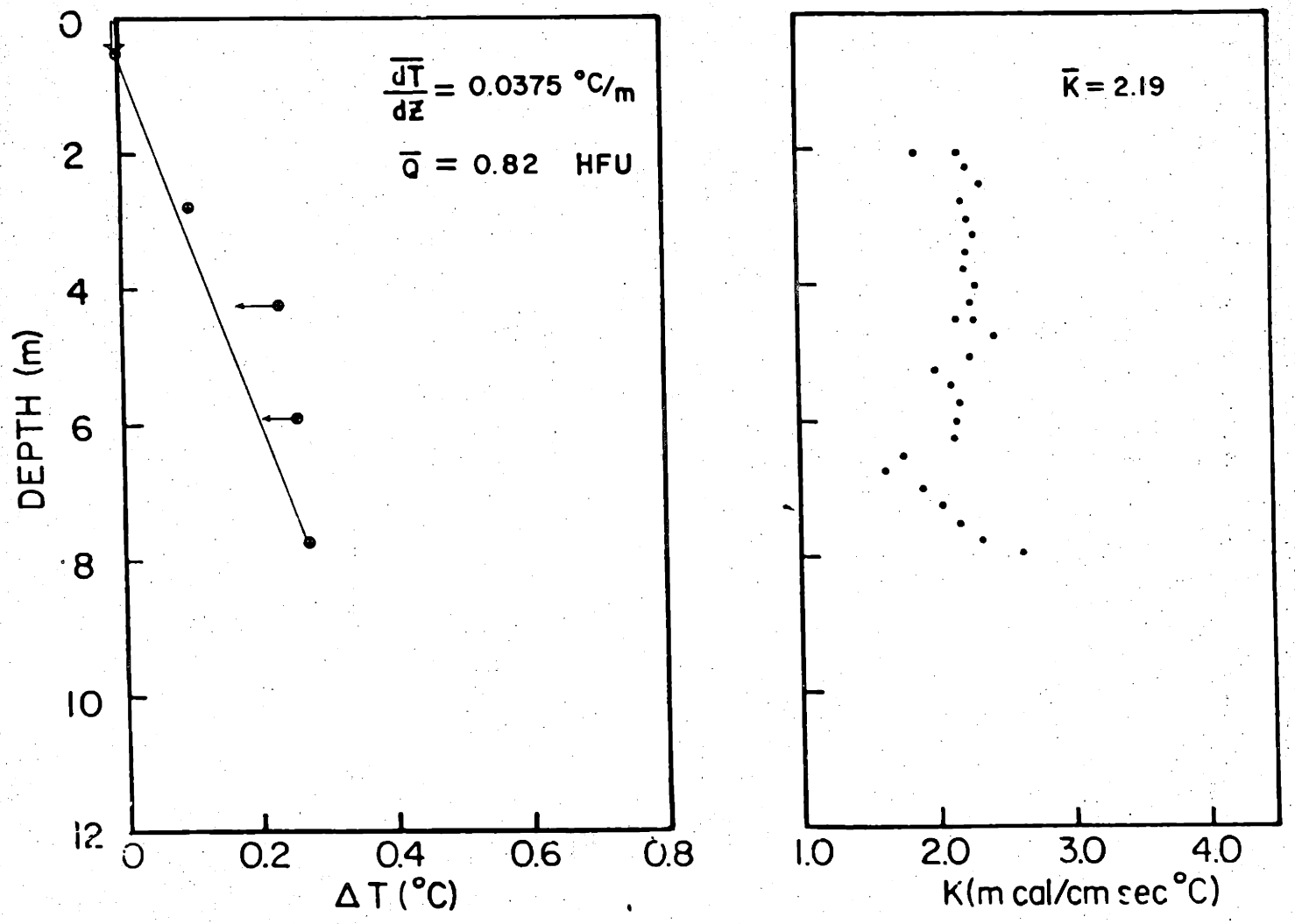

CHAIN 61 HEAT FLOW STATION 59

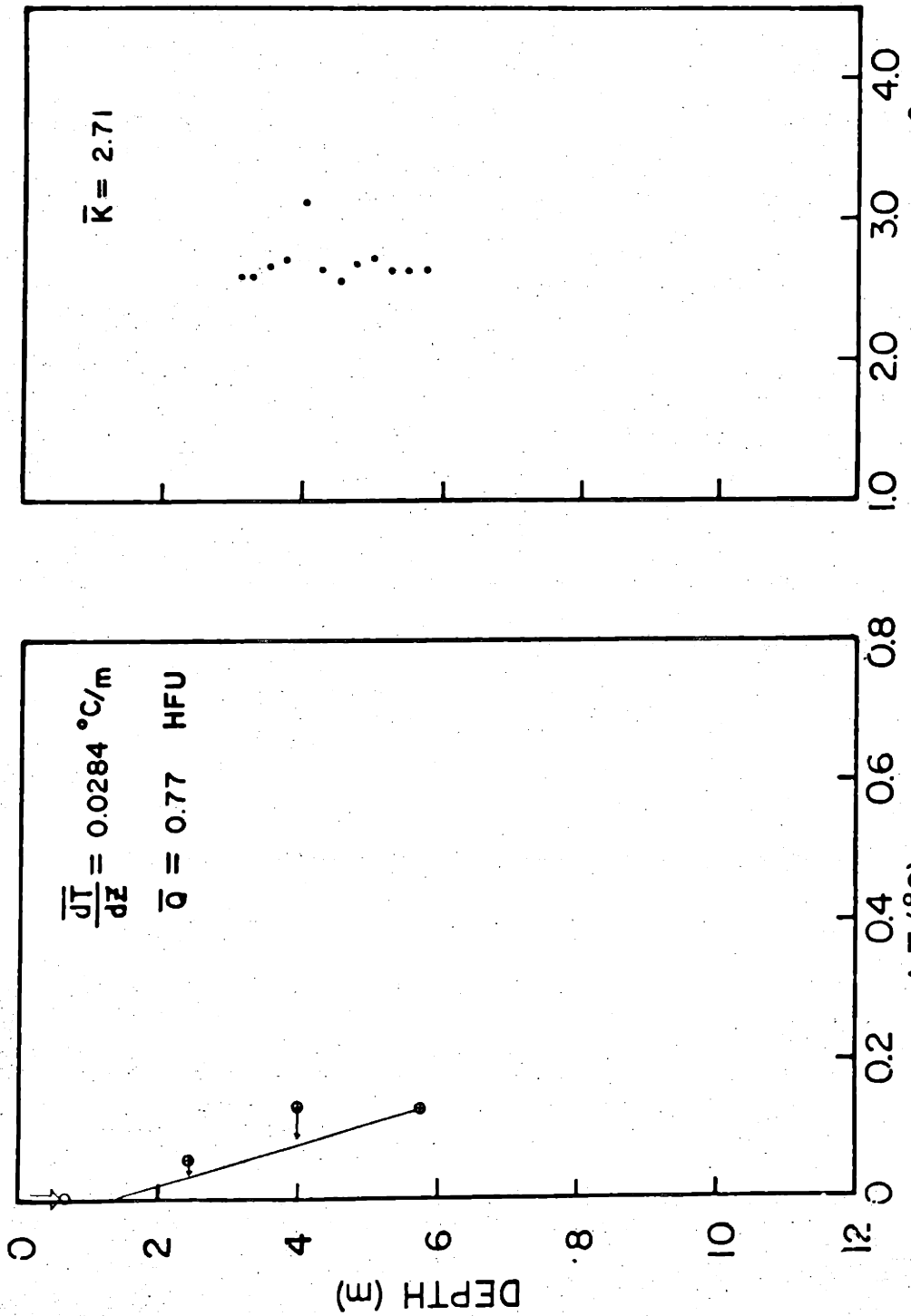

CHAIN 61 HEAT FLOW STATION 62

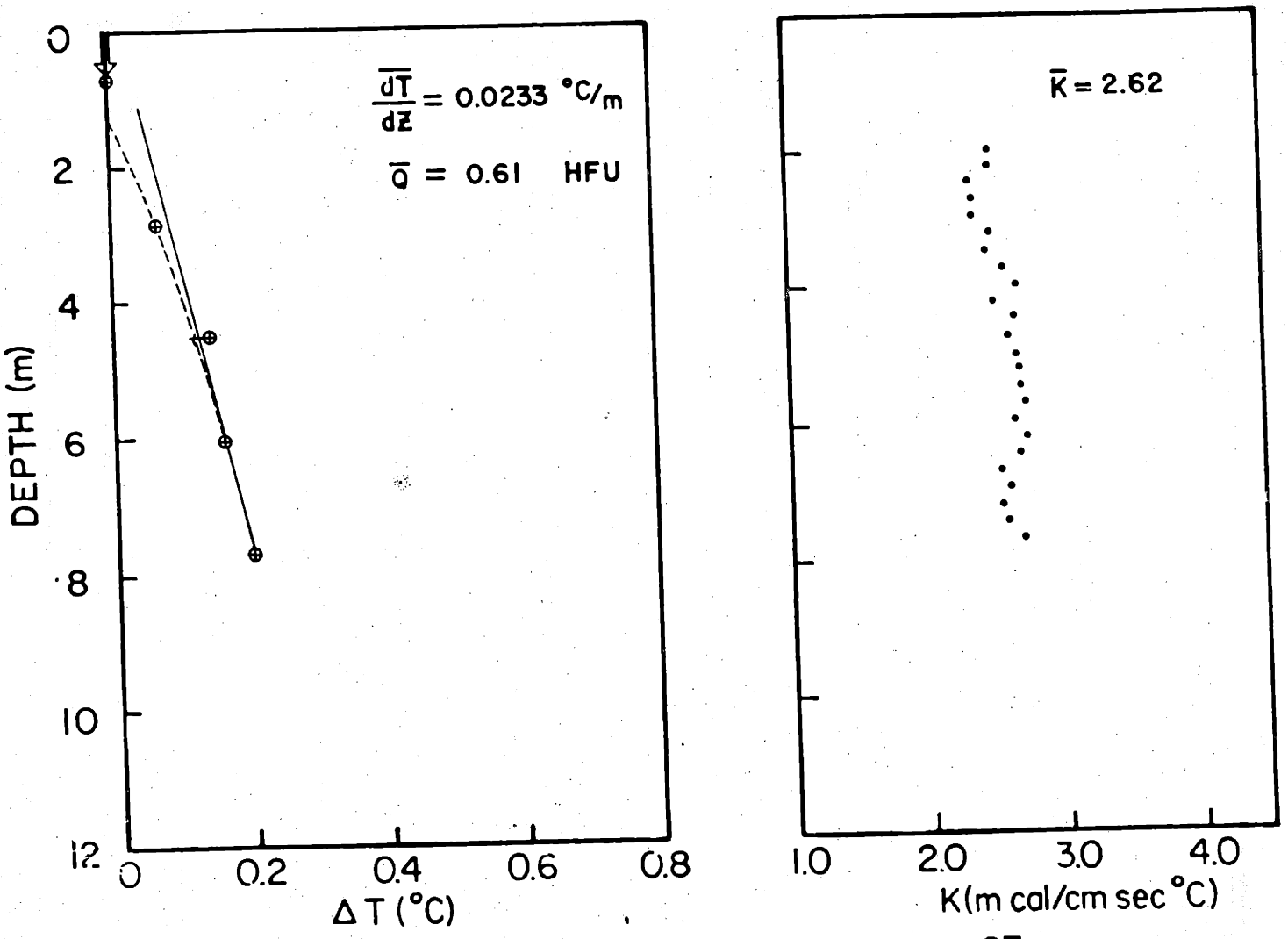

CHAIN 61 HEAT FLOW STATION 63

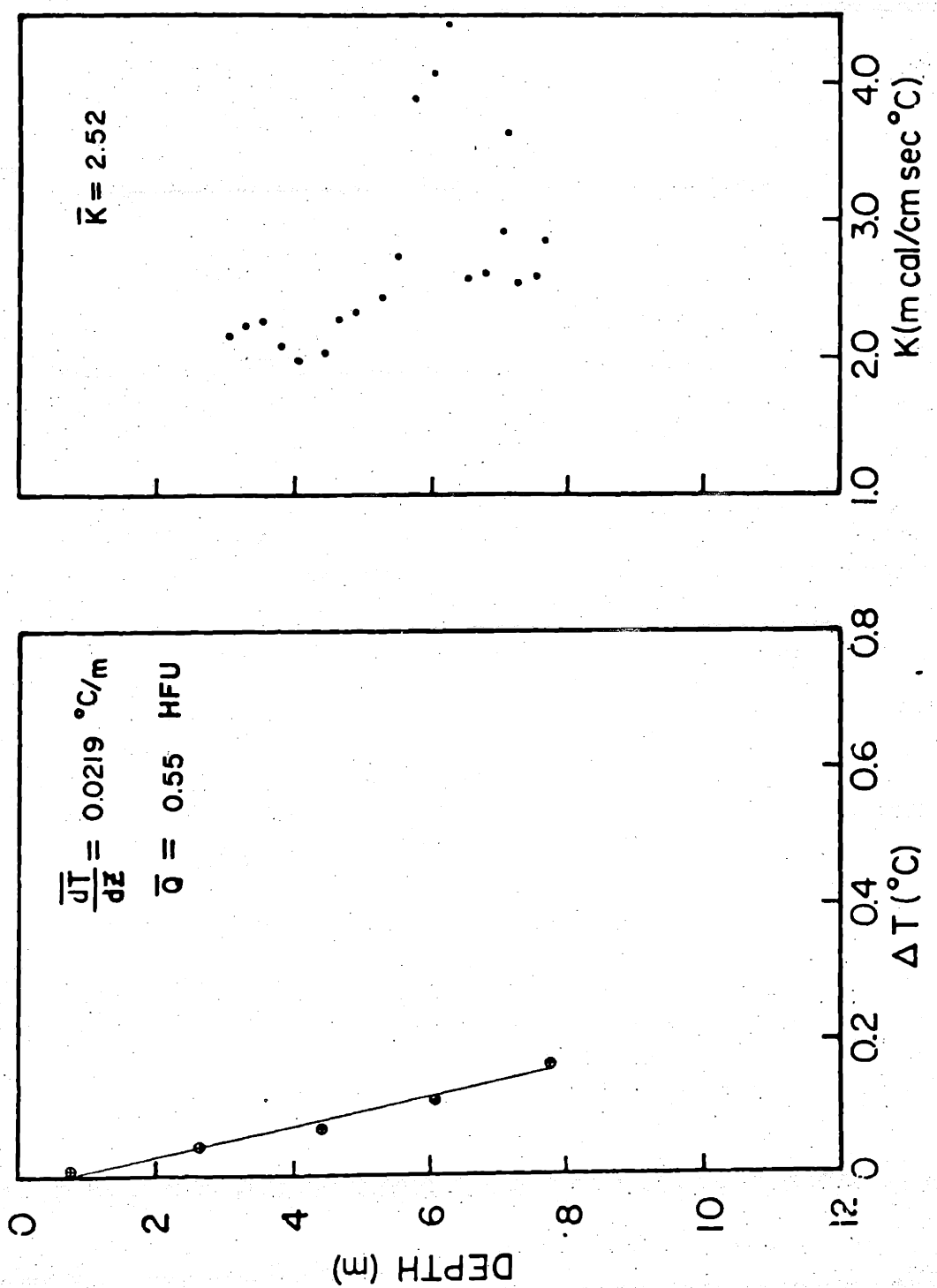

CHAIN 61 HEAT FLOW STATION 64

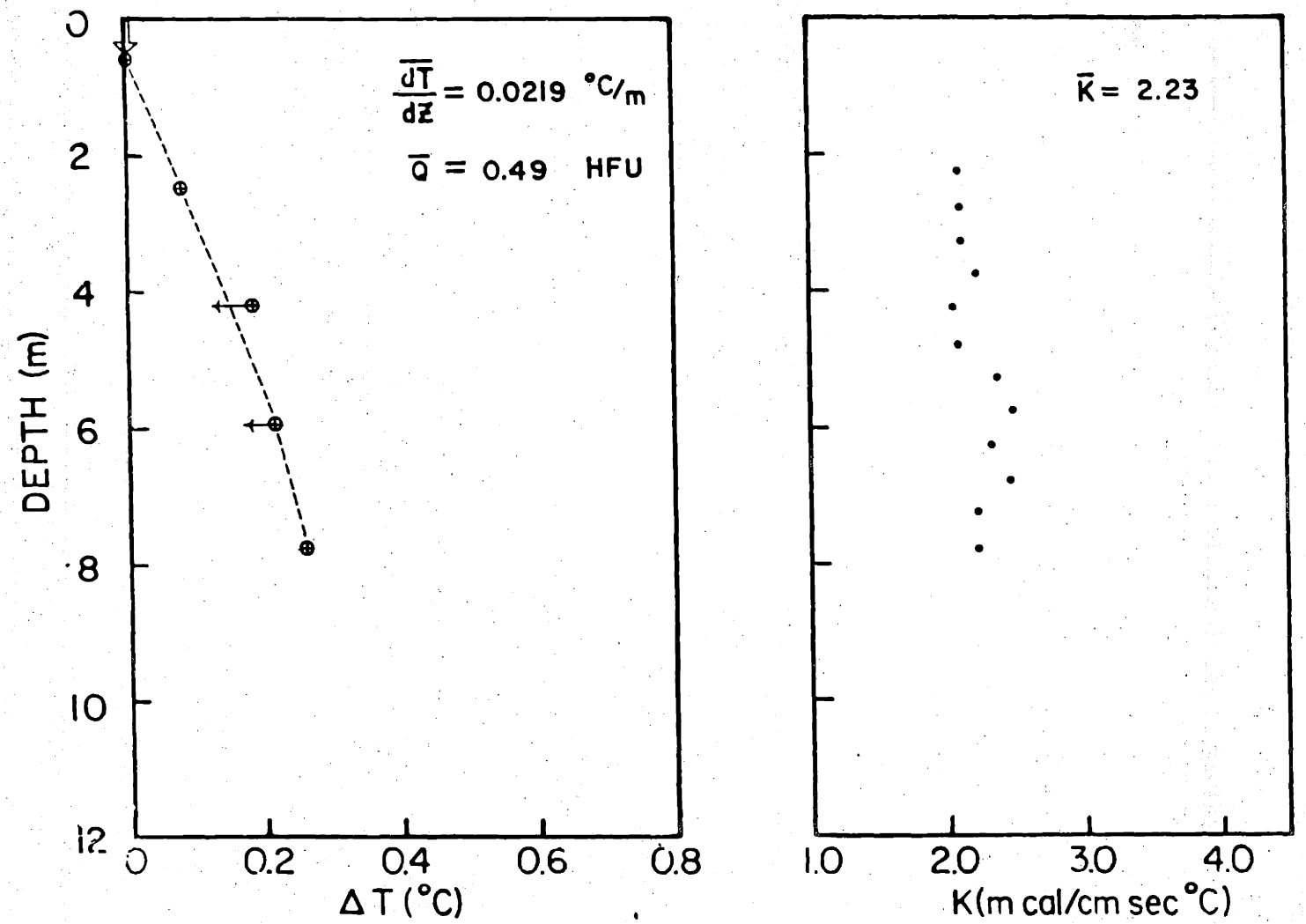

CHAIN 61 HEAT FLOW STATION 65

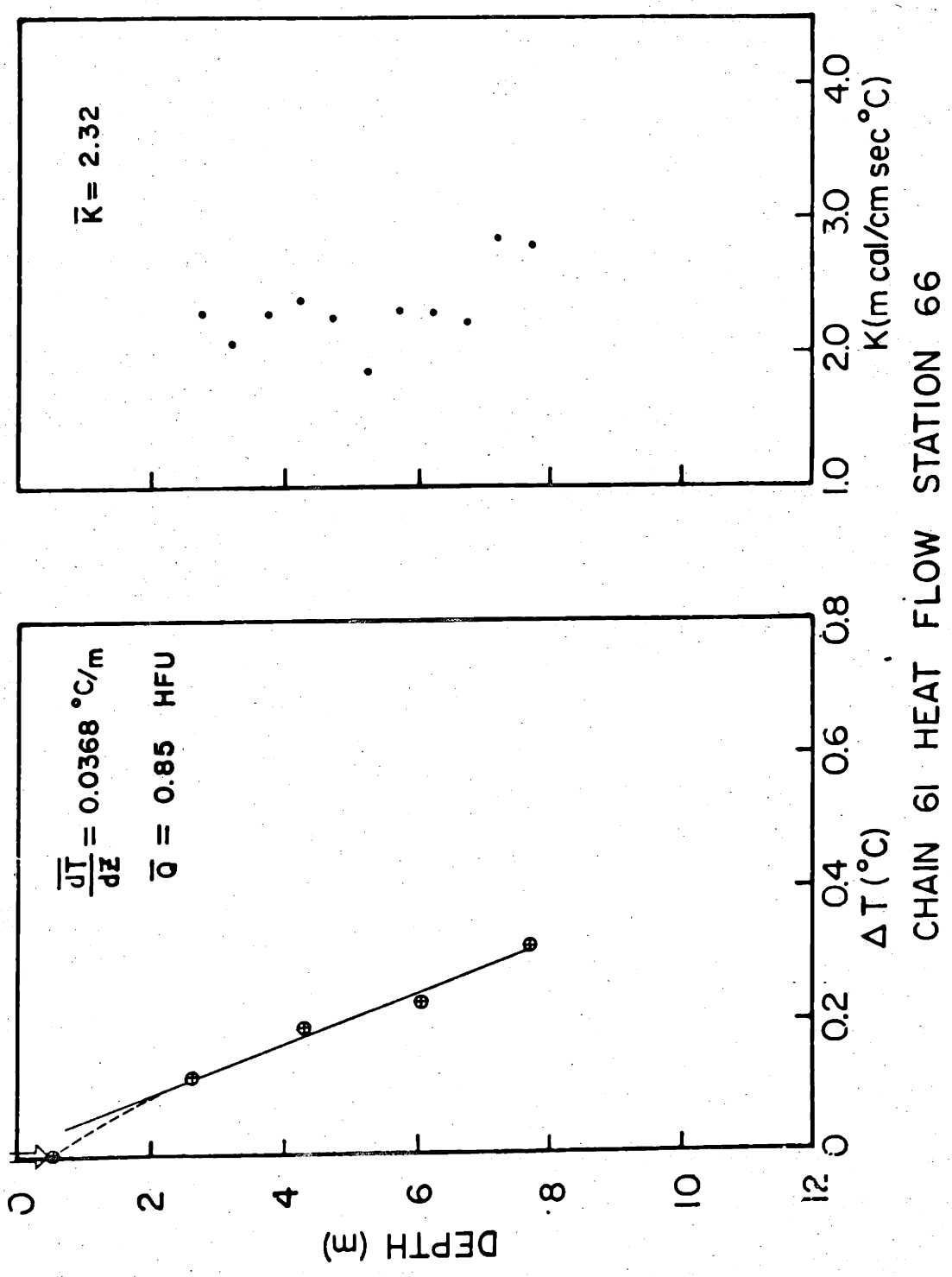
$\overline{\frac{dT}{dz}}$ = 0.0368 °C/m
$\bar{Q}$ = 0.85 HFU
$\bar{K}$ = 2.32
DEPTH (m)
ΔT (°C)
K(m cal/cm sec °C)
CHAIN 61 HEAT FLOW STATION 66

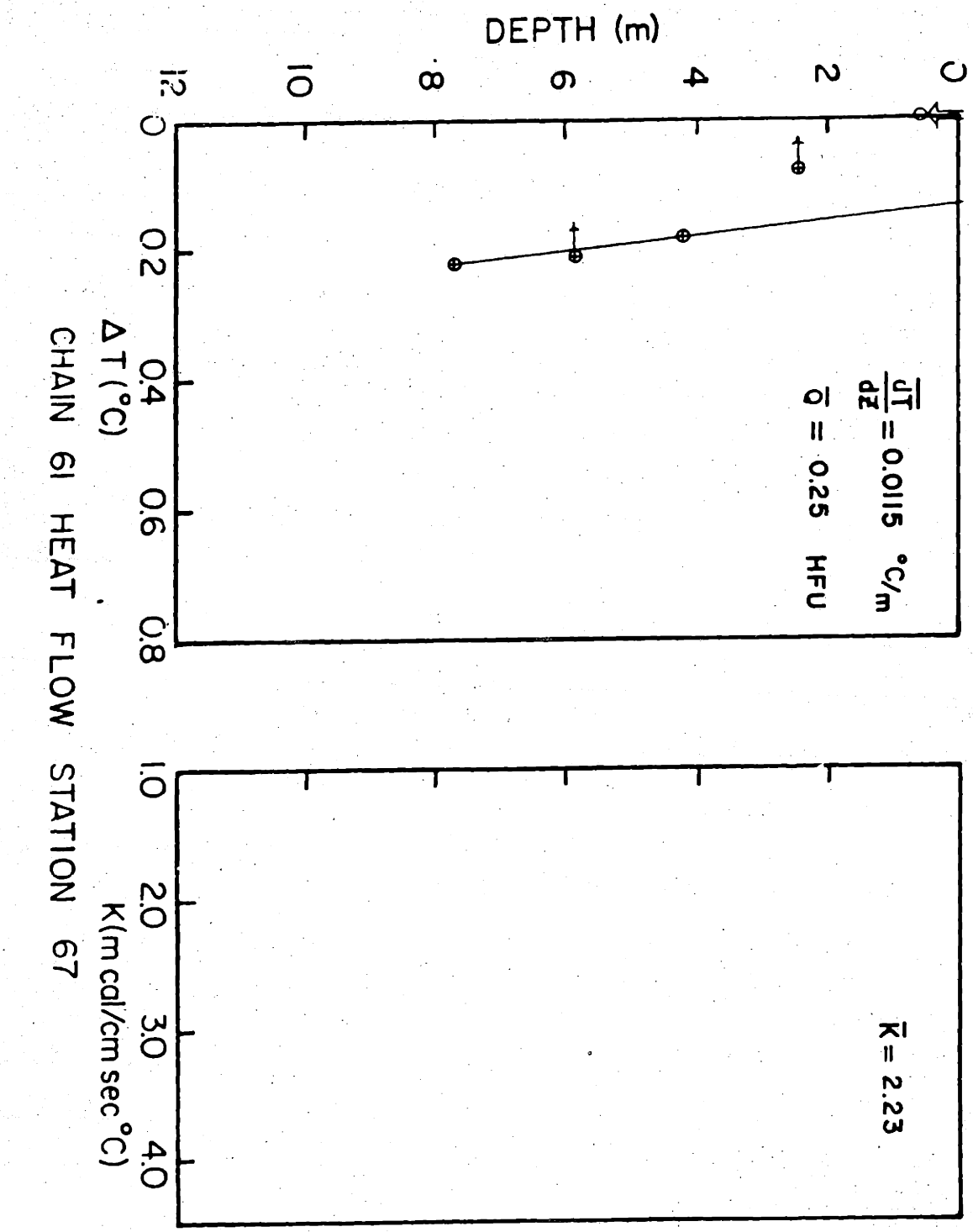

CHAIN 61 HEAT FLOW STATION 67

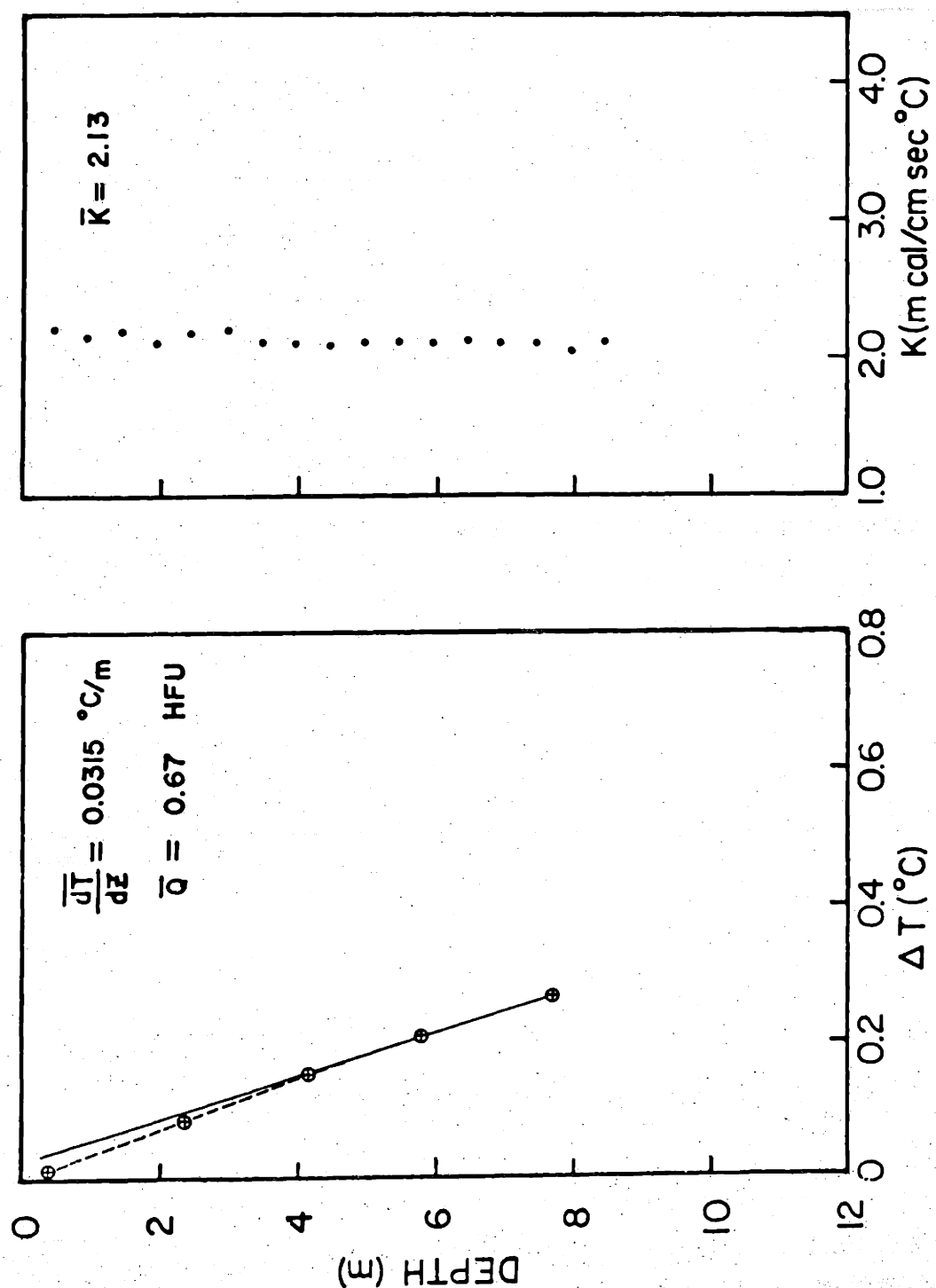

CHAIN 61 HEAT FLOW STATION 68

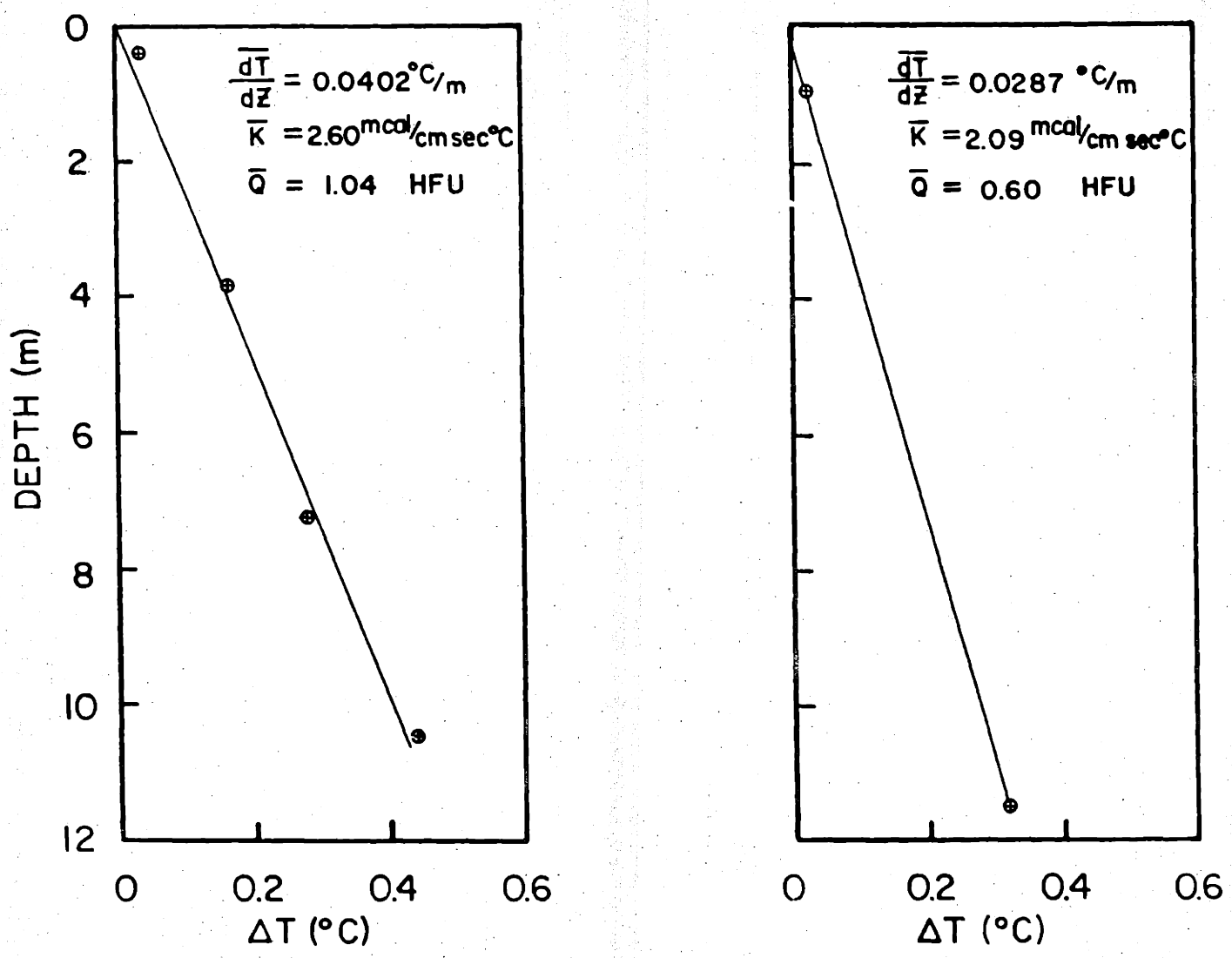

CONRAD 9 HEAT FLOW MEASUREMENTS

STATION 115 STATION 116

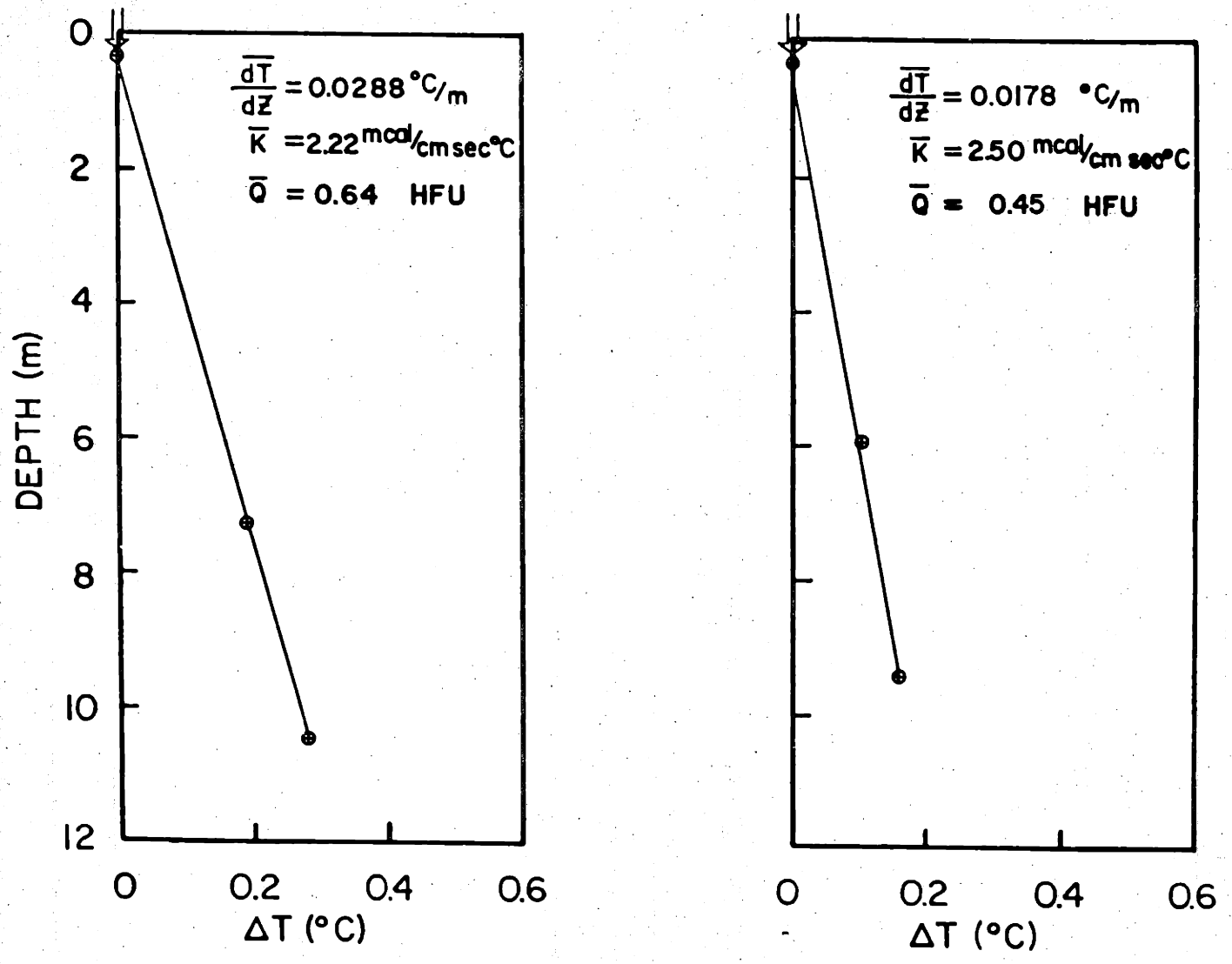

CONRAD 9 HEAT FLOW MEASUREMENTS

STATION 117

STATION 118

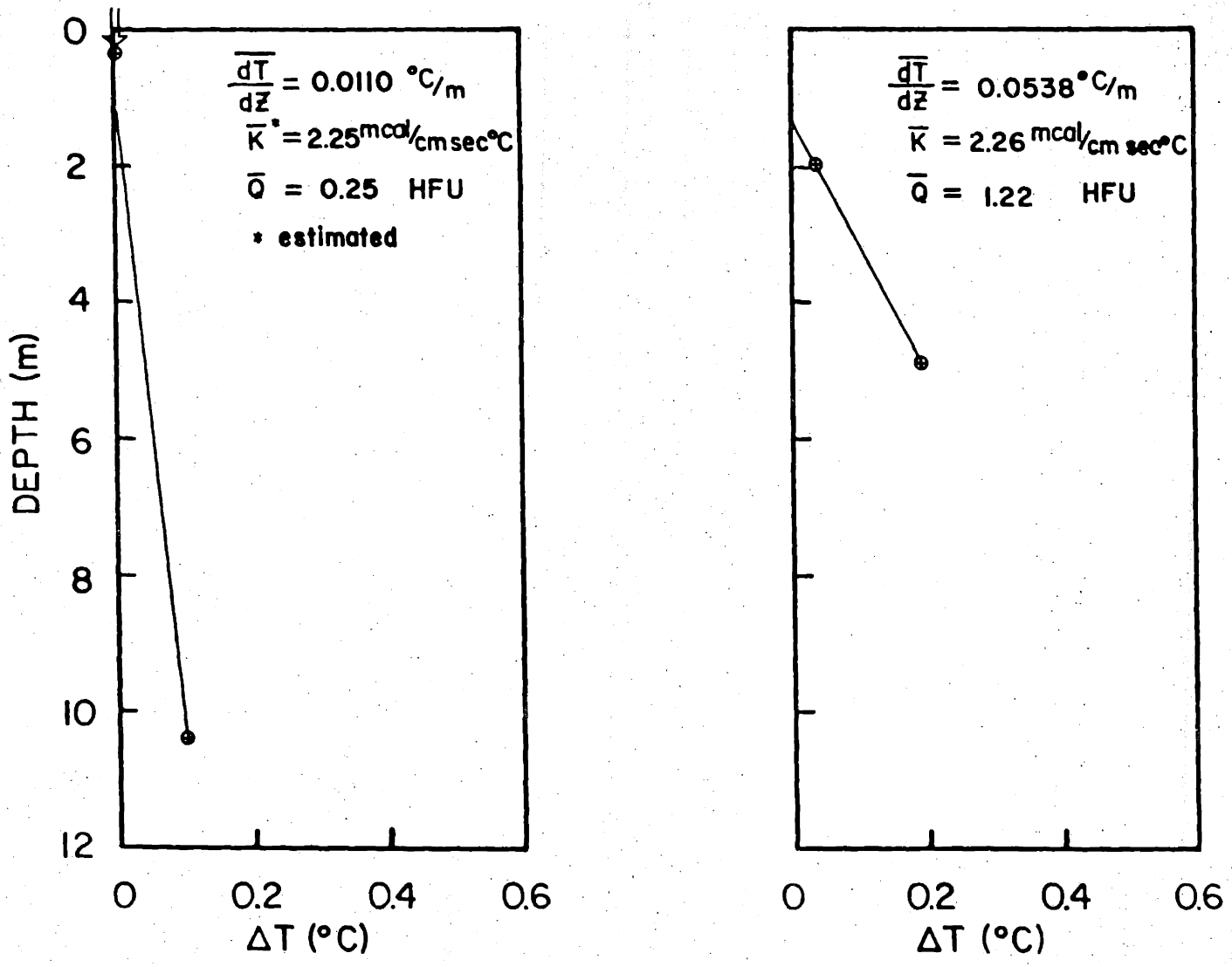

CONRAD 9 HEAT FLOW MEASUREMENTS

STATION 119

STATION 121

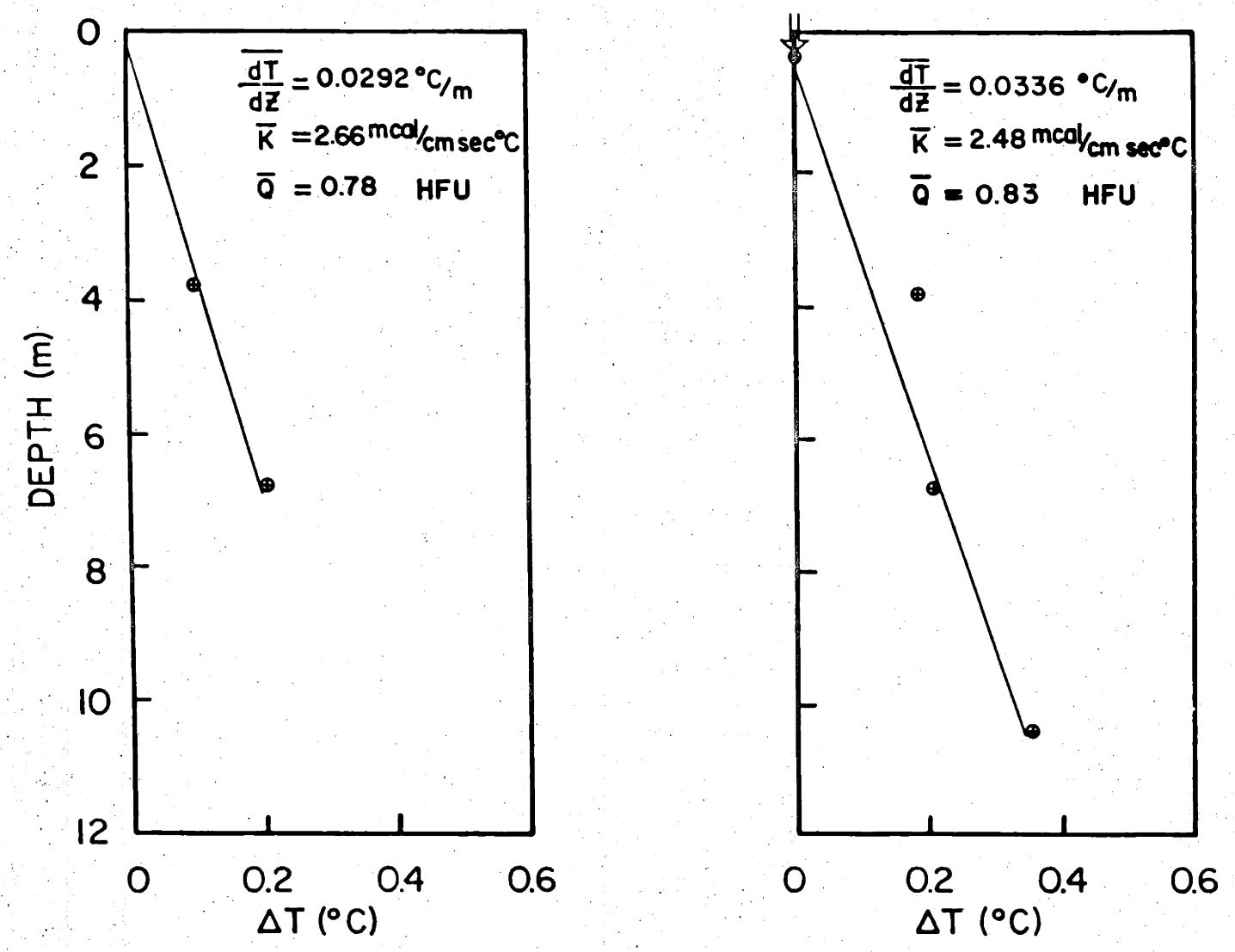

CONRAD 9 HEAT FLOW MEASUREMENTS

STATION 123 STATION 124

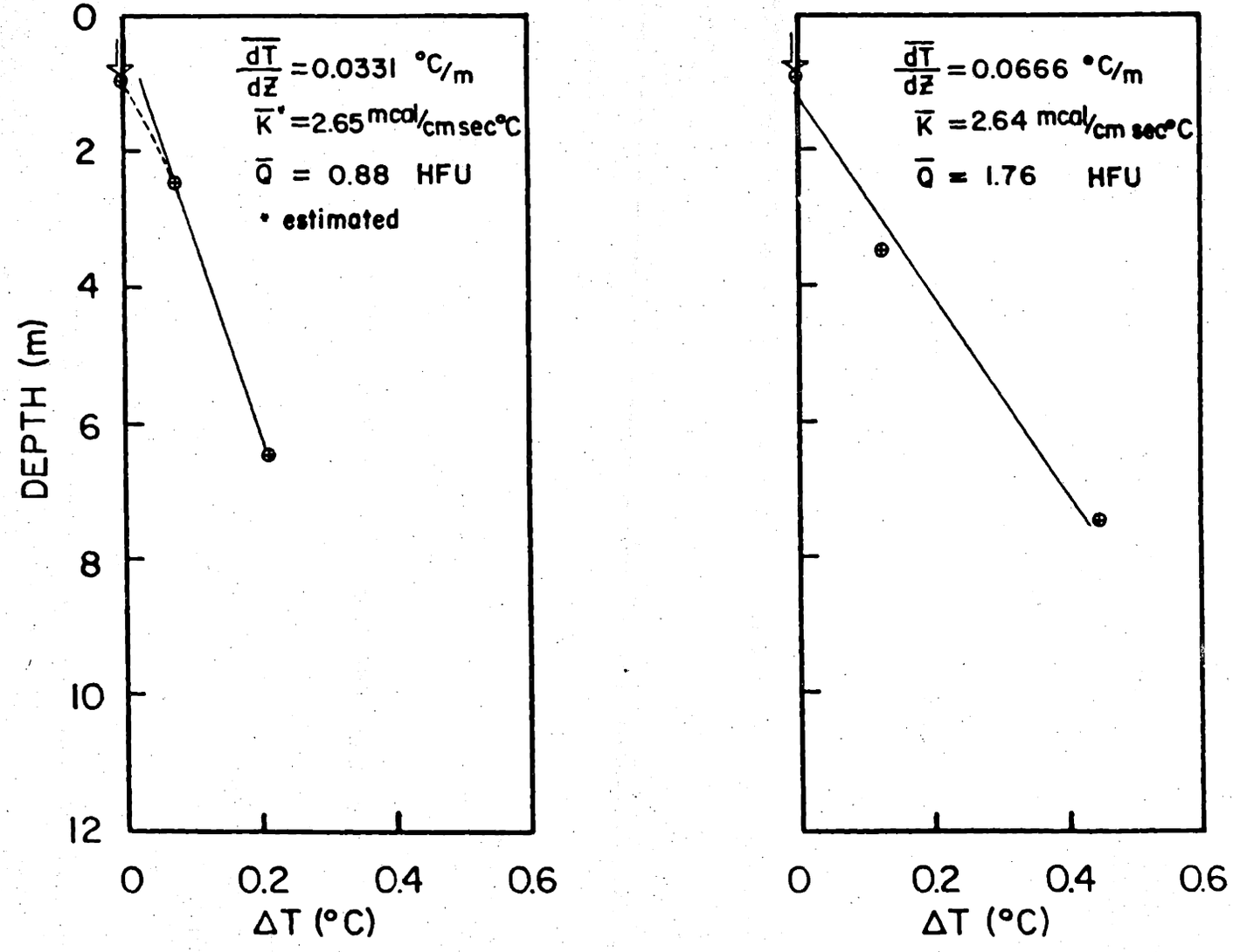

CONRAD 9 HEAT FLOW MEASUREMENTS

STATION 125 STATION 126

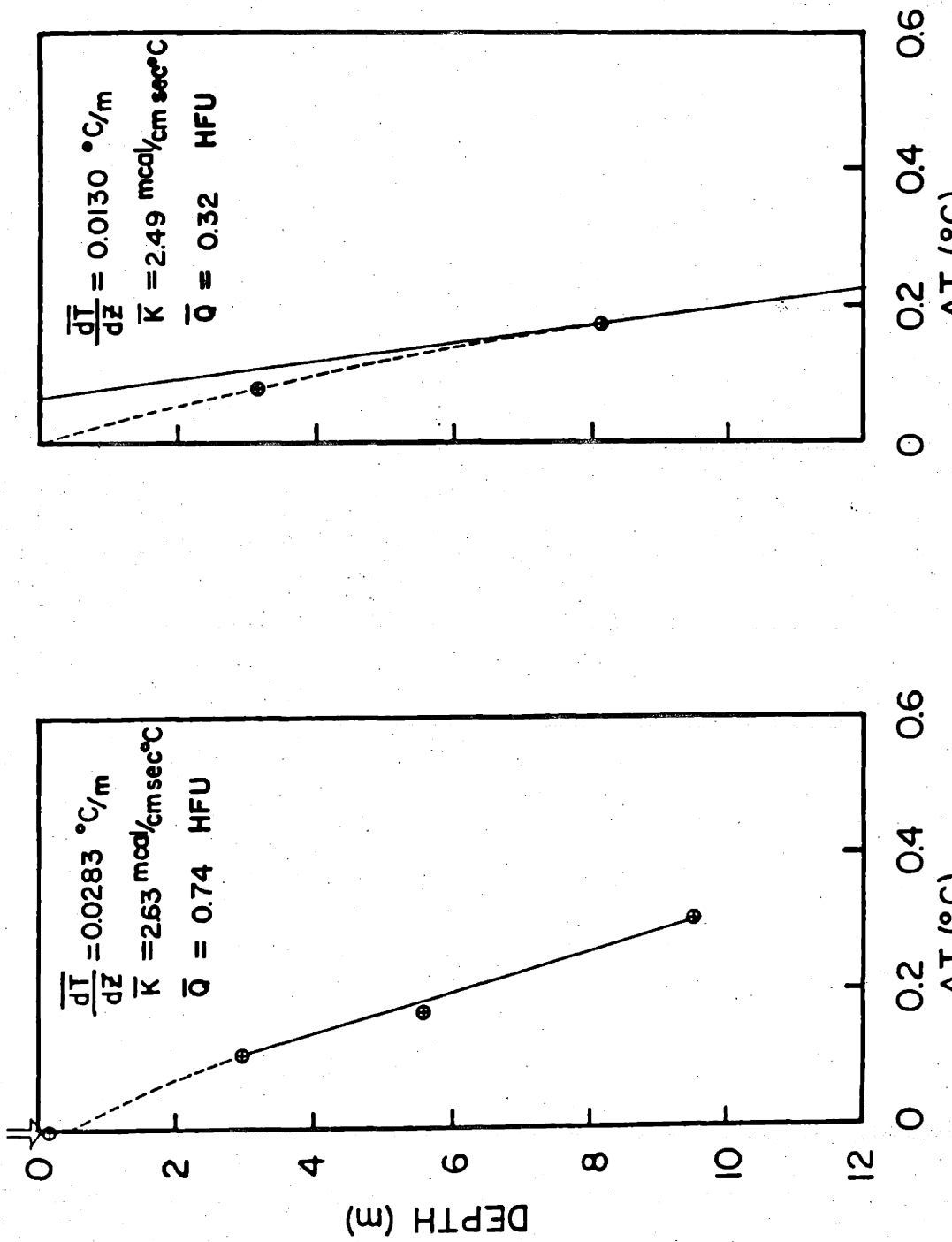

CONRAD 9 HEAT FLOW MEASUREMENTS
STATION 127
STATION 129

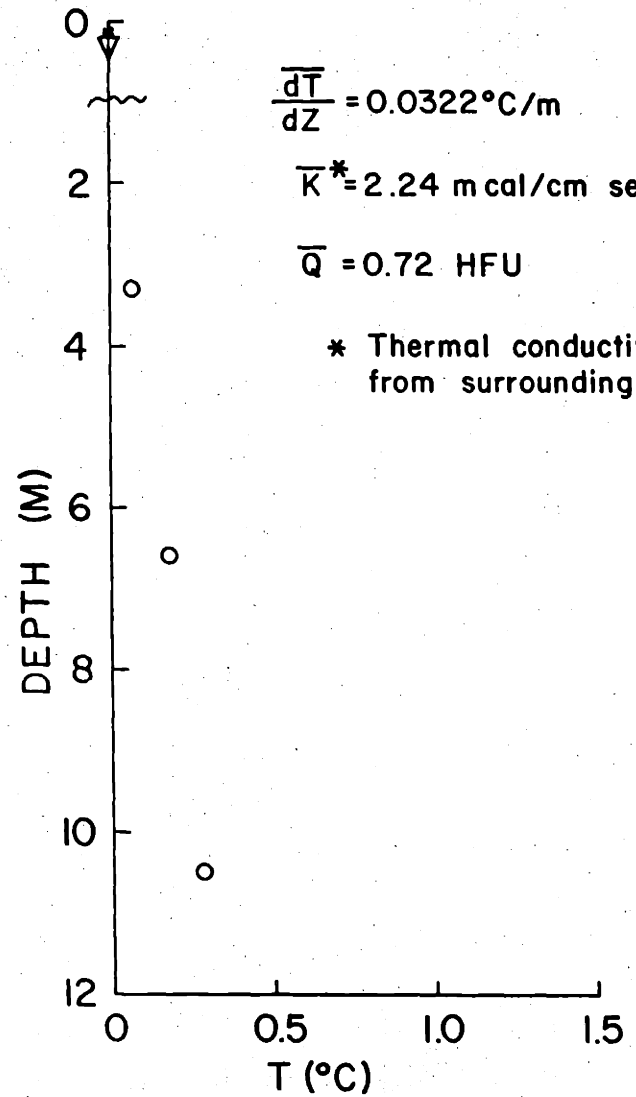

$\overline{\frac{dT}{dZ}}$ = 0.0322°C/m

$\overline{K}^{*}$ = 2.24 m cal/cm sec °C

$\overline{Q}$ = 0.72 HFU

* Thermal conductivity estimated from surrounding stations.

R.V. CONRAD 9 HEAT FLOW STATION 131

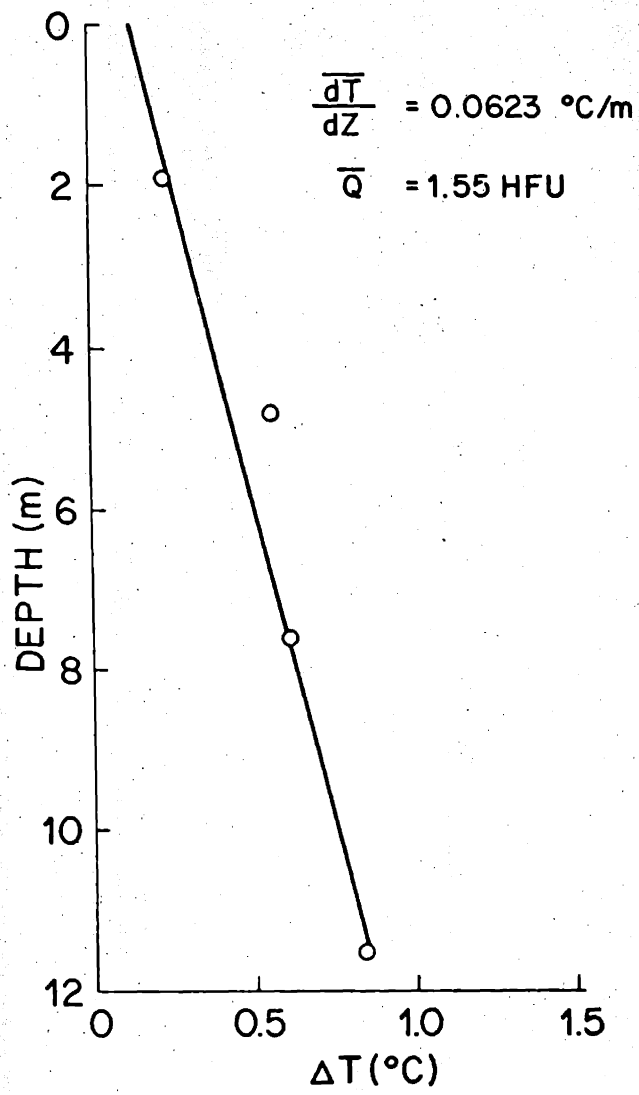

R.V. CONRAD 9

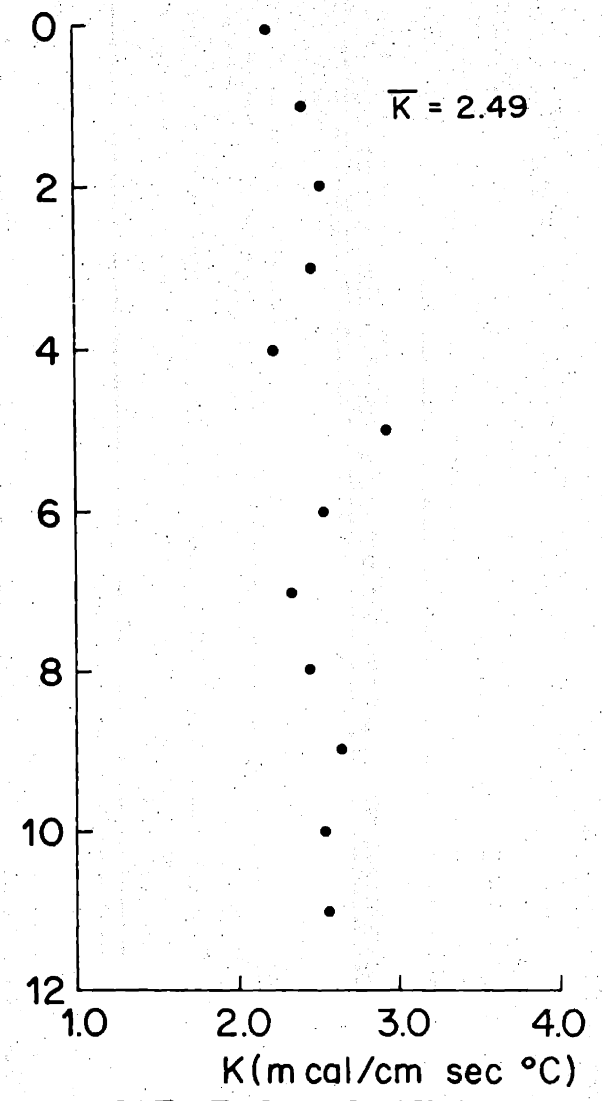

HEAT FLOW STATION 132

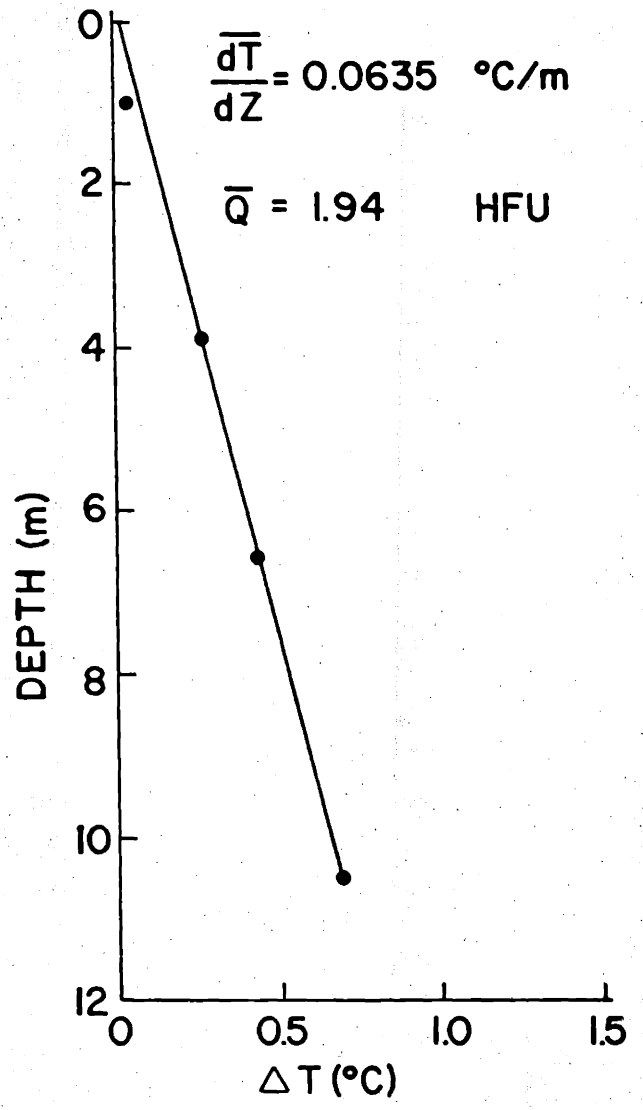

R.V. CONRAD 9

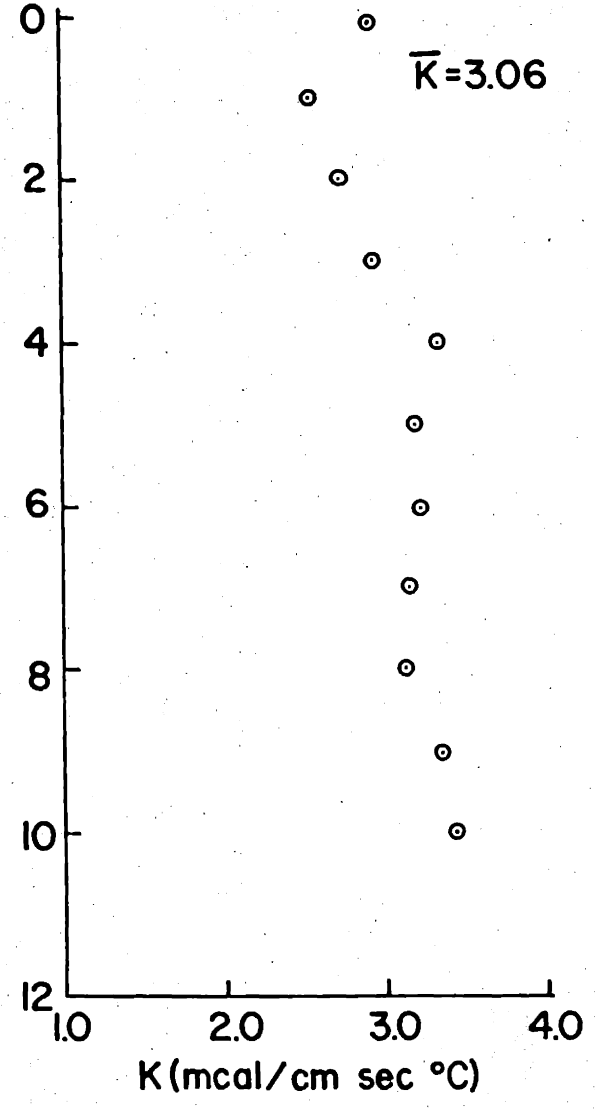

HEAT FLOW STATION 133

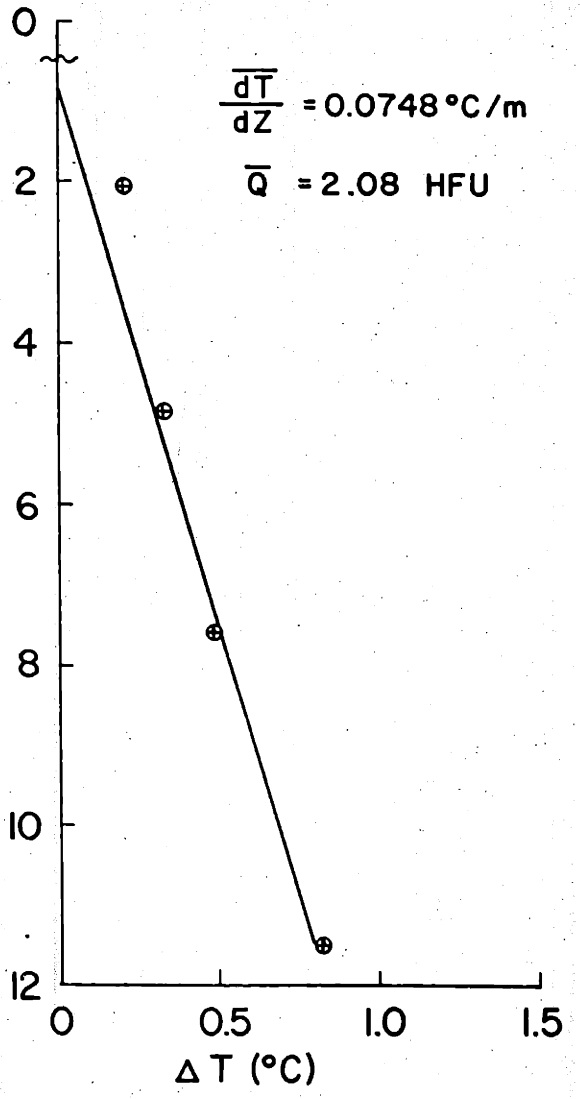

R.V. CONRAD 9

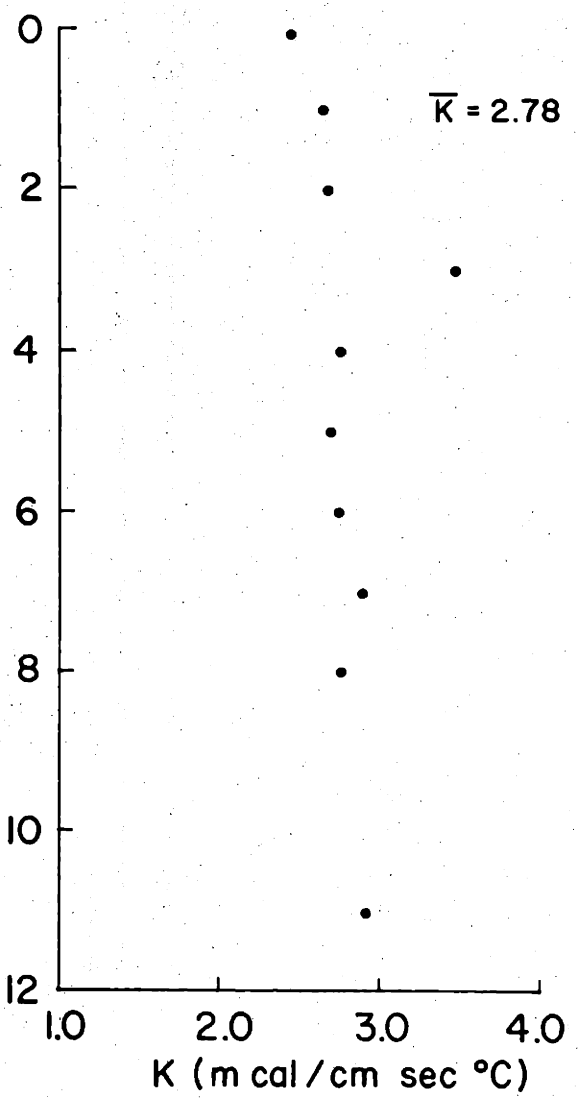

HEAT FLOW STATION 134

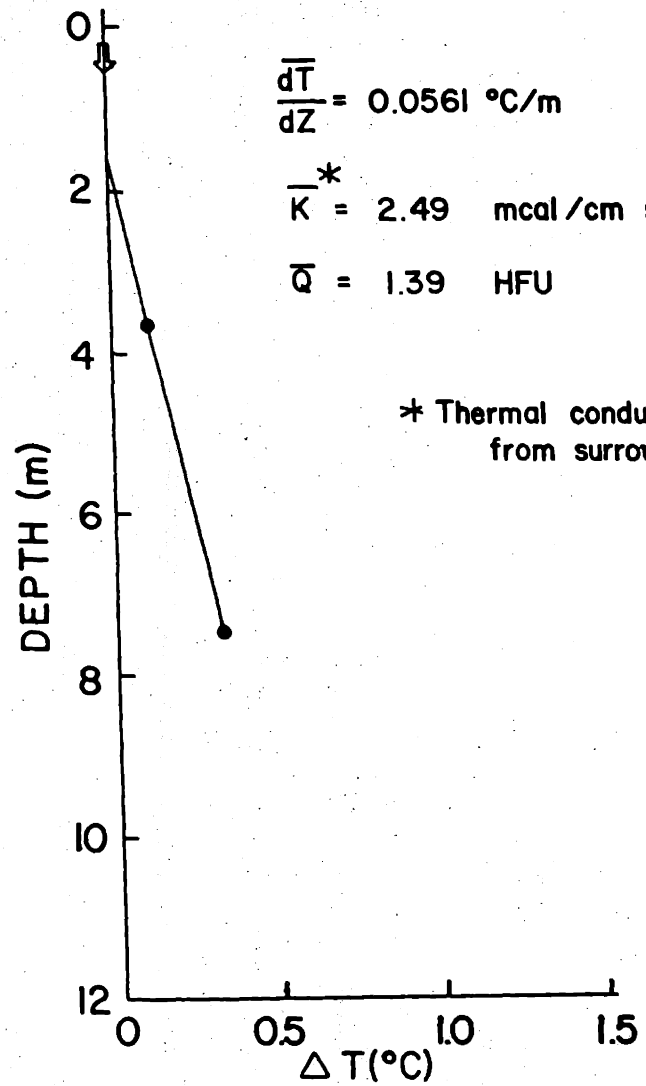

$\frac{\overline{dT}}{dZ}$ = 0.0561 °C/m

$\overline{K}^{*}$ = 2.49 mcal/cm sec °C

$\overline{Q}$ = 1.39 HFU

* Thermal conductivity estimated from surrounding stations

R.V. CONRAD 9 HEAT FLOW STATION 135

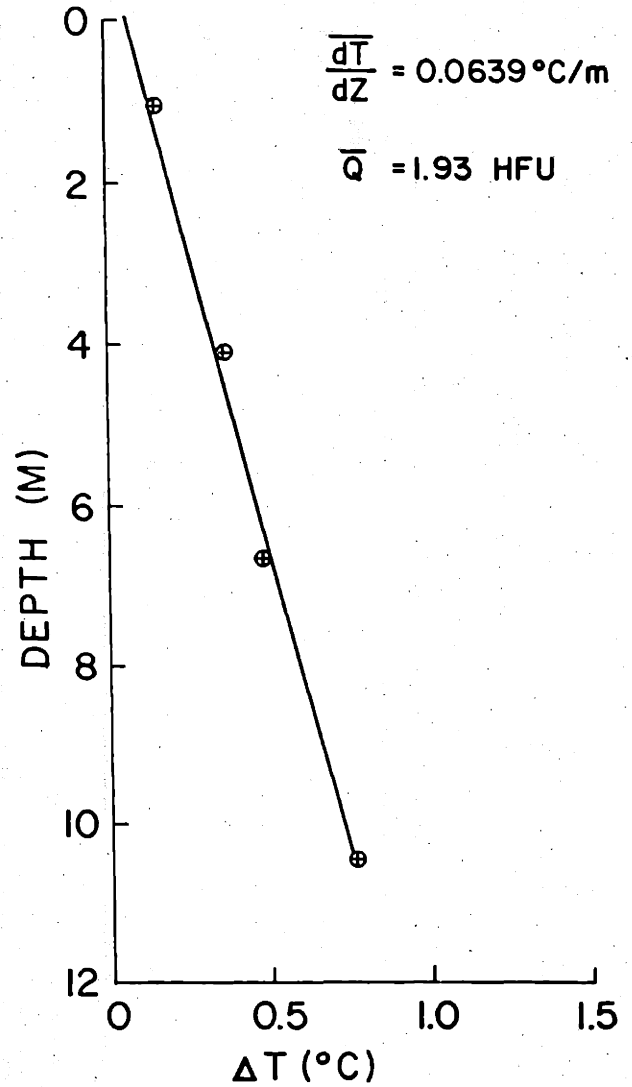

R.V. CONRAD 9

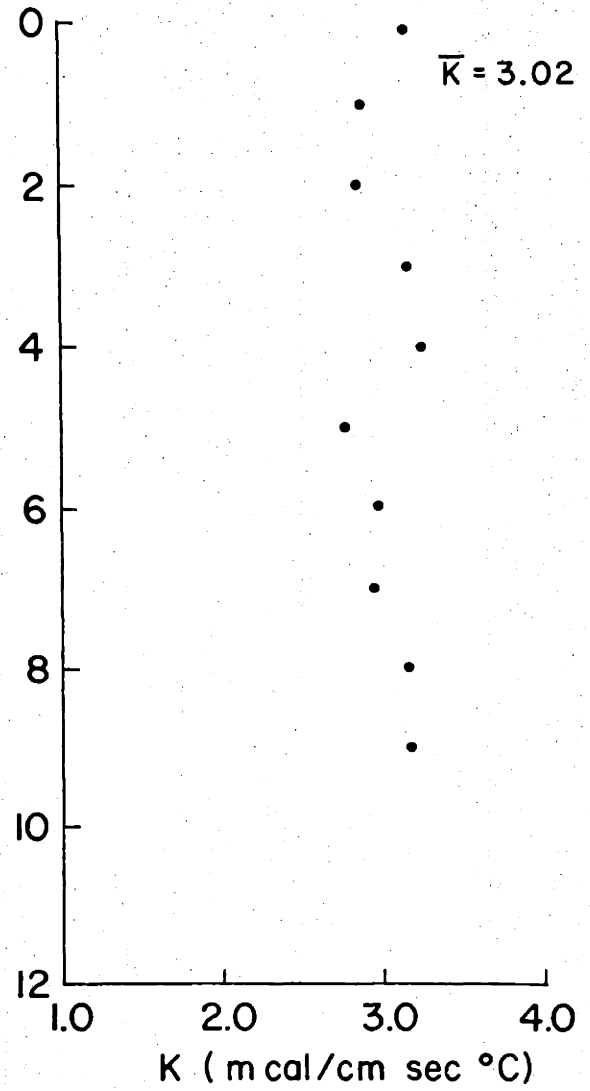

HEAT FLOW STATION 136

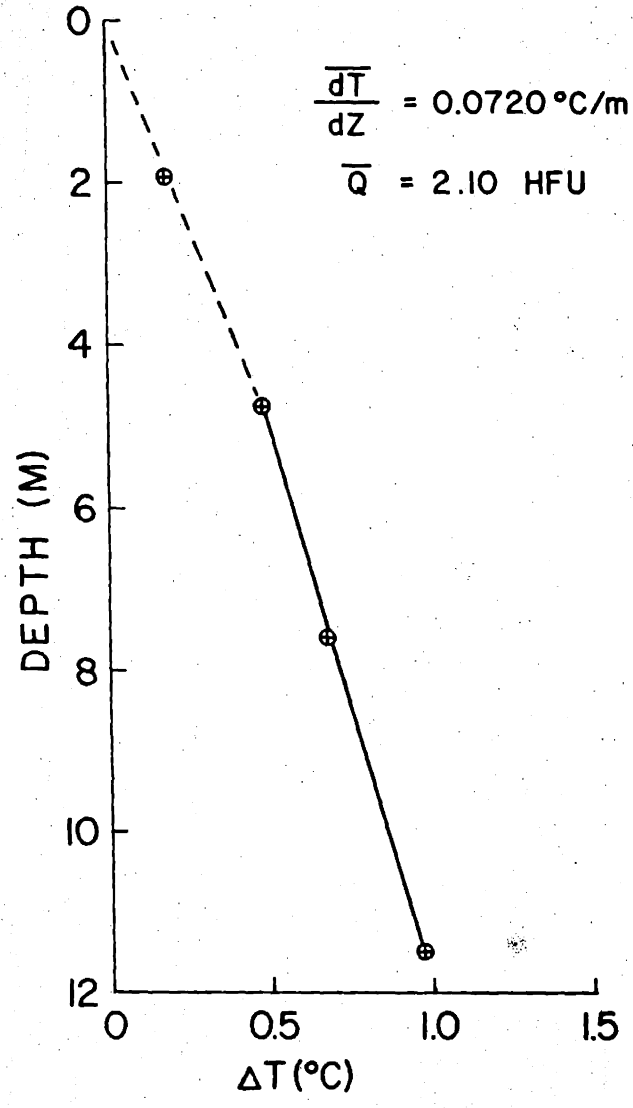

R.V. CONRAD 9

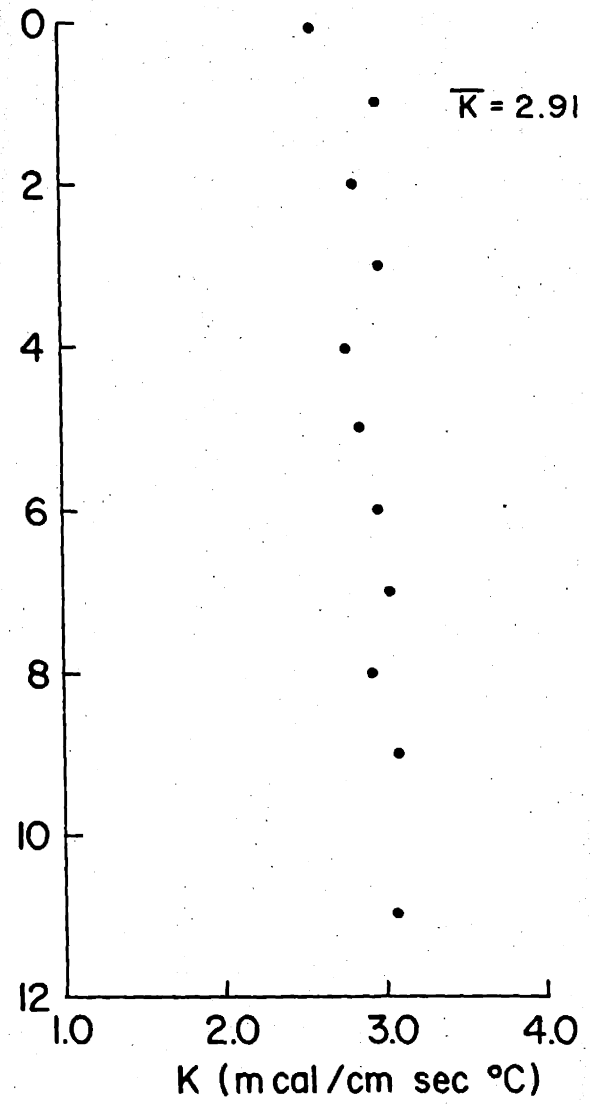

HEAT FLOW STATION 137

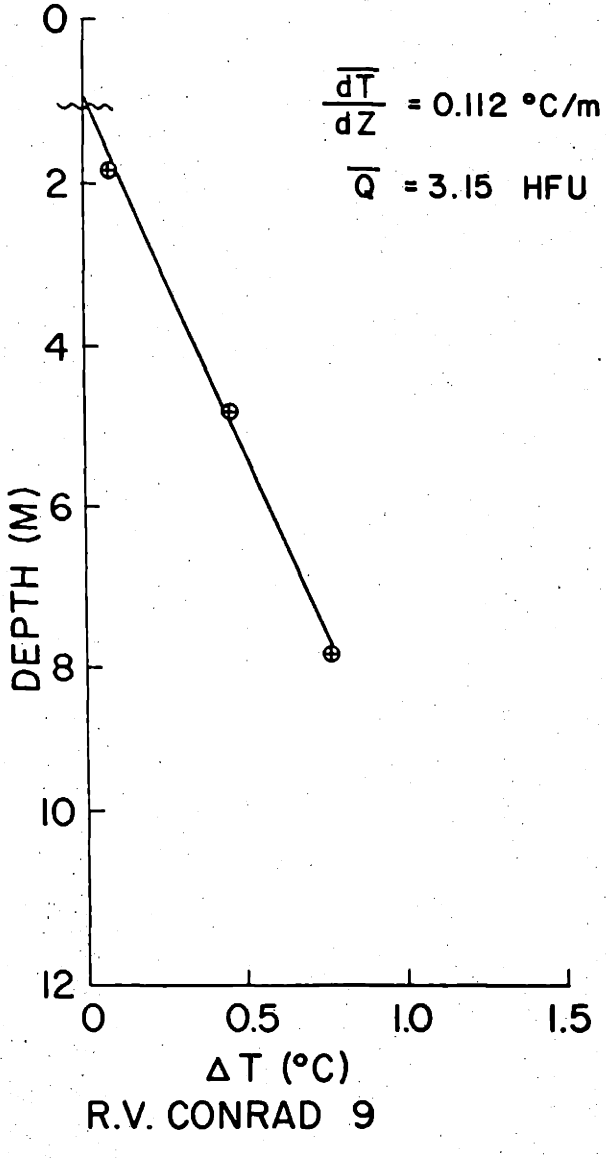

R.V. CONRAD 9

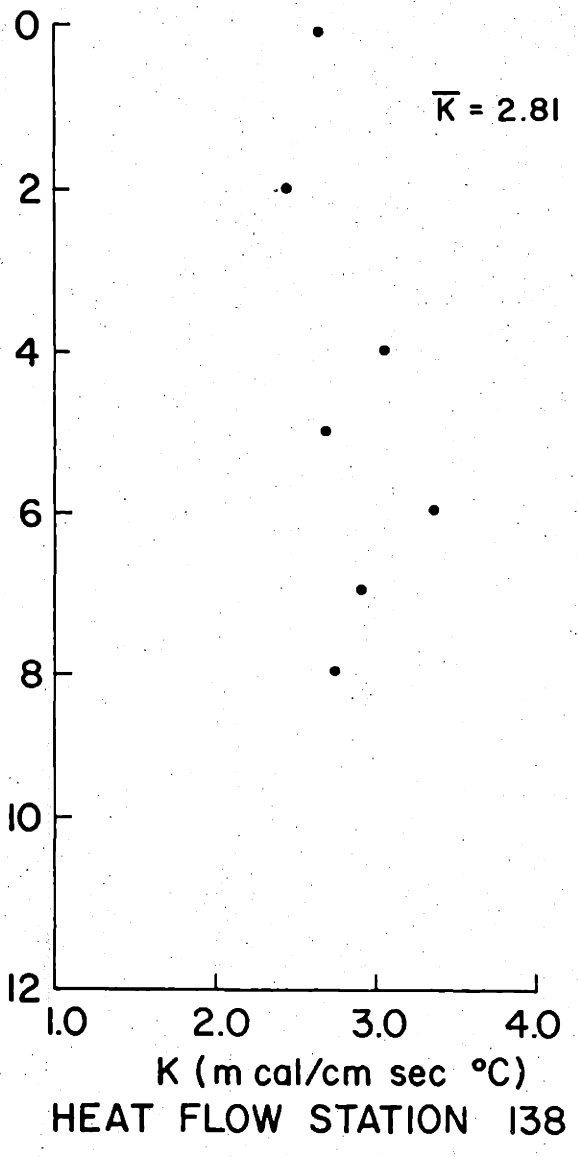

HEAT FLOW STATION 138

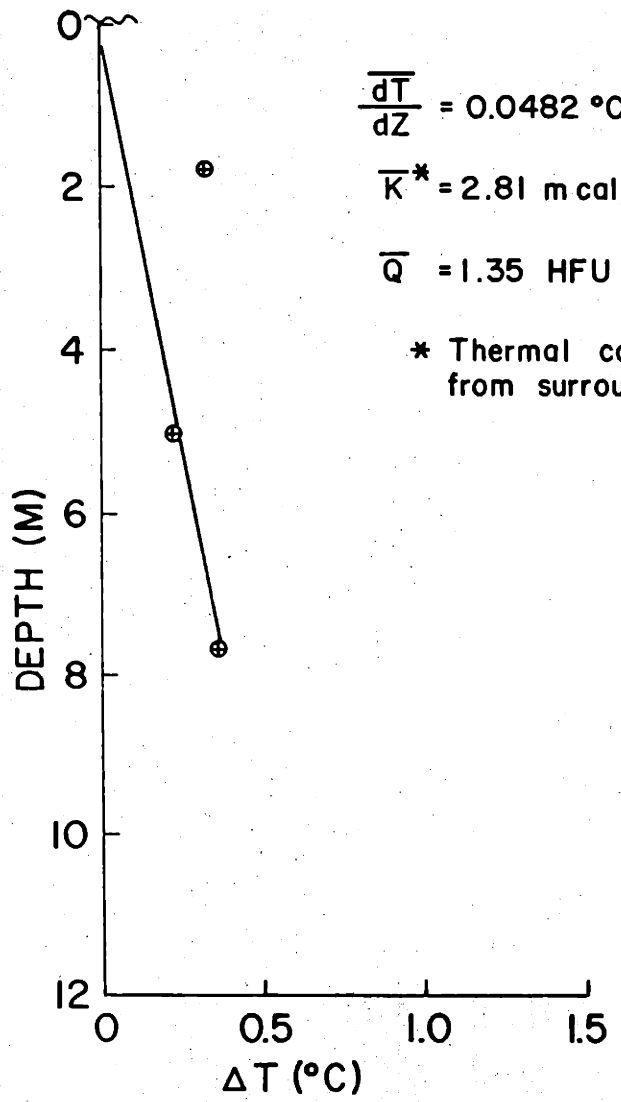

$\overline{\frac{dT}{dZ}}$ = 0.0482 °C/m

$\overline{K}$* = 2.81 m cal/cm sec °C

$\overline{Q}$ = 1.35 HFU

* Thermal conductivity estimated from surrounding stations.

R.V. CONRAD 9 HEAT FLOW STATION 139

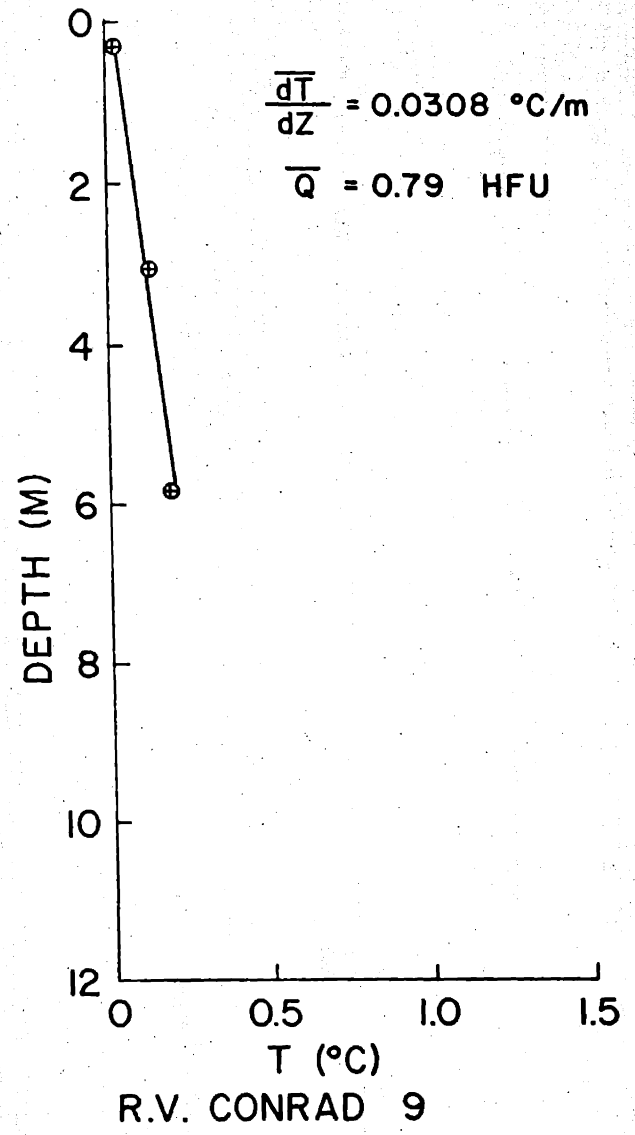

R.V. CONRAD 9

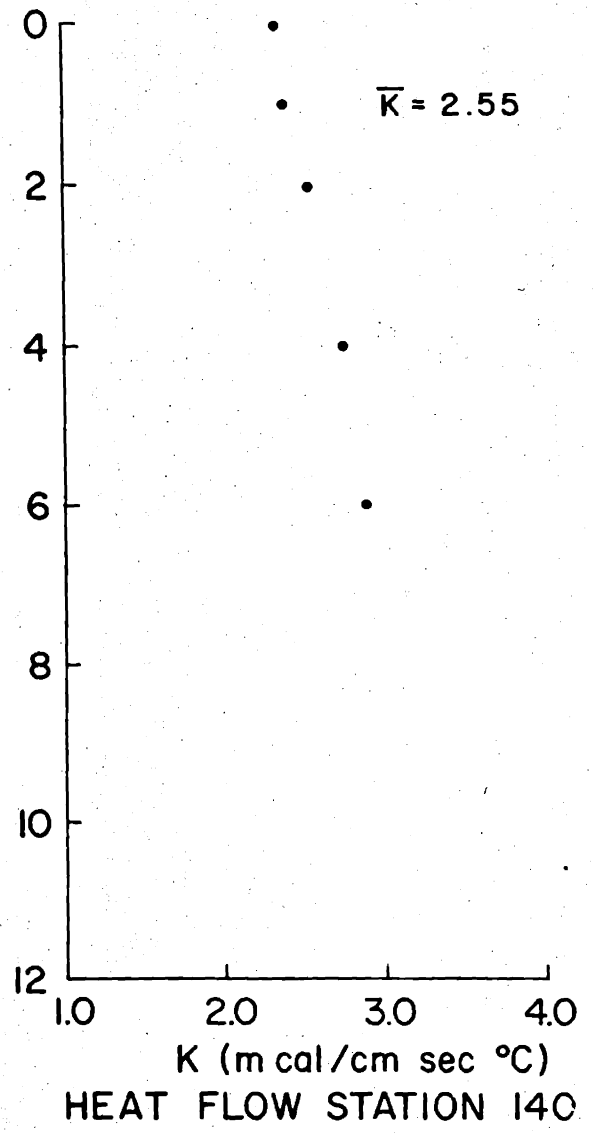

HEAT FLOW STATION 140

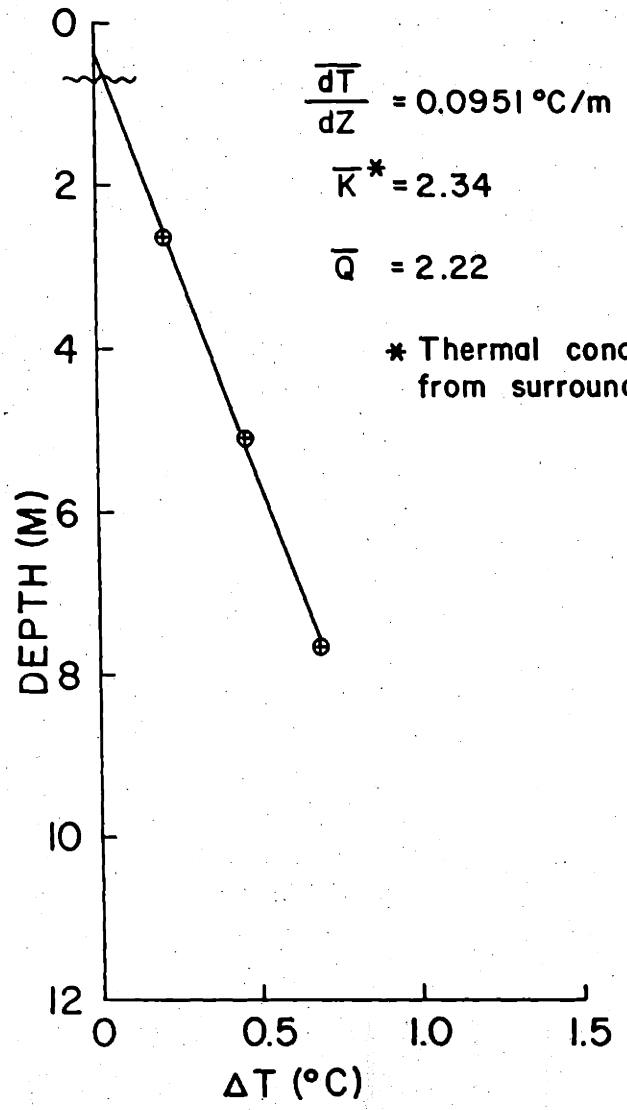

$\frac{\overline{dT}}{dZ}$ = 0.0951 °C/m

$\overline{K}^*$ = 2.34

$\overline{Q}$ = 2.22

* Thermal conductivity estimated from surrounding stations.

R.V. CONRAD 9 HEAT FLOW STATION 141

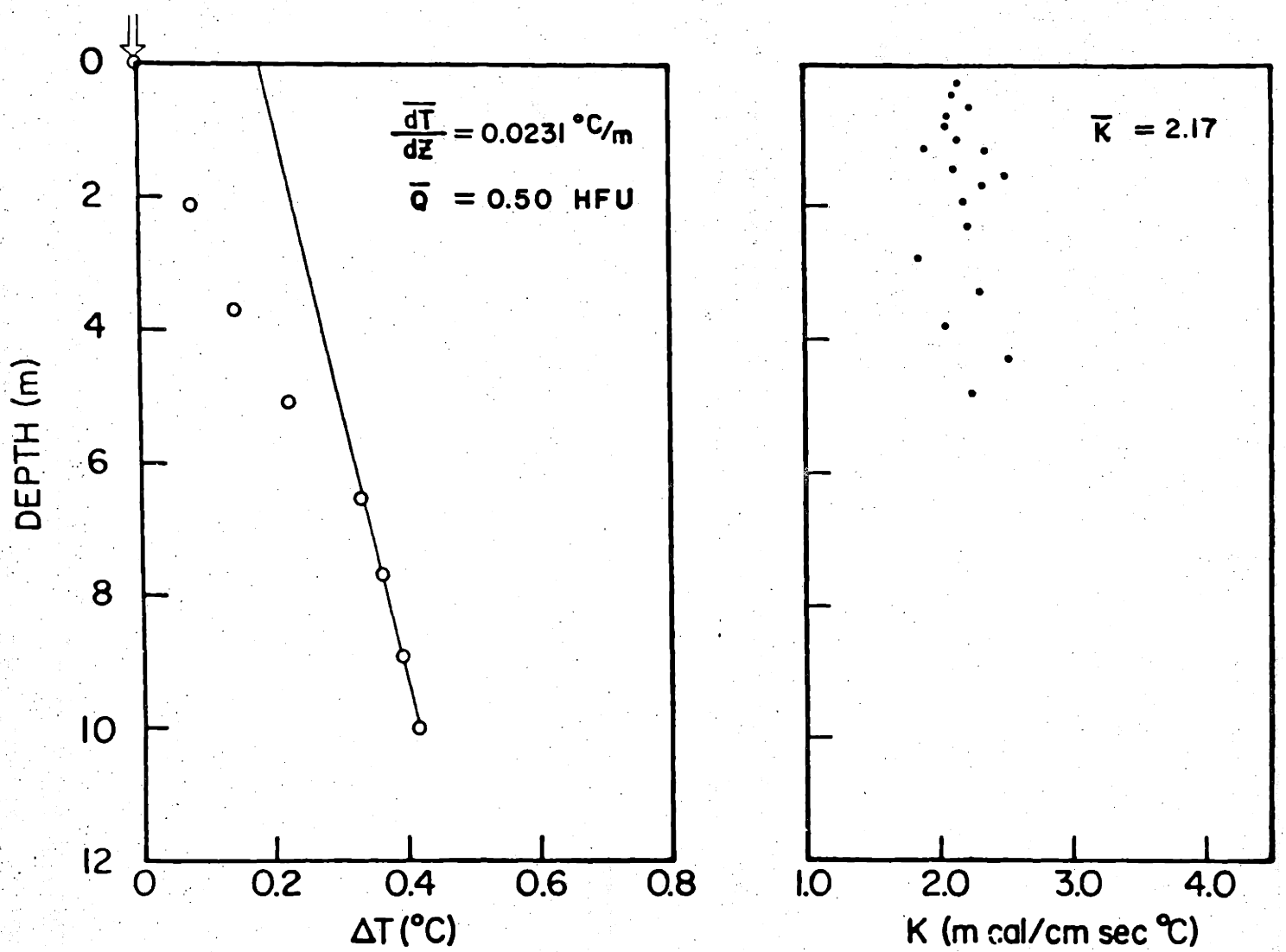

ATLANTIS II-49 HEAT FLOW STATION 1431 P

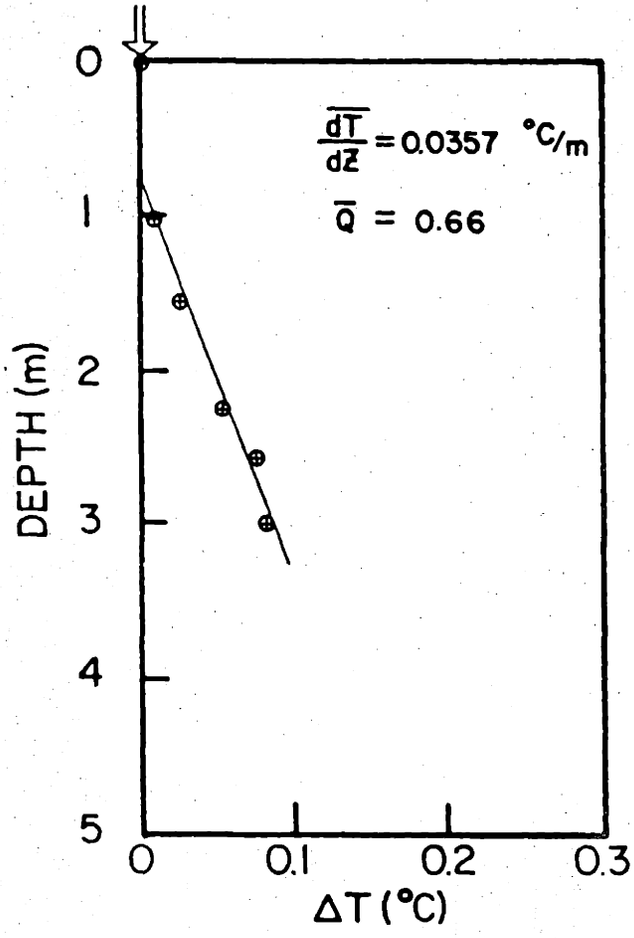

ATLANTIS II-49

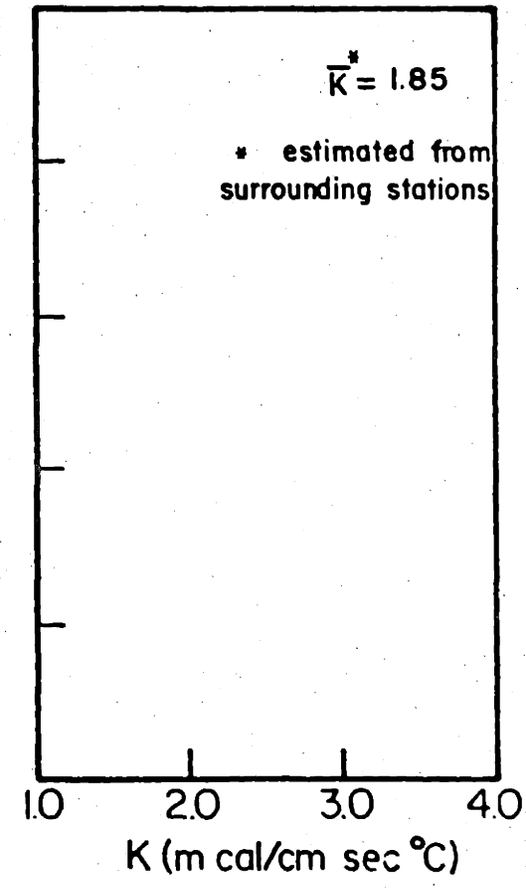

HEAT FLOW STATION 1432 G

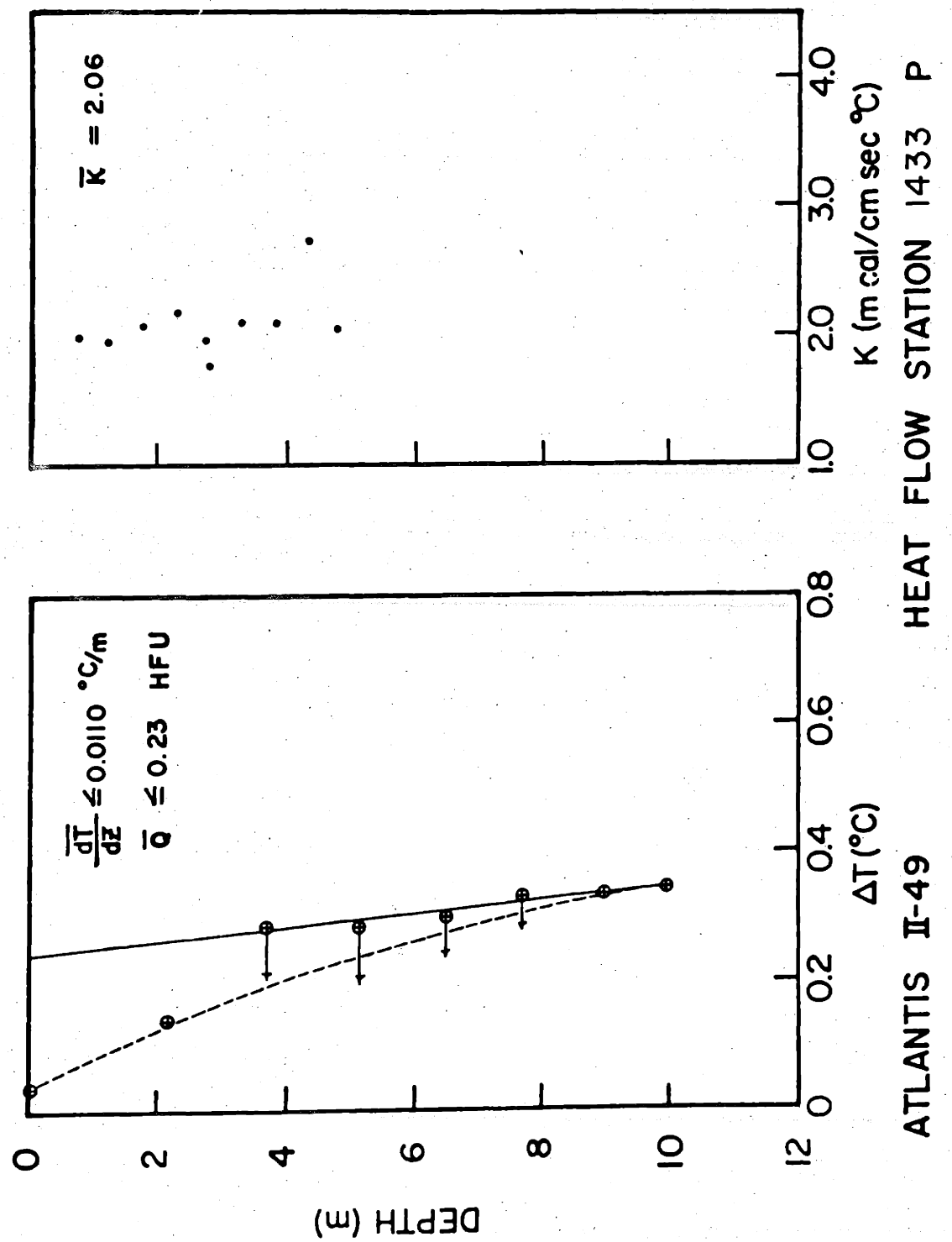

ATLANTIS II-49 HEAT FLOW STATION 1433 P

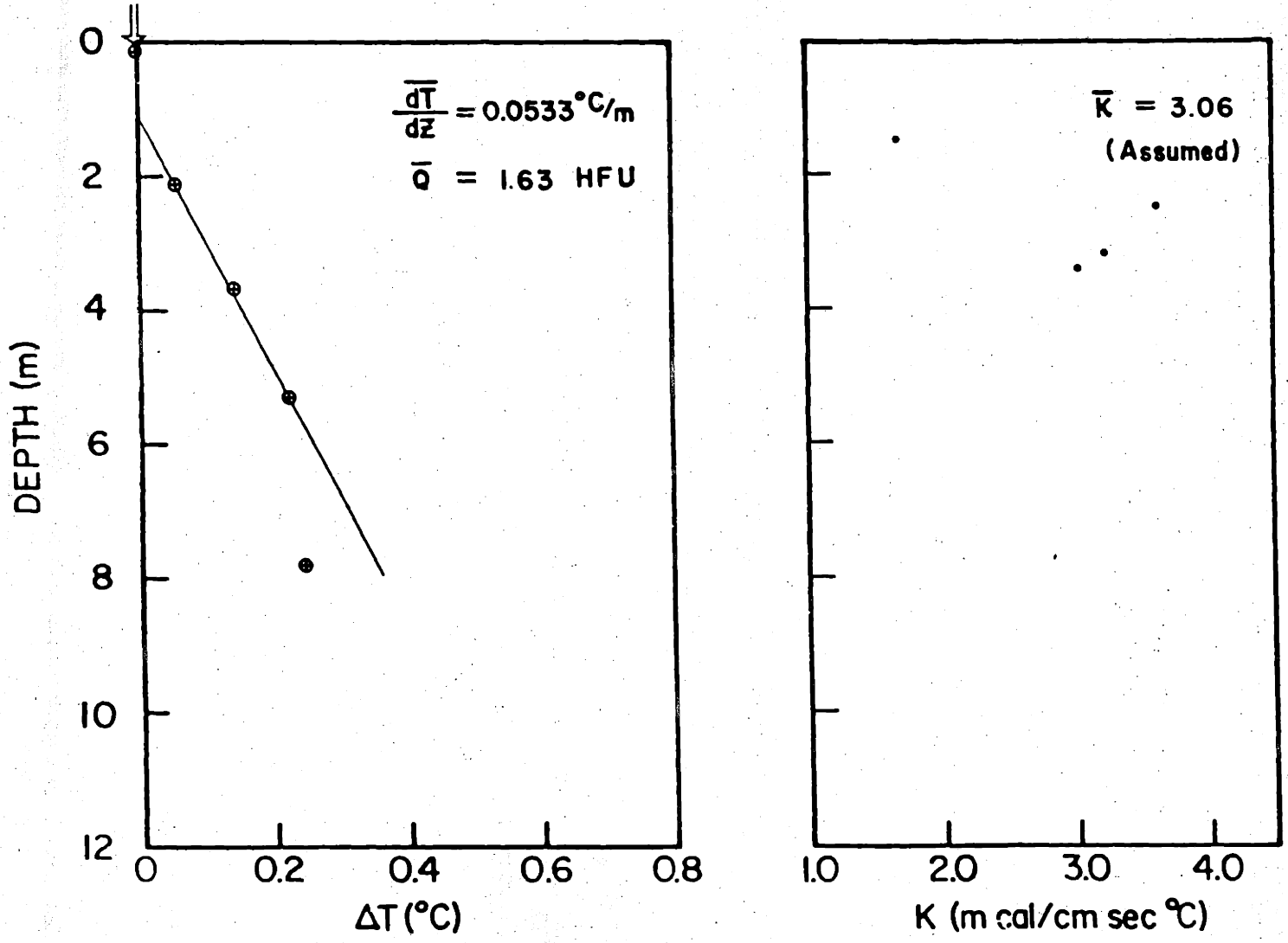

ATLANTIS II-49 HEAT FLOW STATION 1442 P

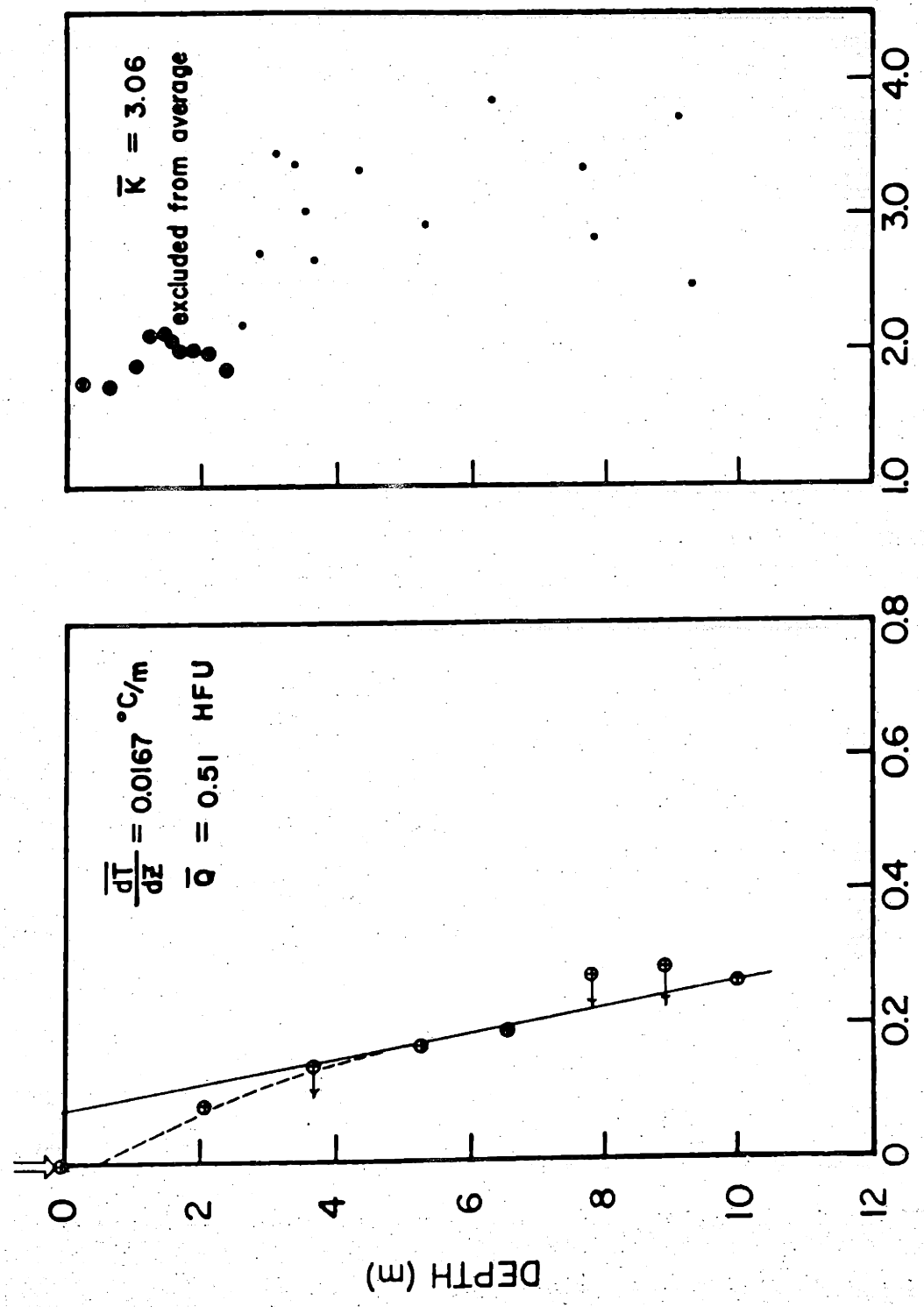

ATLANTIS II-49 HEAT FLOW STATION 1443 P

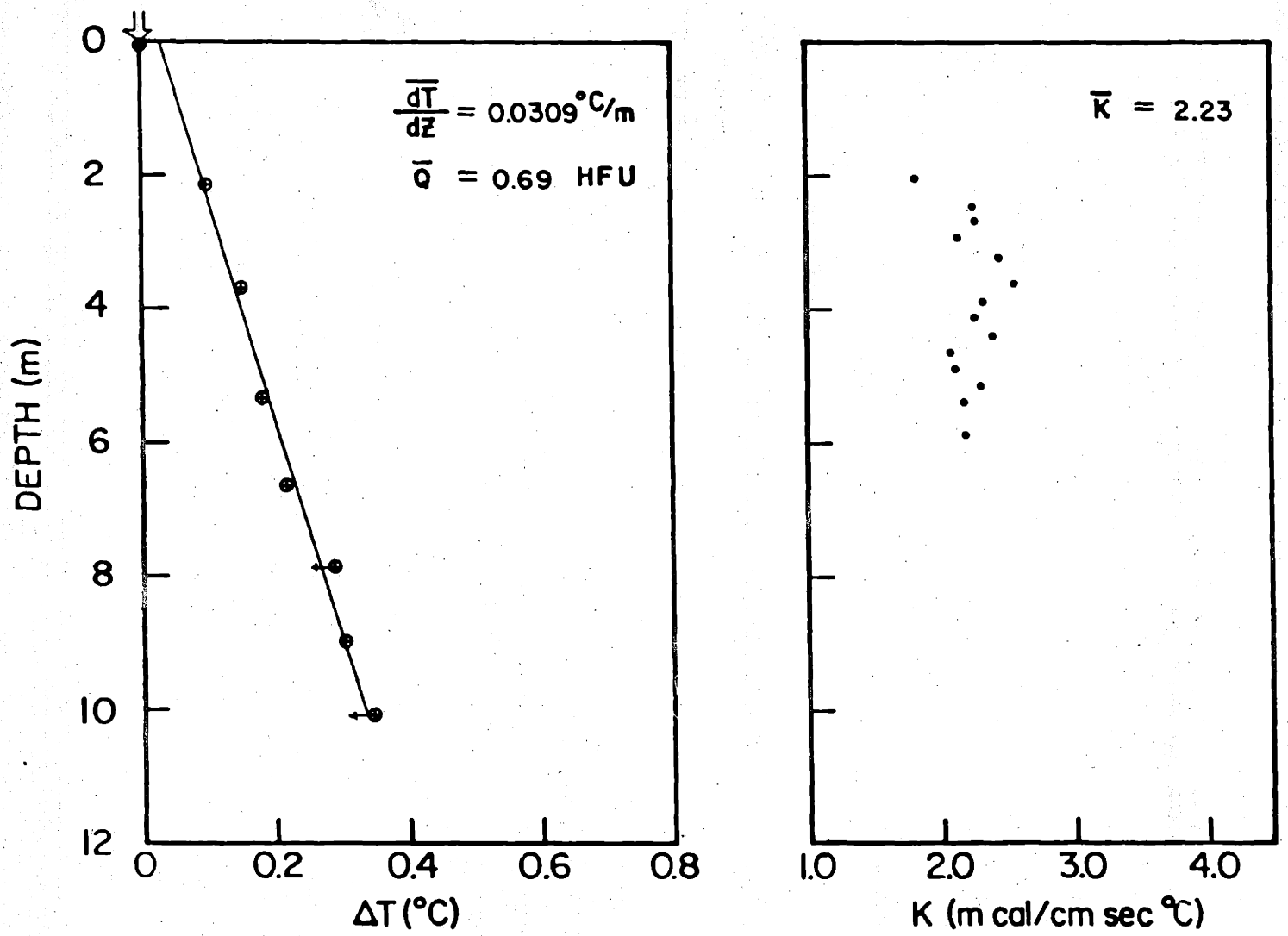

ATLANTIS II-49 HEAT FLOW STATION 1444 P

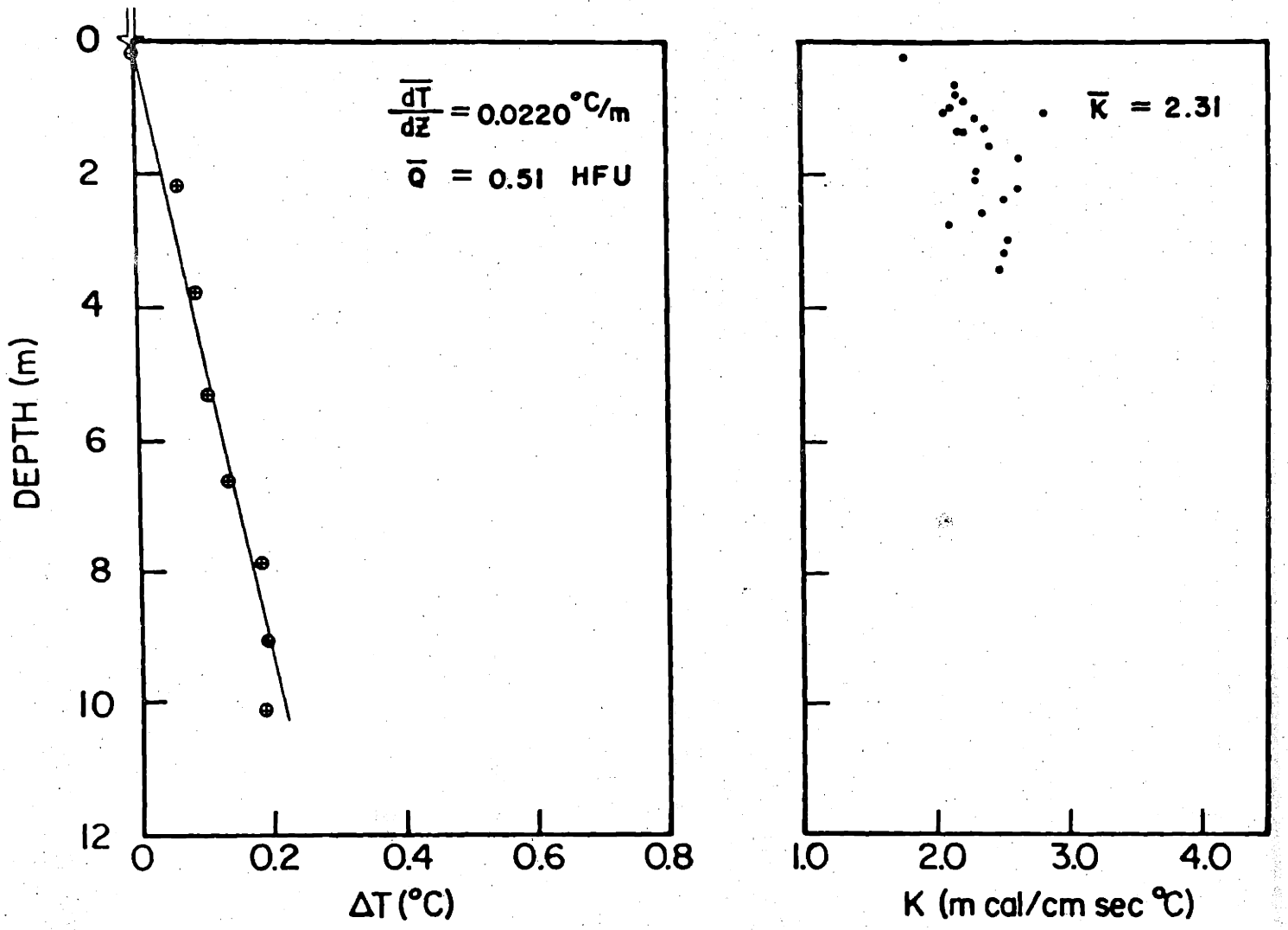

ATLANTIS II-49 HEAT FLOW STATION 1445 P

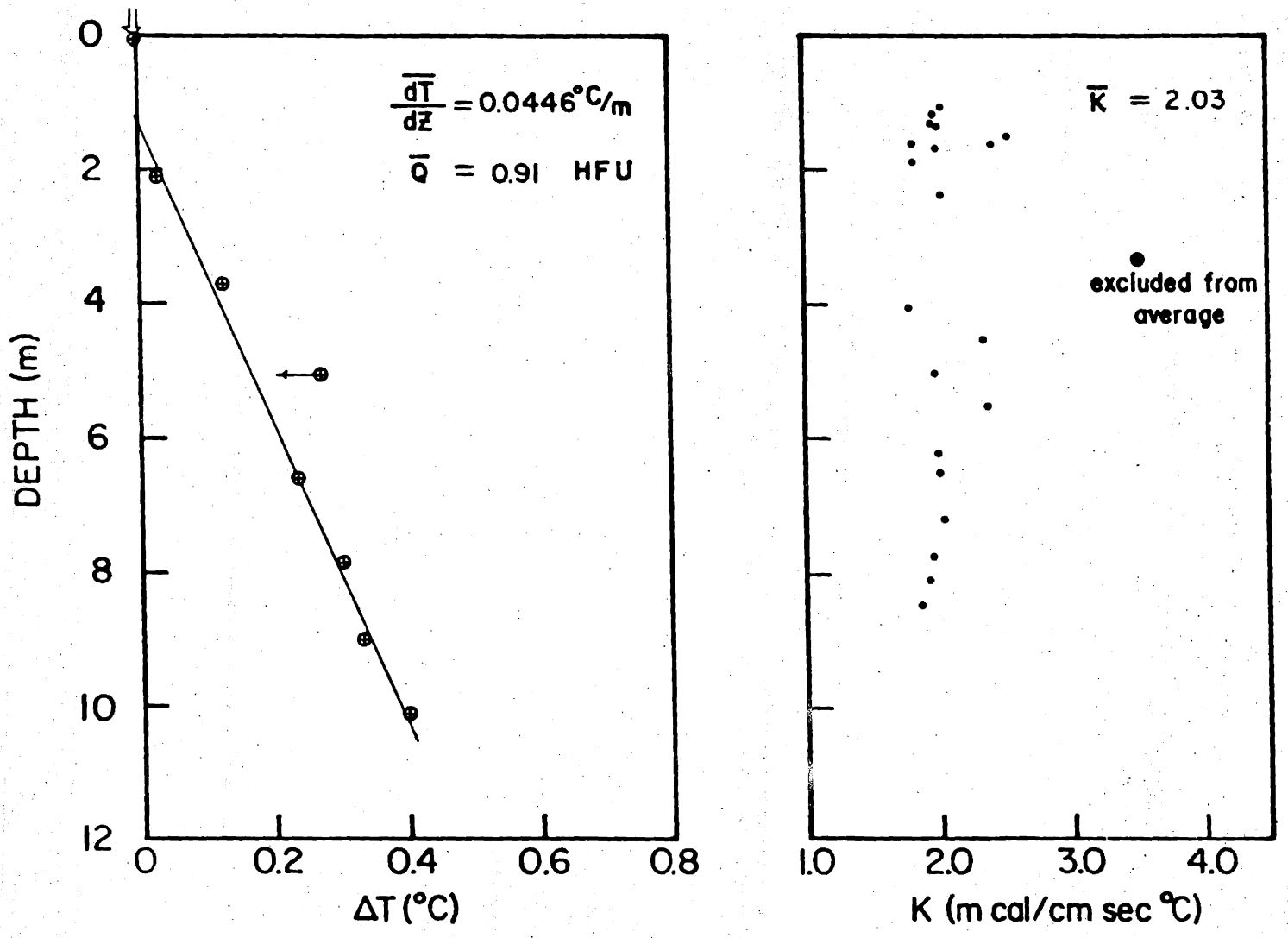

ATLANTIS II-49 HEAT FLOW STATION 1446 P

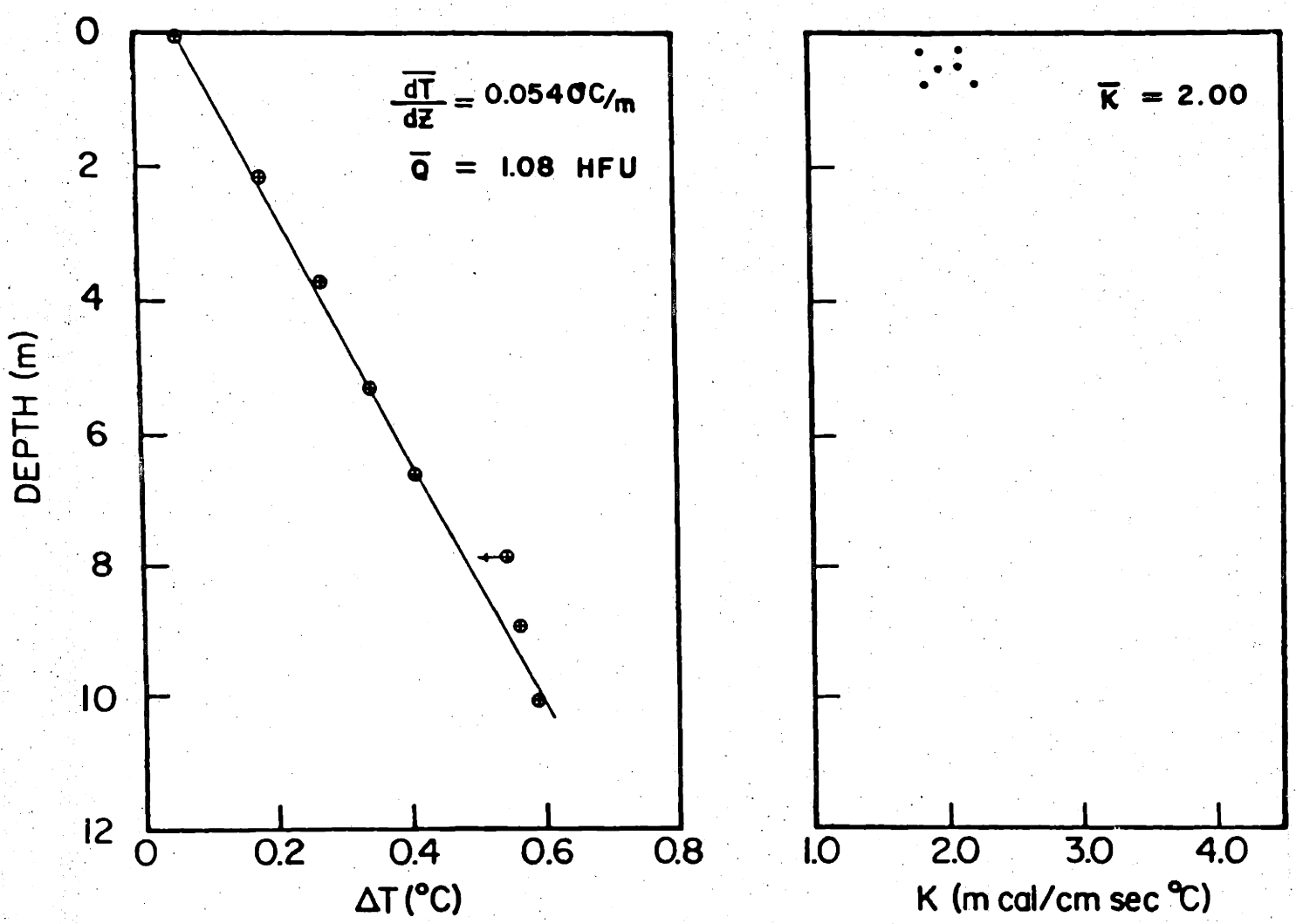

ATLANTIS II-49 HEAT FLOW STATION 1447 P

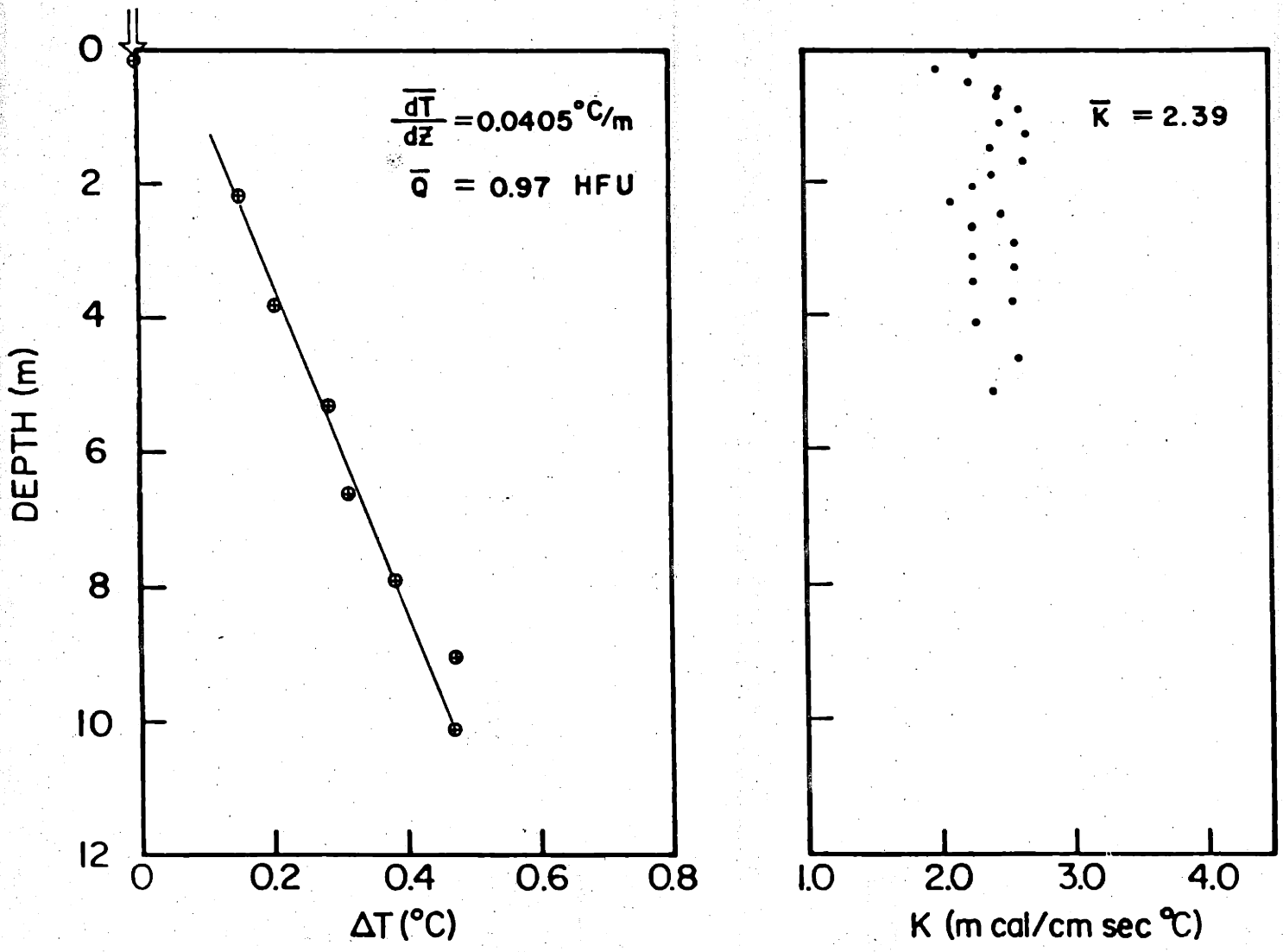

ATLANTIS II-49 HEAT FLOW STATION 1452 P

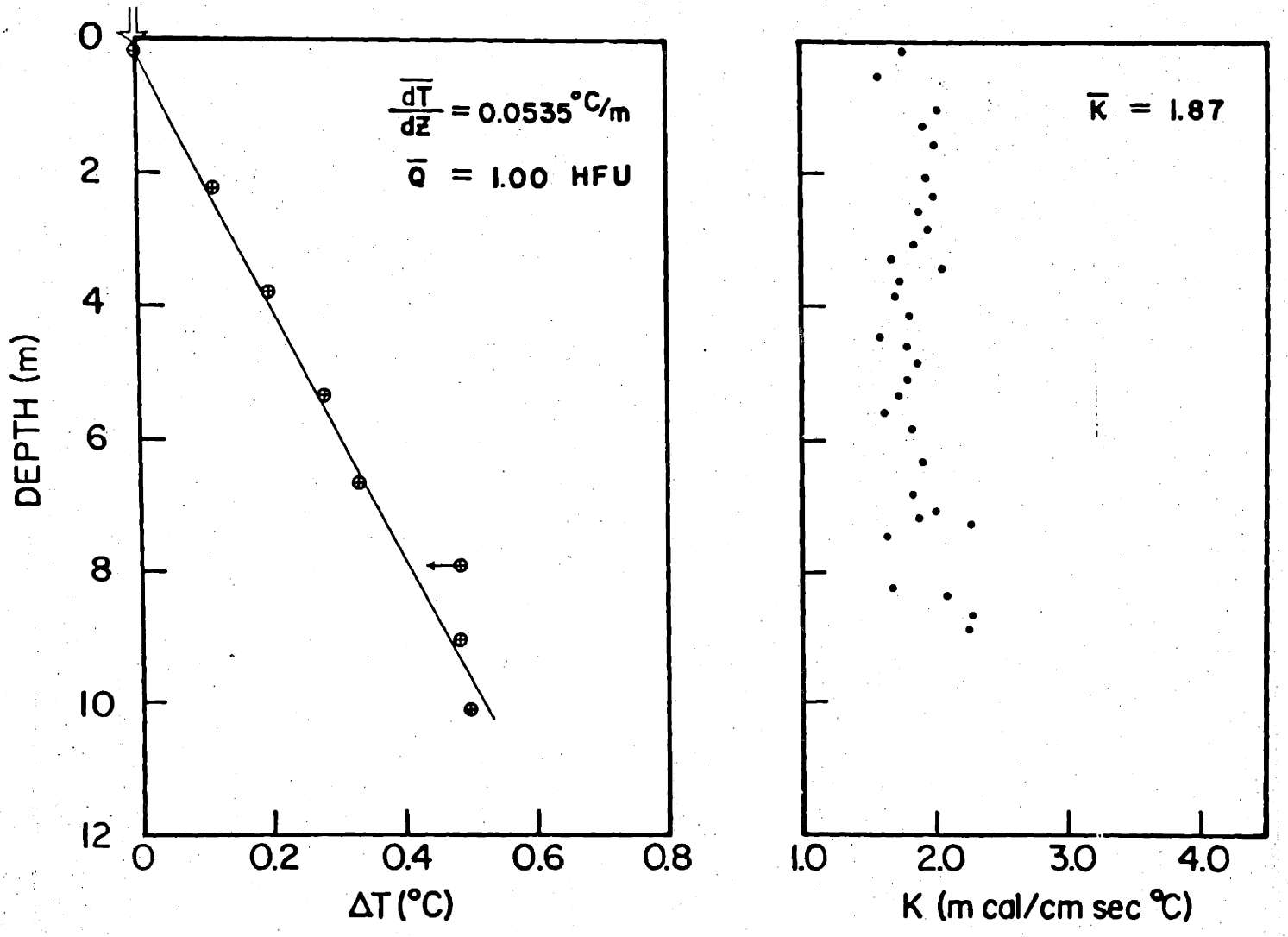

ATLANTIS II-49 HEAT FLOW STATION 1460 P

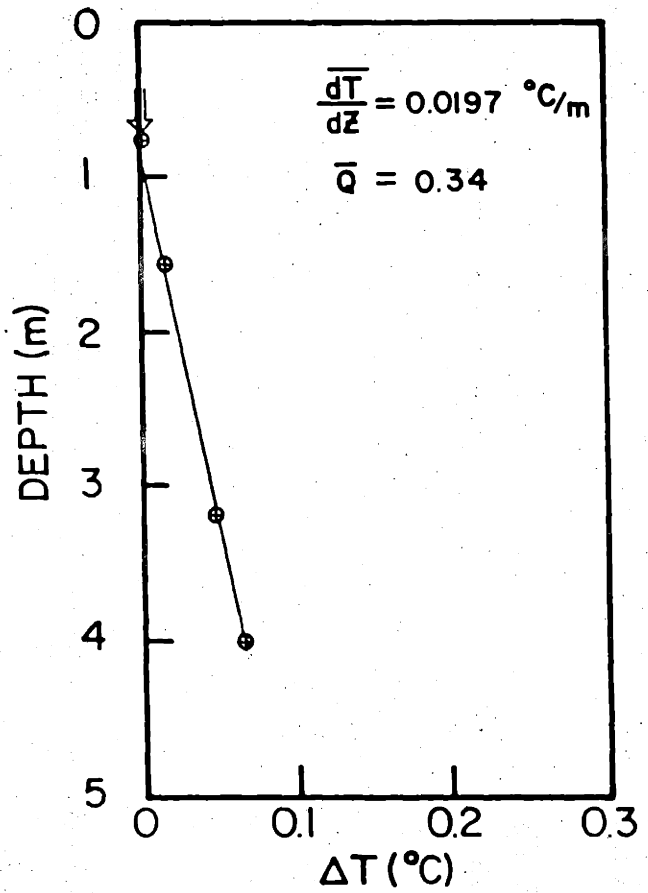

ATLANTIS II-49

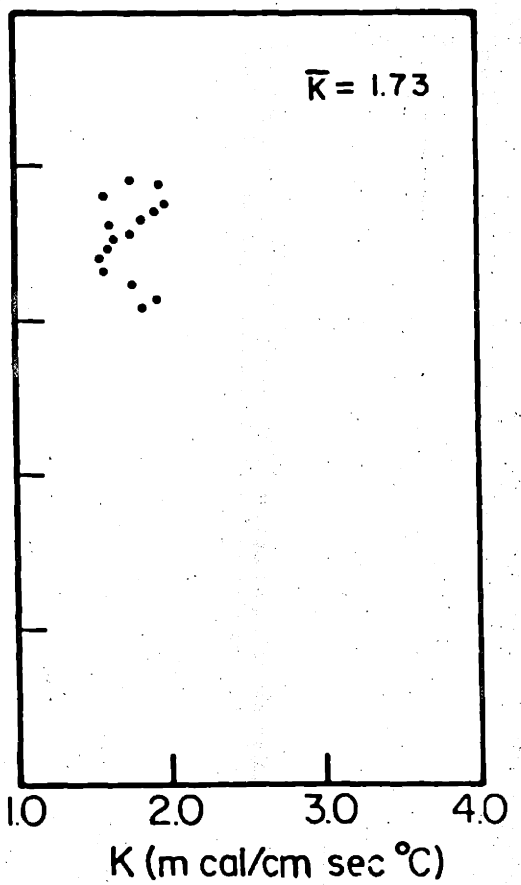

HEAT FLOW STATION 1462 G

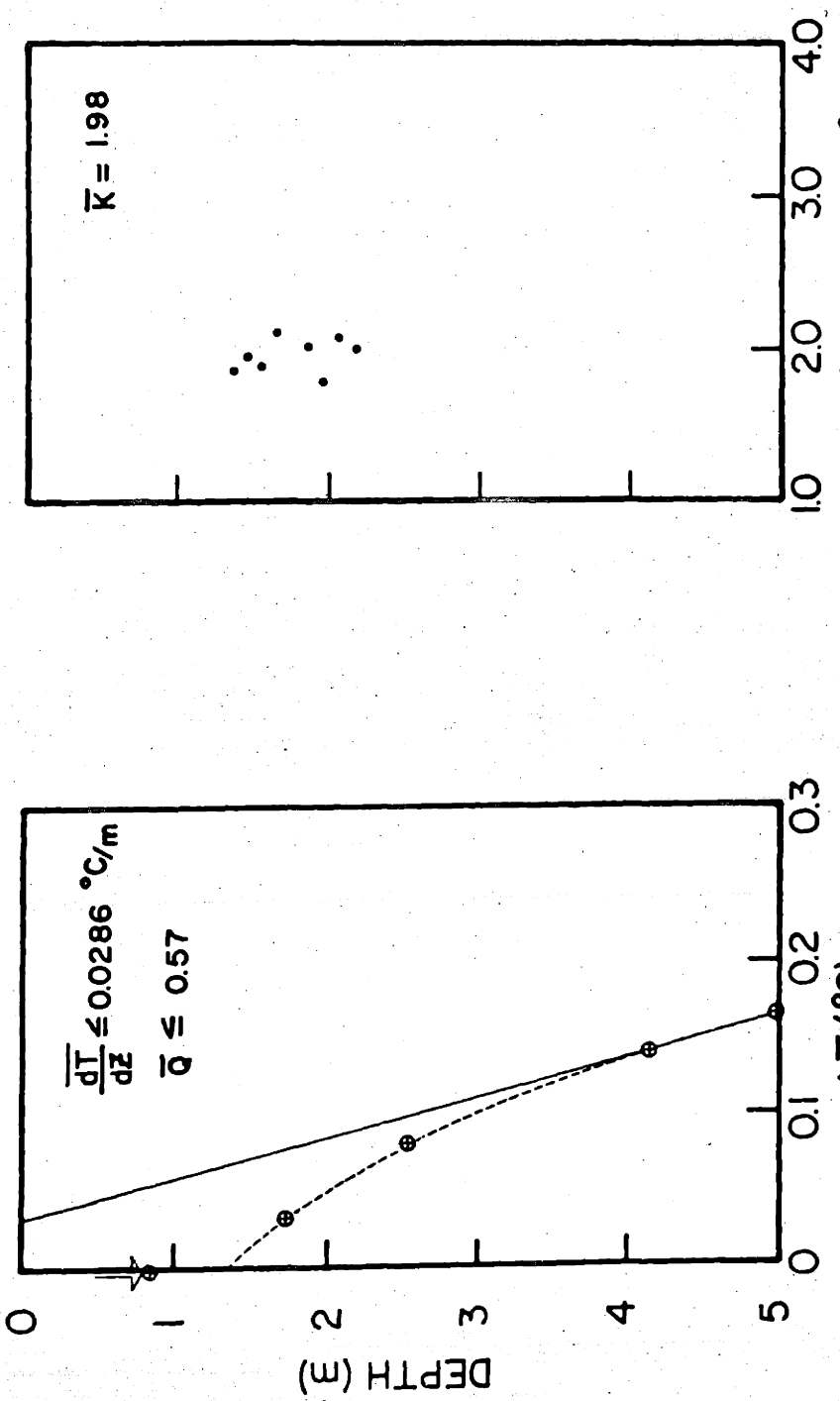

HEAT FLOW STATION 1464 G

ATLANTIS II-49

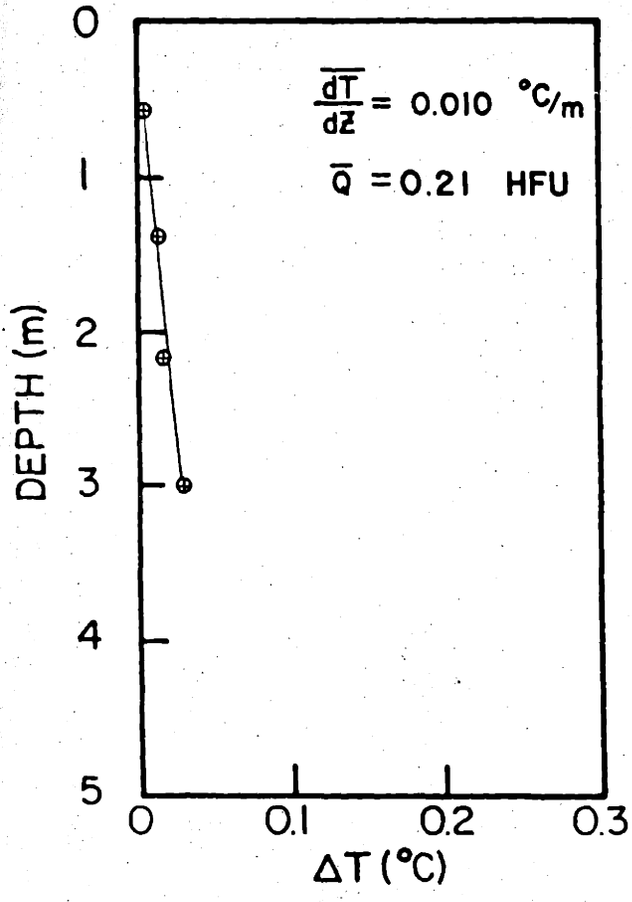

ATLANTIS II-49

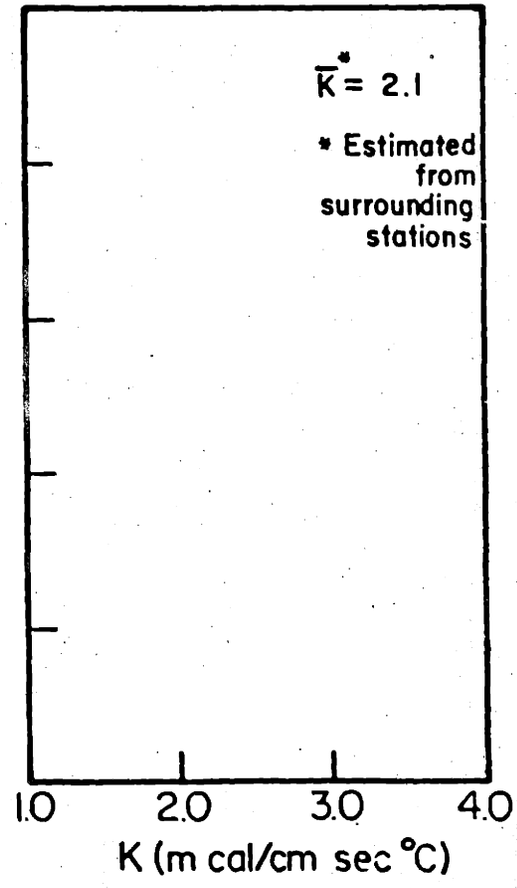

HEAT FLOW STATION 1468 G

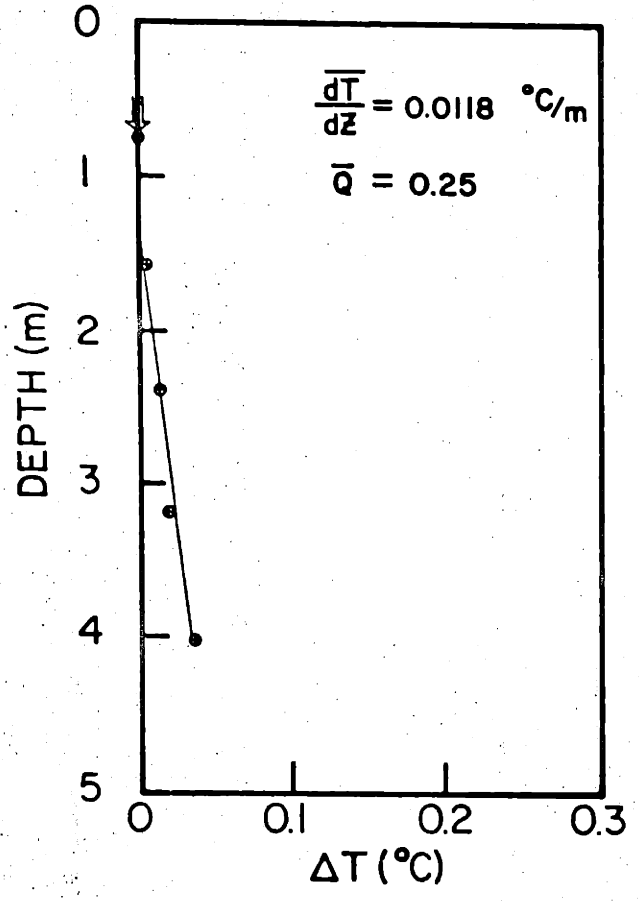

ATLANTIS II-49

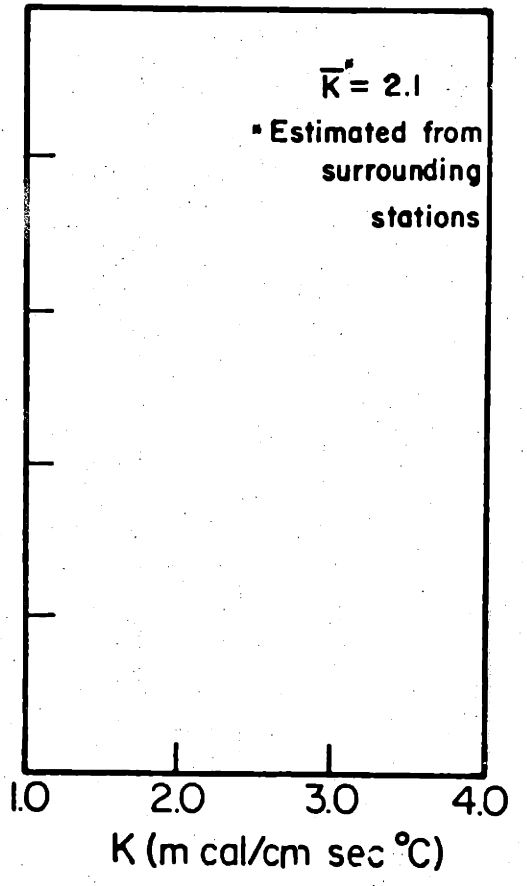

HEAT FLOW STATION 1469 G

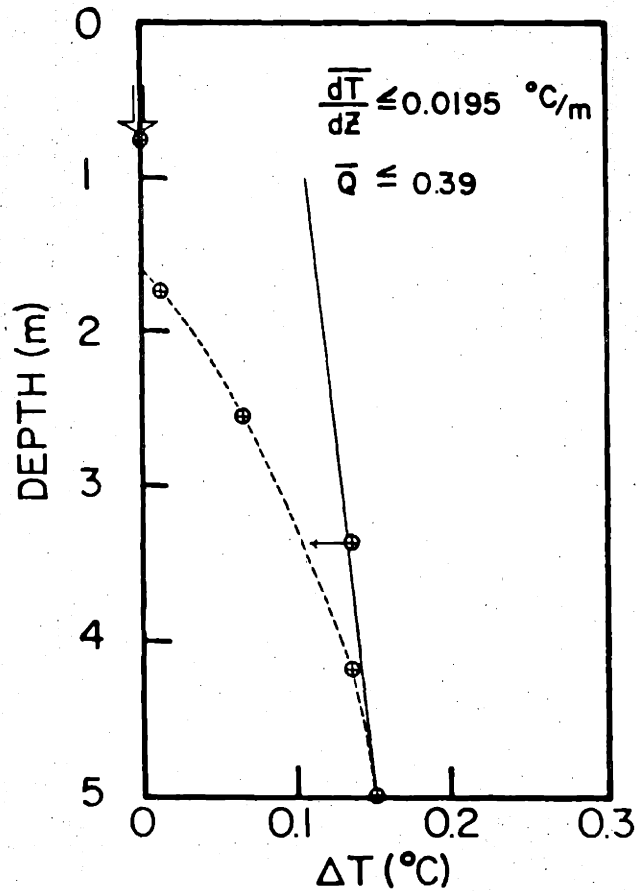

ATLANTIS II-49

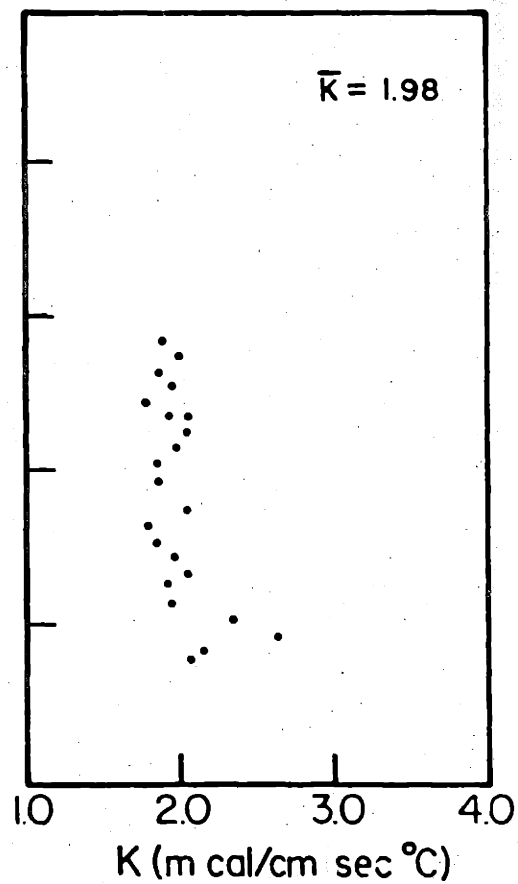

HEAT FLOW STATION 1470 G

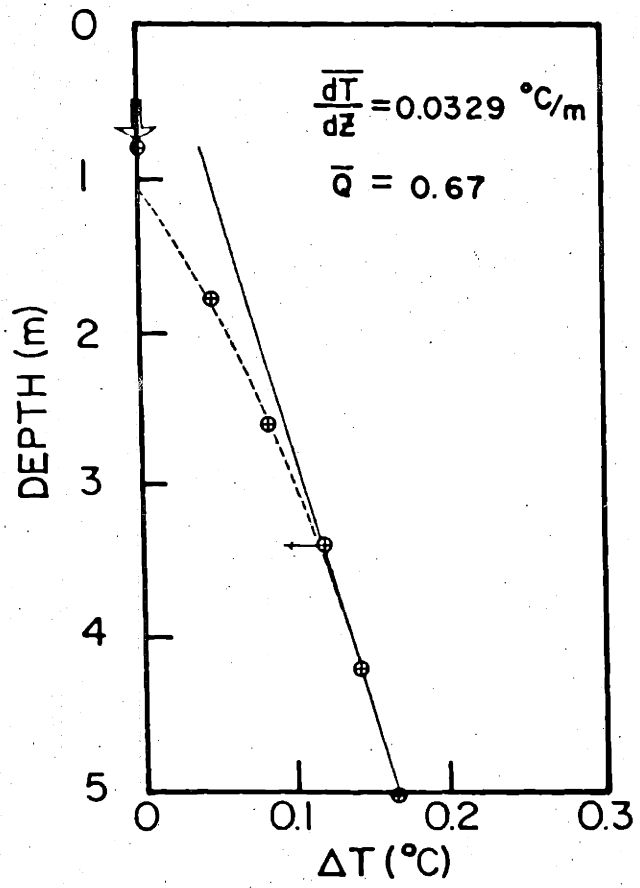

ATLANTIS II-49

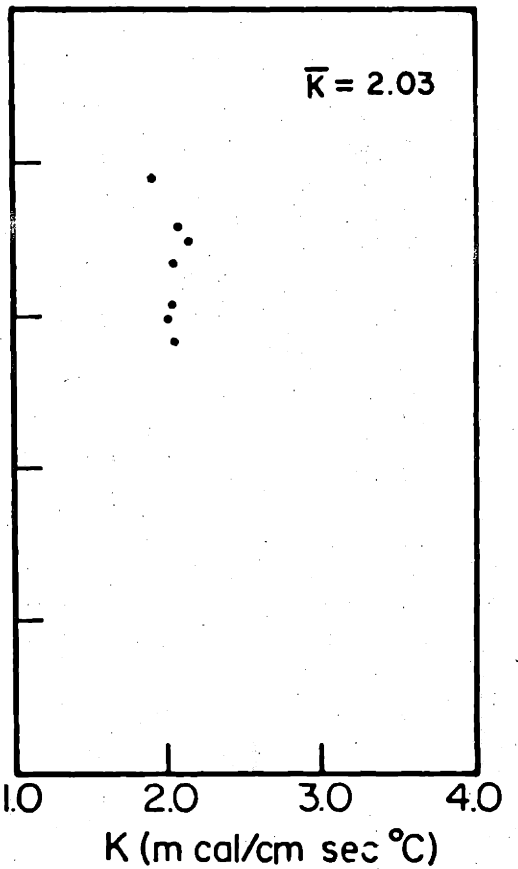

HEAT FLOW STATION 1472 G

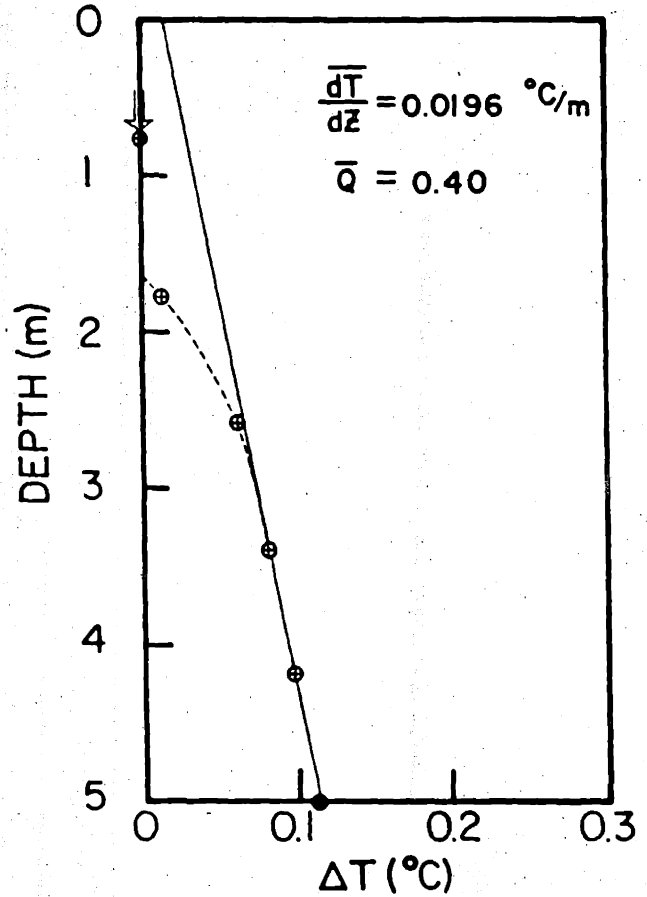

ATLANTIS II-49

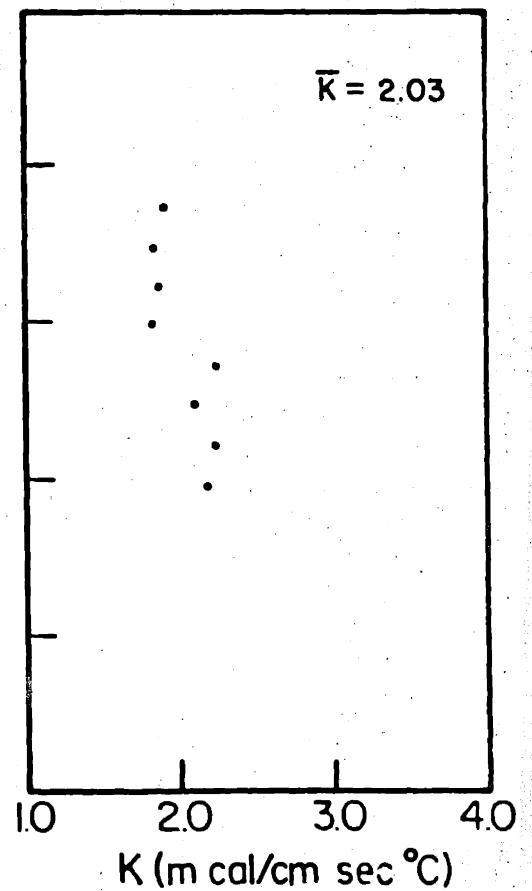

HEAT FLOW STATION 1473 G

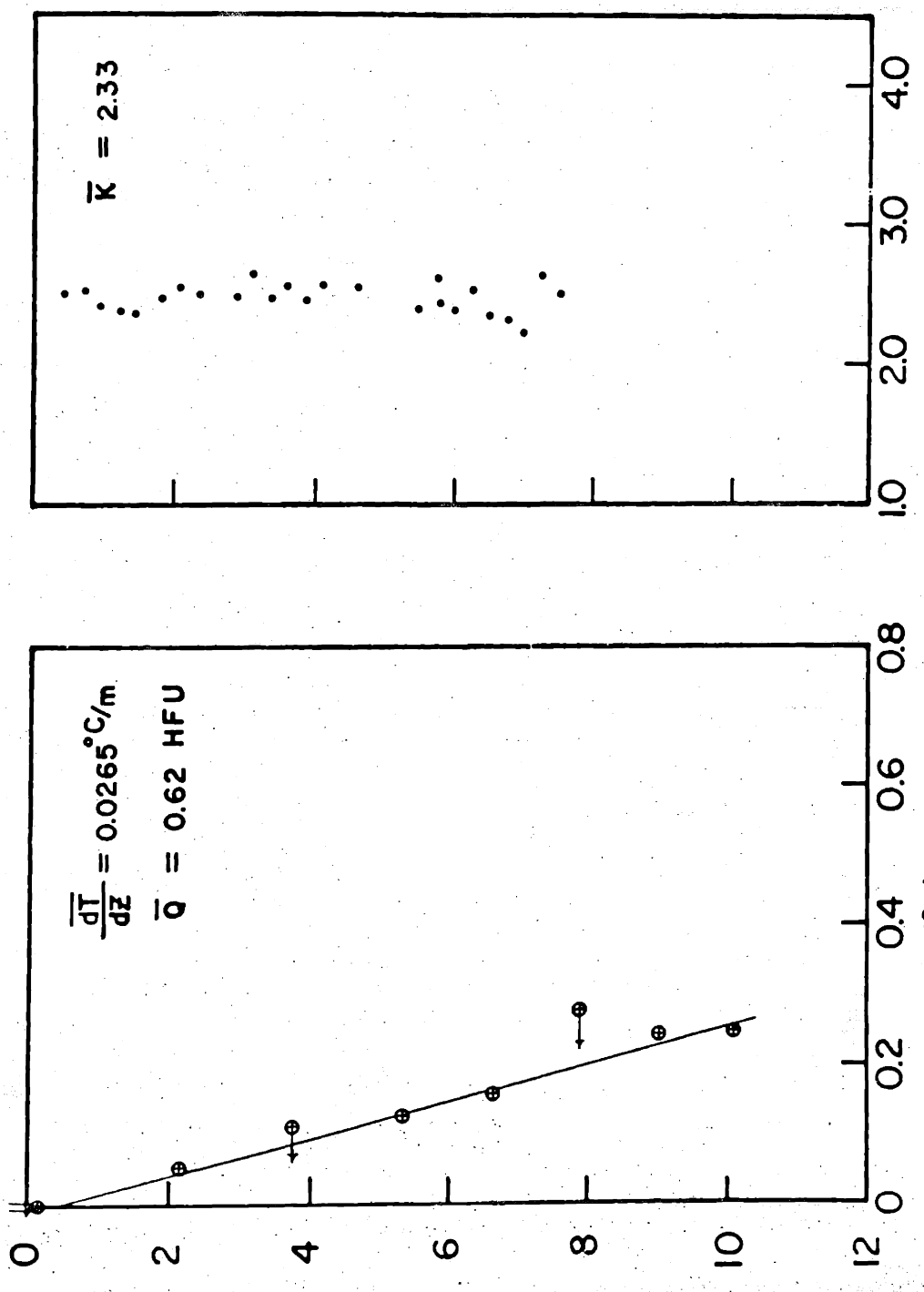

ATLANTIS II-49 HEAT FLOW STATION 1473 P

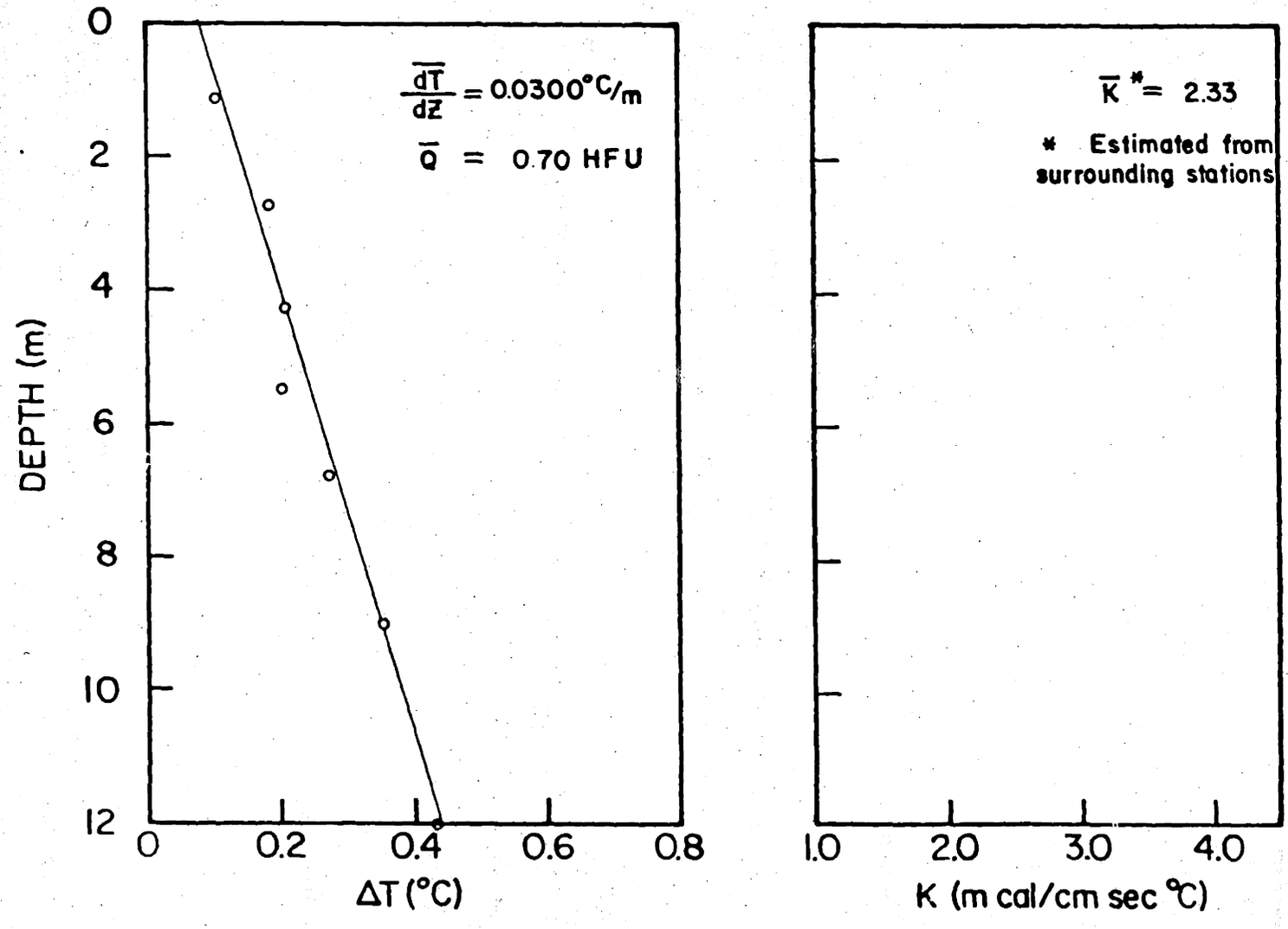

ATLANTIS II-49 HEAT FLOW STATION 1474 P

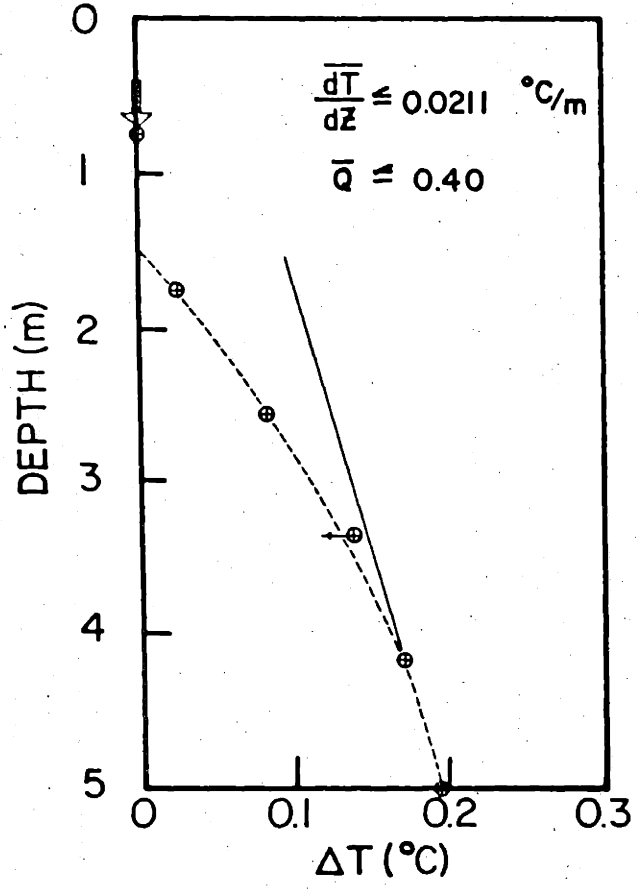

ATLANTIS II-49

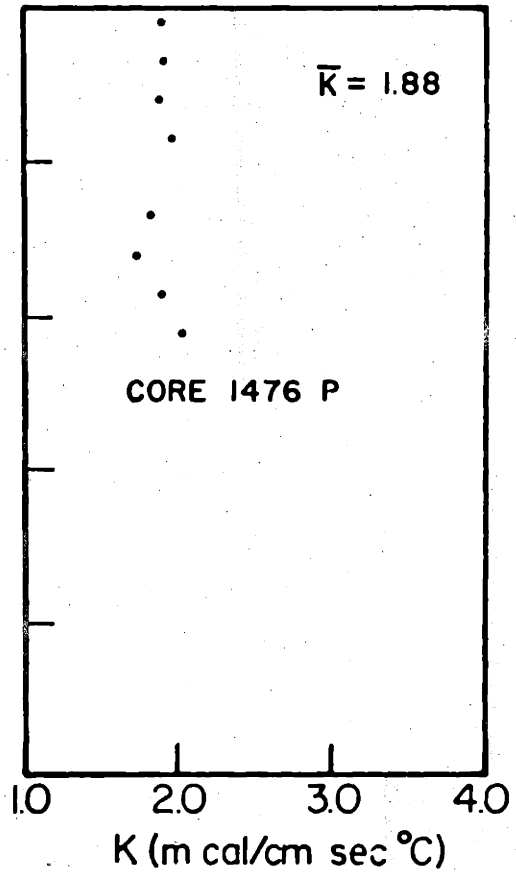

HEAT FLOW STATION 1476 G

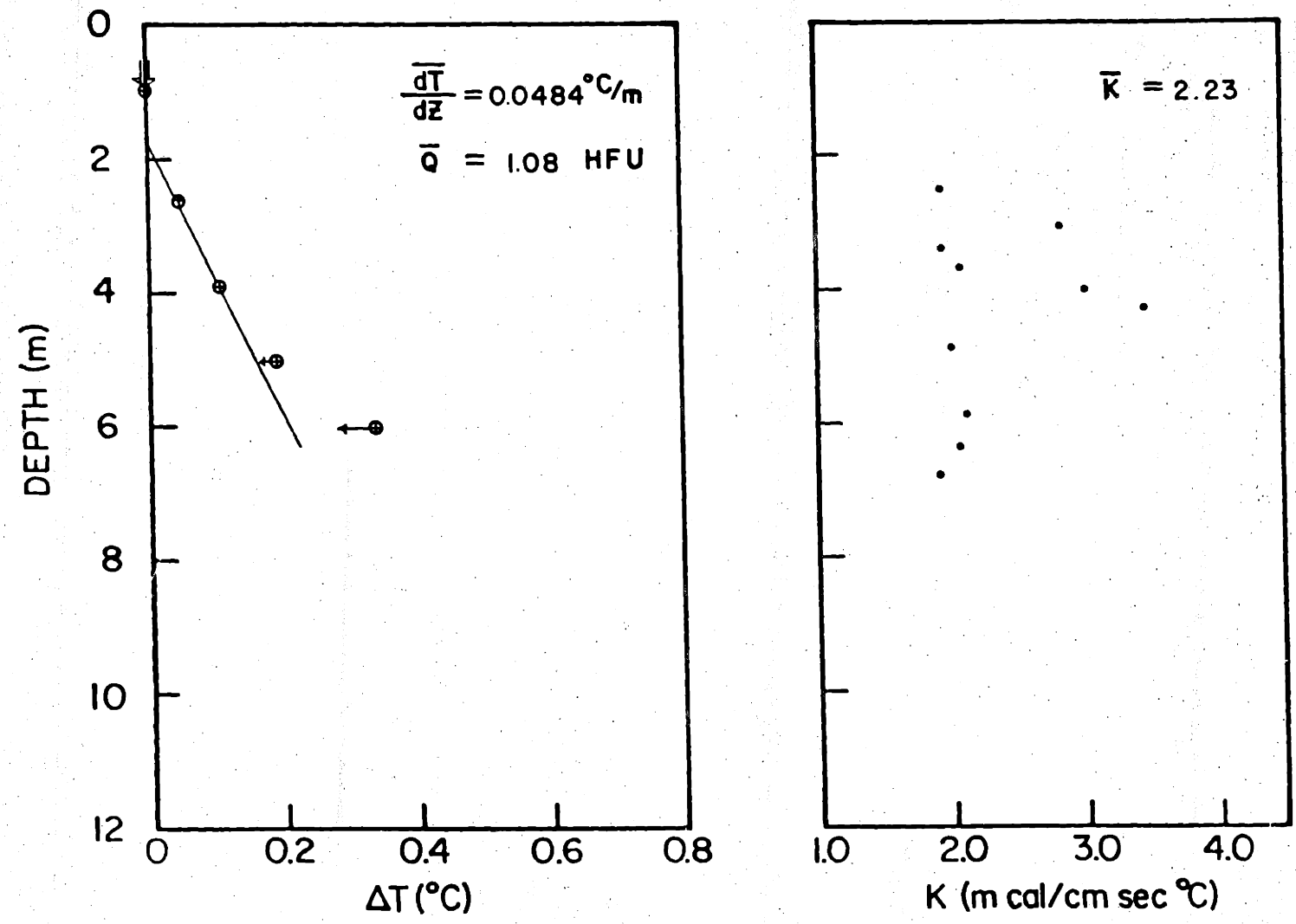

ATLANTIS II-49 HEAT FLOW STATION 1477 P

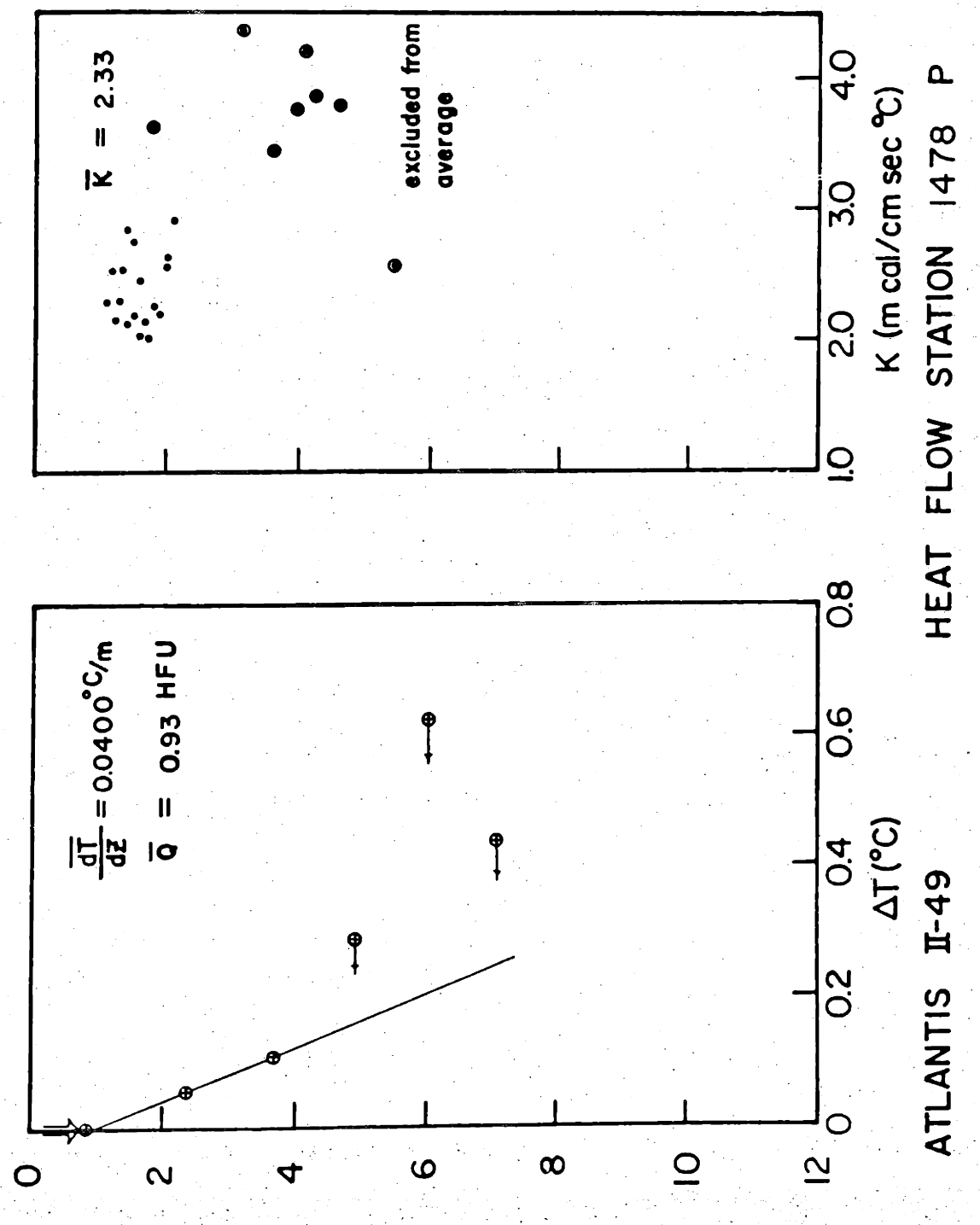

ATLANTIS II-49 HEAT FLOW STATION 1478 P

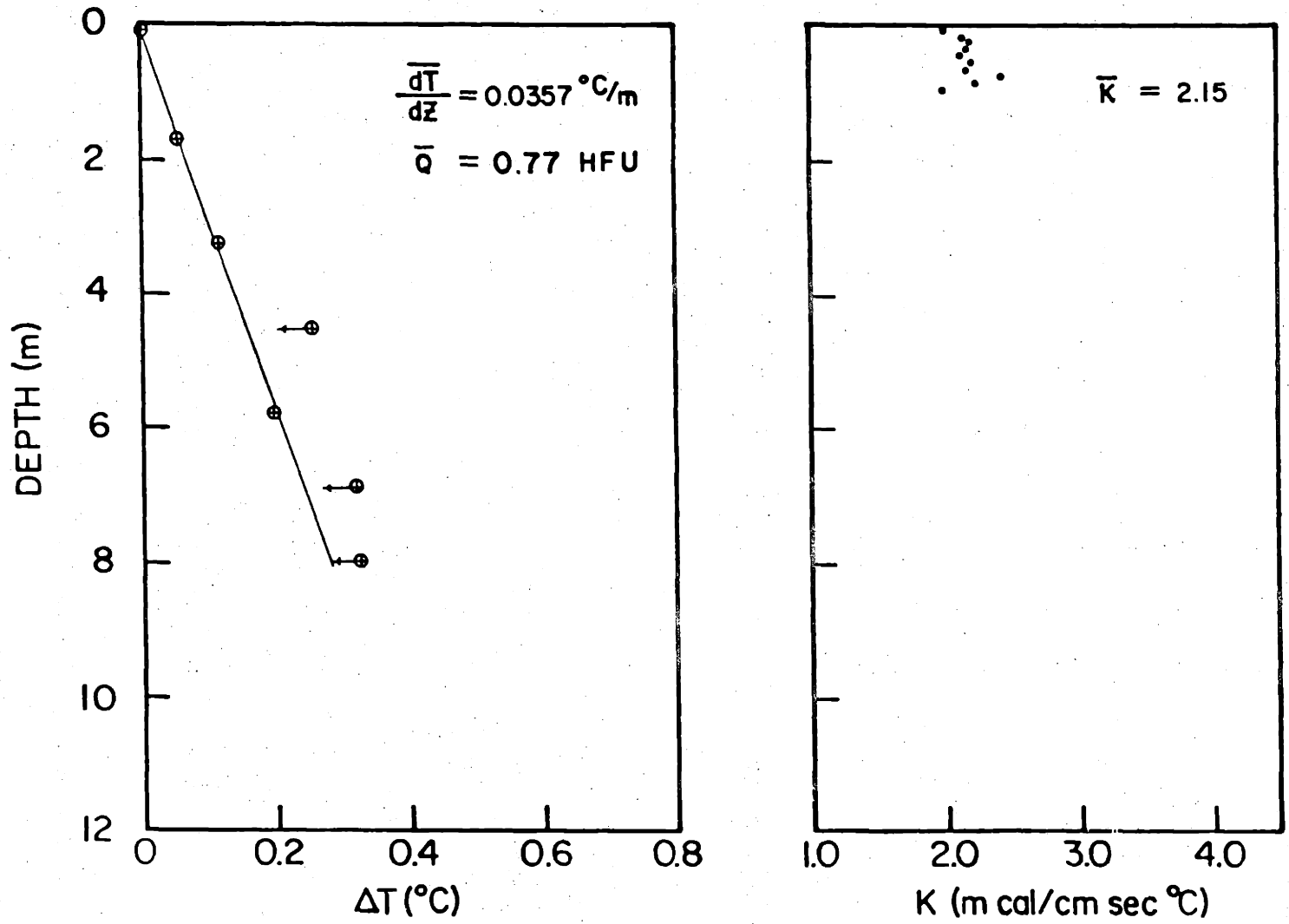

ATLANTIS II-49 HEAT FLOW STATION 1480 P

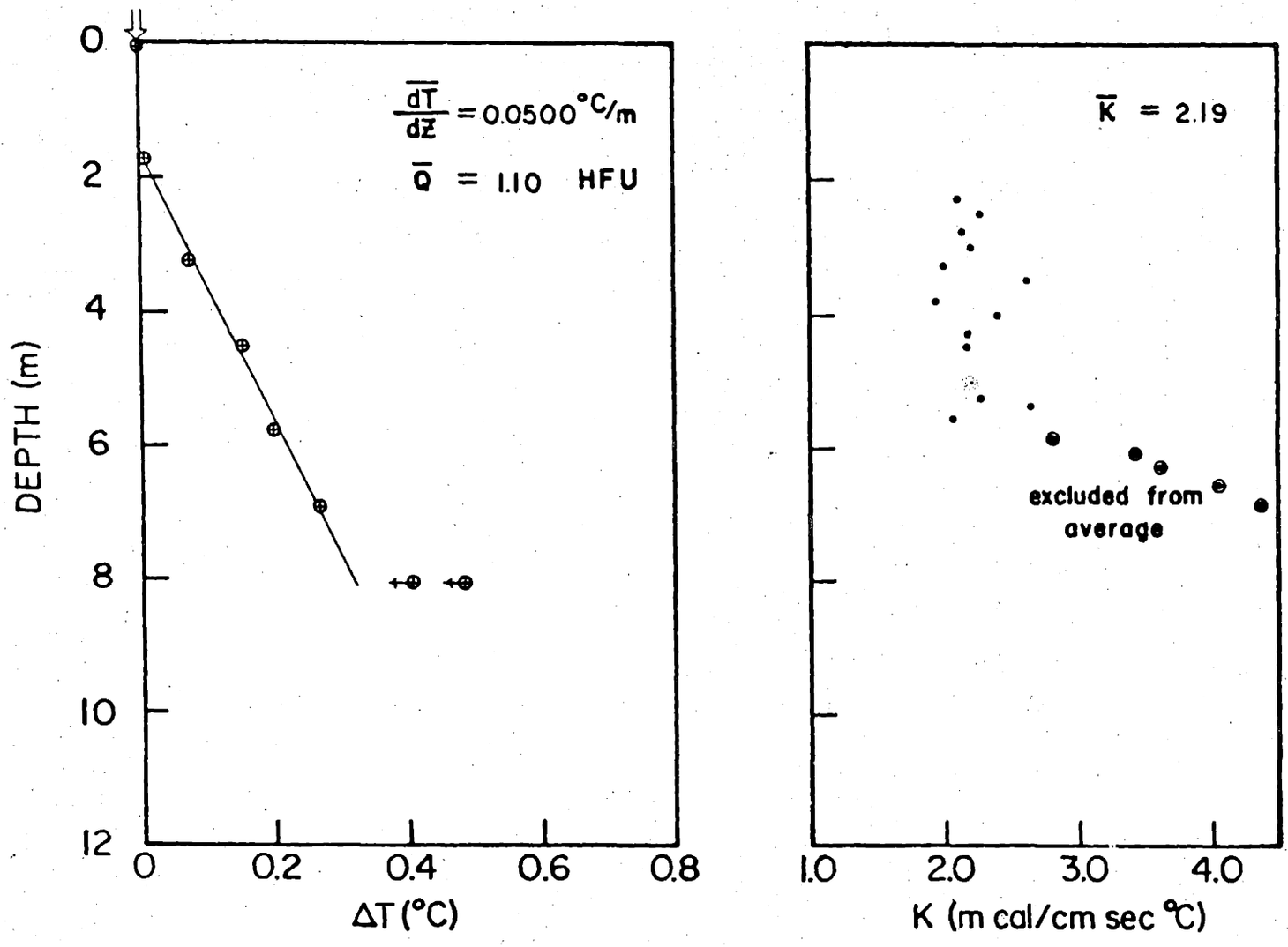

ATLANTIS II-49 HEAT FLOW STATION 1481 P

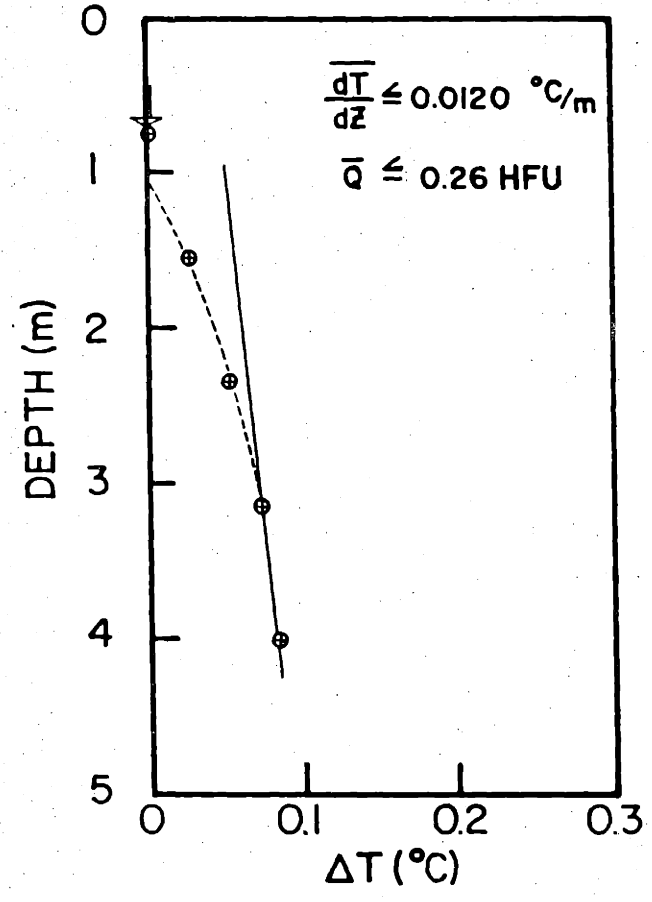

ATLANTIS II-49

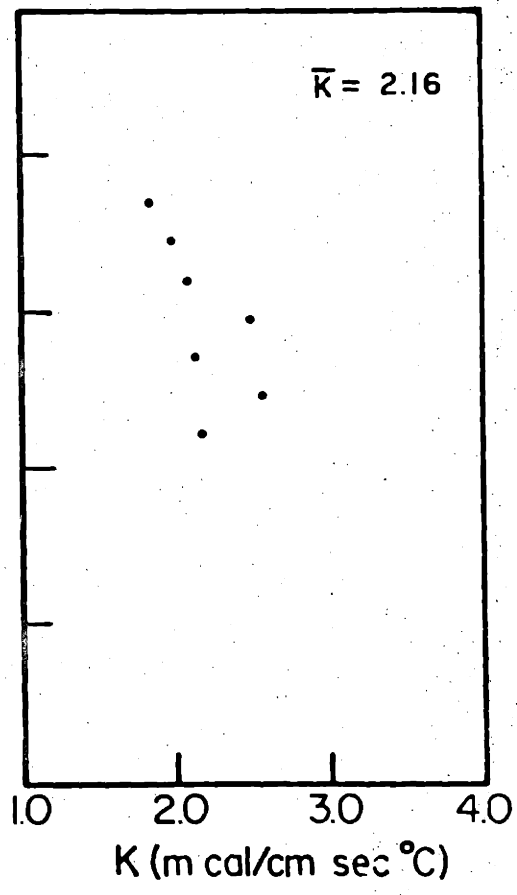

HEAT FLOW STATION 1484 G

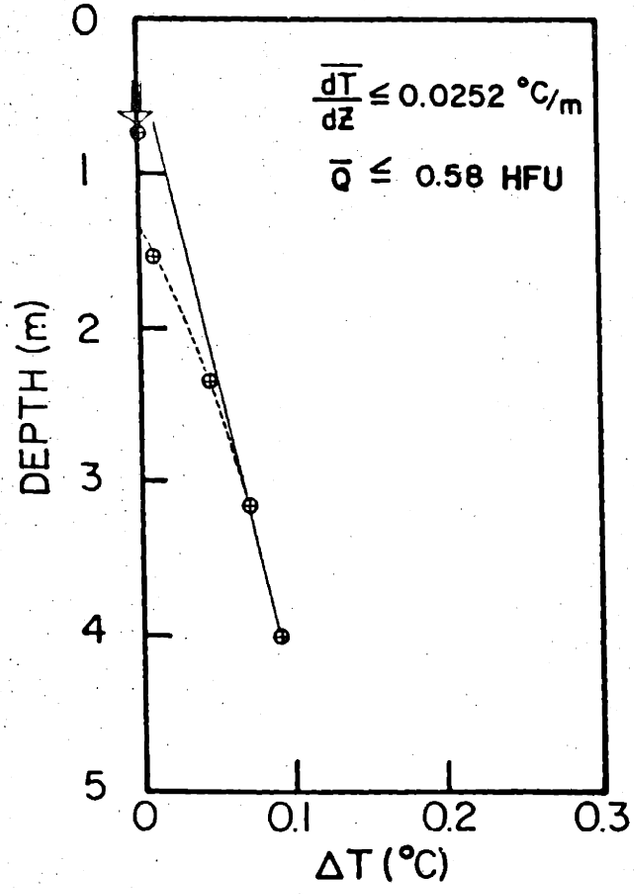

ATLANTIS II-49

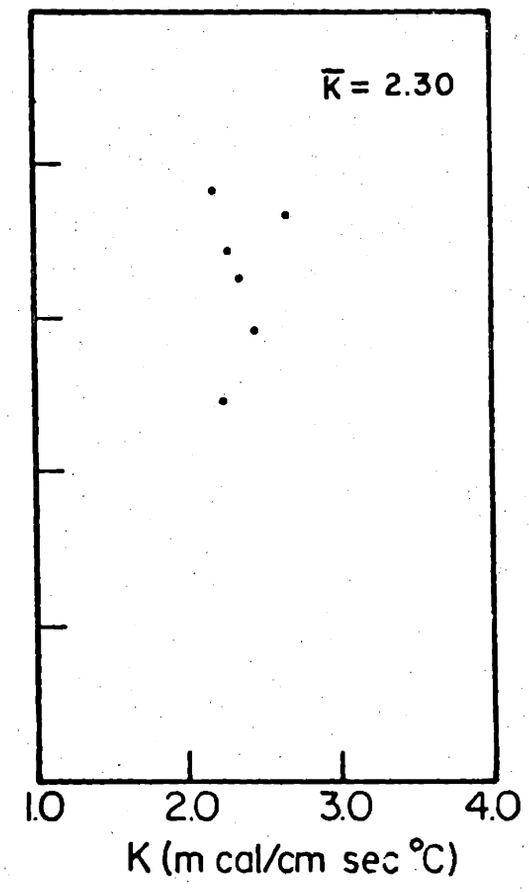

HEAT FLOW STATION 1485 G

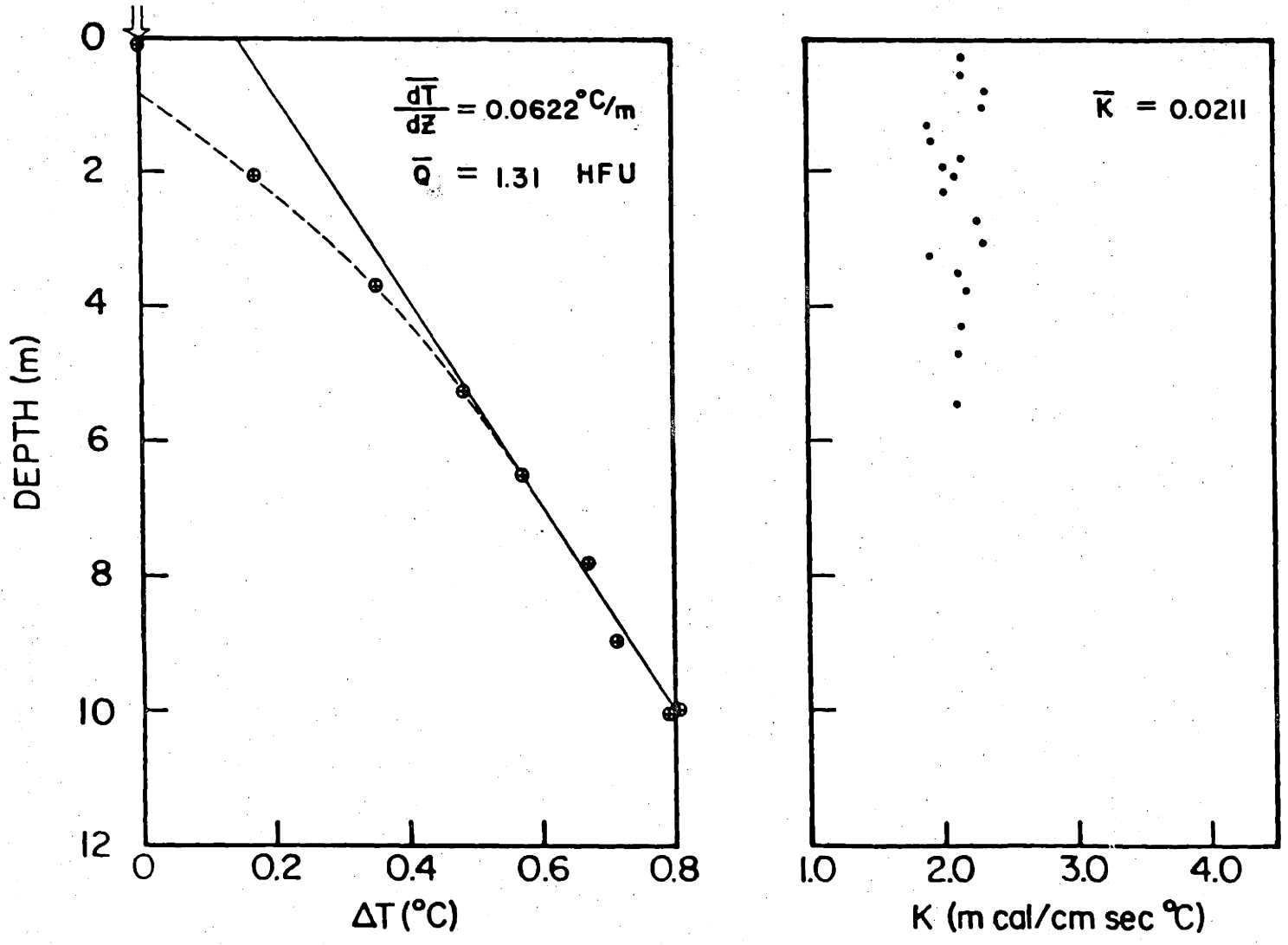

ATLANTIS II-49 HEAT FLOW STATION 1486 P

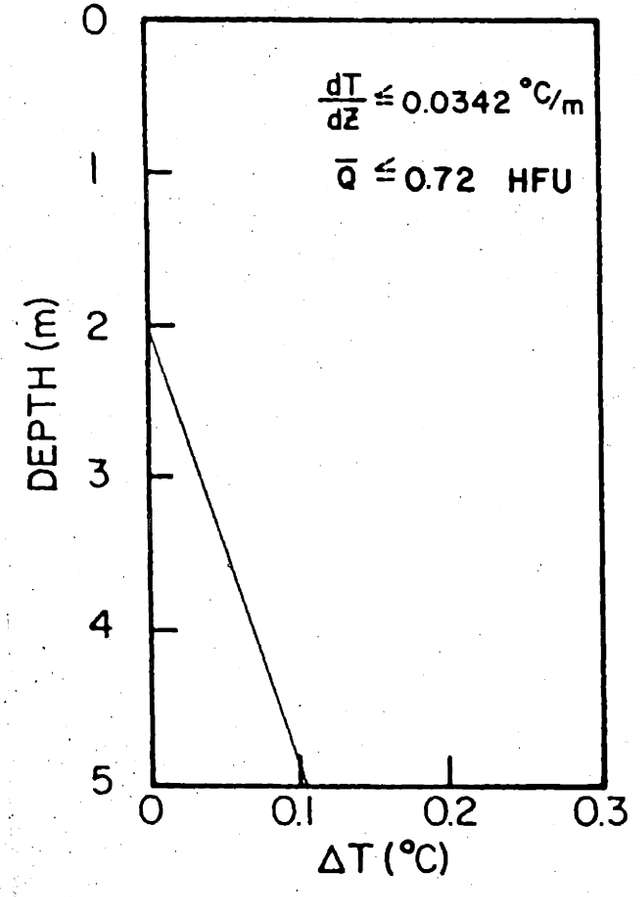

ATLANTIS II-49

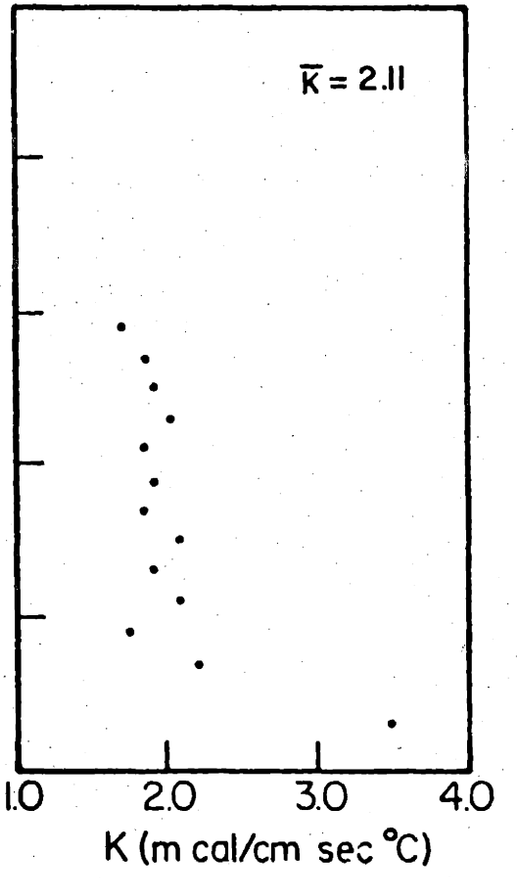

HEAT FLOW STATION 1486 G

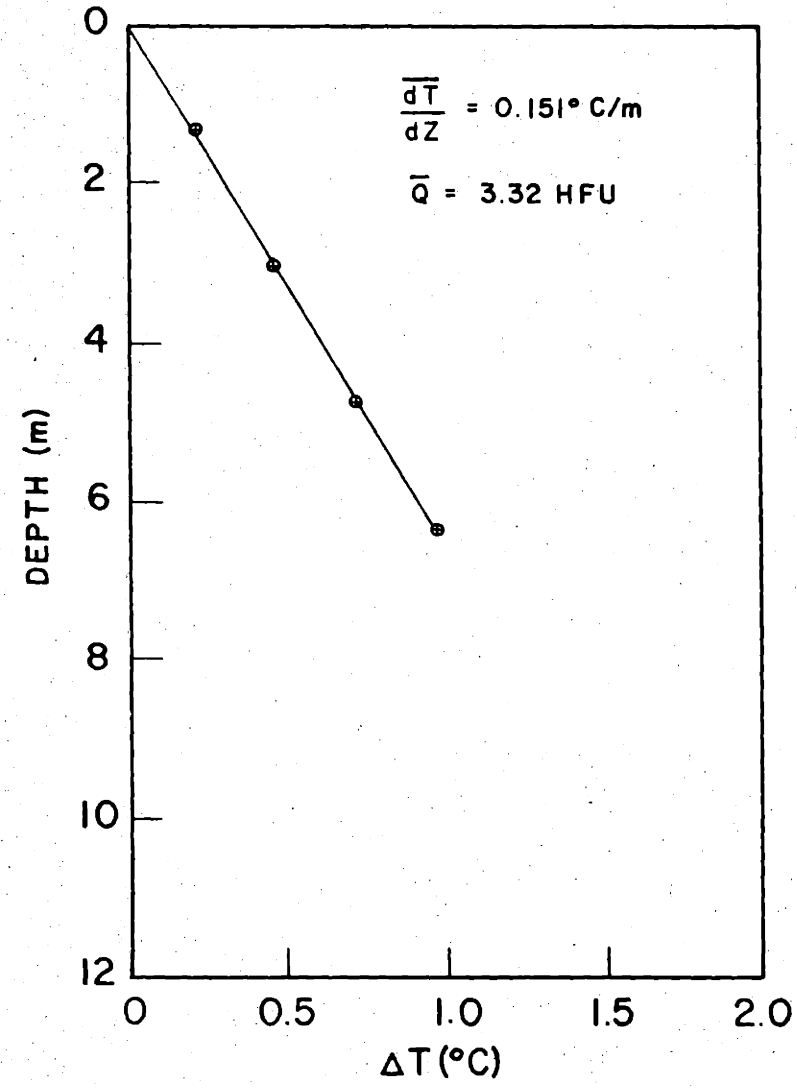

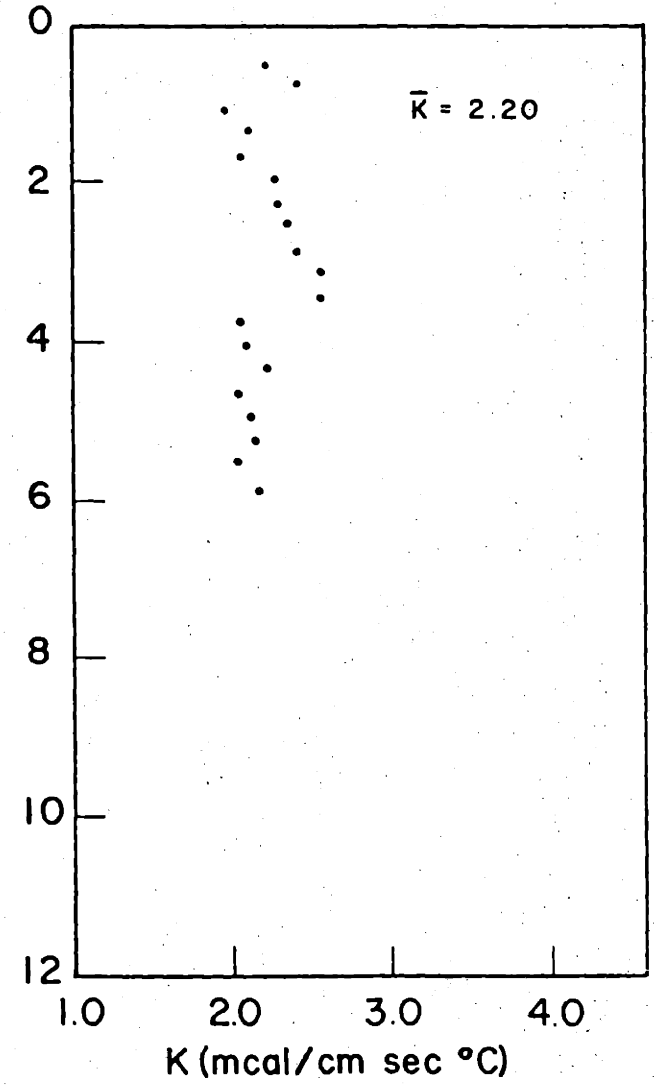

R.V. BANNOCK CT - 69 HEAT FLOW STATION 17

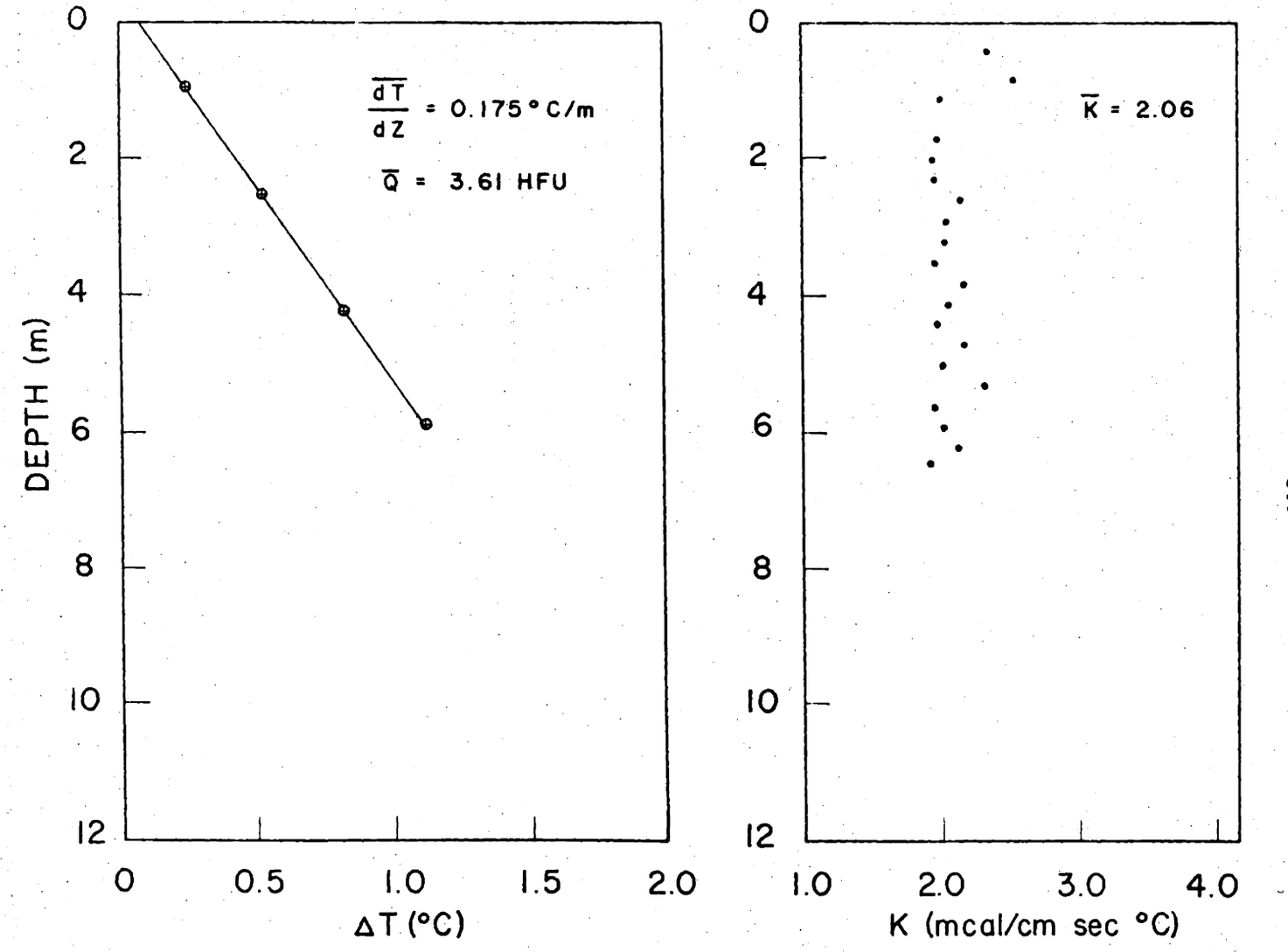

R.V. BANNOCK CT - 69 HEAT FLOW STATION 29

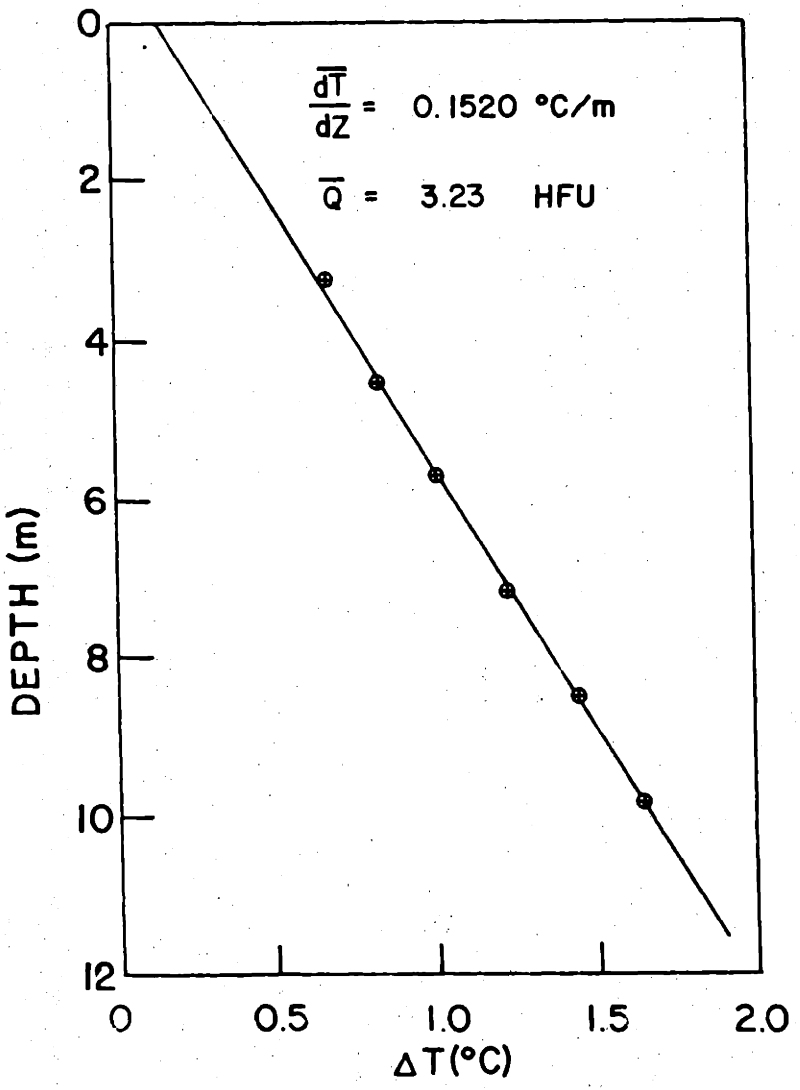

R.V. BANNOCK CT-69

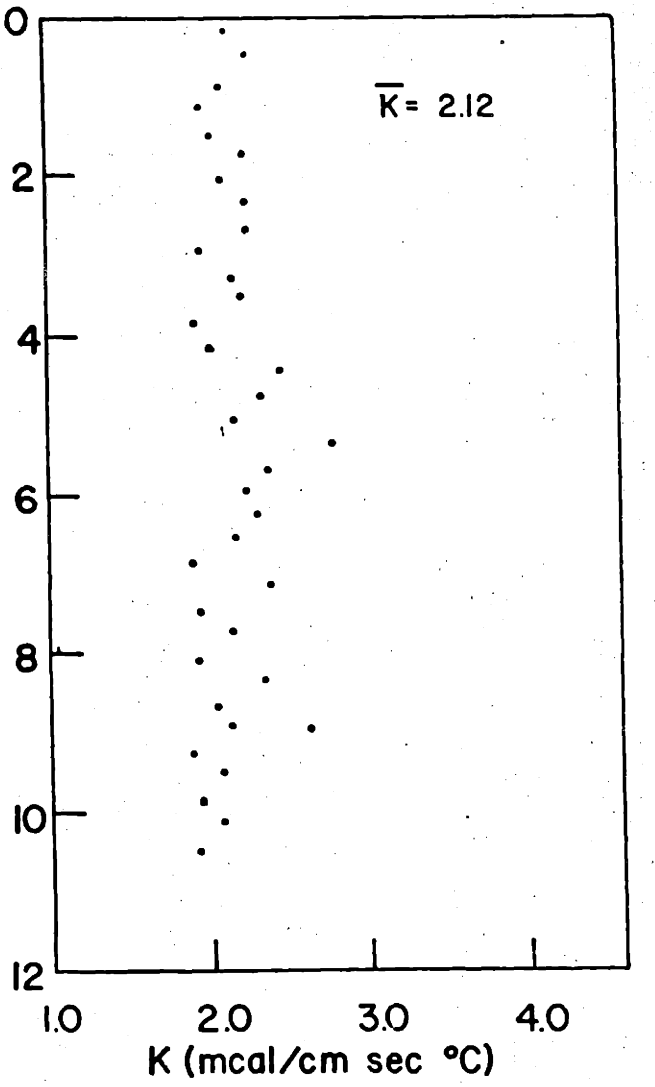

HEAT FLOW STATION 31

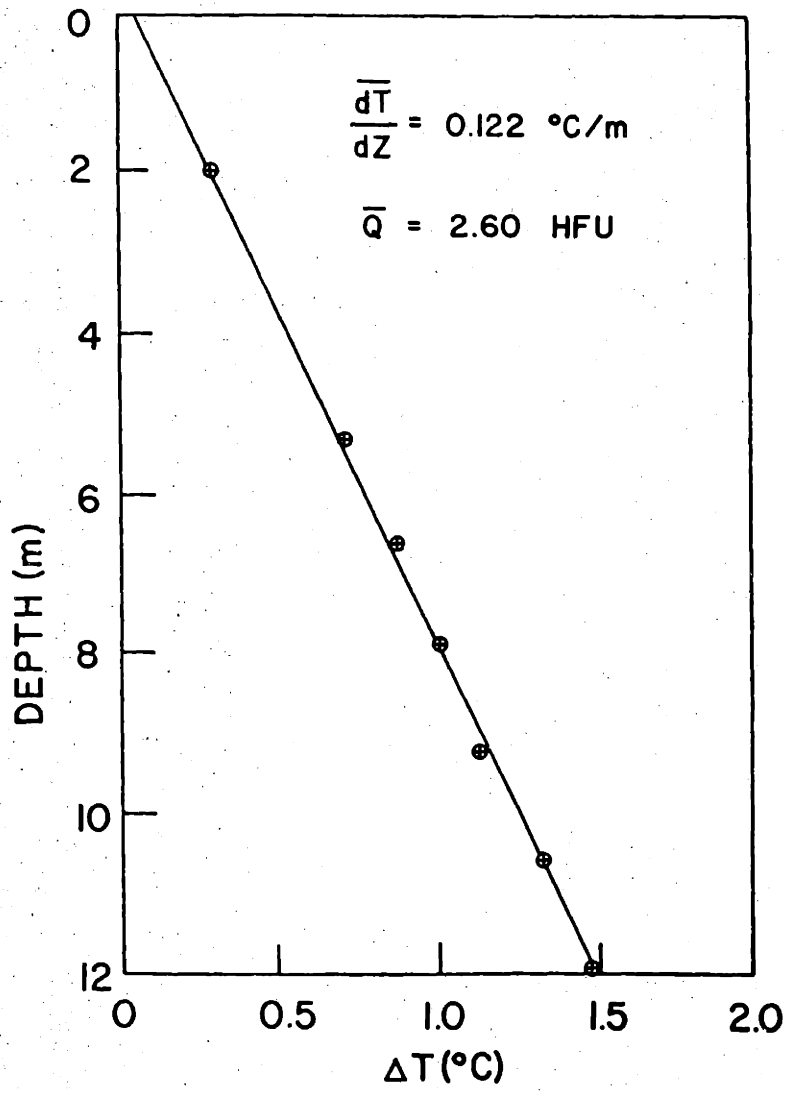

R.V. BANNOCK CT-69

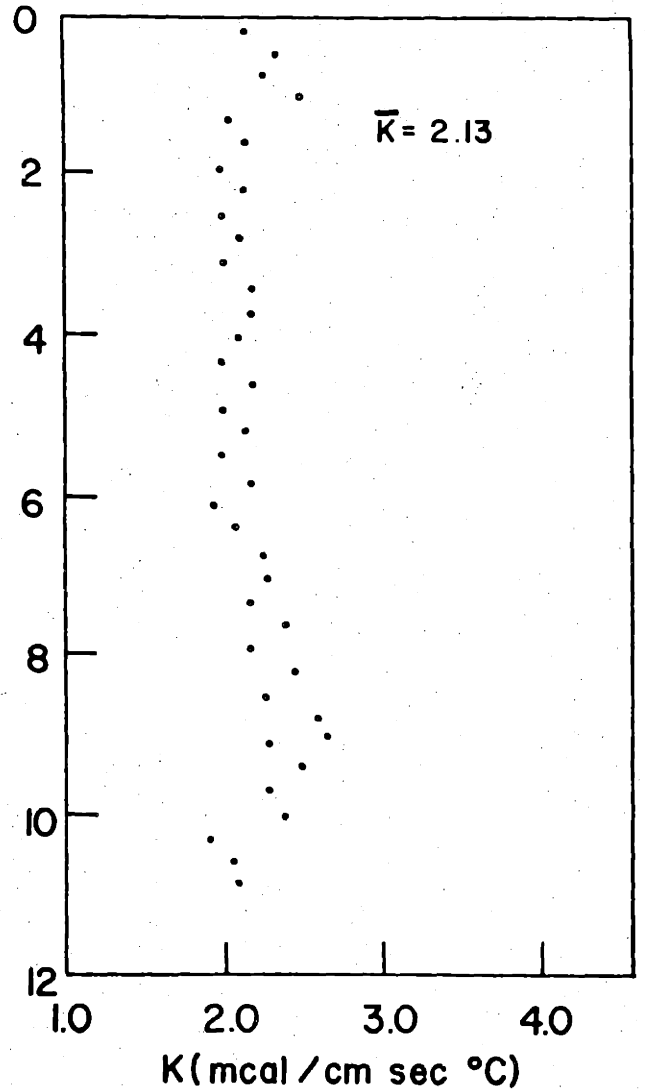

HEAT FLOW STATION 32

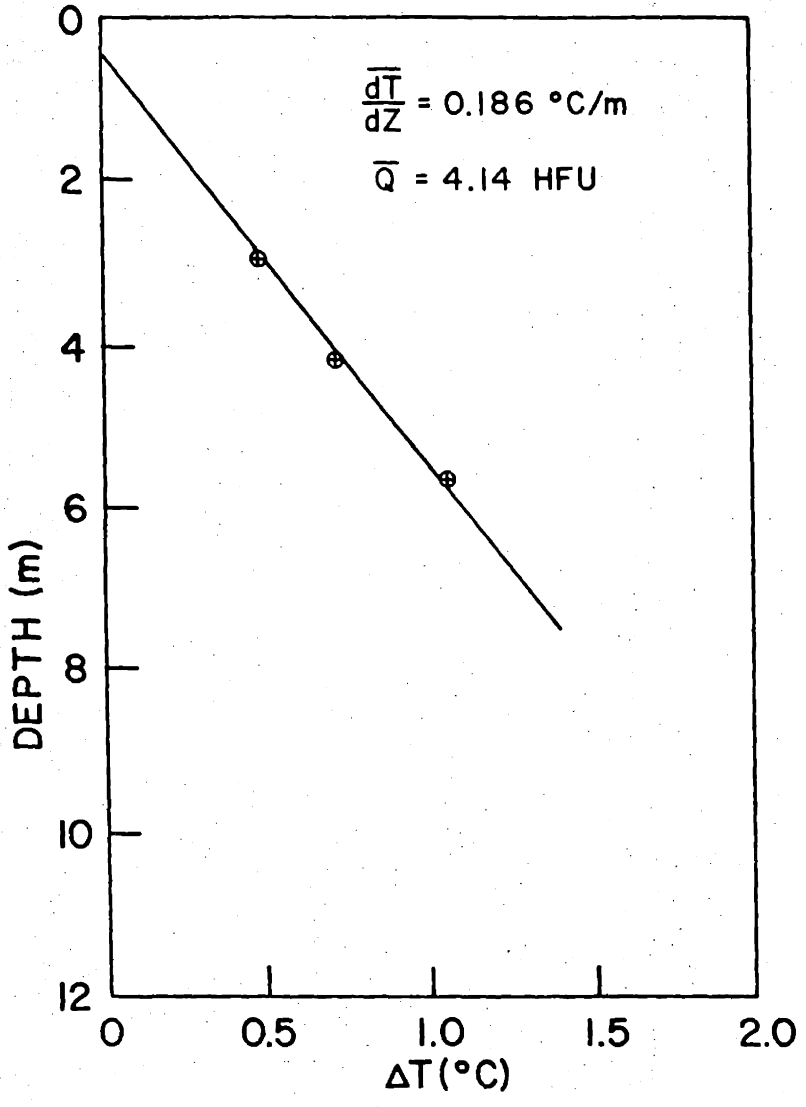

R.V. BANNOCK CT-69

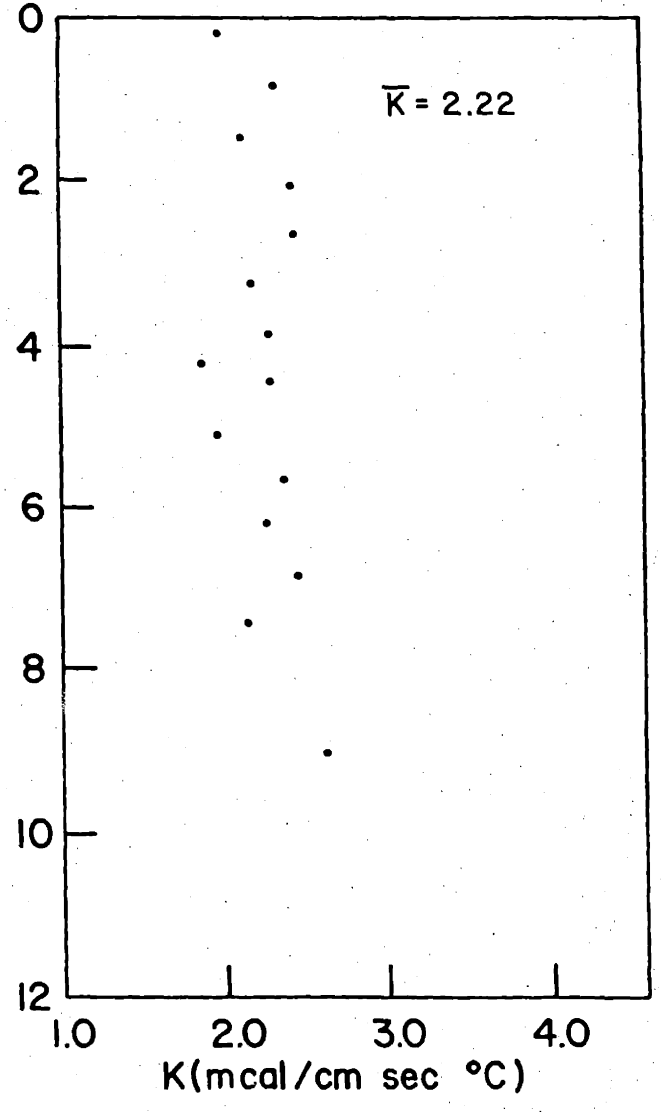

HEAT FLOW STATION 50

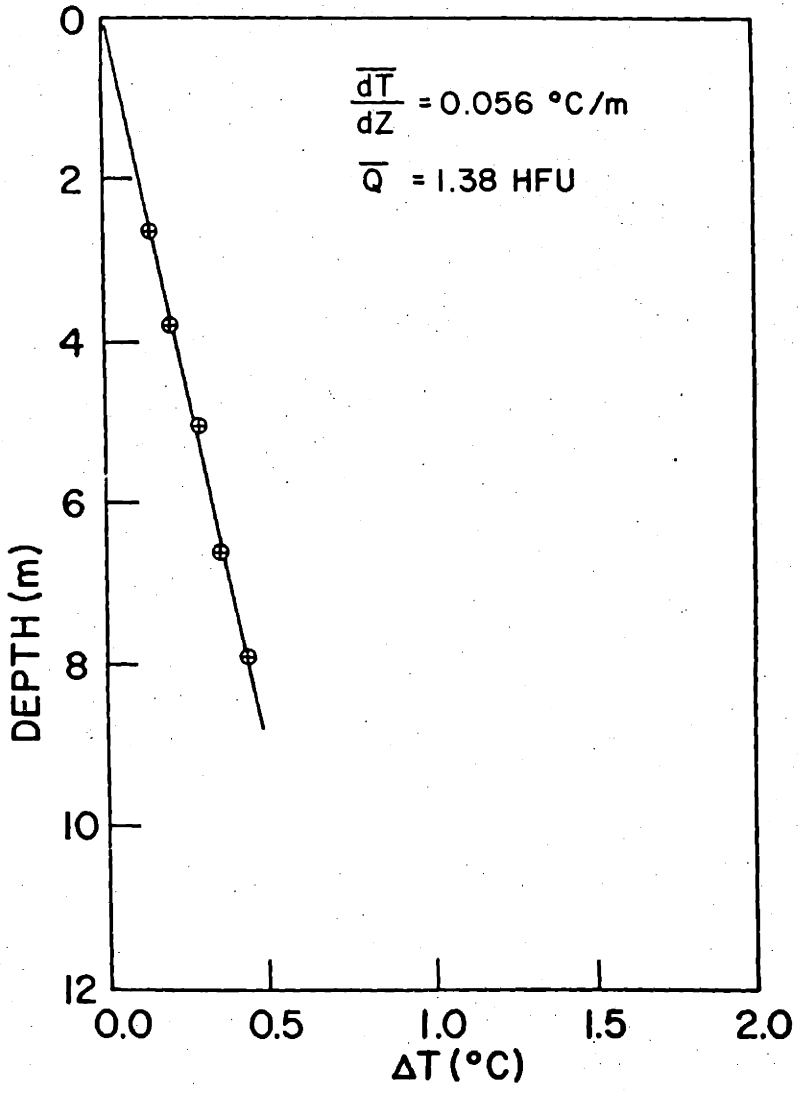

R.V. BANNOCK CT-69

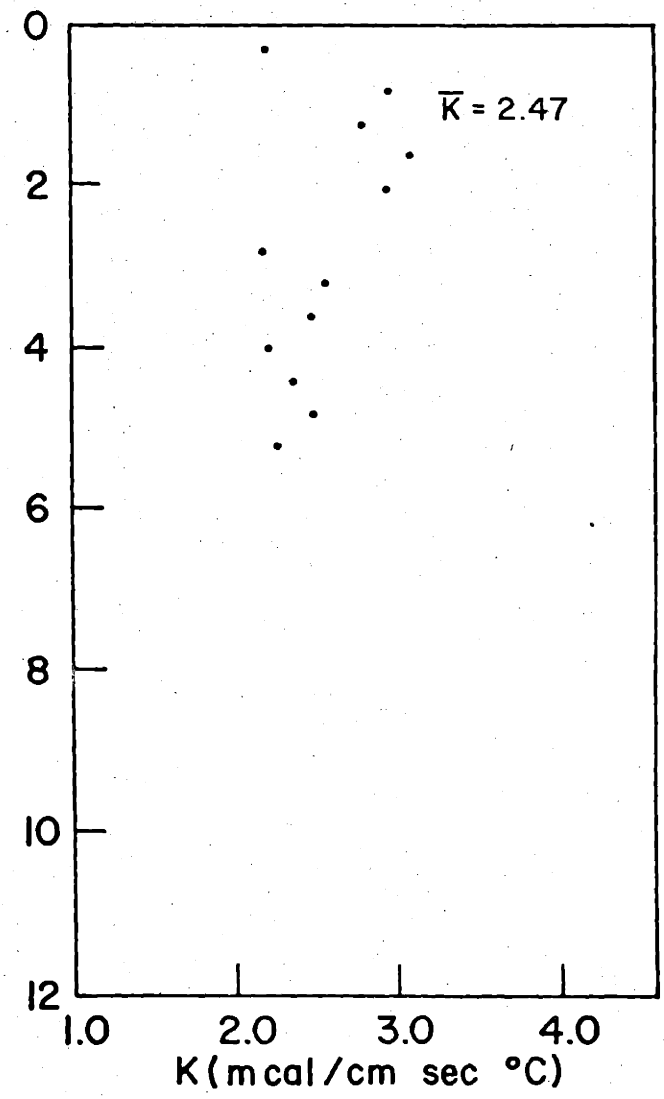

HEAT FLOW STATION 53

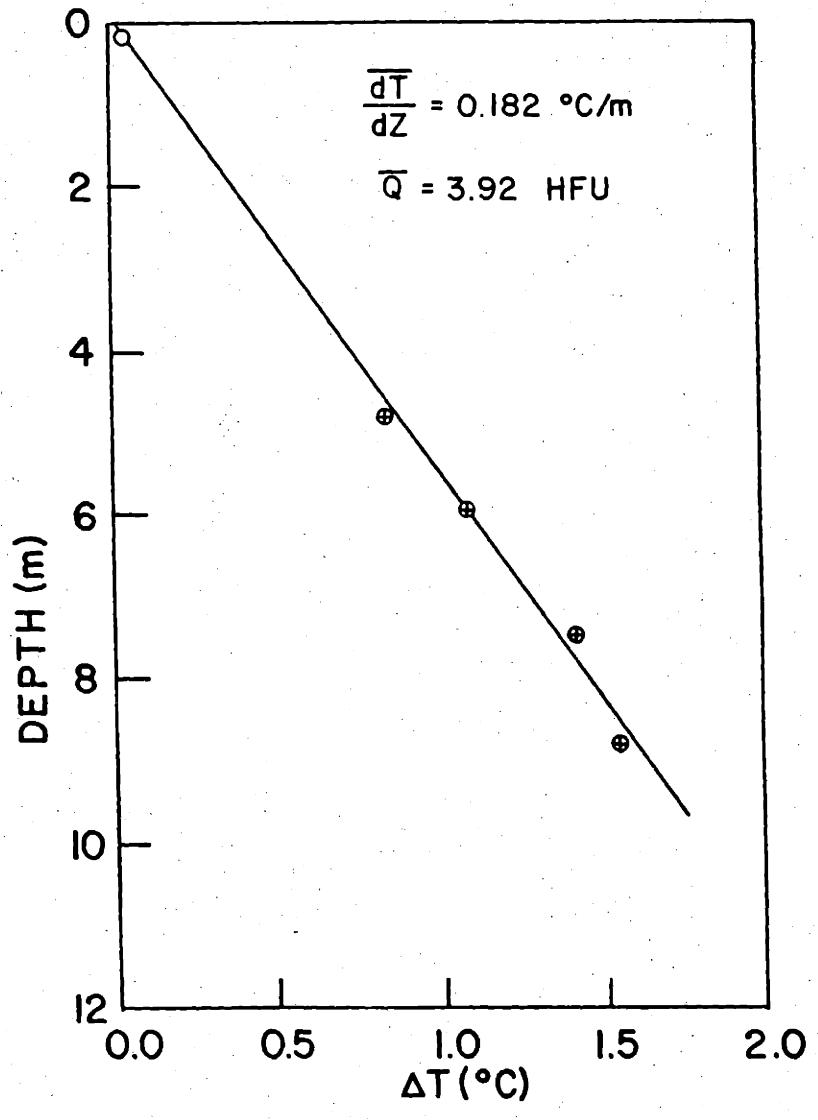

R.V. BANNOCK CT-69

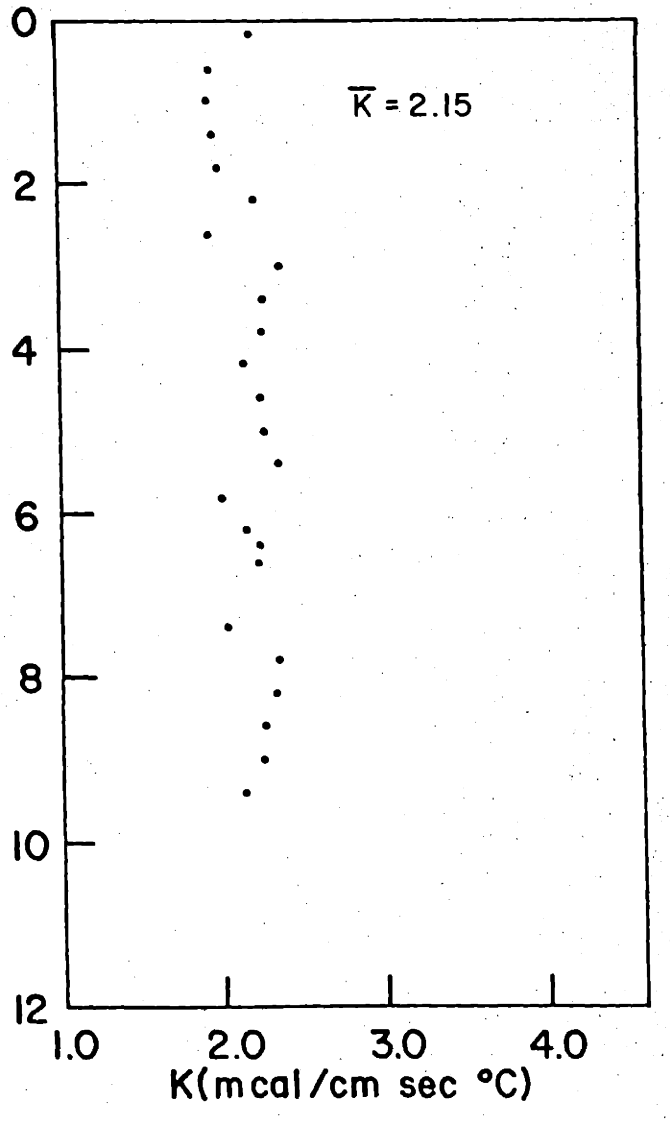

HEAT FLOW STATION 54

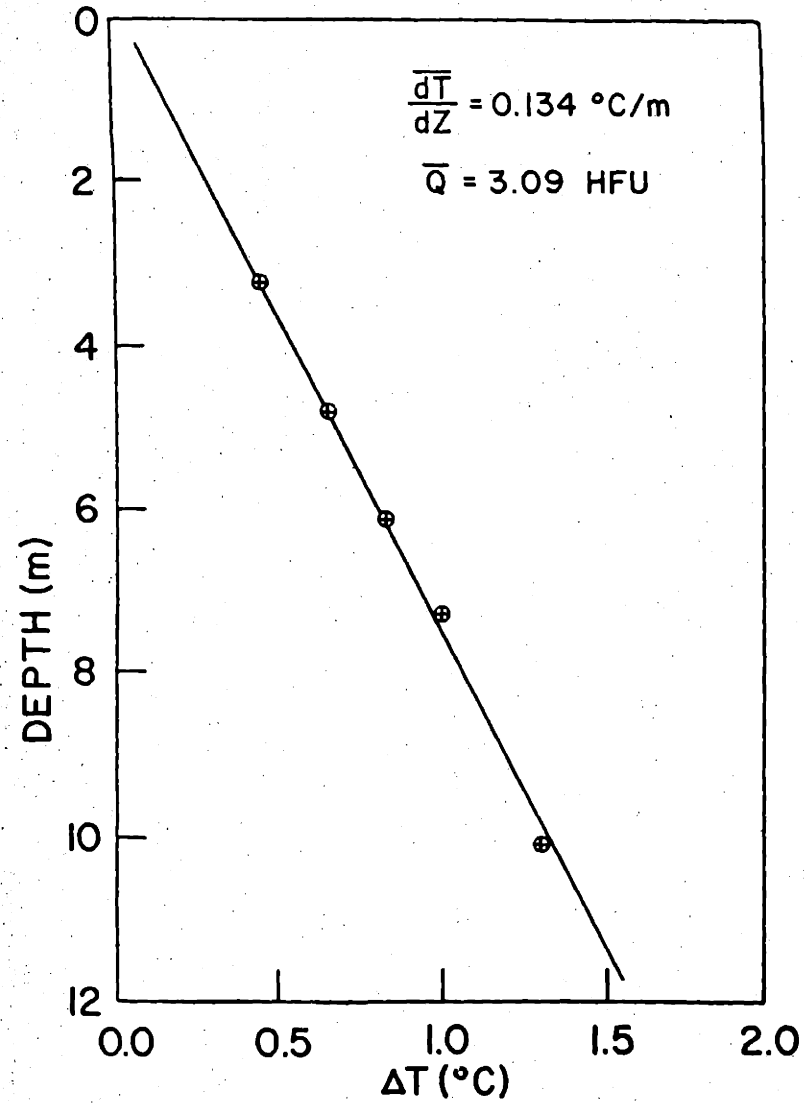

R.V. BANNOCK CT - 69

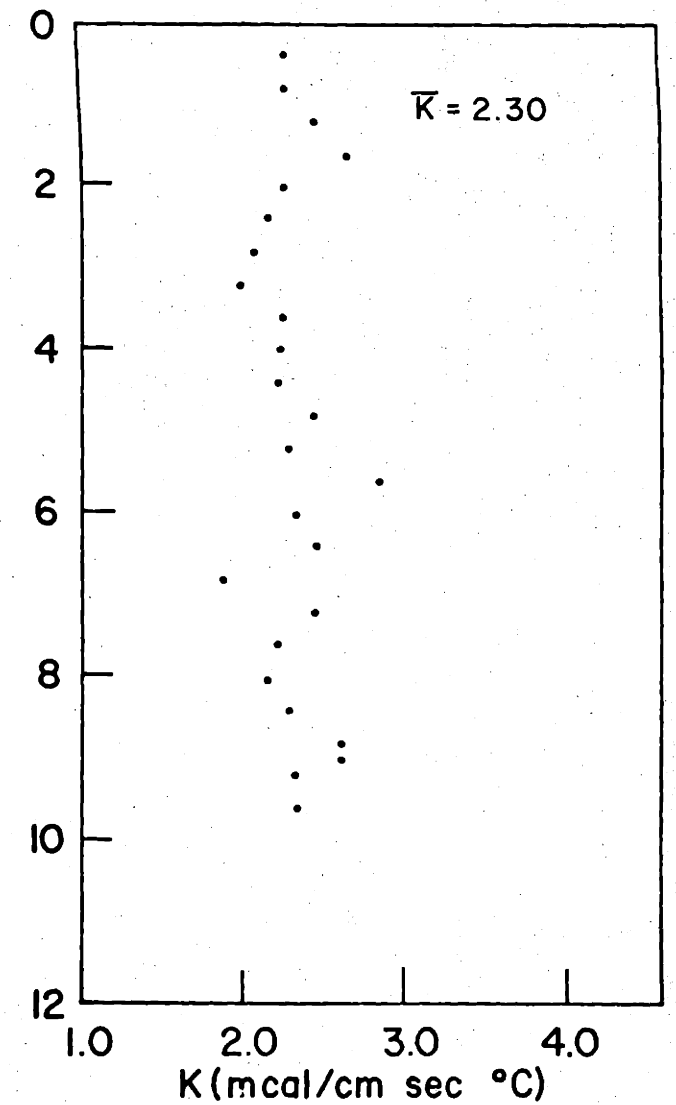

HEAT FLOW STATION 55

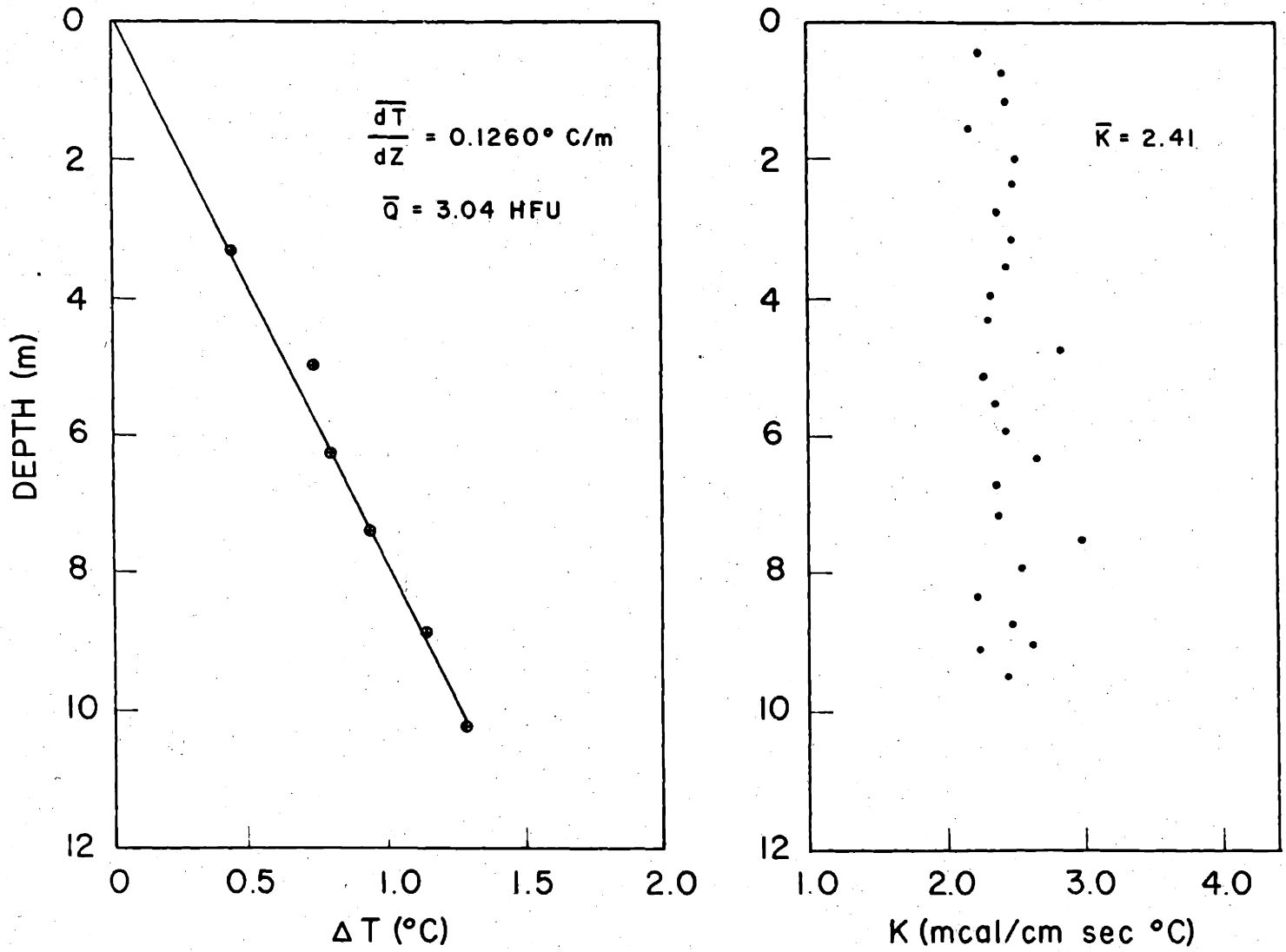

R.V. BANNOCK CT-69 HEAT FLOW STATION 78

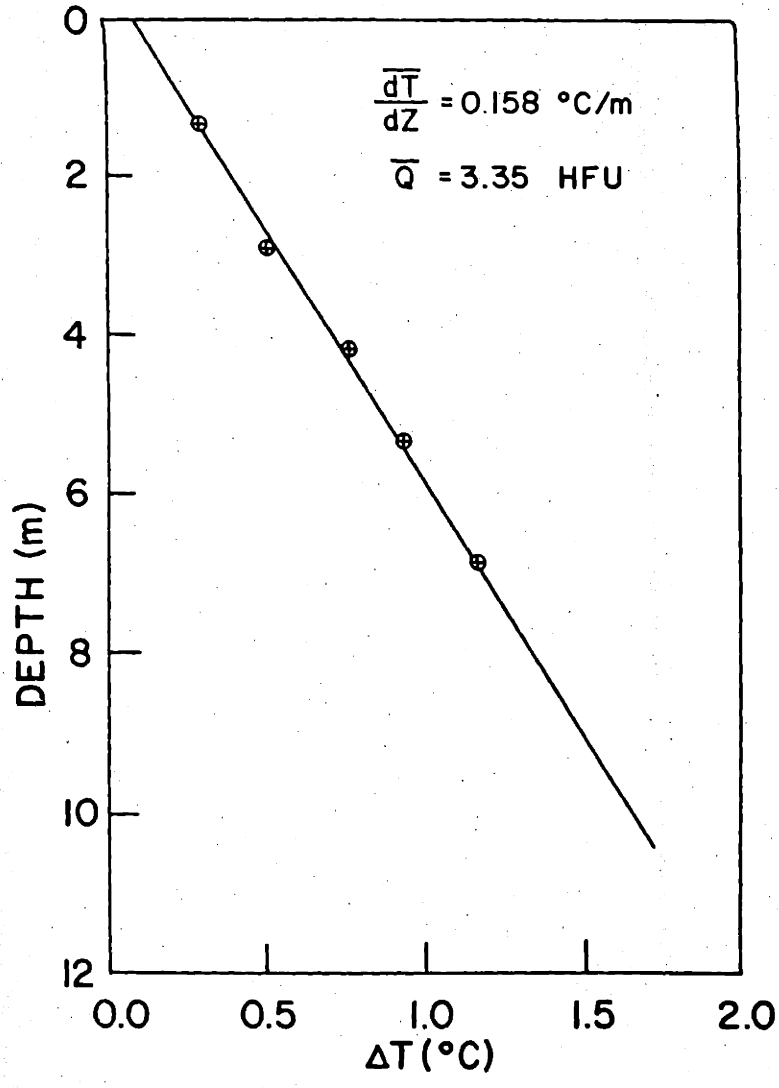

R.V. BANNOCK CT-69

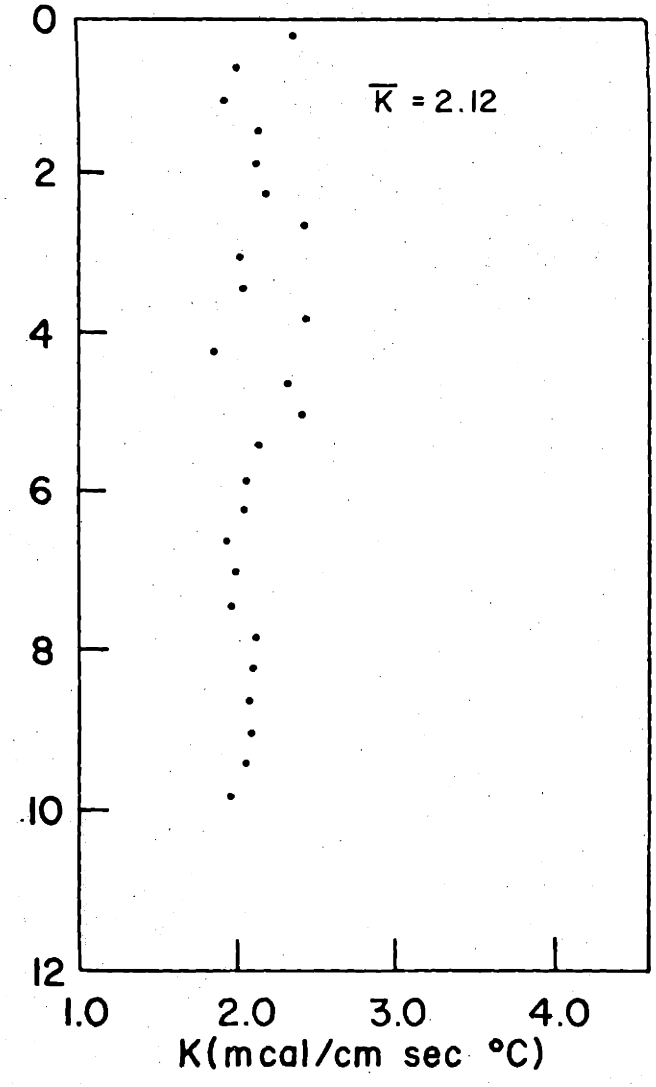

HEAT FLOW STATION 79

APPENDIX III

Thermal Conductivity Data

The results of thermal conductivity measurements made by M.I.T. investigators are presented in the following tables. The position in the core was measured in centimeters from the top or bottom of the core, as noted.

R.V. CHAIN 61 HEAT FLOW STATION 19

MEASUREMENT NUMBER	POSITION (CM)	THERMAL CONDUCTIVITY (CAL/CM SEC DEG C)
24	11.0	0.00226
31	35.0	0.00212
25	50.0	0.00225
32	60.0	0.00213
33	85.0	0.00227
26	100.0	0.00242
27	150.0	0.00242
28	200.0	0.00237
29	250.0	0.00234
30	290.0	0.00232
5	350.0	0.00217
3	400.0	0.00231
2	450.0	0.00196
1	500.0	0.00232
14	550.0	0.00188
15	592.0	0.00216
16	610.0	0.00200
17	650.0	0.00213
18	700.0	0.00219
19	750.0	0.00221
20	800.0	0.00212
21	850.0	0.00197
23	891.0	0.00226
22	955.0	0.00183

THERMAL CONDUCTIVITY CORRECTED FOR SEAFLOOR TEMPERATURE AND PRESSURE

POSITION MEASURED FROM BOTTOM OF CORE

R.V. CHAIN 61 HEAT FLOW STATION 29

MEASUREMENT NUMBER	POSITION (CM)	THERMAL CONDUCTIVITY (CAL/CM SEC DEG C)
1	25.0	0.00252
2	75.0	0.00246
3	125.0	0.00234
4	175.0	0.00231
5	225.0	0.00231
6	275.0	0.00234
7	325.0	0.00227
8	375.0	0.00227
9	425.0	0.00228
10	475.0	0.00227
11	525.0	0.00225
12	575.0	0.00222
13	625.0	0.00218
17	650.0	0.00219
16	700.0	0.00220
15	750.0	0.00217
14	800.0	0.00211
19	850.0	0.00206

THERMAL CONDUCTIVITY CORRECTED FOR SEAFLOOR TEMPERATURE AND PRESSURE

POSITION MEASURED FROM BOTTOM OF CORE

R.V. CHAIN 61 HEAT FLOW STATION 37

MEASUREMENT NUMBER	POSITION (CM)	THERMAL CONDUCTIVITY (CAL/CM SEC DEG C)
2	75.0	0.00197
3	125.0	0.00195
4	175.0	0.00201
5	225.0	0.00192
6	275.0	0.00205
7	325.0	0.00201
8	375.0	0.00201
9	400.0	0.00197

THERMAL CONDUCTIVITY CORRECTED FOR SEAFLOOR TEMPERATURE AND PRESSURE

POSITION MEASURED FROM BOTTOM OF CORE

R.V. CHAIN 61 HEAT FLOW STATION 39

MEASUREMENT NUMBER	POSITION (CM)	THERMAL CONDUCTIVITY (CAL/CM SEC DEG C)
5	55.0	0.00274
4	105.0	0.00277
3	155.0	0.00262
2	205.0	0.00283
1	255.0	0.00273

THERMAL CONDUCTIVITY CORRECTED FOR SEAFLOOR TEMPERATURE AND PRESSURE

POSITION MEASURED FROM BOTTOM OF CORE

R.V. CHAIN 61 HEAT FLOW STATION 40

MEASUREMENT NUMBER	POSITION (CM)	THERMAL CONDUCTIVITY (CAL/CM SEC DEG C)
1	25.0	0.00215
2	75.0	0.00221
3	125.0	0.00209
4	175.0	0.00232
5	225.0	0.00273
6	275.0	0.00176
7	325.0	0.00250
8	375.0	0.00267
9	425.0	0.00268
10	475.0	0.00252
11	525.0	0.00250

THERMAL CONDUCTIVITY CORRECTED FOR SEAFLOOR TEMPERATURE AND PRESSURE

POSITION MEASURED FROM BOTTOM OF CORE

R.V. CHAIN 61 HEAT FLOW STATION 42

MEASUREMENT NUMBER	POSITION (CM)	THERMAL CONDUCTIVITY (CAL/CM SEC DEG C)
15	0.0	0.00214
29	25.0	0.00260
28	50.0	0.00261
27	75.0	0.00258
26	100.0	0.00246
25	125.0	0.00226
30	150.0	0.00248
8	175.0	0.00248
21	190.0	0.00248
22	205.0	0.00259
23	215.0	0.00246
7	225.0	0.00263
24	235.0	0.00260
17	245.0	0.00246
18	260.0	0.00248
6	275.0	0.00243
19	283.5	0.00245
20	292.0	0.00248
5	315.0	0.00261
13	340.0	0.00253
31	365.0	0.00256
14	382.5	0.00250
32	400.0	0.00254
3	425.0	0.00238
9	435.0	0.00213
16	450.0	0.00213
2	465.0	0.00200
12	477.5	0.00213
1	490.0	0.00237
10	493.5	0.00226
11	499.0	0.00235

THERMAL CONDUCTIVITY CORRECTED FOR SEAFLOOR TEMPERATURE AND PRESSURE

POSITION MEASURED FROM BOTTOM OF CORE

R.V. CHAIN 61 HEAT FLOW STATION 46

MEASUREMENT NUMBER	POSITION (CM)	THERMAL CONDUCTIVITY (CAL/CM SEC DEG C)
1	10.0	0.00227
2	30.0	0.00248
3	50.0	0.00250
4	70.0	0.00251
31	80.0	0.00260
5	90.0	0.00262
6	110.0	0.00265
30	115.0	0.00262
33	117.5	0.00248
26	120.0	0.00218
29	127.0	0.00213
7	130.0	0.00207
28	133.0	0.00253
32	135.0	0.00256
27	140.0	0.00263
8	150.0	0.00271
9	170.0	0.00268
10	190.0	0.00265
11	210.0	0.00258
12	230.0	0.00263
13	250.0	0.00253
14	272.5	0.00237
15	285.0	0.00246
16	305.0	0.00250
17	325.0	0.00250
18	345.0	0.00254
19	365.0	0.00245
20	385.0	0.00244
21	390.0	0.00236
22	401.5	0.00210
23	409.0	0.00208

THERMAL CONDUCTIVITY CORRECTED FOR SEAFLOOR TEMPERATURE AND PRESSURE

POSITION MEASURED FROM BOTTOM OF CORE

R.V. CHAIN 61 HEAT FLOW STATION 50

MEASUREMENT NUMBER	POSITION (CM)	THERMAL CONDUCTIVITY (CAL/CM SEC DEG C)
15	10.0	0.00258
14	30.0	0.00245
13	50.0	0.00252
12	70.0	0.00247
22	90.0	0.00261
11	90.0	0.00216
21	100.0	0.00252
10	110.0	0.00258
9	130.0	0.00262
8	150.0	0.00263
7	170.0	0.00261
6	190.0	0.00246
5	210.0	0.00248
4	230.0	0.00244
3	250.0	0.00247
2	270.0	0.00243
1	290.0	0.00245
16	310.0	0.00251
33	320.0	0.00251
23	328.0	0.00246
17	330.0	0.00251
30	338.0	0.00244
34	340.0	0.00241
24	348.0	0.00239
18	350.0	0.00239
28	353.0	0.00231
27	358.0	0.00211
35	360.0	0.00230
29	363.0	0.00235
25	368.0	0.00239
19	370.0	0.00226
31	378.0	0.00219
36	380.0	0.00230
26	388.0	0.00235
20	390.0	0.00212
32	399.0	0.00226

THERMAL CONDUCTIVITY CORRECTED FOR SEAFLOOR TEMPERATURE AND PRESSURE

POSITION MEASURED FROM BOTTOM OF CORE

R.V. CHAIN 61 HEAT FLOW STATION 53

MEASUREMENT NUMBER	POSITION (CM)	THERMAL CONDUCTIVITY (CAL/CM SEC DEG C)
1	10.0	0.00240
2	25.0	0.00238
3	50.0	0.00221
4	75.0	0.00241
5	100.0	0.00193
6	125.0	0.00229
7	150.0	0.00205
8	175.0	0.00197
9	200.0	0.00237
10	225.0	0.00225
11	250.0	0.00216
12	275.0	0.00227
13	290.0	0.00217
14	310.0	0.00235
15	325.0	0.00156
41	337.5	0.00161
16	350.0	0.00158
42	362.5	0.00215
17	375.0	0.00222
18	400.0	0.00233
19	425.0	0.00227
20	450.0	0.00247
21	475.0	0.00225
22	500.0	0.00250
23	525.0	0.00245
24	550.0	0.00183
39	560.0	0.00237
43	565.0	0.00240
38	570.0	0.00234
25	575.0	0.00241
37	580.0	0.00240
44	585.0	0.00232
36	590.0	0.00241
26	590.0	0.00243

THERMAL CONDUCTIVITY CORRECTED FOR SEAFLOOR TEMPERATURE AND PRESSURE

POSITION MEASURED FROM BOTTOM OF CORE

R.V. CHAIN 61 HEAT FLOW STATION 53 (CONTINUED)

MEASUREMENT NUMBER	POSITION (CM)	THERMAL CONDUCTIVITY (CAL/CM SEC DEG C)
45	595.0	0.00242
35	600.0	0.00230
46	605.0	0.00236
34	605.0	0.00209
33	610.0	0.00185
47	610.0	0.00183
32	615.0	0.00187
48	615.0	0.00189
31	620.0	0.00191
49	620.0	0.00198
30	625.0	0.00199
50	625.0	0.00196
29	630.0	0.00198
51	630.0	0.00195
52	635.0	0.00212

THERMAL CONDUCTIVITY CORRECTED FOR SEAFLOOR TEMPERATURE AND PRESSURE

POSITION MEASURED FROM BOTTOM OF CORE

R.V. CHAIN 61 HEAT FLOW STATION 54

MEASUREMENT NUMBER	POSITION (CM)	THERMAL CONDUCTIVITY (CAL/CM SEC DEG C)
8	15.0	0.00222
1	25.0	0.00265
9	30.0	0.00231
10	45.0	0.00245
7	50.0	0.00240
2	75.0	0.00225
6	100.0	0.00239
3	125.0	0.00236
5	150.0	0.00234
4	175.0	0.00228

THERMAL CONDUCTIVITY CORRECTED FOR SEAFLOOR TEMPERATURE AND PRESSURE

POSITION MEASURED FROM BOTTOM OF CORE

R.V. CHAIN 61 HEAT FLOW STATION 55

MEASUREMENT NUMBER	POSITION (CM)	THERMAL CONDUCTIVITY (CAL/CM SEC DEG C)
1	25.0	0.00252
2	75.0	0.00247
3	125.0	0.00244
4	175.0	0.00235
5	225.0	0.00242
6	275.0	0.00242
7	325.0	0.00245
12	350.0	0.00220
8	375.0	0.00226
13	400.0	0.00224
23	410.0	0.00229
18	420.0	0.00233
9	425.0	0.00232
17	440.0	0.00228
14	450.0	0.00225
16	460.0	0.00233
10	465.0	0.00244
22	480.0	0.00208
21	490.0	0.00193
24	500.0	0.00209
15	500.0	0.00224
20	510.0	0.00213

THERMAL CONDUCTIVITY CORRECTED FOR SEAFLOOR TEMPERATURE AND PRESSURE

POSITION MEASURED FROM BOTTOM OF CORE

R.V. CHAIN 61 HEAT FLOW STATION 56

MEASUREMENT NUMBER	POSITION (CM)	THERMAL CONDUCTIVITY (CAL/CM SEC DEG C)
1	25.0	0.00205
13	50.0	0.00212
2	75.0	0.00192
14	100.0	0.00200
3	125.0	0.00199
15	150.0	0.00201
24	175.0	0.00234
4	175.0	0.00240
5	225.0	0.00186
17	250.0	0.00191
6	275.0	0.00208
23	295.0	0.00238
7	325.0	0.00209
18	350.0	0.00217
8	375.0	0.00219
19	400.0	0.00221
9	425.0	0.00210
25	425.0	0.00210
20	450.0	0.00211
10	475.0	0.00221
21	500.0	0.00245
35	500.0	0.00229
34	510.0	0.00208
33	520.0	0.00199
11	525.0	0.00207
32	530.0	0.00195
31	540.0	0.00192
30	550.0	0.00184
22	550.0	0.00185
29	560.0	0.00191
28	570.0	0.00193
12	575.0	0.00195
27	580.0	0.00209
26	590.0	0.00218

THERMAL CONDUCTIVITY CORRECTED FOR SEAFLOOR TEMPERATURE AND PRESSURE

POSITION MEASURED FROM BOTTOM OF CORE

R.V. CHAIN 61 HEAT FLOW STATION 57

MEASUREMENT NUMBER	POSITION (CM)	THERMAL CONDUCTIVITY (CAL/CM SEC DEG C)
23	25.0	0.00228
1	50.0	0.00235
2	75.0	0.00237
3	100.0	0.00251
4	125.0	0.00199
6	175.0	0.00331
7	200.0	0.00225
8	225.0	0.00243
9	250.0	0.00249
10	275.0	0.00246
11	295.0	0.00213
12	325.0	0.00257
13	350.0	0.00184
14	375.0	0.00202
15	400.0	0.00268
16	425.0	0.00256
17	450.0	0.00248
24	475.0	0.00189
5	475.0	0.00246
19	500.0	0.00225
20	525.0	0.00200
21	550.0	0.00236
22	575.0	0.00209
18	475.0	0.00194

THERMAL CONDUCTIVITY CORRECTED FOR SEAFLOOR TEMPERATURE AND PRESSURE

POSITION MEASURED FROM BOTTOM OF CORE

R.V. CHAIN 61 HEAT FLOW STATION 59

MEASUREMENT NUMBER	POSITION (CM)	THERMAL CONDUCTIVITY (CAL/CM SEC DEG C)
23	25.0	0.00234
22	50.0	0.00218
21	75.0	0.00205
20	100.0	0.00193
19	125.0	0.00163
18	150.0	0.00179
17	175.0	0.00216
16	200.0	0.00218
15	225.0	0.00219
14	250.0	0.00214
13	275.0	0.00203
12	295.0	0.00228
11	325.0	0.00246
10	350.0	0.00220
26	350.0	0.00230
9	375.0	0.00228
8	400.0	0.00233
7	425.0	0.00225
6	450.0	0.00227
5	475.0	0.00231
4	500.0	0.00227
3	525.0	0.00223
2	550.0	0.00237
1	575.0	0.00226
24	595.0	0.00221
25	595.0	0.00188

THERMAL CONDUCTIVITY CORRECTED FOR SEAFLOOR TEMPERATURE AND PRESSURE

POSITION MEASURED FROM BOTTOM OF CORE

R.V. CHAIN 61 HEAT FLOW STATION 62

MEASUREMENT NUMBER	POSITION (CM)	THERMAL CONDUCTIVITY (CAL/CM SEC DEG C)
13	0.0	0.00221
1	25.0	0.00263
2	50.0	0.00262
3	75.0	0.00262
4	100.0	0.00270
5	125.0	0.00267
6	150.0	0.00255
7	175.0	0.00262
8	200.0	0.00310
9	225.0	0.00269
10	250.0	0.00265
11	275.0	0.00257
12	295.0	0.00259

THERMAL CONDUCTIVITY CORRECTED FOR SEAFLOOR TEMPERATURE AND PRESSURE

POSITION MEASURED FROM BOTTOM OF CORE

R.V. CHAIN 61 HEAT FLOW STATION 63

MEASUREMENT NUMBER	POSITION (CM)	THERMAL CONDUCTIVITY (CAL/CM SEC DEG C)
24	25.0	0.00271
23	50.0	0.00259
22	75.0	0.00255
21	100.0	0.00260
20	125.0	0.00255
19	150.0	0.00269
18	175.0	0.00274
17	200.0	0.00264
16	225.0	0.00273
15	250.0	0.00270
14	275.0	0.00269
13	295.0	0.00266
12	325.0	0.00261
11	350.0	0.00265
10	375.0	0.00252
9	400.0	0.00268
8	425.0	0.00260
7	450.0	0.00247
6	475.0	0.00250
5	500.0	0.00237
4	525.0	0.00237
3	550.0	0.00234
2	575.0	0.00250
1	595.0	0.00250

THERMAL CONDUCTIVITY CORRECTED FOR SEAFLOOR TEMPERATURE AND PRESSURE

POSITION MEASURED FROM BOTTOM OF CORE

R.V. CHAIN 61 HEAT FLOW STATION 64

MEASUREMENT NUMBER	POSITION (CM)	THERMAL CONDUCTIVITY (CAL/CM SEC DEG C)
1	35.0	0.00286
2	50.0	0.00258
3	75.0	0.00253
4	80.0	0.00255
5	90.0	0.00364
6	100.0	0.00292
7	125.0	0.00260
8	150.0	0.00257
9	175.0	0.00443
10	200.0	0.00406
11	225.0	0.00389
12	250.0	0.00274
13	275.0	0.00243
14	315.0	0.00231
15	340.0	0.00227
16	370.0	0.00203
17	400.0	0.00197
18	425.0	0.00207
19	450.0	0.00226
20	475.0	0.00224
21	500.0	0.00215

THERMAL CONDUCTIVITY CORRECTED FOR SEAFLOOR TEMPERATURE AND PRESSURE

POSITION MEASURED FROM BOTTOM OF CORE

R.V. CHAIN 61 HEAT FLOW STATION 65

MEASUREMENT NUMBER	POSITION (CM)	THERMAL CONDUCTIVITY (CAL/CM SEC DEG C)
6	25.0	0.00222
5	75.0	0.00221
4	125.0	0.00245
3	175.0	0.00231
2	225.0	0.00247
1	275.0	0.00236
12	325.0	0.00206
11	375.0	0.00204
10	425.0	0.00220
9	475.0	0.00210
8	525.0	0.00209
7	575.0	0.00207

THERMAL CONDUCTIVITY CORRECTED FOR SEAFLOOR TEMPERATURE AND PRESSURE

POSITION MEASURED FROM BOTTOM OF CORE

R.V. CHAIN 61 HEAT FLOW STATION 66

MEASUREMENT NUMBER	POSITION (CM)	THERMAL CONDUCTIVITY (CAL/CM SEC DEG C)
1	25.0	0.00276
2	75.0	0.00280
3	125.0	0.00219
4	175.0	0.00227
5	225.0	0.00227
6	275.0	0.00182
7	325.0	0.00224
8	375.0	0.00235
9	425.0	0.00226
10	475.0	0.00204
11	525.0	0.00226
12	568.0	0.00417

THERMAL CONDUCTIVITY CORRECTED FOR SEAFLOOR TEMPERATURE AND PRESSURE

POSITION MEASURED FROM BOTTOM OF CORE

R.V. CHAIN 61 HEAT FLOW STATION 67

MEASUREMENT NUMBER	POSITION (CM)	THERMAL CONDUCTIVITY (CAL/CM SEC DEG C)
1	25.0	0.00208
2	75.0	0.00218
3	112.0	0.00215
4	157.0	0.00226
13	167.0	0.00217
5	213.0	0.00239
6	263.0	0.00228
7	335.0	0.00218
8	385.0	0.00218
9	435.0	0.00204
10	485.0	0.00219
11	525.0	0.00220
12	575.0	0.00225

THERMAL CONDUCTIVITY CORRECTED FOR SEAFLOOR TEMPERATURE AND PRESSURE

POSITION MEASURED FROM BOTTOM OF CORE

R.V. CHAIN 61 HEAT FLOW STATION 63

MEASUREMENT NUMBER	POSITION (CM)	THERMAL CONDUCTIVITY (CAL/CM SEC DEG C)
1	25.0	0.00211
2	75.0	0.00202
3	125.0	0.00209
4	175.0	0.00208
5	225.0	0.00210
6	275.0	0.00209
7	325.0	0.00210
8	375.0	0.00209
9	425.0	0.00206
10	475.0	0.00208
11	525.0	0.00208
12	575.0	0.00216
13	625.0	0.00215
14	675.0	0.00207
15	725.0	0.00216
16	775.0	0.00215
17	825.0	0.00219

THERMAL CONDUCTIVITY CORRECTED FOR SEAFLOOR TEMPERATURE AND PRESSURE

POSITION MEASURED FROM BOTTOM OF CORE

R.V. BANNOCK CT-69 HEAT FLOW STATION 17

MEASUREMENT NUMBER	POSITION (CM)	THERMAL CONDUCTIVITY (CAL/CM SEC DEG C)
2	45.0	0.00220
3	75.0	0.00241
4	105.0	0.00195
5	135.0	0.00210
6	165.0	0.00205
7	195.0	0.00227
8	225.0	0.00228
9	255.0	0.00234
10	285.0	0.00240
11	315.0	0.00257
12	345.0	0.00255
13	375.0	0.00206
14	405.0	0.00209
15	435.0	0.00221
16	465.0	0.00204
17	495.0	0.00211
18	525.0	0.00214
19	555.0	0.00201
20	585.0	0.00219

THERMAL CONDUCTIVITY CORRECTED FOR SEAFLOOR TEMPERATURE AND PRESSURE

POSITION MEASURED FROM TOP OF CORE

R.V. BANNOCK CT-69 HEAT FLOW STATION 29

MEASUREMENT NUMBER	POSITION (CM)	THERMAL CONDUCTIVITY (CAL/CM SEC DEG C)
2	42.0	0.00233
6	79.0	0.00253
5	109.0	0.00193
4	139.0	0.00204
3	169.0	0.00197
7	199.0	0.00194
8	229.0	0.00194
9	259.0	0.00213
10	289.0	0.00205
14	319.0	0.00202
13	349.0	0.00196
12	379.0	0.00218
11	409.0	0.00205
15	439.0	0.00198
16	469.0	0.00219
17	499.0	0.00200
18	529.0	0.00230
19	559.0	0.00193
20	589.0	0.00199
21	619.0	0.00219
22	639.0	0.00191

THERMAL CONDUCTIVITY CORRECTED FOR SEAFLOOR TEMPERATURE AND PRESSURE

POSITION MEASURED FROM TOP OF CORE

R.V. BANNOCK CT-69 HEAT FLOW STATION 21

MEASUREMENT NUMBER	POSITION (CM)	THERMAL CONDUCTIVITY (CAL/CM SEC DEG C)
1	24.0	0.00211
2	48.0	0.00225
3	87.0	0.00208
4	117.0	0.00197
5	147.0	0.00201
6	177.0	0.00221
7	207.0	0.00209
8	237.0	0.00225
9	267.0	0.00224
10	297.0	0.00196
11	327.0	0.00215
12	357.0	0.00221
13	387.0	0.00191
14	417.0	0.00201
15	447.0	0.00246
16	477.0	0.00234
17	507.0	0.00214
18	537.0	0.00229
19	567.0	0.00237
20	597.0	0.00223
21	627.0	0.00230
22	657.0	0.00215
23	687.0	0.00190
24	717.0	0.00233
25	747.0	0.00194
26	777.0	0.00214
27	807.0	0.00192
28	837.0	0.00234
29	867.0	0.00203
30	897.0	0.00212
31	927.0	0.00189
32	957.0	0.00207
33	987.0	0.00192
34	1017.0	0.00207
35	1048.0	0.00191

THERMAL CONDUCTIVITY CORRECTED FOR SEALEVEL TEMPERATURE AND PRESSURE

POSITION MEASURED FROM TOP OF CORE

R.V. BANNOCK CT-69 HEAT FLOW STATION 33

MEASUREMENT NUMBER	POSITION (CM)	THERMAL CONDUCTIVITY (CAL/CM SEC DEG C)
1	15.0	0.00208
2	45.0	0.00228
3	75.0	0.00220
4	100.0	0.00255
5	130.0	0.00198
6	160.0	0.00210
7	190.0	0.00134
8	220.0	0.00200
9	250.0	0.00184
10	280.0	0.00203
11	310.0	0.00197
12	340.0	0.00213
13	370.0	0.00213
14	400.0	0.00204
15	430.0	0.00196
16	460.0	0.00215
17	490.0	0.00195
18	520.0	0.00210
19	550.0	0.00195
20	580.0	0.00214
21	610.0	0.00139
22	640.0	0.00201
23	670.0	0.00221
24	700.0	0.00225
25	730.0	0.00213
26	760.0	0.00226
27	790.0	0.00214
28	820.0	0.00241
29	850.0	0.00223
30	880.0	0.00253
31	910.0	0.00225
32	940.0	0.00249
33	970.0	0.00227
34	1000.0	0.00236
35	1030.0	0.00188
36	1060.0	0.00204
37	1088.0	0.00206

THERMAL CONDUCTIVITY CORRECTED FOR SEAFLOOR TEMPERATURE AND PRESSURE

POSITION MEASURED FROM TOP OF CORE

R.V. RANNOCK CT-69 HEAT FLOW STATION 59

MEASUREMENT NUMBER	POSITION (CM)	THERMAL CONDUCTIVITY (CAL/CM SEC DEG C)
1	22.0	0.00196
2	85.0	0.00230
3	145.0	0.00210
4	205.0	0.00241
5	265.0	0.00241
6	325.0	0.00216
7	385.0	0.00227
8	445.0	0.00229
9	505.0	0.00196
10	565.0	0.00239
11	625.0	0.00225
12	685.0	0.00245
13	745.0	0.00213

THERMAL CONDUCTIVITY CORRECTED FOR SEAFLOOR TEMPERATURE AND PRESSURE

POSITION MEASURED FROM TOP OF CORE

R.V. RANNOCK CT-69 HEAT FLOW STATION 53

MEASUREMENT NUMBER	POSITION (CM)	THERMAL CONDUCTIVITY (CAL/CM SEC DEG C)
1	30.0	0.00217
2	80.0	0.00201
3	120.0	0.00275
4	160.0	0.00303
5	200.0	0.00290
7	280.0	0.00213
9	320.0	0.00252
9	360.0	0.00243
10	400.0	0.00219
11	440.0	0.00231
12	480.0	0.00247
13	520.0	0.00224

THERMAL CONDUCTIVITY CORRECTED FOR SEAFLOOR TEMPERATURE AND PRESSURE

POSITION MEASURED FROM TOP OF CORE

R.V. RANNOCK CT-69 HEAT FLOW STATION 54

MEASUREMENT NUMBER	POSITION (CM)	THERMAL CONDUCTIVITY (CAL/CM SEC DEG C)
1	20.0	0.00220
2	60.0	0.00193
3	100.0	0.00191
4	140.0	0.00195
5	180.0	0.00199
6	220.0	0.00221
7	260.0	0.00193
8	300.0	0.00237
9	340.0	0.00226
10	380.0	0.00227
11	420.0	0.00214
12	460.0	0.00226
13	500.0	0.00227
14	540.0	0.00235
15	580.0	0.00200
16	620.0	0.00214
17	660.0	0.00223
19	740.0	0.00201
20	780.0	0.00234
21	820.0	0.00233
22	860.0	0.00229
23	900.0	0.00227
24	940.0	0.00214

THERMAL CONDUCTIVITY CORRECTED FOR SEAFLOOR TEMPERATURE AND PRESSURE

POSITION MEASURED FROM TOP OF CORE

R.V. BANNOCK CT-69 HEAT FLOW STATION 55

MEASUREMENT NUMBER	POSITION (CM)	THERMAL CONDUCTIVITY (CAL/CM SEC DEG C)
1	40.0	0.00223
2	80.0	0.00227
3	120.0	0.00246
4	160.0	0.00267
5	200.0	0.00228
6	240.0	0.00215
7	280.0	0.00219
8	320.0	0.00200
9	360.0	0.00228
10	400.0	0.00222
11	440.0	0.00224
12	480.0	0.00246
13	520.0	0.00230
14	560.0	0.00287
15	600.0	0.00235
16	640.0	0.00248
17	680.0	0.00190
18	720.0	0.00247
19	760.0	0.00223
20	800.0	0.00219
21	840.0	0.00229
22	880.0	0.00251
23	920.0	0.00233
24	960.0	0.00235
25	995.0	0.00223

THERMAL CONDUCTIVITY CORRECTED FOR SEAFLOOR TEMPERATURE AND PRESSURE

POSITION MEASURED FROM TOP OF CORE

P.V. BANNOCK CT-69 HEAT FLOW STATION 78

MEASUREMENT NUMBER	POSITION (CM)	THERMAL CONDUCTIVITY (CAL/CM SEC DEG C)
1	24.0	0.00224
2	70.0	0.00240
3	113.0	0.00243
4	153.0	0.00218
5	193.0	0.00250
6	233.0	0.00247
7	273.0	0.00235
8	313.0	0.00247
9	353.0	0.00241
10	393.0	0.00233
11	433.0	0.00230
12	473.0	0.00282
13	513.0	0.00229
14	553.0	0.00235
15	593.0	0.00241
16	633.0	0.00265
17	673.0	0.00237
18	713.0	0.00236
19	753.0	0.00209
20	793.0	0.00254
21	833.0	0.00223
22	873.0	0.00245
23	913.0	0.00223
24	949.0	0.00243

THERMAL CONDUCTIVITY CORRECTED FOR SEAFLOOR TEMPERATURE AND PRESSURE

POSITION MEASURED FROM TOP OF CORE

R.V. RANNOCK CT-68 HEAT FLOW STATION 70

MEASUREMENT NUMBER	POSITION (CM)	THERMAL CONDUCTIVITY (CAL/CM SEC DEG C)
1	21.0	0.00239
2	42.0	0.00202
3	102.0	0.00197
4	142.0	0.00214
5	182.0	0.00215
6	222.0	0.00221
7	262.0	0.00245
8	302.0	0.00203
9	342.0	0.00207
10	382.0	0.00245
11	422.0	0.00198
12	462.0	0.00234
13	502.0	0.00243
14	542.0	0.00216
15	582.0	0.00208
16	622.0	0.00206
17	662.0	0.00196
18	702.0	0.00200
19	742.0	0.00193
20	782.0	0.00213
21	822.0	0.00212
22	862.0	0.00203
23	902.0	0.00212
24	942.0	0.00208
25	982.0	0.00193

THERMAL CONDUCTIVITY CORRECTED FOR SEAFLOOR TEMPERATURE AND PRESSURE

POSITION MEASURED FROM TOP OF CORE

P.V. ATLANTIS II HEAT FLOW STATION 1431P

MEASUREMENT NUMBER	POSITION (CM)	THERMAL CONDUCTIVITY (CAL/CM SEC DEG C)
10	35.0	0.00215
17	56.0	0.00211
16	76.0	0.00224
9	99.0	0.00206
15	101.0	0.00206
14	124.0	0.00213
18	136.0	0.00192
8	139.0	0.00235
19	164.0	0.00211
12	175.0	0.00250
7	189.0	0.00234
11	214.0	0.00218
6	251.0	0.00224
5	301.0	0.00185
4	351.0	0.00231
3	401.0	0.00205
2	451.0	0.00252
1	499.0	0.00225

THERMAL CONDUCTIVITY CORRECTED FOR SEAFLOOR TEMPERATURE AND PRESSURE

POSITION MEASURED FROM TOP OF CORE

R.V. ATLANTIS II HEAT FLOW STATION 14338

MEASUREMENT NUMBER	POSITION (CM)	THERMAL CONDUCTIVITY (CAL/CM SEC DEG C)
3	80.0	0.00198
2	130.0	0.00194
1	180.0	0.00206
13	232.0	0.00217
4	275.0	0.00196
12	282.0	0.00177
11	332.0	0.00209
10	382.0	0.00209
9	432.0	0.00271
8	480.0	0.00203

THERMAL CONDUCTIVITY CORRECTED FOR SEAFLOOR TEMPERATURE AND PRESSURE

POSITION MEASURED FROM TOP OF CORE

R.V. ATLANTIS II HEAT FLOW STATION 1443P

MEASUREMENT NUMBER	POSITION (CM)	THERMAL CONDUCTIVITY (CAL/CM SEC DEG C)
4	90.0	0.00271
5	115.0	0.00345
7	155.0	0.00302
8	170.0	0.00265
15	234.0	0.00332
16	331.0	0.00293
17	429.0	0.00384
13	565.0	0.00332
11	585.0	0.00281
12	710.0	0.00371
14	730.0	0.00248

THERMAL CONDUCTIVITY CORRECTED FOR SEAFLOOR TEMPERATURE AND PRESSURE

POSITION MEASURED FROM TOP OF CORE

R.V. ATLANTIS II HEAT FLOW STATION 1444B

MEASUREMENT NUMBER	POSITION (CM)	THERMAL CONDUCTIVITY (CAL/CM SEC DEG C)
10	100.0	0.00183
11	140.0	0.00224
12	165.0	0.00227
13	190.0	0.00214
14	215.0	0.00244
1	250.0	0.00256
2	284.0	0.00232
3	304.0	0.00224
4	334.0	0.00230
5	359.0	0.00209
6	384.0	0.00211
7	405.0	0.00231
8	434.0	0.00219
9	484.0	0.00218

THERMAL CONDUCTIVITY CORRECTED FOR SEAFLOOR TEMPERATURE AND PRESSURE

POSITION MEASURED FROM TOP OF CORE

R.V. ATLANTIS II HEAT FLOW STATION 1445B

MEASUREMENT NUMBER	POSITION (CM)	THERMAL CONDUCTIVITY (CAL/CM SEC DEG C)
4	20.0	0.00177
7	60.0	0.00215
8	75.0	0.00215
9	85.0	0.00221
1	91.0	0.00211
10	100.0	0.00208
2	105.0	0.00281
11	110.0	0.00228
2	111.0	0.00229
12	125.0	0.00237
3	130.0	0.00216
3	131.0	0.00219
13	140.0	0.00267
4	151.0	0.00239
5	171.0	0.00262
6	191.0	0.00229
7	204.0	0.00228
8	218.0	0.00262
9	231.0	0.00250
10	251.0	0.00234
11	271.0	0.00209
12	291.0	0.00255
13	311.0	0.00251
14	331.0	0.00247

THERMAL CONDUCTIVITY CORRECTED FOR SEAFLOOR TEMPERATURE AND PRESSURE

POSITION MEASURED FROM TOP OF CORE

R.V. ATLANTIS II HEAT FLOW STATION 14462

MEASUREMENT NUMBER	POSITION (CM)	THERMAL CONDUCTIVITY (CAL/CM SEC DEG C)
1	10.0	0.00204
0	20.0	0.00197
2	30.0	0.00197
7	40.0	0.00198
3	50.0	0.00257
5	60.0	0.00183
12	63.0	0.00242
4	70.0	0.00199
6	80.0	0.00183
14	136.0	0.00203
8	301.0	0.00177
9	351.0	0.00234
10	401.0	0.00198
11	451.0	0.00239
1	515.0	0.00200
2	547.0	0.00203
3	615.0	0.00204
4	667.0	0.00196
5	704.0	0.00194
6	740.0	0.00187

THERMAL CONDUCTIVITY CORRECTED FOR SEAFLOOR TEMPERATURE AND PRESSURE

POSITION MEASURED FROM TOP OF CORE

R.V. ATLANTIS II HEAT FLOW STATION 1447P

MEASUREMENT NUMBER	POSITION (CM)	THERMAL CONDUCTIVITY (CAL/CM SEC DEG C)
1	25.0	0.00211
1	30.0	0.00182
2	50.0	0.00209
2	55.0	0.00197
3	75.0	0.00223
3	80.0	0.00184

THERMAL CONDUCTIVITY CORRECTED FOR SEAFLOOR TEMPERATURE AND PRESSURE

POSITION MEASURED FROM TOP OF CORE

R.V. ATLANTIS II HEAT FLOW STATION 1452P

MEASUREMENT NUMBER	POSITION (CM)	THERMAL CONDUCTIVITY (CAL/CM SEC DEG C)
1	8.0	0.00228
2	28.0	0.00201
3	48.0	0.00224
13	58.0	0.00247
4	68.0	0.00245
5	88.0	0.00262
6	108.0	0.00248
7	124.0	0.00266
8	144.0	0.00240
9	164.0	0.00265
10	184.0	0.00242
11	204.0	0.00228
12	224.0	0.00210
14	243.0	0.00248
15	263.0	0.00226
16	283.0	0.00259
17	303.0	0.00227
18	323.0	0.00259
19	343.0	0.00225
20	373.0	0.00255
21	403.0	0.00229
22	453.0	0.00261
23	503.0	0.00242

THERMAL CONDUCTIVITY CORRECTED FOR SEAFLOOR TEMPERATURE AND PRESSURE

POSITION MEASURED FROM TOP OF CORE

R.V. ATLANTIS II HEAT FLOW STATION 1460P

MEASUREMENT NUMBER	POSITION (CM)	THERMAL CONDUCTIVITY (CAL/CM SEC DEG C)
1	15.0	0.00174
2	50.0	0.00158
3	98.0	0.00202
4	122.0	0.00192
5	148.0	0.00199
6	200.0	0.00194
7	225.0	0.00198
8	250.0	0.00189
9	275.0	0.00195
10	300.0	0.00193
11	322.0	0.00168
12	332.0	0.00206
13	352.0	0.00174
14	377.0	0.00170
15	402.0	0.00181
16	435.0	0.00159
17	449.0	0.00180
18	475.0	0.00188
19	501.0	0.00180
20	525.0	0.00173
21	550.0	0.00162
22	575.0	0.00183
23	622.0	0.00182
25	671.0	0.00185
26	697.0	0.00202
27	706.0	0.00188
28	718.0	0.00227
29	735.0	0.00163
31	812.0	0.00169
32	826.0	0.00209
33	852.0	0.00228
34	872.0	0.00225

THERMAL CONDUCTIVITY CORRECTED FOR SEAFLOOR TEMPERATURE AND PRESSURE

POSITION MEASURED FROM TOP OF CORE

R.V. ATLANTIS II HEAT FLOW STATION 14626

MEASUREMENT NUMBER	POSITION (CM)	THERMAL CONDUCTIVITY (CAL/CM SEC DEG C)
1	13.0	0.00174
2	18.0	0.00196
3	23.0	0.00158
4	28.0	0.00197
5	33.0	0.00195
6	38.0	0.00181
7	43.0	0.00161
8	47.0	0.00174
9	51.0	0.00161
10	55.0	0.00159
11	59.0	0.00153
12	65.0	0.00157
13	78.0	0.00177
14	88.0	0.00190
15	93.0	0.00181

THERMAL CONDUCTIVITY CORRECTED FOR SEAFLOOR TEMPERATURE AND PRESSURE

POSITION MEASURED FROM TOP OF CORE

R.V. ATLANTIS II HEAT FLOW STATION 1464G

MEASUREMENT NUMBER	POSITION (CM)	THERMAL CONDUCTIVITY (CAL/CM SEC DEG C)
9	37.0	0.00189
8	45.0	0.00197
7	55.0	0.00190
6	65.0	0.00213
5	75.0	0.00203
4	85.0	0.00205
3	95.0	0.00181
2	105.0	0.00208
1	115.0	0.00202

THERMAL CONDUCTIVITY CORRECTED FOR SEAFLOOR TEMPERATURE AND PRESSURE

POSITION MEASURED FROM TOP OF CORE

R.V. ATLANTIS II HEAT FLOW STATION 14706

MEASUREMENT NUMBER	POSITION (CM)	THERMAL CONDUCTIVITY (CAL/CM SEC DEG C)
12	12.0	0.00189
11	22.0	0.00193
13	32.0	0.00188
10	42.0	0.00195
14	52.0	0.00173
9	62.0	0.00192
17	72.0	0.00204
15	72.0	0.00204
8	82.0	0.00198
16	92.0	0.00186
7	102.0	0.00195
6	122.0	0.00202
18	132.0	0.00179
5	142.0	0.00185
19	152.0	0.00197
4	162.0	0.00202
20	172.0	0.00190
3	182.0	0.00197
21	192.0	0.00232
2	202.0	0.00263
22	212.0	0.00214
1	217.0	0.00208

THERMAL CONDUCTIVITY CORRECTED FOR SEAFLOOR TEMPERATURE AND PRESSURE

POSITION MEASURED FROM TOP OF CORE

R.V. ATLANTIS II HEAT FLOW STATION 14726

MEASUREMENT NUMBER	POSITION (CM)	THERMAL CONDUCTIVITY (CAL/CM SEC DEG C)
1	10.0	0.00190
3	40.0	0.00208
4	50.0	0.00214
5	65.0	0.00204
6	90.0	0.00203
7	100.0	0.00200
8	115.0	0.00205

THERMAL CONDUCTIVITY CORRECTED FOR SEAFLOOR TEMPERATURE AND PRESSURE

POSITION MEASURED FROM TOP OF CORE

R.V. ATLANTIS II HEAT FLOW STATION 1473D

MEASUREMENT NUMBER	POSITION (CM)	THERMAL CONDUCTIVITY (CAL/CM SEC DEG C)
17	48.0	0.00242
16	73.0	0.00250
15	98.0	0.00240
14	123.0	0.00237
13	148.0	0.00235
1	133.0	0.00245
2	208.0	0.00254
3	233.0	0.00249
5	283.0	0.00246
6	308.0	0.00262
7	333.0	0.00247
8	358.0	0.00255
9	383.0	0.00245
10	408.0	0.00255
12	458.0	0.00253
27	547.0	0.00236
26	572.0	0.00242
25	597.0	0.00235
24	622.0	0.00251
23	647.0	0.00233
29	672.0	0.00253
22	672.0	0.00230
21	697.0	0.00222
20	722.0	0.00262
19	747.0	0.00240
1	25.0	0.00190
2	50.0	0.00185
3	75.0	0.00187
4	100.0	0.00183
5	125.0	0.00225
6	150.0	0.00210
7	175.0	0.00221
8	200.0	0.00210

THERMAL CONDUCTIVITY CORRECTED FOR SEAFLOOR TEMPERATURE AND PRESSURE

POSITION MEASURED FROM TOP OF CORE

P.V. ATLANTIS II HEAT FLOW STATION 1473G

MEASUREMENT NUMBER	POSITION (CM)	THERMAL CONDUCTIVITY (CAL/CM SEC DEG C)
1	25.0	0.00190
2	50.0	0.00195
3	75.0	0.00187
4	100.0	0.00193
5	125.0	0.00225
6	150.0	0.00210
7	175.0	0.00221
8	200.0	0.00219

THERMAL CONDUCTIVITY CORRECTED FOR SEAFLOOR TEMPERATURE AND PRESSURE

POSITION MEASURED FROM TOP OF CORE

R.V. ATLANTIS II HEAT FLOW STATION 1476P

MEASUREMENT NUMBER	POSITION (CM)	THERMAL CONDUCTIVITY (CAL/CM SEC DEG C)
1	10.0	0.00182
2	35.0	0.00190
3	60.0	0.00189
5	85.0	0.00176
7	135.0	0.00191
8	160.0	0.00172
9	185.0	0.00183
10	210.0	0.00202

THERMAL CONDUCTIVITY CORRECTED FOR SEAFLOOR TEMPERATURE AND PRESSURE

POSITION MEASURED FROM TOP OF CORE

R.V. ATLANTIS II HEAT FLOW STATION 1477P

MEASUREMENT NUMBER	POSITION (CM)	THERMAL CONDUCTIVITY (CAL/CM SEC DEG C)
7	43.0	0.00194
5	103.0	0.00281
4	133.0	0.00193
3	163.0	0.00206
2	193.0	0.00297
1	223.0	0.00343
12	280.0	0.00200
10	380.0	0.00212
9	430.0	0.00206
8	473.0	0.00199

THERMAL CONDUCTIVITY CORRECTED FOR SEAFLOOR TEMPERATURE AND PRESSURE

POSITION MEASURED FROM TOP OF CORE

R.V. ATLANTIS II HEAT FLOW STATION 14780

MEASUREMENT NUMBER	POSITION (CM)	THERMAL CONDUCTIVITY (CAL/CM SEC DEG C)
1	10.0	0.00227
12	20.0	0.00252
2	30.0	0.00227
11	40.0	0.00283
3	50.0	0.00218
10	60.0	0.00243
9	65.0	0.00212
5	90.0	0.00218
13	100.0	0.00241
7	100.0	0.00255
6	110.0	0.00290
14	211.0	0.00435
15	260.0	0.00342
19	297.0	0.00374
16	310.0	0.00415
18	314.0	0.00383
17	360.0	0.00376

THERMAL CONDUCTIVITY CORRECTED FOR SEAFLOOR TEMPERATURE AND PRESSURE

POSITION MEASURED FROM TOP OF CORE

P.V. ATLANTIS II HEAT FLOW STATION 1480G

MEASUREMENT NUMBER	POSITION (CM)	THERMAL CONDUCTIVITY (CAL/CM SEC DEG C)
1	10.0	0.00197
2	20.0	0.00214
3	30.0	0.00218
4	40.0	0.00216
5	50.0	0.00212
6	60.0	0.00219
7	70.0	0.00217
8	80.0	0.00243
9	90.0	0.00222
10	100.0	0.00199

THERMAL CONDUCTIVITY CORRECTED FOR SEAFLOOR TEMPERATURE AND PRESSURE

POSITION MEASURED FROM TOP OF CORE

R.V. ATLANTIS II HEAT FLOW STATION 1491?

MEASUREMENT NUMBER	POSITION (CM)	THERMAL CONDUCTIVITY (CAL/CM SEC DEG C)
9	25.0	0.00209
10	50.0	0.00224
11	75.0	0.00212
12	100.0	0.00219
13	125.0	0.00199
14	150.0	0.00259
15	175.0	0.00191
16	200.0	0.00236
17	225.0	0.00215
18	250.0	0.00216
1	324.0	0.00225
2	334.0	0.00263
3	359.0	0.00205

THERMAL CONDUCTIVITY CORRECTED FOR SEAFLOOR TEMPERATURE AND PRESSURE

POSITION MEASURED FROM TOP OF CORE

R.V. ATLANTIS II HEAT FLOW STATION 1484G

MEASUREMENT NUMBER	POSITION (CM)	THERMAL CONDUCTIVITY (CAL/CM SEC DEG C)
7	26.0	0.00183
6	51.0	0.00189
5	76.0	0.00208
4	101.0	0.00249
3	126.0	0.00215
2	151.0	0.00257
1	173.0	0.00218

THERMAL CONDUCTIVITY CORRECTED FOR SEAFLOOR TEMPERATURE AND PRESSURE

POSITION MEASURED FROM TOP OF CORE

R.V. ATLANTIS II HEAT FLOW STATION 1485G

MEASUREMENT NUMBER	POSITION (CM)	THERMAL CONDUCTIVITY (CAL/CM SEC DEG C)
7	17.0	0.00217
6	32.0	0.00265
5	57.0	0.00217
4	82.0	0.00232
3	107.0	0.00244
1	157.0	0.00212

THERMAL CONDUCTIVITY CORRECTED FOR SEAFLOOR TEMPERATURE AND PRESSURE

POSITION MEASURED FROM TOP OF CORE

R.V. ATLANTIS II HEAT FLOW STATION 14868

MEASUREMENT NUMBER	POSITION (CM)	THERMAL CONDUCTIVITY (CAL/CM SEC DEG C)
1	30.0	0.00213
2	55.0	0.00216
3	80.0	0.00232
4	105.0	0.00230
5	130.0	0.00190
6	155.0	0.00191
7	180.0	0.00215
8	192.0	0.00201
9	205.0	0.00210
10	230.0	0.00202
11	276.0	0.00227
12	304.0	0.00231
13	326.0	0.00193
14	352.0	0.00211
15	376.0	0.00219
16	425.0	0.00215
17	470.0	0.00211
18	540.0	0.00211

THERMAL CONDUCTIVITY CORRECTED FOR SEAFLOOR TEMPERATURE AND PRESSURE

POSITION MEASURED FROM TOP OF CORE